2016

BIOACTIVE POLY(BETA-AMINO ESTER) BIOMATERIALS FOR TREATMENT OF INFECTION AND OXIDATIVE STRESS

Andrew L. Lakes
University of Kentucky, andrewllakes@gmail.com
Digital Object Identifier: http://dx.doi.org/10.13023/ETD.2016.024

STUDENT AGREEMENT:

I represent that my thesis or dissertation and abstract are my original work. Proper attribution has been given to all outside sources. I understand that I am solely responsible for obtaining any needed copyright permissions. I have obtained needed written permission statement(s) from the owner(s) of each third-party copyrighted matter to be included in my work, allowing electronic distribution (if such use is not permitted by the fair use doctrine) which will be submitted to UKnowledge as Additional File.

I hereby grant to The University of Kentucky and its agents the irrevocable, non-exclusive, and royalty-free license to archive and make accessible my work in whole or in part in all forms of media, now or hereafter known. I agree that the document mentioned above may be made available immediately for worldwide access unless an embargo applies.

I retain all other ownership rights to the copyright of my work. I also retain the right to use in future works (such as articles or books) all or part of my work. I understand that I am free to register the copyright to my work.

REVIEW, APPROVAL AND ACCEPTANCE

The document mentioned above has been reviewed and accepted by the student's advisor, on behalf of the advisory committee, and by the Director of Graduate Studies (DGS), on behalf of the program; we verify that this is the final, approved version of the student's thesis including all changes required by the advisory committee. The undersigned agree to abide by the statements above.

Andrew L. Lakes, Student

Dr. Thomas D. Dziubla, Major Professor

Dr. Thomas D. Dziubla, Director of Graduate Studies

BIOACTIVE POLY(BETA-AMINO ESTER) BIOMATERIALS FOR TREATMENT OF INFECTION AND OXIDATIVE STRESS

DISSERTATION

A dissertation submitted in partial fulfillment of the
requirements for the degree of Doctor of Philosophy in the
College of Engineering
at the University of Kentucky

By
Andrew L. Lakes

Lexington, Kentucky

Director: Dr. Thomas D. Dziubla, Gill Professor, Associate Professor of Chemical Engineering

Lexington, Kentucky

2016

ABSTRACT OF DISSERTATION

BIOACTIVE POLY(β-AMINO ESTER) BIOMATERIALS FOR TREATMENT OF INFECTION AND OXIDATIVE STRESS

Polymers have deep roots as drug delivery tools, and are widely used in clinical to private settings. Currently, however, numerous traditional therapies exist which may be improved through use of polymeric biomaterials. Through our work with infectious and oxidative stress disease prevention and treatment, we aimed to develop application driven, enhanced therapies utilizing new classes of polymers synthesized in-house. Applying biodegradable poly(β-amino ester) (PBAE) polymers, covalent-addition of bioactive substrates to these PBAEs avoided certain pitfalls of free-loaded and non-degradable drug delivery systems. Further, through variation of polymer ingredients and conditions, we were able to tune degradation rates, release profiles, cellular toxicity, and material morphology.

Using these fundamentals of covalent drug-addition into biodegradable polymers, we addressed two problems that exist with the treatment of patients with high-risk wound-sites, namely non-biodegradability that require second-surgeries, and free-loaded antibiotic systems where partially degraded materials fall below the minimum inhibitory concentration, allowing biofilm proliferation. Our *in situ* polymerizable, covalently-bound vancomycin hydrogel provided active antibiotic degradation products and drug release which closely followed the degradation rate over tunable periods.

With applications of antioxidant delivery, we continued with this concept of covalent drug addition and modified a PBAE, utilizing a disulfide moiety to mimic redox processes which glutathione/glutathione disulfide performs. This material was found to not only be hydrolytically biodegradable, but tunable in reducibility through cleavage of the disulfide crosslinker, forming antioxidant groups of bound-thiols, similar to drugs currently used in radioprotective therapies. The differential cellular viability of degradation products containing disulfide or antioxidant thiol forms was profound, and the antioxidant form significantly aided cellular resistance to a superoxide attack, similar to that of a radiation injury.

Pathophysiological oxidation in the form of radiation injury or oxidative stress based diseases are often region specific to the body and thus require specific targeting, and nanomaterials are widely researched to perform this. Utilizing a tertiary-amine base-catalyst, we were able to synthesize a high drug content (20-26 wt%) version of the disulfide PBAE previously unattainable. The reduced version of this material created a

linear-chain polymer capable of single-emulsion nanoparticle formulation for use with intravenous antioxidant delivery applications instead of local.

KEYWORDS: Antibiotics, Antioxidants, Oxidative Stress, Hydrogels, Nanoparticles

Andrew L. Lakes

2/3/2016

BIOACTIVE POLY(BETA-AMINO ESTER) BIOMATERIALS FOR TREATMENT OF INFECTION AND OXIDATIVE STRESS

By

Andrew L. Lakes

Dr. Thomas D. Dziubla
Director of Dissertation

Dr. Thomas D. Dziubla
Director of Graduate Studies

February 3, 2016
Date

DEDICATION

I dedicate this body of work and degree to:

Lea Lakes
Jody and Lloyd Vasilakes
Nicholas Vasilakes

For making me strive to be a doctor, *and* an engineer.
Qapla’

ACKNOWLEDGEMENTS

I would like to recognize my primary and co-advisors Drs. Tom Dziubla, J. Zach Hilt, and David Puleo for their outstanding support and continuous thought they have put into not only our work accomplished, but in my development into a scientist who holds critical thinking to the highest of regard.

I would also like to thank my other committee member Dr. Brad Berron for allowing for me to think of new perspectives, and my outside examiner, Dr. Bob Yokel, for his support in mentorship and development.

I thank my lab mates of present and past who have helped me accomplish what I have, partially through letting me "scavenge" their forlorn delectables: Dr. Paritosh Wattamwar, Dr. David Cochran, Dr. Sundar Authimoolam, Prachi Gupta, Vinod Patil, and Mark Bailey. Some out-of-our-lab members have become good friends, and their food-for-thought through long nights have already been much missed: Dr. Robert and Luna Wydra, Dr. Daniel Schlipf, Dr. Matt Dickerson, Andrea Leydet, Dr. Nathanael Stocke, Carolyn Jordan, Angela Gutierrez, Anastasia Hauser, and Jacob Lilly. Special thanks to Dr. Nico Briot and Dr. Dali Qian for SEM expertise, Dr. Jack Goodman for help with mass spectroscopy and Dr. Illona Hoffman for help with X-ray photoelectron spectroscopy.

Finally, I would like to thank the funding support from my two traineeship grants which allowed my research to be possible, as well as allow me to define where my research direction would lead to. These are the National Science Foundation Integrative Graduate Education and Research Traineeship (NSF-IGERT), and the National Cancer Institute Cancer Nanotechnology Training Center (NCI-CNTC).

TABLE OF CONTENTS

LIST OF TABLES

LIST OF FIGURES

Chapter 1. Introduction and Research Goals

1.1 Introduction

Poly(β-amino esters) (PBAE) are a class of biodegradable and biocompatible materials which are polymerized via the reaction of acrylates with amines, i.e. aza-Michael addition, into biofunctional materials. Originally, PBAE polymers found research interest as non-viral gene vectors due to their cationic charge from sterically hindered tertiary amines, which allows for both DNA complexation while possessing a cytotoxicity profile that is significantly lower than that of cationic polymers like polyethylenimine or poly-lysine [1]. Since then, PBAEs have proven to be a highly customizable platform, such as formation into soft/hard tissue-like structures [2, 3], or utilized for a variety of applications in drug delivery [4-6].

To introduce versatile functionality, bioactive molecules may be covalently bonded into PBAE network backbones. If an appropriate group on a molecule of interest is available for reaction (e.g., α,β-unsaturated carbonyls, or primary/secondary amines), a PBAE may be formed without needing to use complex conjugates/leaving groups. For example, our group has previously formulated poly-drug systems through the synthesis of polyphenolic antioxidants, curcumin and quercetin, into acrylated forms through conversion of OH groups [7, 8]. Michael addition of acrylated antioxidants with amines proved advantageous as a pro-drug antioxidant delivery method, whereupon ester degradation, active antioxidant was released. Expanding upon this work, we have developed two different PBAEs utilizing covalent drug addition using primary amine sites already present upon the molecules of interest. By using vancomycin and cystamine to form bioactive and functionalized

biomaterials, we demonstrate the versatility of the PBAE platform for the treatment of infection and oxidative stress.

In the clinical treatment of infection, antibiotic resistance emergence has become a significant concern throughout the world [9]. Stemming from the brisk pace of bacterial evolution by natural selection, bacteria can develop coping mechanisms to overcome antibiotic pressures. Particularly, it has been shown that suboptimal antibiotic treatment at concentrations below the minimum inhibitory concentration (MIC) aids bacterial selection through a differential growth rate of more resistant bacteria [10, 11]. Further, bacterial biofilm formation allows for bacteria to remain in a dense packing, where antibiotic perfusion may be limited, thus protecting inner bacteria from the full concentration of antibiotic. *Staphylococcus aureus*, in particular, is part of the bacterial skin flora and is notorious for prevalence in hospital and community acquired disease [12]. With *S. aureus,* the combination of treatment with sub-optimal antibiotic concentration along with the mutagenic effects of the bacteria's endogenously produced hydrogen peroxide signaling—used as a bacterial quorum sensing molecule—allows for rapid genetic mutation and survival of the fittest against the antibiotic selective pressure [10, 11]. In an attempt to suppress hydrogen peroxide signaling and thus the increased mutagenesis, it is hypothesized that delivering catalase to *S. aureus* would inhibit hydrogen peroxide mediated genetic diversification [13]. Chapter 4 presents a method for the tandem delivery of an antibiotic, vancomycin, alongside the antioxidant, catalase, from a PBAE hydrogel designed for local antibiotic delivery. *In situ* polymerization, a favorable method widely used in tissue adhesives and injectable hydrogels [14-16], was produced through a two-step hydrogel synthesis. First, an acrylate end-capped linear chain macromer was formed,

of which the acrylates were then free radical polymerized to synthesize the hydrogel. We found that tandem delivery was achieved, and that both drugs remained active after free-radical polymerization process. With the release of catalase over an extended period of 19 days, this system could further be studied in reducing the chance of antibiotic resistance emergence.

In local drug delivery, traditional biopolymer implants like polymethylmethacrylate (PMMA) could become colonized if not removed before the drug content is diminished, and thus complication-prone second surgeries are a necessity [17-22]. Alternatively, biodegradable implants are favorable in that they resorb into tissue. Even so, there is risk of bacterial biofilm formation in biodegradable materials for the period after drug release falls below the MIC, but before complete degradation occurs [23-25]. This diffusive burst-release phenomenon was found to be present in our prior hydrogel study found in Chapter 4, and thus Chapter 5 presents a method to overcome the inherent burst release. We synthesized a similarly *in situ* polymerizable PBAE hydrogel, yet covalently incorporated vancomycin into the polymeric backbone in an attempt to slow burst release, and equalize the drug release and material degradation rates. Vancomycin conjugation was performed through the available primary amines, allowing for Michael addition incorporation into PBAE oligomers, which could further be polymerized via free radical polymerization into hydrogels. It was found that the drug release vs degradation rate allowed for vancomycin release up to the completion of degradation, albeit at the cost of increasing the bacterial minimum inhibitory concentration of conjugate vancomycin released.

Pathophysiological oxidative stress related diseases, such as ischemia in diabetes, reperfusion injury in myocardial infarction, certain neurodegenerative diseases like

Alzheimer's, autoimmune disorders like rheumatoid arthritis, pulmonary pneumonitis from radiotherapy, cancer etc. are directly or indirectly caused by increased levels of reactive oxygen species (ROS) and reactive nitrogen species (RNS) [26-30]. Oxidative damage to DNA, lipids, or proteins may cause cellular dysfunction, apoptosis, necrosis, and promote an immune cascade of inflammation, further increasing the generation of ROS/RNS. While cells maintain redox homeostasis during minor events of oxidative burden via a complex system of antioxidant molecules like glutathione, catalase, and superoxide dismutase (SOD), too great an oxidative insult can saturate the cellular defenses and lead to injury.

In Chapter 6, using our experience in covalent addition, we synthesized a PBAE hydrogel for the treatment of oxidative stress via addition of cystamine. Cystamine contains a redox sensitive disulfide bond and may be reduced into thiols to carry out antioxidant scavenging, similar to cellular-based cysteine and glutathione. In hydrogel form, adding a reducing agent converted disulfide bonds into thiols, and decreased the level of hydrogel crosslinking depending upon the cystamine content. Interestingly, the material degradation products showed a significant differential of toxicity towards a human-derived endothelial cell line depending on if in the disulfide or thiol state, as well as concentration of thiol in the starting material. These results support the hypothesis that antioxidant delivery alleviates oxidative injury [31, 32].

With a large body of research on polymeric nanoparticles in the literature, they are a promising technology for drug delivery, whether it be for extended release with long circulating particles or region/cell specific targeting as with antibody or ligand targeted systems [33-36]. Chapter 3 discusses polymeric nanoparticle background and utility in depth. With intent to formulate a polymeric nanoparticle system using our cystamine-

PBAE material for nanoscale antioxidant delivery in such aforementioned applications, we developed a hydrogel with cystamine composed of 100% of the amines, containing between 20-26 wt% cystamine depending on the diacrylate monomer used. This high loading had previously been unattainable due to low solubility and low extent of reaction, but with the addition of a non-nucleophilic base catalyst, it was achievable. This hydrogel could be solubilized upon reduction into thiolated oligomers for single emulsion into thiolated nanoparticles. Chapter 7 covers the PBAE nanoparticle formation where we characterize the material properties and kinetics of the thiolated nanoparticle system. The nanoparticles were found to have a high thiol content over a period of 7 days. This allowed for an extended period of high antioxidant capacity, potentially useful for antioxidant delivery applications, or for applications where high concentrations of thiol moieties would be useful in adding further functional thiol-reactive conjugates such as maleimide, thiol-ene, iodoacetamides, or gold reactions.

1.2 Research Goals

The overall objective of this work was to utilize PBAEs as a biocompatible and biodegradable platform to formulate bioactive biomaterials for the treatment of infection and oxidative stress disease. Four specific aims of this research were investigated:

Chapter 4. Formulate tunable PBAE hydrogels for the tandem release of vancomycin and catalase with application of infection treatment

a. Synthesize PBAE hydrogels with a method for *in situ* polymerization containing vancomycin and catalase
b. Modify degradation and drug release profiles via variation of co-monomer and co-macromer ratios
c. Provide extended antibiotic activity against *S. aureus*
d. Conserve catalase activity after the oxidative free radical polymerization

Outcome and Significance:

Tunable release and degradation rates resulted through variation of the hydrophilic and hydrophobic co-macromers and co-monomer macromers made from poly(ethylene glycol), diethylene glycol, and isobutylamine. Both small (vancomycin, 1.5 kDa) and large (catalase, 232 kDa) molecules were released for an extended period while retaining activity of drugs. Where vancomycin release was slowed from 2 days to 7 days comparing a co-macromer hydrogel (H6:A6 as defined in chapter 4) to a co-monomer macromer system (AH6 as defined in chapter 4) respectively, catalase showed a slower release profile up to when the hydrogels began to fragment 19 days. At catalase drug release 60%

or less, vancomycin release was complete, yet catalase was retained within the mesh, likely due to its large size. The release of two vastly different sized molecules from a single, *in situ* polymerizable biodegradable material is an important delivery method for combinatorial drug treatments in local infections as it 1) reduces the total number of materials required, 2) doesn't required second surgeries for non-degradable material removal, and 3) forms to the surrounding tissue to reduce patient discomfort. Further, the method of co-delivery of an antibiotic with catalase may provide protection against antibiotic resistance emergence through suppression of hydrogen peroxide signaling.

Chapter 5. Achieve equivalent vancomycin release and degradation periods through covalent addition of vancomycin to a PBAE hydrogel as a method to avoid the non-therapeutic period of biodegradable antibiotic implants after drug release is complete yet degradation is not

a. Partially replace isobutylamine with vancomycin during Michael addition in PBAE oligomer formation for covalent addition via vancomycin's reactive primary amine site
b. Formulate for equivalent drug release and degradation periods upon variation of co-monomer ratios to show degradative drug release
c. Maintain antibiotic activity against *S. aureus* after covalent addition

Outcome and Significance:

Covalent incorporation of vancomycin was determined via increased mass of hydrogel degradation products via mass spectroscopy of high performance liquid chromatography peaks that showed antibiotic activity against *S. aureus*

(LC-MS). Further, the drug release and degradation rates were coordinated so as to achieve complete drug release upon completion of degradation as additional evidence of covalent addition. While vancomycin activity was reduced, it was still shown to remain active as a hydrogel degradation product on *S. aureus* at a reduced MIC of 155 µg/mL, from 2 µg/mL un-modified. The technique used in covalent drug addition of vancomycin to the PBAE backbone demonstrated the versatility of PBAE synthesis chemistry. This was used as a method to equalize the period of drug release and hydrogel degradation. The development of locally deliverable antibiotic biomaterials with the lack of a drug release stagnation period is important in the minimization of bacterial biofilm formation without the requirement of second surgeries.

Chapter 6. Formulate a redox sensitive PBAE hydrogel for local treatment of oxidative stress

a. Covalently bond cystamine into a PBAE hydrogel to add disulfide/thiol redox functionality
b. Characterize the significance of cystamine content on variation of biomaterial properties in degradation and drug release
c. Determine differential cytotoxicity of hydrogel degradation products in the thiol and disulfide state on a human cell line
d. Demonstrate reduction of oxidative stress on a human cell line in-depth via cell viability and mitochondrial respiration

Outcome and Significance:

Covalent addition of the disulfide cross-linker, cystamine, into the backbone of a PBAE hydrogel produced bound thiols. Through variation of the cystamine content, under reducing conditions, hydrogels remained intact with <75 mol% cystamine of the amines, and become soluble at ≥75 mol% cystamine of the amines due to increase in reducible disulfide crosslinking. Via degradative drug release, bound thiols were found to be highly biocompatible compared to the disulfide (i.e. oxidized) degradation products for both cell viability and mitochondrial function (IC_{50} (the half maximal inhibitory concentration) = 8.5 mg/mL thiol compared to 0.32 mg/mL disulfide). Cellular fortification of the glutathione/cysteine (i.e. thiol) antioxidant cellular capacity is a potential method of both treatment of oxidative stress in disease, as well as the basis of prophylaxis for such applications as radioprotection of healthy tissues in cancer therapies. This material is promising for antioxidant delivery in that it produced cytocompatible material at a high concentration, allowing for high thiol content as well (IC_{50} 8.7 (mM thiol)) (both numbers for 50 mol% cystamine of the total amines formulation).

Chapter 7. Synthesize thiolated nanoparticles for antioxidant delivery utilizing cystamine-PBAE hydrogel starting material

a. Increase cystamine PBAE hydrogels to use 100% of the amine for increased drug content via use of a Michael addition catalyst
b. Create thiolated linear chain polymers upon hydrogel reduction

c. Synthesize a nanoparticle formulation via single-emulsion of reduced hydrogel material
d. Determine nanoparticle stability and degradation in solution
e. Determine activity of reduced nanoparticle thiols over time

Outcome and Significance:

The use of a non-nucleophilic base catalyst allowed for formation of a purely cystamine and diacrylate hydrogel, previously not achievable without catalysis. Two diacrylates were tested, 1,6-hexanediol ethoxylate diacrylate (HEDA) and diethylene glycol diacrylate (DEGDA), where only DEGDA/CA hydrogels and nanoparticles showed material degradation, hypothesized due to an increased number of aliphatic hydrocarbons in HEDA compared to DEGDA. It was found that these hydrogels when reduced formed thiolated oligomers, which when subjected to single emulsion, turned into controllable sized thiolated nanoparticles (150-400 nm) with activity up to 1 week. These hydrogels were converted into thiolated nanoparticles (up to 3.5 mmol thiol/mg particles), which could be used for not only applications of oxidative stress treatment, but as a cost effective means towards particle functionalization with the thiol moiety without the requirement of expensive conjugates.

Chapter 2: Hydrogels and Polymeric Nanoparticles in Drug Delivery

Based partially upon the book chapter:

> Andrew L. Vasilakes, Thomas D. Dziubla, Paritosh P. Wattamwar. *Polymeric Nanoparticles*, In Rebecca A. Bader, Engineering Polymer Systems for Improved Drug Delivery. Hoboken, NJ: Wiley & Sons, Inc. 2014

2.1 Introduction

Medical devices, whether it be from one of the original ocular prosthetic in-socket implants made from glass as early as 2900 BCE [37], or wooden feet as early as 484 BCE [38], have helped improve quality of life throughout history. While wood and glass were merely mechanical replacements in a loosely anatomical form, they were designed with little intent of biocompatibility, integration or tissue regeneration. Over time, these medical materials and devices have advanced immensely through application-driven interaction of materials with specific biological systems to produce "biomaterials" which elicit favorable tissue response [39-41]. Glass eyes have developed from uncoated spheres which caused inflammation and implant migration, to adding acrylate coatings for sclera adherence, to formation of porous, integrated implants from materials such as hydroxyapatite or polyethylene for muscle and vascular attachment to aid in motility in the late 1980s [42]. As Richard Feynman alluded to in his *There's Plenty of Room at the Bottom* talk in 1959, advances in engineering and biology have followed Feynman's prediction with the nanotechnology revolution spurred on by Norio Tanaguchi, K. Eric Drexler, and President Clinton in 1979, 1986, and 2000 respectively [43]. The field of drug delivery has been opened wide with nanoparticle research, which has been able to create enhanced drug delivery methods, which were previously not possible. For instance, the diffusional barrier of ophthalmic drug entrapped within nano-scale micelles in soft hydrogel contact lenses

has been shown to enable release for up to 30 days, whereas traditional free drug loaded systems show quicker release over only 3 days [44]. Likewise, systemic drug delivery has shown great achievements through nanoparticles and synthetic polymer chemistries. Where traditional cancer chemotherapeutics rely on continual small molecule transfusions, invoking significant side effects, much research has been focused on the area of nanoformulations to increase tumor specific uptake compared to vital organs [45]. With the vast customizability of synthetic polymers, hydrogels and nanoparticles have benefitted greatly.

2.2 Hydrogels

Hydrogels are three-dimensional crosslinked networks of polymer which were originally termed due to their hydrophilic nature, allowing for swelling in water, such as is the case with polyethylene glycol (PEG) based hydrogels [46]. The high water-content from swelling and cross-linked structures are useful properties of biomaterials as they mimic the properties of soft tissue [47]. These swelling properties also allow for drug delivery applications such as the physical capture of molecules, and chemical modification for a variety of applications, and have been highly researched [48]. Conventional, naturally-derived biomedical hydrogels have been used for many years. For instance, collagen sponges have been popular since the 1980s for use in local antibiotic delivery due to being swellable and thus drug loadable, biocompatible, and biodegradable if pre-digested [49]. While hydrogels may also be formed from crosslinking other natural polymers like chitosan, fibrin, or alginate, synthetic polymer hydrogels show the benefits of bottom-up designed, highly controlled chemistry with wide customizability. One important attribute in which synthetic hydrogels excel at, and conventional collagen sponges lack, is the ability

for *in situ* polymerization. *In situ* polymerization allows for liquid monomer solutions to rapidly polymerize into the surrounding tissue geometry upon injection. The result of this tissue conformation is higher surface area contact and less material mobility, reducing levels of inflammation and implant rejection [50]. Nonetheless, *in situ* polymerization conditions must be stringent so as not to incur additional inflammation and toxicity [51]. Although collagen sponge applications are still widespread on the market compared to hydrogels, FDA-approved, *in situ*-formable PEG-based hydrogel alternatives are becoming increasingly available as research advances.

2.2.1 Polymer Selection

Natural polymers such as collagen or hyaluronate, primary components of animal extracellular matrices, have been used extensively for biomedical applications [39, 52] such as collagen wound sponges for tissue regeneration, often after crosslinking with an agent such as glutaraldehyde to form a collagen hydrogel [53]. While many natural polymers, such as collagen, are biocompatible, biodegradable, allow neutrophil infiltration, and are chemically modifiable such as with collagen with fibronectin or antibiotic loading [52], natural polymers often require animal sources and lack the control of chemical reproducibility in which synthetic polymers excel at [39]. Depending on the animal source of the collagen, the region of the animal it was taken from (e.g. type I, III, IV collagen), or if post-crosslinking has been performed all affect drug release and degradation properties. Other natural polymers used in hydrogels include agarose, fibrin, the naturally biodegradable chitosan, or gelatin (hydrolyzed collagen) sponges and fibrin for use as hemostatic dressings [54].

Synthetic polymers have been utilized for biomedical purposes for much of the 20th century, from the non-degradable polymethylmethacrylate (PMMA) used in dentistry applications in the 1930s to polyesters like polyurethane used in catheters, stents, or breast implants later on [55]. One of the first biomedical applications of a biodegradable synthetic polymer was that of sutures using poly(lactic acid) and poly(glycolic acid) copolymers [56, 57]. Since then, polyesters have been researched heavily for a wide variety of applications. However, inflammatory response (described in further detail in Chapter 3) upon implantation of polyesters could lead to implant failure due to reactive oxygen species (ROS) mediated biodegradation. This ROS buildup posed a problem for some applications, such as pacemaker lead insulators, leading to corrosion, but also to the addition of embedded antioxidants such as the polyphenol Santowhite®. Implanted polyester ROS generation was classically utilized in other applications as a beneficial side effect, such as a prophylaxis against capsular contracture of breast implants via the inflammatory response induced fibrous capsule [39, 56, 58]. Beyond polyesters, many other polymers have become popular, such as those depicted in Table 2.2 of Section 2.3.1.1.

2.2.1.1 Poly(β-amino esters)

With intent to deliver DNA or siRNA for gene therapy applications, poly-cationic polymers at physiological pH were sought out due to complexation with the negative charge found on phosphate backbones. While transfection efficiency from highly positively charged polymers, such as hydrogels made from polyethylenimine (PEI) or poly-lysine, were found to be high, the positive charge also showed significant toxicity due to destabilization of cellular membranes [1]. With those materials, there was a tradeoff in effectiveness for toxicity, and thus groups started looking at developing less toxic poly-cationic polymers.

This reduction of toxicity was hypothesized to proceed via formation of polyesters with cationic sidechains to a lesser extent than that of PEI, but still at a great enough concentration to show DNA affinity. However, many of these required expensive coupling reagents or required amine-site protection and post-processing [59-61]. With this in mind, the Langer lab [1] synthesized biodegradable polyesters with tertiary amines through aza-Michael addition of secondary di-amines and diacrylates to form poly(β-amino esters) (PBAEs) without expensive reagents.

PBAEs have been found to show excellent DNA binding and condensation properties, as well as show a much greater cytocompatibility of both linear polymers as well as degradation products, greater than 1-2 orders of magnitude in concentration compared to 25000 Da PEI [1, 62]. While a majority of PBAE applications involve DNA delivery, numerous other applications are continually being produced as well due to their good toxicity profile (similar to PLGA [63]), biodegradability, and customizability into copolymers. These properties allow for formation of pH sensitive materials [64], drug delivery vehicles for hydrophobic [65] and hydrophilic drugs [62], theranostics [66], tissue engineering [67], magnetic hyperthermia [68], and so on. PBAEs synthesized in our lab as hydrogels have been shown to be customizable in degradation period from hours, to weeks, to greater than months [62, 69, 70], show variable cytotoxicity of degradation products depending on co-monomers [63], and display therapeutic degradation products as well [7, 8, 63].

2.2.2 Hydrogel Controlled Release

Contrasting to free drug administration, the drug entrapment offered by hydrogels makes them an advantageous method of extending drug release, minimizing the total number of administrations required. This extended release is highly researched for applications such as invasive surgeries requiring steady concentrations of antibiotic prophylaxis for a long period of time, or as other biodegradable injectable adhesives where multiple surgeries pose risk of further infection. Depending on the polymer choice, some hydrogels are non-degradable and others may biodegrade. Additionally, drugs may be entrapped via physical, affinity, ionic, or covalent methods.

For free drug entrapment via physical means, typically the simple method of imbibition, or drug mixed within the polymer upon polymerization is used (Figure 2.1A). These freely-loaded systems release drug in a diffusive manner, following the concentration gradient surrounding the material, and typically exhibit a burst-release effect where an initially high level of drugs are released (Figure 2.2 A, where M_t/M_∞ defines the mass at a timepoint *t* divided by the total infinite release value to infer the release rate). Typically, release near zero-order (i.e. n=1 in the Power Law, equation 2.31 of section 2.3.7) is more desirable, yet not easily achievable. One method to slow release is to match the material degradation rate with the drug release rate (Figure 2.1B) through utilizing non-interfering drug moieties for conjugation to or crosslinking of the polymer backbone. Non-interfering moieties, for example, being those which are not bioactive and would not negate drug action if modified. Or, the drug molecule could be designed to biodegrade back into the original structure form a method such as drug acrylation to allow ester cleavage back to the original [7]. With covalent addition of this method (Figure 2.2 B, C), therapeutic polymer or drug is released

as degradation products, and will follow the total material degradation rate closely [62, 63]. If the conjugate or crosslinker is a small mass fraction, differences in bond lability, or hydrophilic/hydrophobic effects may incur drug release that doesn't exactly follow the total material degradation pattern (Figure 2.2 B), but with large mass fractions (Figure 2.2 C), the crosslinker has greater effect on the bulk material, and follows the degradation profile closely [63]. For large molecules, like proteins (Figure 2.2 D), degradative release may be produced through simple physical entrapment due to hindrance of diffusion by the network.

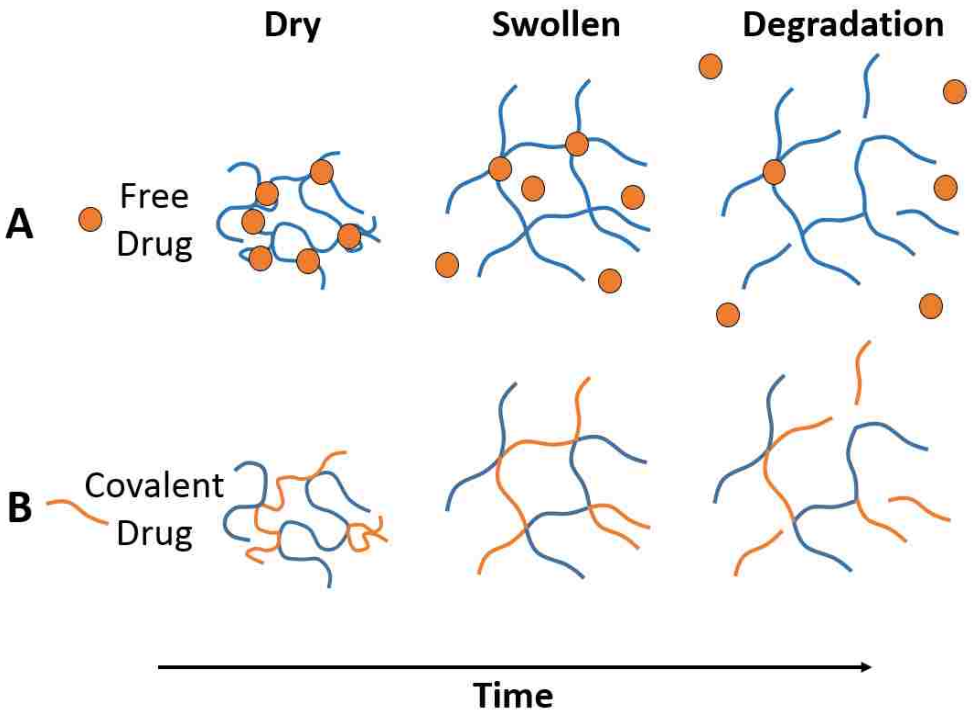

Figure 2.1. Example of degradable hydrogels with A) free or B) covalent drug loading.

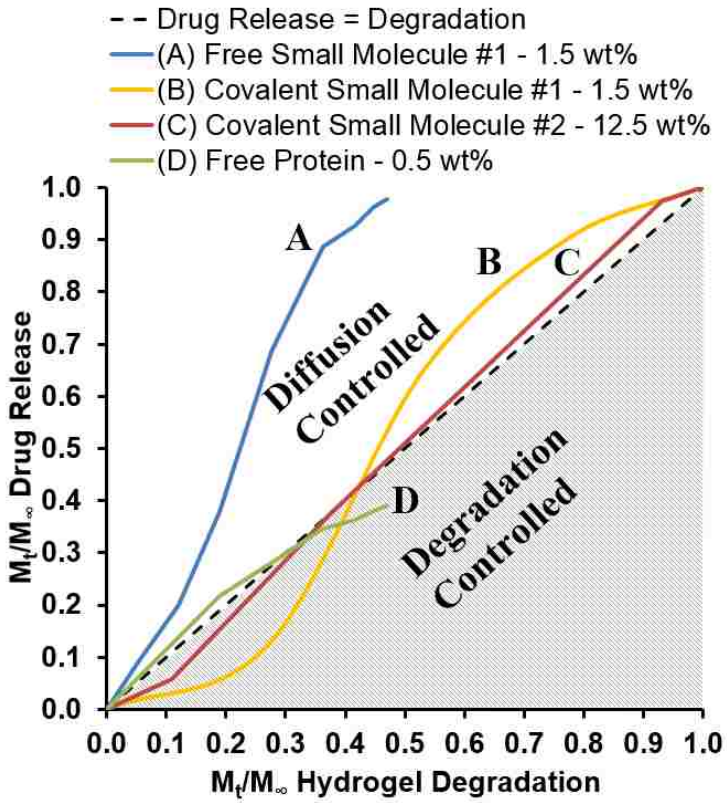

Figure 2.2. Schematic of example drug release profiles from our different PBAE biodegradable hydrogels. A) Freely loaded small molecule showing a diffusive release pattern (1449 Da at 1.5 wt% loading). B) Covalently loaded small molecule showing a release profile near the degradation rate, but with the same total period of release as degradation (1449 Da at 1.5 wt% loading). C) Covalently loaded small molecule showing release very close to equaling the degradation rate (152 Da at 12.5 wt% loading). D) Freely loaded protein showing slightly less than degradative release due to size restriction (230 kDa at 0.5 wt% loading). Data for A and B from [62], C from [63], and D calculated from [70].

2.2.3 Hydrogel Synthesis

Synthetic polymer hydrogels are typically formulated through the crosslinking of monomers into their respective three-dimensional product via covalent, affinity, or ionic methods. Common chemical crosslinking methods include click-chemistry reactions, such as acrylate-amine, thiol-ene/yne, azide-alkyne, and epoxide-amine/thiol, which do not necessarily require the addition of a catalyst for reaction to occur if near stoichiometric conditions [7, 63]. However, catalysts may be beneficial if reaction does not readily occur, such as with excess solvent or reactants which are not particularly reactive [69].

Chemically crosslinked hydrogel reactions are useful for one-pot synthesis of materials, such as *ex vivo* preparation, as they may require addition of heat to occur (e.g. acrylate-amine Michael addition), or utilize cytotoxic monomers/catalysts which would require washing before implantation of the material (e.g. metal catalyst). Other chemical crosslinking methods may be more suitable for *in situ* synthesis, such as free-radical polymerization or the use of photo-initiators [71]. Our group has used free radical polymerization of acrylate-acrylate bonds using ammonium persulfate (APS) with tetramethylethylenediamine (TMED), in which body temperature exposure aids reaction kinetics [62, 70, 72]. There are also affinity formed hydrogels, such as those utilizing biotin-avidin [73], or ionic crosslinked hydrogels utilizing pH sensitive ions for reversible binding [74].

While off-the-shelf monomers may be used directly, a benefit of synthetic polymer chemistry is the ability to tailor polymers for particular uses. And thus, often times custom monomers are formed prior to hydrogelation. For instance, while a monomer of PEG-diacrylate would participate in hydrogel formation with a corresponding crosslinker (e.g.

primary amine, secondary di-amine etc.), formation of a co-polymer macromer/oligomer may be performed for added effect, whether it be simply increasing the polymer mesh size for increased diffusion, or adding functionality such as a drug [8, 62, 75].

Polymer initiation may be started through high chemical potential found in highly reactive substances which produce spontaneous exergonic reactions, such as azide-alkyne Huisgen cycloaddition, or require the initiation of electron movement through chemical redox initiators such as when photo-initiators decompose under electromagnetic radiation to produce free radicals. Once initiated, these reactions propagate until termination may occur for a variety of reasons, such as reaction with a non-propagating species (e.g. oxygen free radical formation interference), or having a lack of substrate concentration to proceed with the reaction.

2.2.3.1 Extent of Reaction

Extent of reaction may be determined by calculation of the degree of polymerization, which is described as equation 2.1 for homopolymers, where *DP* is the degree of polymerization, M_0 is the monomer molecular weight, and M_N is the number average molecular weight. For homopolymers with equal molar quantity of reactants, Carother's equation 2.2 is used to find the number-average degree of polymerization, $\bar{X}_n$, in equation 2.3, where p is the conversion factor, N_0 is the number of monomer molecules initially, and N is the number of final molecules [76].

$$\boldsymbol{DP = \frac{M_N}{M_0}} \tag{2.1}$$

$$\boldsymbol{\bar{X}_n = \frac{1}{1-p}} \tag{2.2}$$

$$p = \frac{N_0 - N}{N_0} \quad \textbf{(2.3)}$$

It can be seen that if a degree of polymerization was 90% (p=0.9), then the number average degree of polymerization for a homopolymer would be 10. When having one monomer is in excess, equation 2.4 is used, where r is the stoichiometric ratio of reactants. For instance, if the stoichiometric ratio is 1, equation 2.2 is re-formed. If a copolymer system is formed, however, equation 2.5 is used, where f_i is the individual functionality per monomer used, and f_{ave} is the average functionality from equation 2.6.

$$\bar{X}_n = \frac{1+r}{1+r-2rp} \quad \textbf{(2.4)}$$

$$\bar{X}_n = \frac{2}{2-pf_{ave}} \quad \textbf{(2.5)}$$

$$f_{ave} = \frac{\sum N_i \cdot f_i}{\sum N_i} \quad \textbf{(2.6)}$$

2.2.4 Hydrogel Characteristic Modeling

Determination and prediction of hydrogel characteristics allows for deeper understanding of material properties. Certain properties are useful to know about synthesized materials, particularly if there is interest in using it as a drug delivery vehicle or biomaterial. Mesh size calculation gives a sense of molecular diffusion, as does the extent of reaction of monomer chains to form oligomers/macromers, relating to the crosslinking chain length, and to identify polymer-solvent interactions which relate to swelling characteristics, important in knowing the amount of imbibed liquid. In 1953, Flory and Huggins developed an equation (known as Flory-Huggins theory) to show crosslinked polymer swelling in water, dependent upon the changes in chemical potential (solved for in equation 2.20

below) [77]. Swelling forces of networks are constrained based upon the elastic properties of the polymer chains, as well as solvent compatibility [46, 78].

2.2.4.1 Change in Chemical Potential Upon Swelling

To produce equation 2.20, which describes the change in chemical potential upon swelling forces, we take example of an isotropic crosslinked hydrogel, and first look at the free energy of the system, ΔG, due to addition of the mixing energy, ΔG_{mix} and elastic energy, $\Delta G_{elastic}$. After differentiation of equation 2.7 with respect to the number of water molecules, N_1, via equation 2.8, the change in chemical potential may be found (equation 2.9), where the pure water chemical potential, $\Delta\mu^{\circ}$, the water within the gel chemical potential, $\Delta\mu_{gel}$, and chemical potential due to elastic effects, $\Delta\mu_{elastic}$ the chemical potential of a hydrogel in solution mixture, $\Delta\mu_{mix}$.

$$\Delta \boldsymbol{G} = \Delta \boldsymbol{G_{mix}} + \Delta \boldsymbol{G_{elastic}} \tag{2.7}$$

$$\boldsymbol{\mu_i} = \left(\frac{\partial \boldsymbol{G}}{\partial \boldsymbol{N_i}}\right)_{\boldsymbol{T,P,N_{j\neq i}}} \tag{2.8}$$

$$\Delta \boldsymbol{\mu} = \boldsymbol{\mu_{gel}} - \boldsymbol{\mu}^{\circ} = \Delta \boldsymbol{\mu_{mix}} + \Delta \boldsymbol{\mu_{elastic}} \tag{2.9}$$

To determine the effect of chemical potential on mixing, the effects of enthalpy upon mixing in equation 2.10 is based upon the lattice model due to equal polymer chain lengths, and simplifies to equation 2.11 as is described in [78]. χ is the Flory-Huggins polymer-solvent interaction parameter (0.426 for PEG-water [79], and decreases with increasing miscibility), and N_1 and v_2 are the number of water molecules and volume fraction of the hydrogel respectively. An example of swelling ratio and χ calculation may be found in Chapter 6 using Hildebrand solubility parameters. Entropy of mixing is found in equation

2.12, ΔS_{mix}, where R is the universal gas constant, N_1 and N_2 are number of molecules of water and polymer respectively, and v_1 and v_2 are the volume fractions of water and polymer respectively, calculated by the equilibrium-state swollen gel.

$$\Delta \boldsymbol{G_{mix}} = \Delta \boldsymbol{H_{mix}} - \boldsymbol{T}\Delta \boldsymbol{S_{mix}} \quad \textbf{(2.10)}$$

$$\Delta \boldsymbol{H_{mix}} = \boldsymbol{kT\chi N_1 v_2} \quad \textbf{(2.11)}$$

$$\Delta \boldsymbol{S_{mix}} = -\boldsymbol{k}(\boldsymbol{N_1} \ln \boldsymbol{v_1} + \boldsymbol{N_2} \ln \boldsymbol{v_2}) \quad \textbf{(2.12)}$$

Adding equations 2.11 and 2.12 into equation 2.10 results in equation 2.13. Since hydrogels are single large molecules the term N_2 disappears, and differentiation of equation 2.13 with respect to the number of water molecules, equation 2.16 is formed, where the volume fraction of water is replaced by equation 2.14 and the universal gas constant, R, with equation 2.15.

$$\Delta \boldsymbol{G_{mix}} = \boldsymbol{kT\chi N_1 v_2} - \boldsymbol{kT}(\boldsymbol{N_1} \ln \boldsymbol{v_1} + \boldsymbol{N_2} \ln \boldsymbol{v_2}) \quad \textbf{(2.13)}$$

$$\boldsymbol{v_1} = \boldsymbol{1} - \boldsymbol{v_2} \quad \textbf{(2.14)}$$

$$\boldsymbol{R} = \boldsymbol{kN_A} \quad \textbf{(2.15)}$$

$$\frac{\partial \Delta \boldsymbol{G_{mix}}}{\partial \boldsymbol{N_1}} = \boldsymbol{RT}(\ln(\boldsymbol{1} - \boldsymbol{v_2}) + \boldsymbol{v_2} + \boldsymbol{\chi v_2}^{\boldsymbol{2}}) = \Delta \boldsymbol{\mu_{mix}} \quad \textbf{(2.16)}$$

Elastic effects from retraction of swelling-expansion are found through using the elastic theory found in Flory [77, 78]. Effects of enthalpy may be ignored due to hydrogels behaving as ideal elastomers where bonds are not stretched. Assuming for isotropic expansion, equation 2.17 is formed using Boltzmann's equation for change in entropy, after differentiation with respect to the number of water molecules, where ρ_{cross} is the

crosslinking density, and V_1 is the molar volume of water in the hydrogel (18 mL/mol). The crosslinking density is defined as equation 2.18, where M_C is the number average molecular weight of crosslinks and $\bar{v}_2$ is the specific volume of the swollen amorphous hydrogel ($1/\rho_s$).

$$\frac{\partial \Delta G_{elastic}}{\partial N_1} = \boldsymbol{\rho_{cross} V_1 RT \left({v_2}^{1/3} - \frac{v_2}{2} \right)} \quad \textbf{(2.17)}$$

$$\boldsymbol{\rho_{cross} = \frac{1}{\bar{v}_2 M_C}} \quad \textbf{(2.18)}$$

Using approximations for chain imperfections and entanglements, equation 2.17 is corrected into equation 2.19 with the addition of a central term, $\left(1 - \frac{2M_C}{M_N}\right)$, where M_N is the number average molecular weight of the polymer utilized for hydrogel formation [78, 80].

$$\frac{\partial \Delta G_{elastic}}{\partial N_1} = \boldsymbol{RT \left(\frac{V_1}{\bar{v}_2 M_C} \right) \left(1 - \frac{2M_C}{M_N} \right) \left({v_2}^{1/3} - \frac{v_2}{2} \right) = \Delta \mu_{elastic}} \quad \textbf{(2.19)}$$

Plugging equations 2.16 and 2.19 into equation 2.9 yields equation 2.20:

$$\boldsymbol{\Delta \mu = RT \left[(\ln(1 - v_2) + v_2 + \chi {v_2}^2) + \left(\frac{V_1}{\bar{v}_2 M_C} \right) \left(1 - \frac{2M_C}{M_N} \right) \left({v_2}^{1/3} - \frac{v_2}{2} \right) \right]} \quad \textbf{(2.20)}$$

2.2.4.2 Crosslinking Molecular Weight and Mesh Size

These methods are also used to predict the crosslinking molecular weight of a hydrogel in water at equilibrium swelling, where $\Delta \mu = 0$, and thus following Flory-Rehner theory, equation 2.20 can be rearranged to produce equation 2.21 [81-83].

$$\boldsymbol{\frac{1}{M_C} = \frac{2}{M_N} - \frac{\bar{v}_2}{V_1} \frac{\left[\ln(1 - v_2) + v_2 + \chi {v_2}^2 \right]}{{v_2}^{1/3} - \frac{v_2}{2}}} \quad \textbf{(2.21)}$$

Similarly, the mesh size of hydrogels may be calculated with equation 2.25 for isotropic swelling, stemming from equation 2.22, where ξ is the distance between two stretched crosslinks, $\left(\bar{r}_o{}^2\right)^{1/2}$ is the root mean square distance between two crosslinks, M_r is the molecular weight of the repeating unit, l is the repeat polymer bond length, and C_n is Flory characteristic ratio (4.0 for PEG [84, 85]) defined as equation 2.23, where n is the number of links per chain from equation 2.24 [81, 86].

$$\boldsymbol{\xi = v_2{}^{-1/3}\left(\bar{r}_o{}^2\right)^{1/2}} \quad \textbf{(2.22)}$$

$$\boldsymbol{C_n = \frac{\bar{r}_o{}^2}{nl^2}} \quad \textbf{(2.23)}$$

$$\boldsymbol{n = \frac{2M_C}{M_r}} \quad \textbf{(2.24)}$$

$$\boldsymbol{\xi = lv_2{}^{-1/3}\left(\frac{2C_nM_C}{M_r}\right)^{1/2}} \quad \textbf{(2.25)}$$

2.2.5 Example Hydrogels in Practice

The original hydrogel application came from Wichterle and Lim [87] who made poly(2-hydroxyethyl methacrylate) (PHEMA) for use as soft contact lenses in the 1950s. Pure PHEMA lenses, however, showed little oxygen diffusion, and thus copolymerization with other hydrophilic acrylates, such as PHEMA-co-methacrylic acid (PHEMA-MAA) or PHEMA-co-tetraethylene glycol dimethacrylate (PHEMA-TEGDMA) has been utilized as spacers to increase the mesh size and allow permeability of oxygen for extended use, as well as modify wettability [88-90]. Hydrogels have since become increasingly popular in application, from wound-healing to organ reconstruction, and have been FDA approved for numerous applications.

For instance, medical adhesives are in use and development to replace sutures due to the lower risk of infection and blood-borne disease from needle use, and the enhanced convenience [16]. Further, chemical hemostatic agents have been shown to be more effective in trauma scenarios where rapid blood loss must be stopped quickly, such as the use of fibrin glue, where thrombin and fibrinogen crosslink into an adhesive network [91]. Popular bioadhesives include those based on cyanoacrylates (e.g. Superglue). These oxidize rapidly from chain nucleophilic addition, such as hydroxyl radical contact air humidity, but are linear chain polymers and are not hydrogels. There are several PEG-based systems, however, such as Coseal®, which is based on formation of branched thio-ester bonds upon reaction of four-armed PEG-glutaryl-succinimidyl ester with four-armed PEG-thiol [91]. Another PEG-based system using PEG-ester and trilysine amine, Duraseal®, is indicated for use to prevent cerebrospinal fluid leakage for dural closure. However, due to the hydrophilicity of PEG-based hydrogels, they exhibit a high swelling ratio, and so care must be used so as not to damage sensitive regions if used [91]. Another, more recent hydrogel application that was FDA approved in 2015 is that of the PEG-based injectable radiospacer, SpaceOAR®, to create a buffer region between the prostate and rectum for prostate cancer radiotherapy with a 3-6 month biodegradation period [15].

2.3 Polymeric Nanoparticles

The central goal of drug delivery is the optimization of the pharmacokinetics/ pharmacodynamics (PK/PD) for a specific medicinal application. To this end, nanoparticles have become a promising drug delivery technology as they are capable of greatly altering the PK/PD of a drug, potentially giving new life to active agents once thought to be unusable. As the PK/PD is determined by the nanoparticle, it is of utmost

importance to define what these properties are, requiring highly specific tuning of the carrier system. One of the classes of nanoparticles which provides the greatest flexibility in tuning, and hence the largest class of nanoparticle studied, is polymeric nanoparticles (PNPs) [92-96].

Importantly, when considering PNPs, it is important to understand what one means as a nanoparticle. According to the National Institute of Health National Cancer Institute National Nanotech Initiative (NIH-NCI NNI), a nanoparticle is any carrier structure who has an aspect ratio less than 100 nm, but greater than 1 nm. This narrow definition has turned out to be quite important for the field of tumor targeting and therapy, however is somewhat limiting considering the range of diseases that must be addressed. For this reason, many researchers have adopted a nanoparticle as being a system whose length scale is less than 1 micron, but most commonly will include particles in the range of 100-400 nm in size due to ease of centrifugation washing and handling, as well as size dependent cellular uptake.

Polymeric nanoparticles can come in various shapes, compositions, and conformations which can be used for a variety of approaches including solubility enhancement, immunogenic masking, controlled release and retention time [96]. Furthermore, PNPs may exhibit unique properties which can allow the particles to flow through vasculature while protecting the active drug until reaching the specific target [97], which can reduce the amount of systemic release and increase local release, allowing the total amount of PNPs and drug administered to be smaller [98, 99].

These advantageous properties can allow simple drug carriers to provide an enhanced delivery effect in comparison to just administration of free-drug. Assuming no change in

bioavailability, but a simple decrease in drug release rate, the advantage of drug delivery via nanoparticles is depicted below in Figure 2.3A as a comparison between a hypothetical situation involving intravenous (IV) injection of free drug vs. drug in a slow releasing PNP carrier.

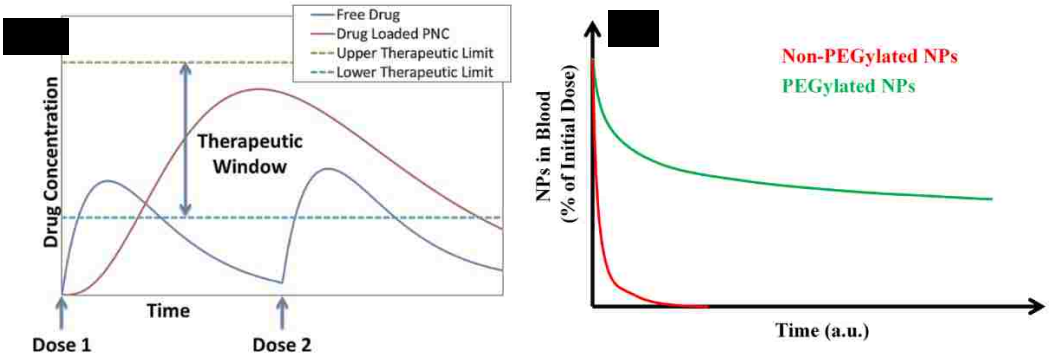

Figure 2.3. Comparison of pharmacokinetics. A.) Schematic of serum drug concentration after IV administration of either free drug or drug encapsulated in PNPs. B.) Schematic representing the effect of PEGylation on particle circulation.

Using IV injection of free drug, total plasma exposure of drug for a given dose is limited because of elimination of the drug. This area under the curve can be maximized by encapsulating the drug in a stealth (longer-circulating) nanoparticle that allows for controlled release. For applications requiring repeated IV injection, utilizing nanoparticles can greatly reduce both the number and frequency of injections necessary to maintain a therapeutic level of drug in the serum. These generalized results are typical in encapsulated drug delivery and give a sampling of the great potential PNPs provide.

2.3.1 PNP Design

In order to understand the advantages offered by polymer-based nanoparticles, it is necessary to understand various design criteria that determine the success of any nanoparticle-based therapy. Some of the important design features of nanoparticles are size, surface functionalization, mechanical properties, loading efficiency, encapsulated drug:carrier ratio, degradation mechanism and biocompatibility of polymer. While the exact structure-function relationships are still being identified, Table 2.1 summarizes the design features that are known to have an impact upon drug delivery parameters.

Table 2.1. PNP properties that affect pharmacological outcomes.

	Pharmacological outcomes				
	Localization			Duration of Therapy	Total Delivered Amount
Design features	Circulation	Tissue/ Cellular	Sub-Cellular		
Surface Chemistry	X	X	X	-	-
Responsiveness	X	X	X	X	X
Size	X	X	X	-	X
Shape	X	X	X	X	X
Mechanical Properties	X	-	X	-	-
Loading Capacity	-	-	-	X	X
Degradation	X	X	X	X	X

2.3.1.1 PNP Material Selection (Biocompatibility and Biodegradability)

PNPs can be formed from a vast array of polymers with a variety of properties including biodegradability, pH sensitivity, temperature responsiveness, reactivity, etc., and choosing the correct polymer and configuration for the PNP application desired may be a challenge. Table 2.2 provides a summary of commonly used polymers in PNP design. Note that this table only summarizes homopolymers and common random copolymers. Any of these polymers can be combined into block co-polymers for PNPs with properties not possible with the homopolymer.

Table 2.2. Classic polymers used in PNP synthesis. Glass transition temperatures (Tg) vary depending on molecular weight. Note that FDA approved indicates whether the polymer has been approved for any biomedical application, not just nanomedicine.

Common PNP Polymers	**Material Class**	**Biodegradation Time**	**Responsiveness**	**Tg**	**FDA Approved**	**Particle Examples**	**References**
Poly(N-isopropylacrylamide) (PNIPAAM)	Polyacrylamide	N/A	Thermal Swelling	135 ºC	Yes	Nanosphere, Nanogel	[100, 101]
Polymethylmethacrylate (PMMA)	Polyacrylate	N/A	Organic Swelling	95 ºC	Yes	Nanosphere	[102-104]
Poly(2-hydroxyethyl methacrylate) (pHEMA)	Polyacrylate	N/A	Hydrolytic Swelling	100 ºC	Yes	Nanosphere	[105, 106]
Polyalkylcyanoacrylate (PACA)	Polyacrylate	Hours to Months	Hydrolysis Ion Pairing	195 ºC	No	Nanosphere	[107-111]
Polyamidoamine (PAMAM)	Polyamide	N/A	pH Conformational Change	-10 ºC to 25 ºC	No	Dendrimer	[112-117]
Polyvinylpyrrolidone (PVP)	Polyamide	N/A	-	180 ºC	Yes	Nanosphere	[118, 119]
Poly(sebacic acid) (PSA), poly(carboxyphenoxypropane) (PCP), etc.	Polyanhydride	Hours to Weeks	Hydrolysis (Surface Erosion)	-	Yes	Nanosphere	[120, 121]

Table 2.2. Continued

Block copolymers	Poly(β-amino ester)	Hours to Years	Hydrolysis, pH Swelling	-	No	Nanosphere, Micelle, Nanogel	[7, 122-125]
Polylactic acid (PLA)	Polyester	Months to Years	Hydrolysis	40 ºC to 60 ºC	Yes	Nanosphere	[126-131]
Poly(lactic-co-glycolic acid) (PLGA)	Polyester	Weeks to Months	Hydrolysis	40 ºC to 50 ºC	Yes	Nanosphere, Micelle, Polymersome, Nanocapsule	[132-136]
Polycaprolactone (PCL)	Polyester	Months to Years	Hydrolysis	-60 ºC	Yes	Nanosphere	[129, 137, 138]
Polyethyleneglycol (PEG)	Polyether	N/A	-	-70 ºC (400 Da)	Yes	-	[139-142]
Polyethylenimine (PEI), PEG-PEI, PLGA-PEI	Polyethylenimine	N/A	-	-25 ºC		Nanosphere, Nanogel	[143, 144]
Polystyrene (PS)	Polystyrene	N/A	-	105 ºC	Yes	Nanosphere	[145, 146]

Owning to their size, nanoparticles are under intense scrutiny regarding their ability to be eliminated from the body. While recent studies have suggested that inert nanoparticles (e.g., gold) are able to be eliminated through the biliary excretion mechanism, it isn't certain how ubiquitous this effect is. As such, biodegradability of PNPs, which circumvents the bioaccumulation concerns, is one of the important properties that sets them apart from other systems. Typically, biodegradable polymers will degrade via either hydrolysis or enzymatic degradation. For instance, PLGA degrades into both lactic and glycolic acids [147], mainly via hydrolysis of ester bonds [147], and chitosan particles degrade in biological systems predominantly through presence of lysozyme and bacterial enzymes in the colon [148] into amino sugars [149]. Given the simple degradation products of PLGA, it is a popular component polymer for a variety of nanospheres, micelles, polymersomes, and nanocapsules systems [133-137] and has already been approved for human use [150, 151].

As overviewed in Chapter 3, poly(β-amino esters) (PBAE) are a new and exciting class of biodegradable polymer. Based upon the Michael addition reaction of amines and acrylates, a wide variety of available monomers exist [47] which can be applied to form polymers in this class, such as to form antioxidant nanogels [8]. The resulting polyester has a pH sensitive hydrolysis [122, 124, 125], allowing for a variety of particle delivery systems, including gene delivery [5]. The flexibility and versatility of PBAEs are very promising, yet given their more recent development, no current PBAE formulations have received FDA approval.

Besides degradation, mechanical properties of certain polymers provide unique advantages over other systems. For instance, the FDA-approved biodegradable polyester,

polycapralactone (PCL), is interesting due to its relatively low glass transition temperature, -60ºC, giving PCL high molecular deformity at body temperature; ease of synthesis; and extended degradation times due to its hydrophobicity [129, 137, 138]. Other groups of polymers used in PNPs can allow interesting effects, such as the thermally induced swelling and shrinking of non-biodegradable poly(*N*-isopropylacrylamide) (PNIPAAM) [100, 101, 152].

While choice of polymer provides control over degradation rate and biocompatibility, polymers do not necessarily contain therapeutic value. Carrier polymers are typically desired to be inert, but recent data suggests that degradation products of biodegradable polymers can induce immunogenic response from host cells/tissue, raising questions about their biocompatibility [153-155]. One of the approaches to improve biocompatibility of polymers is to conjugate anti-inflammatory drugs (e.g. aspirin, small molecule antioxidants) to the polymer or incorporate these drugs into the polymer backbone [8].

2.3.1.2 PNP Surface Chemistry – "Stealth" Considerations

PNPs, as any nanoparticle system, show biological interaction due to the physiochemical effects at their surface. In order to design particles with unique functional surfaces (e.g., active targeting), it is first important to understand what the natural response to the "basic" particle configurations is. In general, nanoparticles administered into blood are rapidly cleared by the mononuclear phagocyte system (MPS). This response is a result of both size effects, (e.g., filtration, impaction, occlusion) and surface recognition, which is characterized by the accumulation of serum proteins and factors onto the particle surface (i.e. opsonization). The amount and type of proteins adsorbed depend on hydrophobicity and surface charge of particles, with charged nanoparticles being cleared much more

rapidly as compared to their neutral counterparts [156]. In fact, by developing surfaces that resist protein adsorption and other factor accumulation, it is possible to have a nanoparticle that is no longer readily recognized by the MPS and thereby possesses extended circulation times [157, 158]. This “stealth” property is classically seen in hydrophilic, or neutral polymers that do not possess hydrogen bonding donors. PEG is the most common polymer used to achieve this stealth capacity, an effect utilized for over 40 years [159]. PEGylation forms a hydrophilic layer around PNPs, which allows them to resist recognition by opsonins, thereby circumventing immune response from macrophages (Figure 2.3B) [160]. PEG brush density also has an effect upon circulation time; typically, with greater density comes greater circulation time [161], unless the greater density causes other adverse effects such as increased instability [160]. Recently, there have been other PNP polymer coatings using polysaccharides that have no natural receptors [162].

Importantly, there are limitations to the use of PEG, which has increased the demand for alternative stealth polymers. For instance, as PEG is a non-biodegradable polymer, there are restrictions as to the maximum molecular weight that can be used. Currently, one of the largest in market PEG molecule being used is in PEGASYS®, which is a PEGylated interferon with a PEG chain weight of 40 kDa to increase retention in blood circulation [34]. The molecular weight restriction is due to the kidney’s maximum size restriction in clearing molecules in the blood stream of around 60 kDa, which avoids the concern of bioaccumulation [159]. Further, as PEG is limited in the number of conjugation sites and mechanical properties, these additional polymer systems increase the flexibility of PNP design available to the formulator without having to sacrifice circulation potential.

2.3.1.3 Size, Shape and Mechanical Properties

Circulation of nanoparticles also depends on their size and shape (Table 2.3). Depending on stealth properties of particles, spherical nanoparticles with sizes less than ~8 nm results in rapid urinary excretion, whereas spherical particles with sizes in excess of 1 μm result in rapid clearance due to filtration effects in the microvasculature. While there exists some degree of controversy in the literature regarding the exact size cut offs, a more inclusive statement is that PEGylated particles with sizes between 20 nm and 1 μm possess prolonged circulation times [163]. The exact extent differences are very system dependent and are still being elucidated. Particle shape also has a profound effect on circulation life, cell attachment and cellular uptake [164]. An example of this is given by PEG-containing diblock copolymer filomicelles, which have shown a circulation half-life approaching ~ 1 week [165]. Filomicelles, which are flexible polymeric micelles with a large aspect ratio, align with blood flow to avoid vascular collisions, extravasation and phagocytosis. Geng et. al. showed that under flow conditions, spherical and short filomicelles were readily phagocytosed as compared to longer filomicelles [165]. Rigidity of particle also affects their phagocytosis. Rigid particles are readily phagocytosed as compared to soft particles [166]. Filomicelles have also been used outside of systemic circulation applications for the mimicking of oral mucin networks via a layer-by-layer deposition approach [167].

As polymers can be composed from a wide variety of chemistries and can be processed into a variety of shapes and forms, each of the above mentioned design criteria can be tuned for specific application. Flexibility in polymer synthesis and nanoparticle formulation methods have made PNPs one of most widely studied drug delivery methods.

Table 2.3. Examples of PNP configurations *in vivo*.

Particle Type	Material	Size Range	Carrier t1/2	Drug t1/2	Drug	Formulation	References
Micelle	mPEG-PLA	30-60 nm	<1 h (human)	12 h (human)	Paclitaxel	Ring-opening polymerization	[168, 169]
Micelle	PBLA-Polyester-PEG	80 nm	2 h (mouse)	9 h (mouse)	Paclitaxel	Nano-precipitation	[170]
Micelle	PEG–poly(aspartic acid)-DOX	40 nm	-	73 h (human), 98 hr (mouse)	Doxorubicin	Ring-opening polymerization	[171, 172]
Polymersome	PEG-Polybutadiene	100 nm	28 h (mouse)	-	-	Film-rehydration	[173]
Nanocapsule	PMMA in HPMC	350 nm - 10 µm	-	9 h (rat)	Tacrolimus	Emulsion, spray drying	[174, 175]
Nanosphere	PEG-Chitosan	150 nm	63 h (mouse)	-	-	Double emulsion	[176]
Nanosphere	PEG-PVA	130 nm	1 h (mouse)	-	-	Double Emulsion	[176]
Nanogel	Polysaccharide–PEG	145 nm	18 h (mouse)	-	-	Nano-precipitation/Michael-addition	[177, 178]
Dendrimer	PEG-polyester-DOX	22,550 Da	72 min (mouse)	-	Doxorubicin	Divergent polymerization	[179, 180]
Print™	PEG	200 nm	3.3 h (mouse)	-	-	PRINT	[181]

2.3.1.4 Particle Type

Given the extensive array of chemistries and mechanical properties available in polymers, there is conceptually no limit to the forms and designs of PNPs that can be made. While the particle types of micelles and dendrimers have many uses, of particular interest to our research in linear chain and crosslinked polymers were nanospheres, polymersomes, and nanogels.

2.3.1.4.1 Polymeric Nanospheres and Nanocapsules/Polymersomes

Polymeric nanospheres, nanocapsules, and polymersomes are composed of polymers which can collapse on themselves or assemble in solution, and have unique geometry described in Figure. 2.4. The categories of nanocapsules/polymersomes and nanospheres differ in that nanospheres are generally solid to the core, where nanocapsules/polymersomes will usually have either a crosslinked surface with a vacant interior that is formed by polymerization in solution, or bilayer through amphiphilic self-assembly [182, 183]. This means that nanospheres can have drug loaded throughout the particle matrix, where nanocapsules/polymersomes generally encapsulate the drug within the interior vacancy, or within the polymer shell [184]. Many of these nanospheres and nanocapsules/polymersomes are formed using amphiphilic di-block copolymers, which allows loading of hydrophobic drugs into the core for increased bioavailability.

Pulmonary drug and gene delivery is an application in which PNPs are promising, as it avoids certain pitfalls of inhalables. Some difficulties in inhalable pulmonary drug delivery are the natural mucin clearance mechanisms, phagocytosis by deep lung macrophages, variable thickness of the mucin layer, and scar tissue from smokers. Interestingly, as inert

PEGylated PNP surfaces are known to enhance vascular circulation times, PEGylation of PNPs also enhance their mucopenetrative properties [185].

Composition, size, and surface charge are important in efficacy of drug deposition and cytotoxicity [186]. PLGA chains covalently modified onto PVA backbones can produce polymeric nanospheres which have tunable properties, such as a fast or slow degradation rate to deliver drugs appropriately depending on the pathophysiology. Nanocapsules/polymersomes (or polymer vesicles), synthetic polymer-based analogs of phospholipid liposomes are composed of self-assembled di/tri-block copolymers [e.g. PEG-PLA, PEG-PBD(poly butadiene), PEG-poly(propylene-sulfide)-PEG] [187, 188] (for detailed review, refer to [189]). Like liposomes, nanocapsules/polymersomes have a large internal aqueous domain that can be used for loading hydrophilic drugs. The thicker membrane of nanocapsules/polymersomes (~9-22 nm as compared to ~3-4 nm for liposomes) makes them a more robust carrier that can resist membrane deformation forces which commonly disrupt liposomes [187]. Also, owing to the higher PEGylation density of the nanocapsule/polymersome surface, nanocapsules/polymersomes have a two-fold higher circulation life (20-30 hours in rats) as compared to liposomes [173]. Nanocapsules/polymersomes have been used to load significant amounts of hydrophilic and hydrophobic anticancer drugs into aqueous core and membrane respectively [142, 190, 191]. Nanocapsules/polymersomes can also be used for simultaneous loading of both water-soluble and water-insoluble small molecule drugs [192].

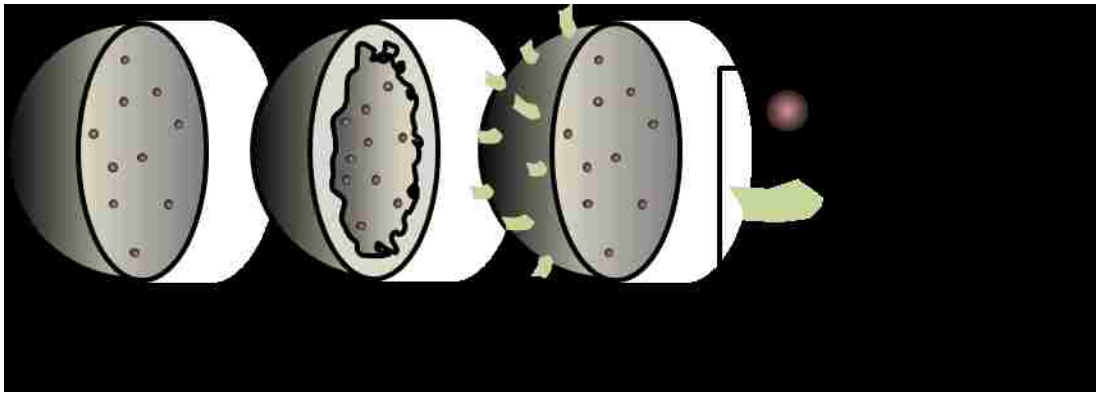

Figure 2.4. Cross-section structural examples of a drug containing A) nanosphere B) nanocapsule or polymersome C) nanosphere with active targeting.

2.3.1.4.2 Nanogels

Aspects of both hydrogels [193] and nanoparticles make polymeric nanogels a very exciting and promising drug delivery system. Through variation of the crosslinked structure, size, and material selection, a multitude of options and effects are possible [177, 194-198]. The biggest difference between nanogels and other polymeric nanoparticles is that their structure is crosslinked either physically or chemically and will hydrolytically swell, and, depending on the polymers and crosslinking chemistry used, degradation can be pH responsive which has been extensively utilized as a passive targeting technique [197, 199]. This swelling force when in an aqueous environment can be produced through protonation/deprotonation, which will increase mesh size until equilibrium is met with the crosslinks' tension force. There are also nanogels which are temperature sensitive, such as those formed from poly(N-vinylcaprolactam) (VCL) [200], poly(N-isopropylacrylamide) (PNIPAAm) [152], or poly(oligo(ethylene glycol methacrylate)) (pOEGMA) [201]. Figure 2.5 shows the structure of a surface modified spherical nanogel.

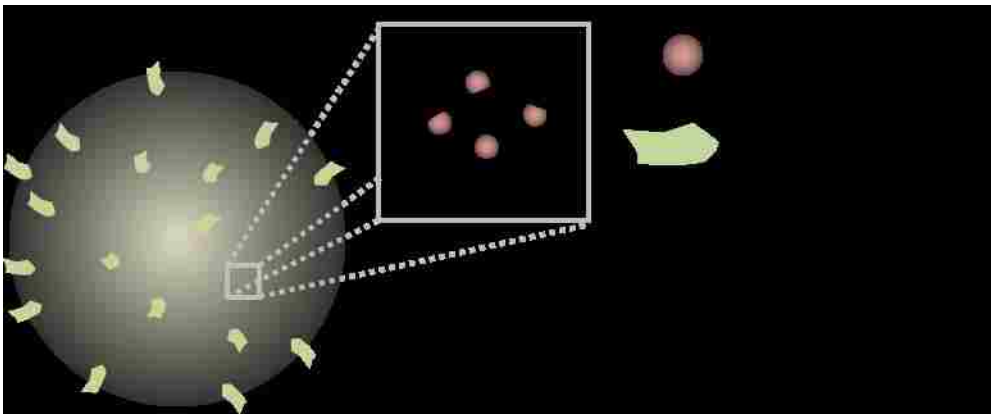

Figure 2.5. Structure of a nanogel with zoomed in section showing crosslinking.

2.3.2 PNP Formulation Methods and Targeting

2.3.2.1 Nano-Precipitation

There are several different routes of synthesis to prepare nanospheres and nanocapsules as well as different methods and results of drug loading and targeting. The simplest approach for nanoparticle formulation is that of nano-precipitation [202]. Generally, the polymer and drug are dissolved in an organic solvent, then added to an aqueous solution being stirred vigorously in which the organic solvent is either quickly evaporated or is diffused into the aqueous phase, which acts as an anti-solvent for the polymer and drug. The polymer then precipitates rapidly, creating nanoparticles [127, 136]. To remain stable, these particulates are then either stabilized by surfactants in the solution or through charge repulsion on the nanoparticle surface. As particles are formed directly by the rate of solvent diffusion and polymer aggregation, initial polymer solution viscosity, polymer MW, and concentration greatly impact the final size of the precipitated particles [69].

As an organic system is often used, it is important to ensure that adequate removal of the toxic solvent phase is achieved. Solvent extraction may be performed through evaporation if it has a high vapor pressure, through complete lyophilization of the solution, centrifugal washing steps, or tangential flow filtration.

2.3.2.2 Nanogel Synthesis

Synthesis of nanogels typically includes crosslinking polymer chains in an already formed PNP [195] through a technique such as emulsion polymerization [197]. For physically crosslinked nanogels, one can perform nano-precipitation [196], which physically binds polymer strands together. Physical crosslinking can be fairly simple, as Nagahama [196]

showed. Briefly, they formed a macromer in DMSO of PLA and dextran and then, dropwise, added water with dissolved protein to this solution under fast mixing to precipitate the polymer into a physically crosslinked nanogel. Physical crosslinking is dependent upon material selection; some diblock polymers will form micelles, others will form nanogels. Nowak [203] used polypeptides to form nanogels and showed that chain conformations (α-helix, β-sheet, or random) of the hydrophobic portion of the amphiphilic block copolymer, as well as the use of a diblock or random block copolymer, make a difference as to whether a micelle or nanogel is formed through physical interactions. Drug loading can be performed through a few different methods. A simple technique is to imbibe the formed nanogels in a drug dissolved solution which will cause the nanogels to swell and increase their mesh size. Drying will effectively collapse the nanogels and encapsulate the drug. Another method is that of direct addition of the drug in solution before the nanogels polymerize. For the technique previously described in Shidhaye [197], one can add drug to the aqueous phase with the polymers before initiating polymerization. Our group has successfully synthesized covalently-bound antioxidant nanogels consisting of quercetin [7, 8] into PBAE nanogels through a single-phase reaction precipitation method with a secondary amine under dilute conditions in acetonitrile. To increase aqueous stability, the polymer was PEGylated as well. These covalently-bound antioxidant nanogels have the benefit of only showing activity upon release of degradation products through ester hydrolysis, allowing for cellular uptake of highly hydrophobic drugs that otherwise would show low bioavailability.

2.3.3 Nanoparticle Targeting

For enhanced selectivity and function in nanoparticle drug delivery, surface modification with specific targeting molecules is popular [204-206] and provides a means to further decrease the amount of drug administered and reduce toxic side effects of the drug that does not reach the intended target. The two main categories of targeting PNPs to a specific location for drug delivery are passive and active targeting. Passive targeting is the use of natural shape/size to determine the localization of PNPs. Active targeting involves the use of an affinity based recognition sequence (e.g. ligand/receptor, antigen/antibody) to determine the distribution of PNPs.

2.3.3.1 Passive Targeting

Currently, passive targeting has been the only FDA approved approach to nanoparticle drug delivery. Most commonly, passive targeting involves utilizing the effects of passive transport principles to reach the desired location. The best example of this is the enhanced permeation and retention (EPR) effect. In areas of highly vascular permeability (e.g., sites of inflammation or some cancerous tumors), nanoparticles that are long circulating can slowly accumulate in the interstitial space. Ideally, extravasated particles can be taken up by the local cells and deliver active drug. Size is an important factor in EPR passive targeting of PNPs administered via systemic drug delivery as it impacts the effective biodistribution throughout the body. If nanoparticles are being used for the treatment of solid tumors, then the size range for the nanoparticles used should be around 10-500 nm [207], where the most effective average size is between 50-200 nm [207]. Tight junctions between healthy endothelial cells will not allow nanoparticles around 10 nm and up to pass

through, but in tumor tissues, nanoparticles can typically fenestrate between the loose junctions up to around 500 nm. In general, though, sizes of 5-250 nm have potential for most drug delivery applications [33] [208].

Another example of passive targeting mechanism is that of pH responsiveness in anti-cancer treatment and other pH sensitive applications where the polymer carrier releases drug at a higher rate either through degradation or via cationic repulsion effects. For instance, in the treatment of colitis, PLGA/methacrylate copolymer nanospheres were loaded with budesonide, a corticosteroid, and delivered to a murine model. In comparison to conventional enteric-coated microparticles, the nanospheres released drug with a strong pH-dependence in the colon and showed superior colon targeting with greater concentration in both non-inflamed and inflamed tissue [209].

Micelles sensitive to pH are particularly popular for anti-cancer drug delivery in which the lowered pH of tumors is utilized with passive targeting and the EPR effect [99, 210, 211]. An example of a method that involves passive targeting via pH sensitivity through polymer design is the use of an amphiphilic diblock copolymer with a hydrophobic poly(β-amino ester) [212] or another acid-sensitive group [98, 99, 210, 213] as the micelle core in combination with a hydrophilic head group. Another example of pH sensitive targeting is by harnessing increased hydrogen bonding at lower pH to extend molecules via repulsion in the corona which may help release the carried drug more readily [210].

2.3.3.2 Active Targeting

Active targeting presents an opportunity to further deliver drug to the desired target tissue. Contrary to passive targeting mechanisms, these coatings can prevent the drug carriers from being swept away from the active site by simple passive transport. This is due to site

specific interactions of the targeting molecule, which can promote endocytosis of the nanoparticles and allow cytoplasmic drug delivery. The production cost of peptides and antibodies, however, increases the cost of the engineered drug delivery system. As with passive targeting, active targeting can occur either with a single level of targeting or multiple levels of targeting. At additional cost, advantages to multi-level active targeting are that you can target more surface area by attacking multiple levels at once, and you have the option of having one drug delivery vehicle being able to treat multiple diseases either separately or together. The addition of targeting groups for both tumor cells and vessels with a tumor-penetrating peptide allows for much greater tumor area covered in comparison to passively targeted nanoparticles.

2.3.3.3 Antibodies

Based upon their method of production, antibodies are available in two main types: monoclonal or polyclonal. Monoclonal antibodies target only one specific epitope on the surface of an antigen. They are molecularly homologous with only one variable region. Polyclonal antibodies represent a heterogeneous population of antibodies that, while targeting the same antigen, can recognize a variety of epitope domains on an antigen. Further, polyclonal antibodies can contain different clones that recognize the same epitope, but with vastly different affinities. For this reason, monoclonal antibodies are the preferred choice for PNP targeting, as they express a much more consistent targeting potential, greatly reducing batch to batch variability. Monoclonal antibodies also may be more easily tailor-made by being produced from gene-modified hybridomas in large supply in the lab. If recombinant polyclonal antibodies can be produced through the use of gene libraries for optimization, they may also be useful to target disease-specific antigens [214]. One concern

with monoclonal antibodies, compared to other targeting, is possible immune activation from nonspecific RES uptake. In addition, their large size inhibits movement through vasculature and passive transport across endothelium [95, 215]. A potentially more useful method was shown in the literature where a mimetic-antibody peptide was used in lieu of the real antibody. The results showed that there was reduced affinity of the mimetic antibody towards the tumor, but the mimetic antibody showed greater tumor inhibition [215].

Example antigens for angiogenic tissue are NG2 (a proteoglycan surface indicator of pericytes) and ED-B (a form of fibronectin). These are all selectively produced in tumor vessels, and antibodies have been developed to target these sites to use in delivering toxins [216]. However, a significant pitfall to the active targeting coatings which target angiogenesis, is that angiogenesis also occurs in tissue with wound repair occurring. The occurrence of cancer treatment coinciding with inflammation or an injury could cause serious malfunction with the normal wound repair processes and pose risk to the patient, thus patients would have to be carefully selected for this option.

An anti-ovarian cancer targeting molecule is folate (vitamin B9). This vitamin is important in rapidly dividing cells, as in the case of cancerous tissue. By surface modifying nanoparticles to include a folate receptor binding molecule, these nanoparticles can go through endocytosis to enter into the cytoplasm for drug delivery [204, 217]. Folate receptor binding molecules include folic acid and a monoclonal antibody which binds to the folate receptor [218].

While systemic targeting is predominantly used in PNP cancer therapy applications, antibody targeted PNPs are also used in gene therapy. Cationic PNPs form electrostatically-

stable complexes with DNA and are a widely-used alternative to viral gene delivery vectors [219]. An advantage of using antibody targeted nanoparticles in gene therapy is that a 70 nm nanoparticle can hold around 2,000 small interfering RNA (siRNA) segments, while keeping the contents safe from external exposure, compared to conjugated antibodies without a nanoparticle carrier, which can only hold less than 10 unprotected siRNA strands [205]. Microparticles and other carriers can have a payload of molecules the same as, if not greater than, that of nanoparticles. However, nanoparticles excel in navigating tumor fenestrations and then delivering drug to the cytoplasm [204], helping bypass multidrug resistance through entering the cell via receptor-mediated endocytosis [220].

2.3.3.4 Target Epitope Selection

Importantly, if active targeting is to be used, selection of the target epitope must be carefully considered. For instance, for cellular targeting, the target should be present on the luminal surface of exposed cell types to be detected during circulation. In particular, this often means the vascular endothelium. Further, the epitope should be spatially and temporally available, i.e. not be down regulated or hidden under times of pathology. For example, adhesion of activated blood cells and accelerated shedding inhibit targeting to some constitutive endothelial determinants [221]. On the other hand, determinants exposed on the endothelial cells under pathological conditions (e.g. selectins) have a distinct transient surface expression profile, which may permit selective drug delivery to pathologically altered endothelium, but require exact timing of administration to match duration of target availability. Ideally, the target should not be present in cells other than the intended target. Targeting should not cause harmful side effects in the vasculature. Binding of targeted drugs may cause shedding, internalization, or inhibition of endothelial

determinants, which may be detrimental. For example, thrombomodulin, a surface protein responsible for thrombosis containment, is abundantly expressed in the pulmonary vasculature, providing high pulmonary targeting specificity [222]. Yet, its inhibition by antibodies may provoke incidences of thrombosis that prevents clinical potential for drug delivery. Ideally, engaging of the target should provide therapeutic benefits, such as inhibition of pro-inflammatory molecules.

2.3.4 Particle Characterization

Ultimately, the success of PNPs is not guaranteed if they are not effectively characterized. Surprisingly, most failures of particles during development have been, in part, due to ineffective characterization of the particles. PNP shape, surface properties and morphology can be determined through imaging, such as scanning electron microscopy (SEM), transmission electron microscopy (TEM) or atomic force microscopy (AFM). Size distribution of PNPs can be checked via nanoscale imaging such as SEM or TEM, or can be analyzed by using dynamic light scattering (DLS). Determining zeta-potential of PNPs is useful to determine both charge properties of a surface coating and to see if the charge is appropriate for biological use systemically. Surface charge of PNPs is important in determining their stability in suspension, their propensity to aggregate in blood flow, their cellular uptake characteristics and their likelihood to adhere with oppositely charged particles or cellular membranes [96]. Zeta potential of nanoparticles in dispersion can be measured using laser Doppler electrophoresis (LDE). Characterization techniques like Fourier transform infrared spectroscopy (FTIR), nuclear magnetic resonance (NMR), or x-ray diffraction (XRD) can be used to determine chemical groups on the PNP surface.

The stability of PNP's, an important characteristic to determine, can easily be checked through looking for degradation products over time in stabilizing media or by checking polydispersity over time. Nanoparticles which aggregate once delivered intravenously can be fatal, thus surface modification to reduce that chance is often necessary [223].

Checking the loading characteristics of PNPs can be as straight forward as simply dissolving/swelling PNP in organic solvent to extract the encapsulated drug or degrading the PNP via a method which does not inhibit or destroy the active drug. For instance, if the drug does not degrade in the presence of acid, lowering the pH to dissolve acid hydrolyzed PNPs is a quick method of degradation, and the concentration of drug released in the supernatant can be determined through an analysis technique such as HPLC, UV-Visible spectroscopy, fluorometry or mass spectroscopy. Encapsulation efficiency (EE) is a very commonly used definition to describe the amount of drug actually loaded into the nanoparticles versus the total amount of drug which was added to the solution of PNP synthesis, as described in equation 2.26:

$$\frac{\text{Mass drug loaded into PNP}}{\text{Mass drug added to synthesis solution}} = \text{EE} \tag{2.26}$$

An easy way to determine EE is to keep track of the mass of drug added to the synthesis solution, form the PNPs, and then centrifuge them into a pellet or perform gel permeation chromatography. Supernatant can then be used to back calculate the encapsulated drug, or a release study can be done with the PNPs to determine drug released.

2.3.5 Biodistribution

Biodistribution can be determined by both invasive and non-invasive methods. Typically, invasive methods involve histology of targeted organs and tissues after set time periods to

detect a marker. For instance, if radiolabeled nanoparticles are used, the tissues can be placed in a gamma counter for comparison over time to find the concentration dynamics. Non-invasive methods are promising in that histology is not required. For instance, if targeted radiopaque PNPs are administered *in vivo*, the subject can be x-ray imaged over a period of time to establish biodistribution [224]. Radio-opaque polymers can be formed through adding salts containing heavy metals, or materials such as iodine which absorb x-rays. Molecular imaging utilizes distinct biomarkers in biological systems to perform characterization at the molecular and cellular level. By delivering a signal-providing, or signal-dampening, probe to a targeted area, 2D and 3D imaging can be produced of that area [225]. A similar branch of molecular imaging, radiogenomics, can detect gene expression radiometrically without performing histology [226]. Different signals can be added to PNPs, such as radioisotopes, which produce either positrons or photons for use in PET (positron emission tomography) or SPECT (single-photon emission computed tomography), respectively, or contrast agents for use in MRI (nuclear magnetic resonance imaging) or optical imaging, etc. Each imaging technique has benefits and caveats due to different sensitivities and approaches. There are many good articles discussing this topic [225, 227-229].

Biodistribution of nanoparticles is often reported with both the total percent of the injected dose (%ID) as well as organ-normalized through the percent injected dose per gram of organ tissue (%ID/g). Through collection of blood samples at the time of tissue harvesting or euthanasia, a localization ratio (LR) may be determined, to analyze differences in nanoparticle localization compared to systemic background, by dividing the organ %ID/g by the blood sample %ID/g. Similarly, if an active targeting agent is used, it may be

compared to a non-targeted control via the immunospecificity index (IS), found by diving the targeted organ LR by the non-targeted organ LR.

2.3.6 Biocompatibility and Cytotoxicity of PNPs

All systemically injected materials must pass basic safety criteria in order to be approved for use. Owing to the burgeoning area of nanoparticle therapy and the complexity involved, this characterization can be quite extensive and challenging. However, the principles of determining safety are relatively simple to understand and provide a guiding-light to consider as one develops new PNP strategies. At the simplest level, the PNP should be nontoxic, non-immunogenic, non-inflammatory, non-teratogenic, non-thrombogenic, non-bioaccumulating and be stable in blood [230]. As toxicity is easily evaluated in *in vitro* studies and provides a useful indicator of biological toxicity, PNPs should be first evaluated by determining the effect of particles and their degradation products on cellular viability. Cell type selection can be made based upon the application of interest. Similar to the cellular uptake of PNPs, the cytotoxicity of PNPs can be size, shape, zeta potential, and surface chemistry dependent. Kim et. al. [231] demonstrated size-dependent cytotoxicity of polypyrrole nanoparticles (PPy NPs). Human lung fibroblasts and mouse alveolar macrophages were treated with monodispersed PPy NPs of different sizes (20, 40, 60, 80 and 100 nm). PPy NP cytotoxicity correlated to their size and was in the following order: 60 nm > 20 nm > 40 nm > 80 nm > 100 nm.

Cytotoxicity may be determined by measuring cell viabilities after treating them with different concentrations of PNPs. Before choosing an appropriate cell viability assay, it is necessary to understand what each assay is measuring as an endpoint and how that correlates with cell viability. Assays are available to measure endpoints like cell

proliferation, number of live cells, number of dead cells, and mechanism of cell death. MTT (3-[4,5-Dimethylthiazole-2-yl]-2,5-diphenyl tetrazolium) is a colorimetric assay to measure cell proliferation where the active reductase enzymes in viable cells reduce MTT to a purple-colored formazan product. As a result, formazan formation is directly proportional to the number of viable cells in a culture. However, MTT can also directly react with reducing agents (e.g. polyphenolic antioxidants) to produce formazan crystals. In cases where such reducing agents are involved, MTT or other assays that rely on reductase activity may overestimate cell proliferation [232]. The luminescence-based ATP assay, where luminescence originates from conversion of luciferin to oxyluciferin by a luciferase in presence of ATP, measures luminescence intensity to determine ATP concentration in cells which is an indicator of cell viability [231]. Live/Dead® assay is a fluorescence based assay to differentiate live cells from dead cells by simultaneously staining with green fluorescent Calcein-AM to indicate intracellular esterase activity (marker of live cells) and red-fluorescent ethidium homodimer-1 to indicate loss of plasma membrane integrity (marker of dead cells). Methods of detection for Live/Dead® assay include fluorescent spectroscopy, fluorescent imaging or flow-cytometry, and it can be used to determine total number of live and dead cells in a culture. To determine the mechanism of cell death, apoptotic and necrotic cells can be differentiated by detecting phosphatidylserine with FITC bound annexin V and propidium iodide [233]. Furthermore, mitochondrial membrane potential can be measured with flow-cytometry to determine if a loss of membrane potential has occurred, a sign of apoptosis in some systems. This can be performed by adding fluorochromes which reflect the membrane potential via fluorescence. In case of slow degrading biodegradable PNPs, measuring cytotoxicity of

PNPs after short term exposure (24 – 72 hrs) may not be enough and it is equally important to separately determine cytotoxicity of water-soluble and insoluble degradation products of PNPs.

While cell viability assays are a good indicator of overall cellular response to a toxin, they do not reveal much about the mechanism of toxicity. Recently, a lot of attention is also being given to biomaterial-induced inflammatory response which is inextricably linked to cellular oxidative stress, where cellular antioxidant defense mechanisms are overwhelmed by excessive generation of reactive oxygen species (ROS) and reactive nitrogen species (RNS) [7]. 2',7'-dichlorodihydrofluorescein diacetate (DCFH-DA) is commonly used as a marker of oxidative stress in cells [234]. DCFH-DA, a non-fluorescent form of the dye, is taken up cells and cleaved to a non-fluorescent DCFH (2',7'-dichlorodihydrofluorescein) by active esterases in the cell. DCFH can the then react with a variety of ROS and RNS (hydrogen peroxide, peroxynitrite, hydroxyl radical, lipid peroxides, thiol radicals, etc.) to form fluorescent DCF (2',7'-dichlorofluorescein). Oxidative stress in the cells can be quantified by measuring DCF fluorescence. Since DCF reacts with variety of ROS and RNS, it does not provide information about specific oxidative species involved or about sub-cellular compartments (e.g. cytoplasm, plasma membrane) that are at risk of damage by ROS/RNS. Cellular proteins can be measured for their 3-nitrotyrosine (3NT) and protein-bound 4-hydroxy-2-trans-nonenal (HNE) content, which are specific markers for protein damage by RNS and lipid peroxidation, respectively [234].

A typical and problematic contaminant in nanoparticle formulations is that of the endotoxin lipopolysaccharide (LPS). LPS, originating from gram negative bacteria, is pyrogenic and a major hurdle of nanoparticle formulations in pre-clinical studies due to cytotoxicity [235].

Endotoxin levels can be determined via a simple assay, such as the lumilus amebocyte lysate (LAL) assay, which may give a positive result through clot formation, turbidity, or chromogenicity depending on the test used. The other common method of evaluation for pyrogenic contamination is an *in vivo* rabbit test where qualitative results are measured after injection. Removal of LPS from nanoparticles is very troublesome due to the high surface area to volume ratio of nanoparticles [235], resistance to heat, pH, and inability of removal via sterile filtration, so sterile design and practices may be the most effective method of non-contamination compared to post-processing removal.

2.3.7 PNP Drug Release and Pharmacokinetic Modeling

Modeling release characteristics of drugs from PNPs not only gives insight about the release/degradation mechanism in a new PNP formulation, but also helps in choosing PNP design to obtain desired release profiles. Fick's second law of diffusion in spherical coordinates, equation 2.27, is a common starting point for modeling drug release from PNPs, and it describes the change in concentration, C, of drug in a sphere of radius r over time t. D is the diffusivity and a is the constant radius of the sphere. Since Fick's second law only describes diffusion, it is not an end-point equation for PNPs which are degradable or exhibit relaxation effects.

$$\frac{\partial C}{\partial t} = D\left[\frac{\partial^2 C}{\partial r^2} + \frac{2}{r}\frac{\partial C}{\partial r}\right] \tag{2.27}$$

For 1-dimensional diffusion in the radial axis and sink conditions, initial and boundary conditions can be stated as:

$$t = 0 \qquad 0 < r < a \qquad C = C_1$$

$$t = 0 \qquad r = 0 \qquad \frac{\partial C}{\partial t} = 0$$

$$t > 0 \qquad r = a \qquad C = C_0$$

where a is the PNP radius, C_1 is the initial concentration in the PNP and C_0 is the concentration in the surrounding bulk fluid. The series solution to equation 2.27 is given by Crank et. al. as equation 2.28:

$$\frac{M_t}{M_\infty} = 1 - \frac{6}{\pi^2}\sum_{n=1}^{\infty}\frac{1}{n^2}\,exp\left[\frac{-Dn^2\pi^2 t}{a^2}\right] \tag{2.28}$$

For short times, equation 2.28 can be simplified to equation 2.29:

$$\frac{M_t}{M_\infty} = 6\left[\frac{Dt}{\pi a^2}\right]^{1/2} - 3\frac{Dt}{a^2} \tag{2.29}$$

Modeling using non-sink conditions can also be very useful. If the drug delivery is to be in an area where drug may accumulate, such as PNPs meant to be delivered to a tumor site, Fick's second law can be used to derive numerous variations by simply changing the boundary conditions. Historically, the Higuchi equation, originally derived for a slab geometry and simplified in equation 2.30, has been the modeling workhorse of diffusive drug delivery [236], showing diffusion following Fick's second law for the first 60% of release. $\frac{M_t}{M_\infty}$ is the mass fraction of drug released at time t from the total amount contained at $t = 0$, and K is a constant which depends on each system. Over the years, this equation has been the basis for many other equations which take into account other geometries and has been derived from a simple pseudo-steady state diffusion model. Equation 2.31, typically called the power law, further expands the Higuchi equation into describing the mechanism of drug release by combining diffusive effects with $t^{1/2}$ and relaxation with

t^1, as seen in equation 2.32. This equation superimposes both relaxation/swelling based transport and pure Fickian diffusion by allowing alteration of the power n, and again can be used to describe the first 60% of release.

$$\frac{M_t}{M_\infty} = Kt^{1/2} \tag{2.30}$$

$$\frac{M_t}{M_\infty} = Kt^n \tag{2.31}$$

$$\frac{M_t}{M_\infty} = K_1 t^{1/2} + K_2 t \tag{2.32}$$

However, the power values of 0.5 and 1 are useful only for slab geometry, and power values have been derived for systems with other geometries [237]. Concerning spherical geometry, when the exponent n is equal to 0.43, the release mechanism is that of Fickian diffusion. An exponent between 0.43 to 0.85 is described as transport utilizing both Fickian and case-II swelling, and an exponent of 0.85 is defined as purely case-II relaxation transport. Trivially, a power value of 0 would give no release and 1 would give zero-order release, independent of time.

While the power law is useful in quick characterization, there are some draw backs in the assumptions made: the particle size distribution must be narrow, sink conditions must always be attained, diffusion must only occur in one direction, edge effects must not exist, the diffusivity of drug must remain constant, the polymer carrier must not dissolve, and the drug must be suspended such that it is much smaller than the thickness of the system [236]. Considering drug delivery applications, sink conditions occur when drug is released into an area where the limiting condition is the rate of diffusion of drug from the PNPs, and diffusion of the drug into the surroundings is fast. If the drug is released into an area where

local concentration buildup occurs, this model will not fit. If the particle size distribution is tight, setting up an easy experiment with sink conditions is very simple. An example experiment would be to put the PNPs into a dialysis bag, and that bag into a large volume of drug release medium. Then, by calculating the drug release from the particles, the initial and final mass of drug release is known, and parameters K and n can be obtained by fitting the data to a plot.

Nanoparticles may release drugs following several different mechanisms. Possible mechanisms of release include diffusion and degradation of the polymer chains. Diffusion of the drug can occur from the surface, through an expanded polymer matrix, through the wall of a nanocapsule, or through a combination of these processes. Degradation can occur due to hydrolysis of bonds which may increase the mesh size in nanogels or lead to the dissolution of nanospheres, nanocapsules, dendrimers, or micelles.

A common equation used in modeling of drug release from nanoparticles is equation 2.33.

$$\mathbf{C}_{drug}(\mathbf{t}) = \mathbf{A}\mathbf{e}^{-\propto \mathbf{t}} + \mathbf{B}\mathbf{e}^{-\beta \mathbf{t}} \qquad \textbf{(2.33)}$$

This equation is a bi-exponential function which describes at time *t* the concentration of drug in a nanoparticle. A is a diffusion constant, B is a degradation constant, and α and β are rate constants. When it comes to more rigorous modeling, there are variety of different methods to simulate PNPs, and these methods can be categorized by their end goal. If one is interested in interaction at the molecular level, a macroscale approach will not be as useful as molecular dynamics or Monte Carlo simulations. Molecular dynamics and Monte Carlo simulations rely on molecular interactions, thermodynamics, and kinetics to carry out the simulation. Microscale methods can include Brownian dynamics modeling or dissipative particle dynamics [238]. While molecular dynamics simulations can be more

intricate in the modeling of PNPs, there is a large downside in that it usually requires intensive and extensive computation.

2.3.8 Compartmental Modeling

Related to drug release, pharmacokinetics can be described through the use of compartmental modeling. Briefly, each compartment describes a biological transport barrier or container, such as the circulatory system, different organs, RES, or cellular barriers. The end-goal is to be able to determine concentration at any time in any compartment. The simplest compartmental model is a single compartment model that describes first-order elimination of a drug following a single bolus injection (equation 2.34). For instance, if drug loaded PNPs are injected intravenously and have a single, constant clearance mechanism without any other interaction with any parts of the body, this can be modeled as a single compartment. Solving equation 2.34 for the initial condition yields equation 2.35. The constants can be determined through physiologically relevant studies.

$$\frac{dC}{dt} = -k_{out} * C(t) \qquad C(0) = C_0 \tag{2.34}$$

$$C(t) = C_0 e^{-k_{out}t} \tag{2.35}$$

Each compartment, in addition to the first, can be organized in the fashion necessary to describe the prescribed conditions. Where a single compartment may only utilize simple input and output, a two compartment model can show equilibrium effects where drug may be transiently contained. For instance, Figure 2.6 describes this concept as a block diagram. Utilizing a form of the base equation 2.34, the necessary equations can be derived from a mass balance of inputs and outputs.

$$V_1 \frac{\partial C_1}{\partial t} = Q_{in} C_0 + k_{21} C_2 V_2 - k_{12} C_1 V_1 - Q_{out} C_1 \quad \textbf{(2.36)}$$

$$V_2 \frac{\partial C_2}{\partial t} = k_{12} C_1 V_1 - k_{21} C_2 V_2 \quad \textbf{(2.37)}$$

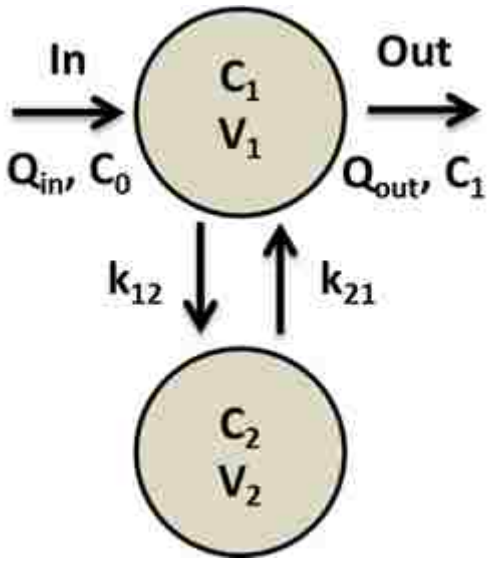

Figure 2.6. 2-compartment model showing equilibrium with a second compartment corresponding to equations 2.36 and 2.37.

A simple example of Figure 2.6 is when compartment #1 is the blood space and compartment #2 is tissue space of a particular organ. Blood flows through the organ, and there is local buildup in the tissue space of the organ. This is a simple model, but compartments to represent additional organs or drug depots can be added to increase model accuracy; however, determining appropriate parameters for more complicated models can be challenging.

2.3.9 Example PNPs in Practice

While there are numerous PNP products in development [33], and several currently in the clinical trial phase [33, 168], there are currently no FDA approved synthetic polymeric nanoformulations. However, nanoformulations made from organic polymers (e.g. proteins) and liposomes do exist, such as the popular albumin-based Abraxane® for paclitaxel delivery approved in 2005 [34, 239]. Interestingly, the story of Abraxane® provides an excellent illustration of the importance in delivery vehicle choices. Paclitaxel is a highly hydrophobic anticancer agent that is difficult to deliver in therapeutically relevant doses without some mechanism to increase solubility. Prior to Abraxane®, the most common formulation to achieve this was based upon a non-ionic surfactant, Cremophore EL®, and ethanol mix (Marketed as Taxol®). This mixture is considered to be a predecessor to PNP as, upon injection, Cremophore EL® forms a micelle which aides in dispersing and solubilizing paclitaxel [168]. Unfortunately, Cremophore EL® has significant side effects, including neuropathy and hyper sensitivity. Furthermore, the Cremophore EL® micelle has rapid clearance rate compared to free paclitaxel, which requires more drug to be injected to be effective [168, 240]. In 2005, Abraxis Bioscience (acquired by Celgene in 2010) received FDA approval to market Abraxane®. Abraxane® is a 130 nm nanoparticle

composed of Albumin-bound paclitaxel. Albumin is a long circulating serum protein that is a natural carrier of vitamins and many other different hydrophobic molecules. As such, it was hypothesized that particles composed of albumin would both enhance paclitaxel solubilization and provide improved circulation times. However, it was also found that albumin aides in the transcytosis of the substance it is carrying into endothelial cells by forming caveolae [241]. This effect, in addition to the improved pharmacokinetics with reduced side effects, is a classic example of just how PNP can be designed to improve drug therapy.

Conceptually, a more straight forward approach is to create a micelle system that is less toxic, more stable and has a longer circulation half-life than Cremophore EL®. Currently in a phase IV clinical trial in the USA, is Genexol-PM®, which has been approved for paclitaxel delivery in South Korea since 2007. Genexol-PM® uses a diblock copolymer of poly(ethylene glycol)-co-poly(lactic acid) (PEG-PLA), which fulfills many of these requirements, and is indicated for breast cancer treatment (Figure 2.7).

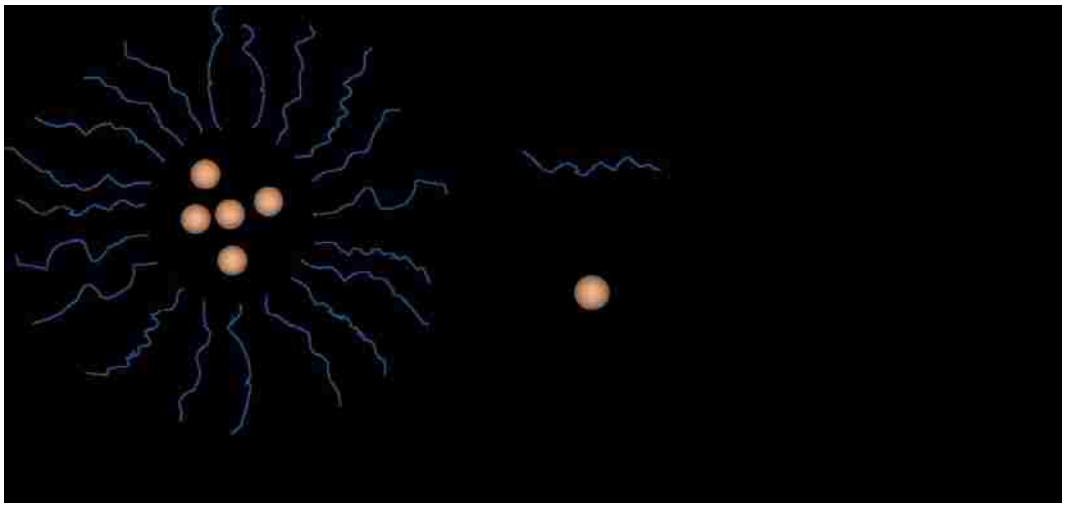

Figure 2.7. Schematic description of paclitaxel loaded Genexol-PM®. Polyethylene glycol, a hydrophilic non-ionic polymer, has excellent anti-adhesive properties, which permits evasion of the mononuclear phagocytic system (MPS), the cell system responsible for the clearance of large particles from circulation. Poly(D,L-lactic acid) is a biodegradable hydrophobic polymer. The diblock copolymer of these polymers results in a micelle system that is more stable, and contains a hydrophilic shell that imparts a longer circulation half-life compared to other nanoparticle systems. This prolonger circulation time resulted in an increase in tumor accumulation due to the enhanced permeation and retention effect (EPR) [168].

2.4 Conclusions

Advances in biomaterials have bridged the historic gap between material science and tissue response for the betterment of patients in a wide variety of applications. Research into synthetic hydrogels has opened the field of local drug delivery for enhanced therapeutic delivery and tissue-like properties. Similarly, nanoparticle properties allow for (but are not limited to) enhanced systemic delivery systems which may evade immune response, or utilize antigens for fast cellular uptake, a property which traditional small molecule drugs lack. As is discussed in Chapter 3, through the understanding of biocompatibility, immune response, and inflammation, biomaterials may be designed to effect a response in complex redox systems for the inhibition of infection and oxidative stress diseases.

Chapter 3. Mechanisms of Infectious and Oxidative Stress Disease

Thiol redox metabolism text partially taken from the book chapter:

> Prachi T. Gupta, Andrew L. Lakes, Thomas D. Dziubla. *A Free Radical Primer*, In Dziubla: Oxidative Stress and Biomaterials: the Science, Challenges and Opportunity. (In Prep.)

3.1 Introduction

Across the world in 2012, all diseases accounted for 49.2% of all deaths, with the remainder from accidental death or "other" causes [242]. Of those disease-related deaths, ischemic heart disease accounted for the leading cause in high income countries (158 deaths out of 100,000 population), and in low income countries lower respiratory infections were the leading cause (91 deaths out of 100,000 population) [242]. In general, many disease-related deaths were implicated with either infection or oxidative stress, such as lower respiratory tract infections or diarrheal diseases, and ischemic/hypertensive heart disease, stroke, chronic obstructive pulmonary disease, cancer, and neurodegenerative disease. While great medical progress has been made in disease treatment, there still remain large numbers of deaths of preventable disease. It is apparent that the shift in cause of deaths away from infectious disease in first world countries is through thorough antibiotic access, advanced medical technologies, and national healthcare systems. Nonetheless, first world countries are afflicted by not only the aforementioned oxidative stress diseases, but also must act swiftly against the increasing rates of antibiotic resistance emergence that is raging across the third world [243, 244]. Through the engineering of new smart materials to enhance delivery of drugs to counteract DNA, protein and lipid damage via oxidative stress mechanisms, as well as those to reduce the propensity for antibacterial resistance emergence are of high importance throughout the world. In this chapter, oxidative stress

disease and bacterial infection mechanisms are discussed in the context of drug delivery methods and devices.

3.2 Cellular Respiration

With primary function of the production of the nucleotide adenosine triphosphate (ATP) in animals, mitochondrial function is very important for cellular energy regulation, and dysfunction can lead to apoptosis and disease [245, 246]. Electron transport of protons across mitochondrial membranes in aerobic respiration, used in the Kreb's cycle or the citric acid cycle (TCA), produces oxidant byproducts of superoxide and hydrogen peroxide due to oxidative phosphorylation of adenosine diphosphate (ADP) to ATP.

In discovering the mechanism of apoptosis, i.e. programmed cell death, there was observation of mitochondrial dysfunction showing loss in cytochrome *c* into the cytosol, and early autolytic morphologies in damaged mitochondria exhibiting swelling, and a small ATP production loss, which was compensated for by increased glycolysis, yet increased reactive oxygen species (ROS) as well [247-249]. Later, it was found that the complex apoptotic process involves pro-apoptotic factors changing mitochondrial permeability to release both second mitochondria-derived activator of caspases (SMACs), which activate cytotoxic caspases, and cytochrome *c*, which is necessary for the formation of the apoptosome, a protein complex holding contents which would otherwise damage nearby cells, allowing phagosomes to eliminate its contents safely, similar to the utility of peroxisomes to harbor hydrogen peroxide for use as an oxidizing agent such as lipid metabolism [250].

3.2.1 Cellular Redox State

Within the eukaryotic cellular environment, there exists an equilibrium between oxidants and antioxidants [251]. The cellular redox state is based upon the concentration of these oxidizing and reducing agents present in various cellular regions, as well as extracellular state. Many oxidants and antioxidants exist and play important roles in cellular function and health. Different cellular compartments, meant for different processes, require different reduction potentials, or the likelihood of electron transfer between species, to function properly. Reduction potentials are typically calculated via the Nernst equation. At homeostasis, cytoplasm typically holds a reduction potential between -260 to -200 mV, allowing the high reducing environment to act as a buffer against oxidative injury. Due to respiration processes, mitochondria are protected to an even greater extent with a reducing potential around -280 mV, with -330 mV in liver mitochondria due to increased glutathione (GSH) transport for toxin removal as well [250]. The endoplasmic reticulum (ER), however, holds a reducing potential around -189 mV due to the oxidative processes the ER carries out, with most glutathione species entrapped as mixed protein disulfides, which can be converted to GSH to aid in protein folding procedures [250].

3.2.1.1 Thiol Redox System

Paramount to achieving a functional cellular environment is the complex network of oxidizing and reducing molecules and proteins, required to maintain correct reaction conditions for the cellular machinery to carry out. Major players of redox processes are defined in Figure 3.1. Of particular interest to our antioxidant polymer work is that of the thiol redox system, involving the small molecule antioxidant, glutathione (GSH), which

contains an antioxidant thiol group and is the most abundant small molecule in eukaryotic cells. Synthesized within the cell from the three amino acids, glutamate, glycine, and cysteine, GSH production is rate limited by cysteine content, a semi-essential amino acid in biology. Cysteine transported from extracellular space is in the disulfide form, termed cystine [252]. Reaction of cysteine with glutamic acid in presence of glutamate-cysteine-ligase (GCL) followed by reaction with glycine via glutathione synthetase (GSS) results in GSH production [252]. GSH may act in several mechanisms as an antioxidant, whether directly through electron donation to reactive oxygen or nitrogen species in the intracellular or extracellular space, or via enzymatic routes such as with glutathione S-transferase (GST) to irreversibly reduce toxic species like lipid peroxides and protein carbonyls [253]. In addition to direct chemical reaction with oxidative species, GSH participates in several mechanisms to regenerate other important antioxidant enzymes such as glutathione peroxidase (GPx), glutaredoxin (GRX), and peroxiredoxins (Prxs) non-specifically. Oxidized glutathione (GSSG) may be reduced back to GSH via glutathione reductase (GR), which is driven by NADPH and the glucose-6-phosphate dehydrogenase (G6PD) cycle via oxidation of NADPH to $NADP^+$. There are also other thiol-based oxidoreductases such as thioredoxin, which utilizes cysteine thiol-disulfide exchange (instead of GSH), and is regenerated with thioredoxin reductase, similarly utilizing NADPH for regeneration akin to GSSG with GR.

Depending on the compartment of the cell, redox equilibrium may vary. For instance, the cytosol (GSH:GSSG 100:1) and nucleus (GSH:GSSG >100:1) maintain a reducing environment [254, 255], whereas the endoplasmic reticulum (GSH:GSSG of 1-3:1 [256], where disulfide bonds fortify the protein structures), mitochondria (GSH: GSSG of 20-

40:1 [255]), secretory pathways, and extracellular space (GSH:GSSG 20:1 [257]) have a high concentration of oxidants comparatively. It is important to note that extracellularly, while the GSH:GSSG ratio is around 10-20:1, cysteine and cystine are in greater concentration by about an order of magnitude, and maintain the oxidative environment around cysteine:cystine of 0.2:1 [257]. In a similar manner, NADPH is a reducing coenzyme involved in processes like fatty acid synthesis, and is required to drive various redox reactions in the metabolic pathway. Therefore, NADPH:$NADP^+$ (200:1) ratios are found to be in same order of magnitude as for GSH/GSSG redox equilibrium. On the other hand, another coenzyme NADH plays an essential part in both reduction and oxidation in general, hence a significant concentration of both oxidized and reduced form is maintained in the cell with NAD^+ at greater concentration. Cytoplasmic NADH which is produced by oxidation of cytoplasmic NAD^+ acts as an electron donor and is transported to the mitochondrion to reduce mitochondrial NAD^+ to NADH, which in turn is oxidized again during oxidative phosphorylation to generate ATP. It is postulated via several experimental studies that NAD^+/NADH ratio in cytoplasm is around 700:1, though the overall cellular ratio varies between 0.5:1 to 4:1. This ratio is involved in regulation of several metabolic enzymes such as glyceraldehyde 3-phosphate dehydrogenase, and pyruvate dehydrogenase used in conversion of pyruvate to acetyl-CoA.

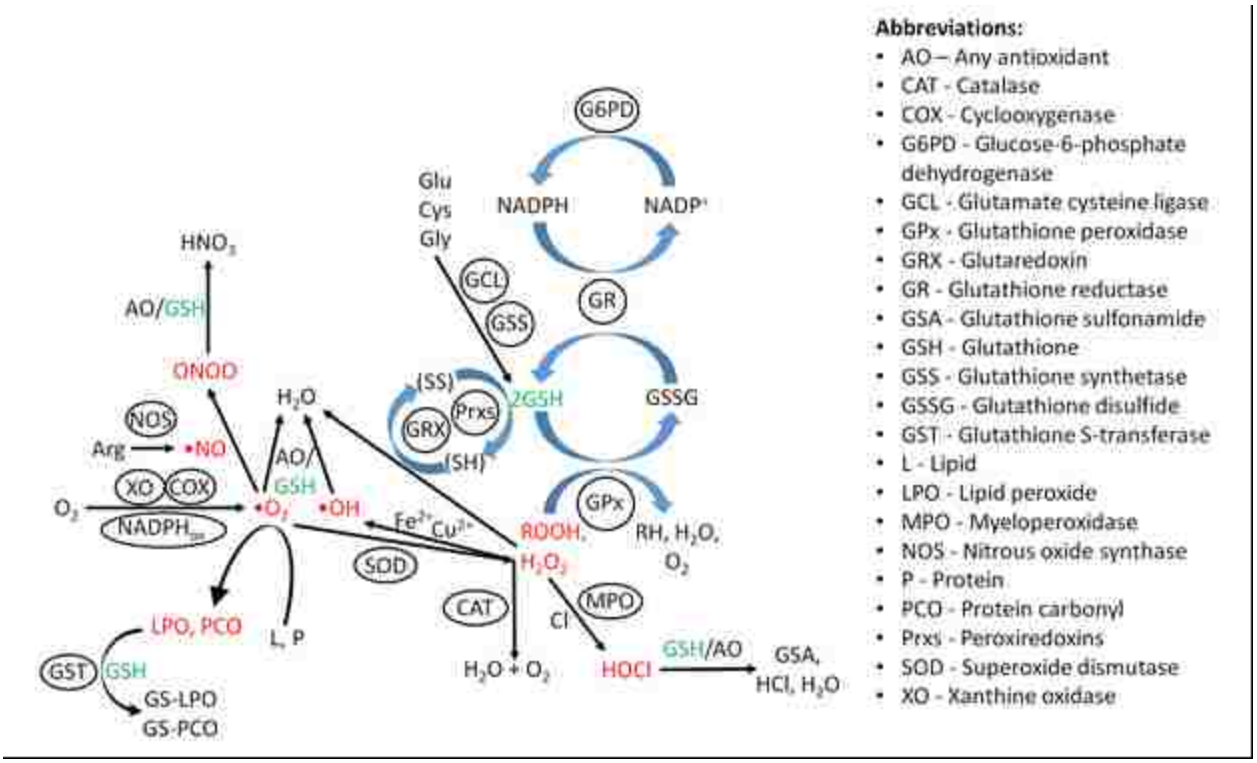

Figure 3.1. Significant cellular redox molecule interactions. Green: glutathione processes.

Red: oxidant species reduced by glutathione processes.

3.3 Immune Response

Infection and inflammation are closely tied and yet may occur independently, for inflammation may occur without infection (e.g. mild cellular damage or disease), or pathogenic infection may occur with a species which evades a host's immune response (e.g. HIV/AIDS). Bacteria and microorganisms display key surface markers, which animals have evolved an innate immune response to in an effort to ward off pathogenic colonization. This response may vary from minor acute inflammation upon injuring a toe from lysed cells releasing inflammatory cytokines, to disabling autoimmune disorders like rheumatoid arthritis where chronic inflammation is intensely damaging to joints in the extremities. This damage is due to continuous production of reactive radical species, creating an imbalance of oxidants to antioxidants, termed oxidative stress. Sepsis, a state of systemic inflammation, occurs due to an out of control immune response to initial infection. With a death rate of roughly 25-80% of patients for uncomplicated to complicated disease, sepsis is a serious disease affecting about 18 million people per year [258]. For each of these diseases, research involving controlling antioxidant delivery is ongoing, involving mitochondrial function protection [258-260]. Another link between infection and oxidative stress-induced disease exists in one of the causes of gastric cancer. *Helicobacter pylori* infection plays a role in that increased gastric immune response creates an oxidative burden upon the stomach lining, causing mutagenic effects over time [261].

To combat these problems, the immune system, consisting of the innate and adaptive immune systems, is charged with removal of foreign bodies to prevent infection, and with the signaling of cellular dysfunction from disease or tissue damage. Cells of the innate immune system contains pattern recognition receptors (that co-evolved with pathogens)

which contain conserved pathogen associated molecular patterns used in detection. There are also damage-associated molecular patterns which are chemosensed by a variety of cell-signaling molecules released from cellular dysfunction, apoptosis, or necrosis [262]. The adaptive immune system is driven by detection of unique antigens via dendritic cells, which initiate and modulate immune response. Upon stimulation of dendritic cells from detection of an antigen in the tissue involved, these dendritic cells present antigens to B and T lymphocytes for antibody production and antigen removal via differentiation into additional B cells, macrophages, and killer T cells [263]. This release of cytokines during the process of antigen detection is paramount towards the end goal of receiving aid in the area of concern via local and circulating immune cells. The duration of immune response, whether it be innate or adaptive response, may be defined as either acute or chronic.

3.3.1 Acute Inflammation

As a means to mobilize appropriate cells to the area of the immune event, acute inflammatory response is initiated by release of event-related signaling molecules. In the case of infection, cytokines are released from immune cells, such as the interleukin family and eicosinoids, a complex, unsaturated fat-derived family involved in leukocyte attraction (e.g. leukotrienes), vasodialation, and thrombosis (e.g. prostaglandins). Lipopolysaccharide (LPS) (the outer membrane layer on gram-negative bacteria) is a well-known prostaglandin inducer (cyclooxygenase 2 synthase in particular) [264]. Bacterial infections are primarily destroyed through neutrophil and monocyte phagocytosis via oxidative bursts of superoxide which are membrane and wall destructive. Further, this superoxide may convert to hydrogen peroxide, and combine with chloride ions to produce hypochlorous acid when protonated via reaction with myeloperoxidase, causing the

characteristically green color found in neutrophil containing mucus, such as a runny nose during sickness.

Similarly with the wound-healing process, after platelet-derived triggering of immune response from collagen contact (if there is hemorrhage), or parenchymal cellular damage/activation (if no hemorrhage), the acute inflammatory phase is primarily neutrophils phagocytosing cellular debris via oxidative burst destruction, later arriving monocytes which also phagocytose debris, and digestion of proteins through secreted proteases [265, 266]. For leukocyte extravasation to occur into an infected or damaged region (Figure 3.2 A), signaling molecules are released from macrophages such as the inflammatory cytokine tumor necrosis factor alpha (TNF-α), and others like interleukins-1 and 6, causing upregulation of G protein coupled receptors on endothelial cell surfaces (Figure 3.2 B) [265]. Circulating leukocytes chemosense cytokines (Figure 3.2 C) and after expressing L-selectin initially adhere to endothelial cells via cluster of differentiation 34 (CD34). Upon attachment (Figure 3.2 D), L-selectin is shed due to CD34 attraction, and leukocytes roll towards endothelial junction, mediated by P-selectin and E-selectin, where leukocytes are triggered via platelet endothelial cell adhesion molecule 1 (PECAM-1) to produce further integrins, and tight adhesion occurs via inflammatory cell adhesion molecule 1 (ICAM-1) and vascular cellular adhesion molecule 1 (VCAM-1). Then, PECAM-1, ICAM-1, and VCAM-1 modulate leukocyte transmigration through the endothelial junction (Figure 3.2 E) [267]. Once complete with the task of initial cellular debris cleanup or infection control (Figure 3.2 F), these leukocytes apoptose for clearance via macrophages (Figure 3.2 G), and the rest of the wound-healing process proceeds with angiogenesis and collagen deposition [268, 269]

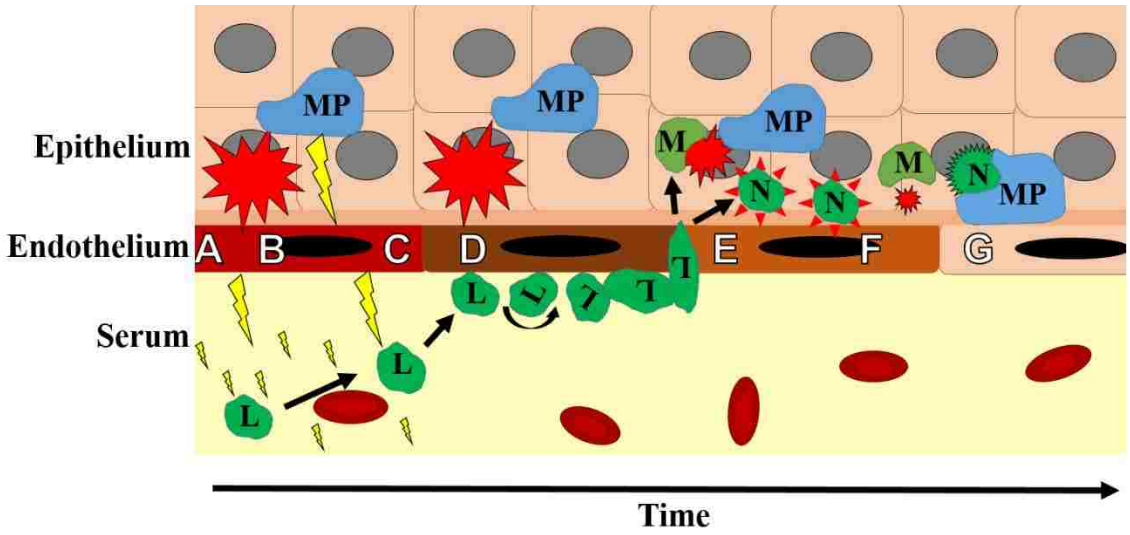

Figure 3.2. Example leukocyte recruitment and extravasation scheme. Red burst indicates cellular damage. Yellow lightning indicates cytokines. MP = macrophage, L = leukocyte, M = monocyte, N = neutrophil.

3.3.2 Chronic Inflammation and Oxidative Stress

Where the acute immune response is vital for disease control and damaged tissue treatment, chronic inflammation may occur when this response becomes dysregulated. This can occur from oxidative stress tissue damage through continuous leukocyte extravasation, due to autoimmune disease, such as type-1 diabetes towards β cells, ischemia/reperfusion injury, or radiation injury for example, causing significant cell death. Typical of a chronic wound, leukocyte extravasation may occur beyond the typical wound healing period (Figure 3.3A). Continuing digestion of cells and surrounding tissue without reduction of leukocyte influx (Figure 3.3B) can cause complications such as infection, or even cancer due to the increase in the cell repair cycle (Figure 3.3C). Mitochondrial damage from excess ROS leads to increased mitochondrial permeability, and the release of ROS into the cytoplasm (Figure 3.3D). This release turns into a chain reaction of mitochondrial dysfunction, termed ROS-induced ROS-release [270].

A main proponent in the function of wound healing is the transcription factor, nuclear factor kappa B (NF-κB). Activated by cell signaling from distress or infection, NF-κB upregulates a series of inflammatory cytokines such as IL-1 and TNF-α [271]. In serious wounds, or wounds complicated by diseases like diabetes where there is limited blood perfusion to tissues, a positive feedback loop may occur where continuing NF-κB expression signals for more TNF-α, thus more leukocyte recruitment and more cellular destruction. NF-κB dysregulation is also implicated in cancer development and drug resistance due to NF-κB being an apoptosis inhibitor, thereby increasing cellular proliferation [271].

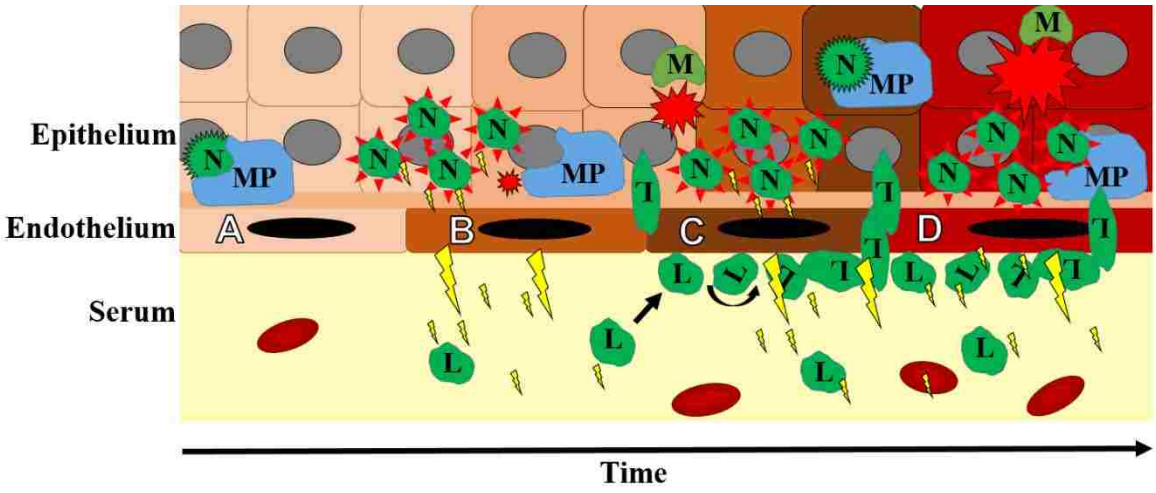

Figure 3.3. Example chronic leukocyte recruitment and extravasation scheme. Red burst indicates cellular damage. Yellow lightning indicates cytokines. MP = macrophage, L = leukocyte, M = monocyte, N = neutrophil.

3.3.3 Biomaterial Biocompatibility

When foreign objects are implanted within the body, immune response follows the acute inflammatory pathway, namely, an influx of white blood cells to the region. If the immune system finds digestion of the material is not possible, the next best option is to contain the foreign body. This occurs through the deposition of opsonins, a complex of proteins such as fibrinogen, IgG, and others on the biomaterial surface (i.e. fibrous capsule formation) [272]. If a continuous oxidative environment is interred upon a biomaterial, it may cause implant failure, such as the case with corrosion of metallic and polyurethane leads in pacemakers [273]. However, depending on the mechanical properties of the implant, surface coatings, and drugs eluted, the inflammatory response can be minimized, allowing the biomaterial to exist in harmony with the immune system [274]. Of high importance is the relationship of the material to the surrounding tissue. That is, if a material is deposited into soft tissue, a soft biomaterial should be used, such as a hydrogel so as to reduce excessive tissue friction and motion. Likewise, rigid implant materials such as PMMA polymers or stainless steels are a better option for bone remodeling. While some surface roughness is desirable to reduce implant motion, excess surface roughness may induce implant erosion, leading to small particle debris further increasing immune response, fibrous capsule thickness, and therefore the chances of implant failure [275, 276]. For biodegradable materials, implant erosion is desirable, but the composition of degradation products must be chosen wisely so as to be non-cytotoxic. Popular examples of these cytocompatible biodegradable materials in clinical use are poly(lactic acid), poly(glycolic acid), and their co-polymers of poly(lactic-co-glycolic acid). Nonetheless, even these

cytocompatible materials produce degradation products that induce an oxidative stress response [153].

Systemically delivered nanomaterials may also be opsonized through white blood cell attack in circulation. This often occurs within seconds in circulation [277]. To avoid unwanted immune system interaction and increase circulation periods (if desired), nanoparticles have often been coated with molecules, such as the polymer polyethylene glycol (PEG). This effect is hypothesized to occur through inhibition of protein adherence via compression of hydrophilic PEG chains upon van der Waals attraction of proteins, whereby the new high energy state creates a repulsive force great enough to block adhesion [278]. However, a certain PEG density must be attained for PEG chains to stand on end in the "brush" configuration (which decreases surface area for opsonin adherence), and with at least a molecular chain weight of 2000 or greater for adequate blocking effects due to elasticity [161].

Since mitochondrial damage can cause oxidative stress feedback loops, mitochondrial health is an important factor in determining cytotoxicity of biomaterial degradation products. Seahorse Bioscience has produced an assay, Seahorse XF, which measures oxygen consumption rates [279]. Through subsequent additions of specific materials, respiratory measurements such as the maximum respiratory capacity, spare respiratory capacity, ATP production, proton-leak, and non-mitochondrial respiration all may be measured. Our group has utilized this method to compare cytotoxicity of materials, for instance finding that thiol-containing degradation products provided higher mitochondrial protection against oxidative stress than the same material oxidized to contain disulfide bonds [63].

3.4 Treatment of Inflammation and Oxidative Stress

There are many causes of acute inflammation for non-disease, injury-related conditions (e.g. tendinitis, back pain, contusions) in which common treatment practices involve administration of analgesics and/or anti-inflammatories to the patient. Most commonly, these are in the form of non-steroidal anti-inflammatory drugs (NSAIDs), such as the non-prescription drugs, ibufropen, acetylsalicylic acid, and naproxen. NSAIDs are popular for mild treatment due to being non-steroidal (non-habit forming) and non-narcotic (non-opioid). These function through cyclooxygenase (COX) inhibition of COX-1 and COX-2 and prostaglandin-endoperoxide synthases 1 and 2, which are used in prostaglandin and thromboxane synthesis (prostanoids) [264, 280]. Superficially, COX-1 generates prostanoids in system-wide tissues, while COX-2 produces prostanoids at the tissue site of inflammation [281]. While many NSAIDs are non-specific in COX inhibition, other common over-the-counter pain-relievers, such as acetaminophen, are only central nervous system COX-2 inhibitors, thus reducing pain, but not inflammation at the tissue site [282]. However, NSAIDs which inhibit both COX-1 and COX-2 show a greater extent of gastric complications compared to COX-2 selective inhibitors [281]. COX-2 also is implicated in cancer development due to on-site inflammatory response. While NSAIDs show a cancer preventative effect on colorectal cancers, due to COX-2 inhibition, their chemopreventive effects are not well established for other cancer types [283, 284].

A variety of diseases exist in which chronic inflammation is implicated, and reduction of oxidative stress is key to treatment. Treatment may vary from short to long-term NSAID or acetaminophen prescription for mild joint pain with osteoarthritis. Or for cases of extreme impairment, such as with rheumatoid arthritis, additional prescription of anti-

rheumatic drugs, such as methotrexate, the first line drug which shows multiple mechanisms of immune suppression [285]. These systems, however, are administered as non-targeted, systemic delivery systems. Drug delivery could be improved through delivering higher doses over an extended period to the tissue of relevance, without inducing unintended toxicity to other organs [286, 287]. Due to the minimization of cellular oxidation via glutathione intracellularly, thiol-based antioxidant delivery systems have been studied for the effect of increasing glutathione cellular concentrations. Unfortunately, glutathione is not readily taken up by cells, and remains in the bloodstream to be oxidized, excreted, or degraded into cysteine [288]. Cysteine, one of three amino acid building blocks for glutathione, may be delivered, but it is also rapidly oxidized as well and shows organ toxicity [289], but is useful in applications such as acetaminophen overdose in the form of N-acetyl-cysteine [290]. Our group has created disulfide based biomaterials which may be reduced to produce bound-thiols [63, 69]. When bound, or upon biodegradation of the material, these thiol groups show antioxidant effects, and have shown cytoprotection under oxidative stress conditions [63].

Another application using an antioxidant thiol-based treatment is the disease of radiation pneumonitis (RP). RP is a chronic inflammatory disease complication of the lungs due to scar tissue buildup after lung cancer radiation therapy. With roughly 10%-20% incidence, RP is a common side effect [291, 292]. As cells contain a very high water content, the effect of high energy radiation is ionization with formation of free radicals and ROS. While these are the driving force for the use of radiation therapy for the destruction of cancer tumors, they may cause undesirable side effects with healthy tissue contact. Of particular interest for the inhibition of RP onset, is the health of endothelial cells in lung capillaries.

Inflammatory response stems from endothelial cell signaling, and resulting damage from radiation therapy will trigger a cascade of events. Due to the acute inflammatory response, cell adhesion molecules and other inflammatory cytokines are upregulated on and around the cellular surface to recruit white blood cells and platelets, and the tight junctions between endothelial cells become more relaxed to allow extravasation [293, 294]. These neutrophils give off oxidative bursts, furthering the oxidative stress in the area. It has been observed that activated macrophages can be found within one hour of lung irradiation [295]. While the effect of this leukocyte transmigration may be beneficial for injury scenarios to reduce chance of infections, the inflammatory response of the lung has been shown to be widespread, and even in cases may occur also in the opposite lung of which was targeted. This describes the extent of non-beneficial oxidative stress, and the purpose for which radioprotectant drug delivery may be used in these situations. By quenching ROS in these extraneous areas through delivery of a radioprotectant, oxidative damage could be minimized, and lung function would be improved.

Perhaps the greatest challenge of all radioprotection is to not protect the tumor, utilizing a mechanism of differential treatment. This is why the controversial amifostine is the only FDA approved radioprotectant, for with its sulfur-protecting phosphate head group, it has been shown to readily cleave (leaving a free thiol head group) in the presence of alkaline phosphatase (AP) [296-298]. Further, it is claimed that there are reduced AP levels expressed only in cancerous tissues, whereas all normal tissues contain baseline levels. With this, if amifostine is near a tumor, it will not become free radical scavenger, whereas any other tissue, it will become a radioprotectant. While this drug may sound useful, it is used under the discretion of the oncologist, and is often not used [291, 292, 296, 297, 299-

304]. Amifostine causes undesirable side effects, such as hypotension and vomiting, which are often detrimental towards the treatment. Another confounding factor, however, which may elucidate the meager results of using amifostine is that AP is also present in the blood serum. Since amifostine is delivered as a free drug intravenously (IV), amifostine (WR-2721) is likely to turn into its free thiol form in the blood stream (WR-1065), perhaps describing both the high dose required, and side effects. Further, it has been shown that predominant uptake of this molecule is via the disulfide configuration (WR-33278), requiring oxidation, where it is then uptaken via a polyamine transporter, as the disulfide version is similar to spermidine, and further reduction within the cell to become active. Thus, there still remains a gap in lung cancer radiotherapy, where an endothelial cell-targeted drug delivery system could aid the patient's recovery in reduction of RP onset through radioprotection.

While inflammatory diseases and ageing incur oxidative stress on the cellular environment, systemic antioxidant delivery has been shown to be a double edged sword. Reviews of diet supplementation with antioxidants have shown no effect at low levels, and an increasing rate of mortality at higher doses [305]. One mechanism for this is that even though the antioxidant, vitamin E, can sequester free radicals, it also suppresses the tumor suppressor protein p53 [306, 307]. p53 is involved in tumor suppression through initiating apoptosis from faulty DNA repair, and thus the systemically lowered p53 levels may allow for increased cellular proliferation of tumors which would otherwise be apoptosed, posing a hazard for at-risk populations (e.g. smokers) [308]. Targeted antioxidant delivery methods are a promising field to control oxidative stress in specific tissues, while avoiding unintended systemic toxicities.

Due to the importance of NF-κB in the wound healing process and in cancer progression, molecules which suppress NF-κB expression have been studied for anti-inflammatory and anti-cancer treatment. One class of antioxidant molecules, which suppresses NF-κB expression and thus are also anti-inflammatory, are those of flavonoids, with examples such as curcumin, apigenin, quercetin, and resveratrol [309-311]. Similarily, targeted delivery methods may be required for successful treatments as NF-κB inhibition not only lowers inflammatory response, but also increases rates of leukocyte apoptosis, potentially harming normal tissues immune response [271].

3.5 Bacteria in Infectious Disease

Bacteria have persisted for over 3.7 billion years [312], evolving into a vast array of an estimated 10^7 to 10^9 species [313], with some living from the depths of the earth to the void of space. Bacteria have been co-evolving with the rise of eukaryotic species since their onset 1.8 billion years ago, as well as with *Homo* genus 2.8 million years ago, resulting in 37% of current *Homo sapiens sapiens* genes containing bacterial/archaeal homologs [314]. From 600-800 species of bacteria compose the oral cavity flora [315], with approximately 1000 more species composing the gut flora [316]. Although many of these bacterial species are beneficial and aid to crowd out pathogens, opportunistic infections are still a common occurrence. Across the world in 2012, these infections or diseases caused death from diarrhea (1.5 million deaths) to lower respiratory infections (3.1 million deaths) [242].

With the advent of the antibiotic era, prophylaxis against bacterial infection has progressed greatly from Ignaz Semmelweis's hand washing [317] to local and/or systemic

administration of antibiotics for routine injuries from a laceration to complex surgical procedures. For deep infection, wound treatment through IV and oral antibiotics requires from weeks to months of delivery to ward off infection in patients, if at all [318]. Sometimes severe wound infections can emerge in sites with limited blood perfusion, forming hard-to-eliminate biofilm infections. These biofilms often require antibiotic concentrations much higher than the minimum inhibitory concentration (MIC) of planktonic bacteria (Figure 3.4), thus requiring toxic concentrations [319]. To avoid this systemic toxicity while still treating the wound, it is common to follow systemic antibiotic delivery with local antibiotic delivery if the wound is serious, or chronic infection occurs [320, 321]. Additionally, in local antibiotic delivery, it is important to maintain an antibiotic concentration greater than the MIC of the targeted bacteria. *Staphylococcus aureus* has the ability to induce biofilm formation due to the presence of sub-MIC antibiotics, further establishing bacterial presence in the afflicted area. In the case of vancomycin and *S. aureus*, it has been shown that biofilm formation is up to four times greater with sub-lethal antibiotic delivery [322]. While local antibiotic delivery improves antibiotic access to the infection, it is at the cost of invasive surgery required for implantation into deep sites. Research into biomaterials for these purposes of efficient local antibiotic delivery is extensive, and biomaterials for these purposes have been used in practice for many years [323].

3.5.1 Antibiotics

Found as part of the natural bacterial skin flora on humans, *S. aureus*, has particular virulence in infection and is common in infection of open wounds, or causing such diseases as osteomyelitis, endocarditis, or sepsis before or due to surgery [324-326]. Treatment of

these infections is routine via antibiotics. Major antibiotic classes include those found in Table 3.4. Antibiotics may work through a variety of mechanisms of action to inhibit or kill bacteria (bacteriostatic or bactericidal respectively). For instance, the class of beta-lactam antibiotics mimic D-alanyl-D-alanine, the terminal amino acid residue on *N*-acetylmuramic acids and *N*-acetylglucosamines used in peptidoglycan synthesis. D-alanyl-D-alanine normally binds with DD-transpetidases (i.e. penicillin binding proteins) to complete cell wall synthesis. However, beta-lactams are competitive binders and inhibit the process. Other antibiotics such as vancomycin, a type of glycopeptide, work similarly through inhibiting cell wall growth. Conversely, glycopeptides competitively bind to D-alanyl-D-alanine to disrupt cell wall synthesis, opposite to the affinity of beta-lactams. Additionally, antibiotics typically work for gram-positive, gram-negative, or are broad-spectrum and inhibit both types of bacteria. Gram-positive bacteria contain a thick outer cell wall, whereas gram-negative bacteria contain a thin cell wall, surrounded by an outer membrane. Via a Gram stain test, bacteria which collect large amounts of crystal violet dye within the peptidoglycan layer are considered gram-positive. Beyond this, bacteria may also be classified as obligate aerobic, anaerobic, facultative anaerobes, aerotolerant, or microaerophiles which determines their preferred environment.

Table 3.1. Overview of common antibiotics via class and mechanism.

Class of Action	Mechanism of Action	Antibiotic Class	Examples	Activity*
Protein Synthesis Inhibiton	30S Inhibition	Aminoglycosides	Streptomycin	G-
			Gentamicin	
		Tetracyclines	Tetracycline	B
			Doxycycline	
Cell Wall Inhibition	Binds to Penicillin Binding Protein	Beta-lactams	Penicillins	
			Cephalosporins	
	Binds to D-alanyl- D-alanine	Glycopeptides	Vancomycin	G+
			Teicoplanin	
	Bactoprenol Inhibition	Polypeptides	Bacitracin	B
	Increased Permeability via LPS Surfactant		Polymyxin B	G-
Nucleic Acid Inhibiton	Topoisomerase Inhibitors	Quinolones	Ciprofloxacin	B
			Levofloxacin	
	Antifolates	Sulfonamides	Mafenide	B
			Sulfamethizole	
	RNA Synthesis	Rifamycins	Rifampicin	M
	DNA Inhibiton	Nitrofurans	Nitrofurantoin	B
		Nitro-imidazoles	Metronidazole	

* G+ gram-positive. G- gram-negative. B broad-spectrum. M antimycotic.

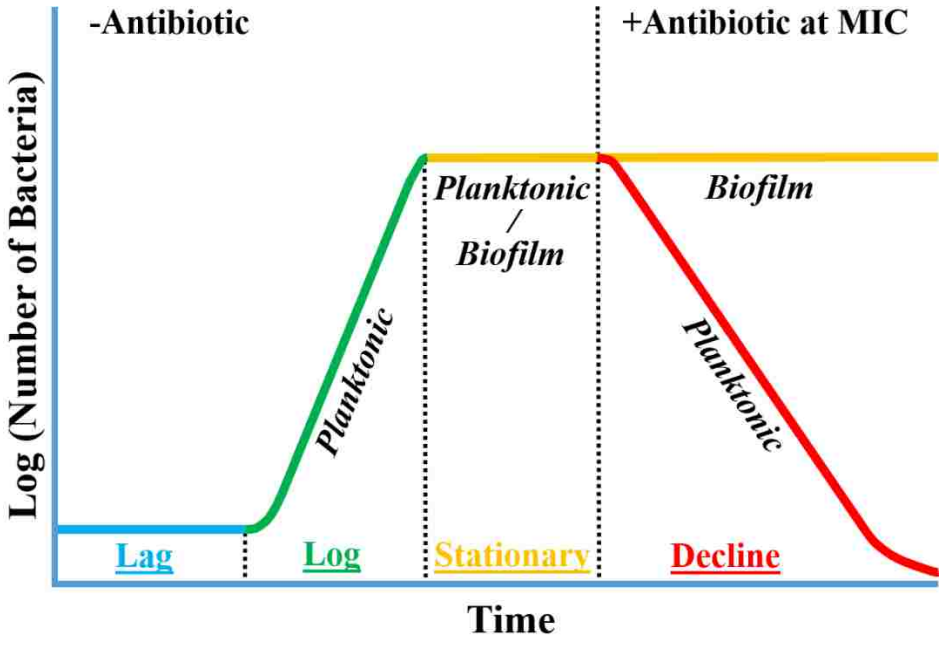

Figure 3.4. Log scale of the number of viable bacteria versus time. Bacterial binary fission typically occurs in four stages: 1) "lag phase" where growth is initially slow due to metabolic adaptation of the surrounding conditions, 2) "log phase" where growth follows an exponential increase in cell numbers due to uninhibited growth conditions, 3) "stationary phase" where bacterial numbers have reached a critical maximum concentration, usually due to nutrient limitation or depletion, and duplication equals cell death, and, if conditions are no longer cell supporting, whether it be severe lack of nutrients, acid build up, or environmental effects 4) "decline phase" where bacterial death is dependent upon the particular conditions. In this instance, the decline phase is induced by the presence of an antibiotic at the minimum inhibitory concentration (MIC) for the particular bacteria, and thus planktonic bacteria, with less resistance to antibiotic concentrations, declines in numbers whereas the biofilm remains viable.

3.5.2 Antibiotic Resistance Emergence

Where antibiotics provide essential treatment for many types of injuries as prevention or treatment from bacterial infection, non-discretionary or overuse may cause unintended ramifications, such as antibiotic resistance. For example, due to poor prison conditions, overcrowding, and low treatment compliance, Tomsk, Russia in the late 1990s had an outbreak of tuberculosis among inmates [327]. Between 1998 and 2002, the World Health Organization (WHO) implemented the directly observed treatment, short-course (DOTS) program to reduce rates of infection by ensuring antimycotic administration compliance. However, during that period rates of multi-drug resistant tuberculosis doubled for both the number of new cases, as well as previously treated cases. This was in part due to the lack of patient screening for antibiotic susceptibility before treatment, and treatment of patients already resistant to the first line drugs of rifampin and isoniazid. To address this, the WHO in combination with other institutions such as Partners in Health (PIH) ran drug susceptibility testing for each patient and administered personalized regiments of first and/or second line treatments with multiple antibiotics in parallel, dropping rates dramatically [327].

Increased rates of antibiotic resistance put the method of parallel drug treatment at risk, however. With slow progress at the pharmaceutical level due to the immense cost of drug development, the number of novel antibiotics with unique mechanisms of action created through the industry pipeline is not competing with the emergence of resistant bacteria to these antibiotics [9]. While traditionally combinatorial drug delivery of synergistic antibiotics has shown beneficial effects towards inhibiting bacterial resistance, with the advent of multi-drug resistance bacteria, these approaches are becoming less effective over

time [328, 329]. While technically any bacterial strain may become resistant to antibiotics, even without contact, several different bacterial species are at high risk due to their pathogenicity. The WHO has determined seven strains of importance: *Staphylococcus aureus*, *Escherichia coli*, *Klebsiella pneumonia* due to their propensity for hospital and community-acquired disease, and S*treptococcus pneumoniae*, Nontyphoidal *Salmonella*, *Shigella* species, and *Neisseria gonorrhea* for their community-acquired disease. While other bacteria may propose a higher health risk factor if infected, like multi-drug resistant tuberculosis, they are less widespread throughout the world and affect fewer patients [330]. One mode of resistance to antibiotics may occur when substrate specificity changes with mutation. For example, a common mode of resistance to vancomycin in gram-positive bacteria is where the bacterial synthesis of D-alanyl-D-alanine is replaced with D-alanyl-D-lactate, and thus there is no longer competitive binding and peptidoglycan synthesis is not inhibited. Other mechanisms may occur, such as diffusional barriers via increased crosslinking density of the cell wall, reducing the penetration of vancomycin—a large molecule of 1449 Da—at the site of cell wall growth in the inner peptidoglycan layer. This diffusional barrier to vancomycin is intrinsic in gram-negative bacteria due to the lipopolysaccharide (LPS) cell membrane layer, whereas the gram-positive bacterial exterior is made from low-density lipoteichoic acids upon the peptideglycan layer, and is permeable.

3.6 Biofilms, Oxidative Stress, and Antibiotic Resistance Emergence Treatment

Biofilms are naturally occurring bacterial structures that help protect colonies from unfavorable environmental conditions, such as presence of antibiotics, and help the colony proliferate. These biofilms can protect *S. aureus* from vancomycin with an increased MIC

from ten to thousands fold higher [331-333], dangerously reducing the ability for systemic antibiotics to work effectively. To form a biofilm, cells will attach to a surface and accumulate into an agglomeration through cell-cell adhesion, increasing the biofilm colony in size through division. Within these biofilms, quorum sensing may occur, which is the ability of many cells in a region to detect each other's presence and react as a group based on the concentration of auto-inducing molecules. This intercellular signaling turns on or off genes and allows biofilms to react as a community to changing conditions or population. For example, *Pseudomonas aeruginosa* evade initial immune detection through slow propagation in low numbers, and only begin to rapidly replicate in log-phase (see Figure 3.1) once a certain quorum sensed concentration is achieved, essentially causing a surprise attack to the immune system.

Naturally, biofilms show a highly increased mutation frequency when compared to planktonic bacteria [13], which aids in antibiotic resistance emergence. In aerobic bacteria, this is largely due to the nature of respiration where ROS such as hydrogen peroxide, hydroxyl radicals, and superoxide are endogenously produced, which can exhibit the effect of hormesis in bacteria [13, 334]. Namely, while sometimes helpful, the ROS concentration produced is high enough to form DNA lesions and can potentially either kill the bacteria, or produce genetic variance from a once homogeneous culture, especially in those cells with a negative DNA repair mutation.

Hydrogen peroxide has formative roots within the cell from dismutated superoxide via NADPH oxidases after respiration [335, 336]. Superoxide is highly reactive with iron-sulfur proteins, has a short life within the cell due to superoxide dismutase, and is not very cell membrane permeable, rendering it not very useful as a ROS signaling molecule. Once

superoxide is in the presence of SOD, it is catalyzed into hydrogen peroxide. Hydrogen peroxide also reacts with iron-sulfur cluster-containing proteins to participate in the Fenton reaction to produce hydroxyl radicals, but otherwise it is less reactive than the other ROS formed and can thus play as an extracellular signaling molecule since it can be permeable through the cell membrane [335].

Sub-lethal application of certain antibiotics upon planktonic cultures of *S. aureus* can induce a mutagenic affect through DNA mutation through additional ROS formation once the bacteria stops normal function [10, 11]. Being highly clinically relevant, this effect has been touched upon in research to be a factor in causing antibiotic resistance emergence in chronic infections where lengthy antibiotic application is utilized on the patient. This is an effect that may also be induced simply through addition of an oxidizing species, such as hydrogen peroxide, where both show attenuation through simultaneous application of an antioxidant [10, 11].

While frugal antibiotic use and/or prescription may cut back on resistance emergence, determining methods to deliver antibiotics without the concern of resistance is an important field of study. Methods such as finding antibiotics which do not tend to form resistance (e.g. peptides like defensins which aid killing of phagocytosed bacteria via cationic membrane disruption) are a promising field, but due to their difficulty in drug delivery, and elevated importance of these in human innate immune response infection control, continuing research is required [337-339]. An alternate route of reducing resistance emergence is to change the bacterial mechanisms by inhibiting their function. Of importance to our studies, hydrogen peroxide disruption may affect *S. aureus* biofilm

function through inhibition of quorum sensing and mutagenic effects, although literature is preliminary on the effects [13, 340].

3.7 Conclusions

There is an inexorable relationship between oxidative stress, immune response, infection, and their respective diseases. Through understanding the mechanisms of infectious and oxidative stress disease, scientists have been able to create boundless strategies for disease treatment. Although multidrug resistant bacteria are on the rise, so is research involving clever new small molecules and biomaterial drug delivery systems to solve this problem. In a similar light, oxidative stress disease treatment has been developing steadily as well. With high levels of primary research in controlled drug delivery to specific tissues and molecules involved in immune response, oxidative stress disease treatment outcomes may become increasingly favorable in the future.

Chapter 4. Antibiotic and Antioxidant Delivery for Control of Local Infection and Antibiotic Resistance

4.1 Introduction

The combined impact of infection and oxidative stress related injuries may be treated with local antioxidant protein therapy alongside other traditionally used small molecule antibiotics. Operations with open wounds or surgeries with risk of bacterial biofilm infection, e.g. osteomyelitis and mediastinitis, create a serious threat to patient health, and thus prophylactic or re-operative administration of multiple drugs systemically and locally are commonly used in treatment. However, management of wound site infections has become increasingly complicated by the emergence of antibiotic resistant bacterial strains [341-346]. Regardless of whether resistant infections are a result of primary infection with an already resistant strain or a result of *de novo* emergence of resistance within the patient, the existence of these strains is the natural result of evolutionary pressures placed upon the bacteria as a result of antibiotic usage. Any new antimicrobial strategy that does not employ mechanisms to suppress this emergence of resistance is effectively just a “stop-gap” measure in the battle against wound infections.

In order to prevent adaptation within a population, evolutionary engineering principles developed in HIV antiviral therapy should be employed [347]. Primarily, multiple stress mechanisms that work in an independent (orthogonal) fashion can adjust the evolutionary fitness landscape to make adaptation unlikely [348-350]. Recent studies on development of resistance within *P. aeruginosa* strains demonstrated an accelerated rate of strain variation within the population [340, 351]. Even for populations developed from a single bacterium, it was found that this increase in variation was stimulated by endogenous

oxidative stress from the environment and was suppressed *in vitro* by administration of various antioxidants. This generation of reactive oxygen species (ROS) can be produced in biofilms due to a redox imbalance in biofilms [352], sub-lethal antibiotic pressures [353, 354] which can activate the SOS response [353, 355-357], as well as deactivate several anti-ROS genes, such as *katA* which produces the antioxidant enzyme catalase [340, 358-360]. Through poor repair of DNA and RNA lesions in an aerobic environment [361, 362], this lack of ROS protection can lead to genetic frame-shifts and the bacteria may become multi-drug resistant through radical-induced mutagenesis [10, 11, 324, 363, 364].

This ability to rapidly diversify during colonization and film formation combined with the suboptimal delivery of antibiotics to bone tissue form the ideal conditions for creating antibiotic resistant infections. Thus, bone infections are a situation where this reemergence is likely to occur. Local treatment provides a practical approach of achieving effective dosing while providing a means of reducing adverse systemic effects [20]. However, various clinical evaluations have demonstrated that due to the concentration gradients established and insufficient low level activity, local release can promote strain resistance [20, 365]. It is possible that local antibiotic delivery coupled with the ability to suppress bacterial diversification may overcome this drawback to localized delivery. One such strategy is the co-delivery of vancomycin with the antioxidant enzyme, catalase, which is an enzyme that can convert the pro-diversification signal, hydrogen peroxide, into oxygen and water. Catalase has one of the highest turnover numbers (k_{cat}) of all of the enzymes, making it an ideal candidate to decrease endogenous oxidative stress within bacterial species. It has been used in many polymeric applications for the purpose of reducing oxidative stress [97, 366, 367]. However, as oxidative stress plays an important role in

antimicrobial actions [368], it is not clear if this co-delivery would attenuate the antimicrobial effects.

Often it can be beneficial to deliver molecules in tandem from an implantable biomaterial. However, the delivery of a small molecule alongside a large molecule (e.g. protein) represents a significant drug delivery challenge. This is due to the vast size difference of small molecule drugs and proteins (2-3 orders of magnitude), making extended release of each from a single biomaterial a difficult task. In the design of a drug releasing hydrogel, it is the interaction between the drug being released, material composition, and structural arrangements which dictates the kinetics. Through variation of hydrophilic and hydrophobic bulk hydrogel content, and mesh size, drug diffusion rates readily change. Further, the rate of biodegradation can greatly influence release rates through systemic increase in mesh size. Therefore, we sought to create a biodegradable hydrogel readily tuneable in composition properties so as to facilitate release of both small and large molecules.

Poly(β-amino ester) hydrogels, a class of cross-linked hydrophilic polymers that are known for their soft tissue-like properties [369-371] and for their applications in drug delivery [372, 373], can be formulated *in situ*, providing an ideal vehicle for drug delivery to especially irregular, hard to treat areas [371]. Further, PBAE hydrogels were selected as a test platform due to widely tuneable degradation rates [374]. Linear chain macromers were chosen based on their characterized degradation properties, stemming from their hydrophilic/hydrophobic polymer composition [374]. These vancomycin and catalase co-loaded PBAE macromers were polymerized into hydrogels using a free radical polymerization method. Loaded hydrogels were characterized for their activity towards

H_2O_2 reduction and *in vitro* degradation and release properties. *Staphylococcus aureus*, a gram-positive bacteria common in infection and found in skin flora, was used to test the vancomycin activity [329, 375].

4.2 Materials and Methods

4.2.1 Materials

All reagents were used as received. *O*-phenylenediamine (OPD), ammonium persulfate (APS), trimethylethylenediamine (TEMED), and isobutylamine (IBA) were purchased from Sigma–Aldrich (St. Louis, MO). Bovine liver catalase (242,000 M_W) and horseradish peroxidase (HRP) (44000 M_W) were purchased from Calbiochem (EMD Biosciences, San Diego, CA). Poly(ethylene glycol) 400 diacrylate (PEGDA) and diethylene glycol diacrylate (DEGDA) were purchased from Polysciences, Inc. (Warrington, PA). All other reagents and solvents were purchased from Sigma–Aldrich.

4.2.2 Macromer Synthesis

The base polymer is formed through combination of two basic components, an acrylate and an amine. The acrylates used were PEGDA and DEGDA, and the amine used to participate in Michael addition was isobutylamine. These were previously formulated into the naming scheme of A = DEGDA, H = PEGDA, 6 = IBA according to [5, 372]. To form the AH6 poly(β-amino ester) macromer used in these experiments [376], diethylene glycol diacrylate and poly(ethylene glycol) 400 diacrylate were added to a flask in a 3:1 molar ratio and heated to 85°C, after which isobutyl amine (IBA) was added in a 1.2:1 molar ratio of diacrylate to amine and let to react for 24 hours under constant stirring. The H6 and A6

macromers were synthesized by reacting the corresponding diacrylate and amine (IBA) for 48 and 16 hours, respectively, in a similar method as reported previously (Figure 4.1 A) [71, 372]. In both the cases, a 1.2:1 molar ratio of diacrylate to amine was used. All macromers were stored at 4˚C until further use.

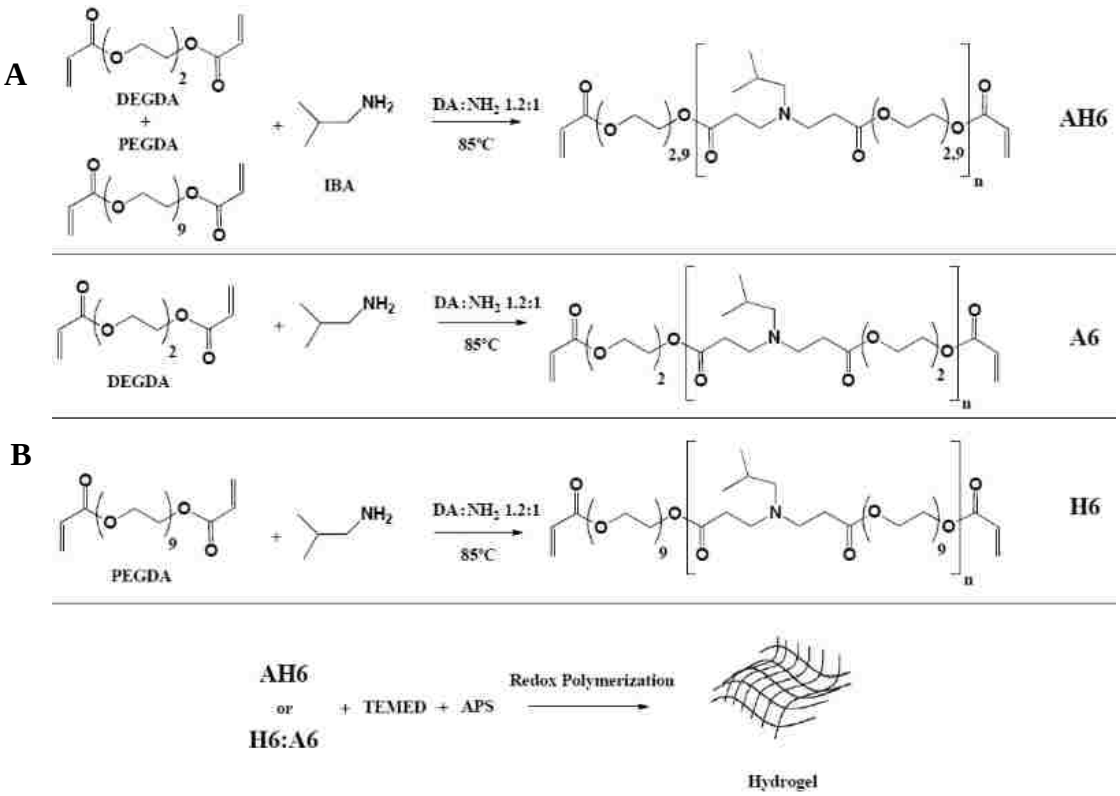

Figure 4.1. Reaction scheme of A) macromer synthesis and B) hydrogel synthesis.

4.2.3 Hydrogel Synthesis

Hydrogels were synthesized from PBAE macromers using free radical polymerization. Both the hydrogels utilizing varying wt% of H6 and A6 macromer and AH6 macromer were formed using the same polymerization procedure (Figure 4.1 B). Approximately, a total mass of 1 g of H6 and A6 macromers were weighed and mixed. APS was used as a free radical initiator, and TEMED was used as an accelerator/catalyst. About 1.5 wt% (based on total macromer weight) of DI water was mixed into 1.5 wt% (based on total macromer weight) APS. Finally, 0.5 wt% (based on total macromer weight) of TEMED was added to the macromer followed by addition of the APS solution. The reaction mixture was mixed and transferred to a closed rectangular mould, formed between two glass plates separated by 1.5 mm Teflon moulds, and wrapped in paraffin film. The reaction was continued at room temperature overnight to ensure maximum polymerization. The hydrogels were cut into 7 mm diameter x 1.5 mm thick discs for both the degradation and release studies.

Catalase loaded PBAE hydrogels were synthesized in a similar method as explained above. However, 0.1 wt% of catalase (based on total macromer weight) was dissolved in 1.5 µL DI H_2O/mg enzyme and thoroughly mixed into the macromer mixture before addition of APS and TEMED. Vancomycin loaded PBAE hydrogels were synthesized similarly, but 1.5 wt% vancomycin (based on total hydrogel mass) was directly mixed in with the macromers. Co-loaded vancomycin plus catalase hydrogels were synthesized by combining the two previous techniques.

4.2.4 Degradation

In order to study the degradation properties of different PBAE hydrogels, the hydrogel samples were incubated at 37 °C in phosphate buffer saline solution (PBS) (pH=7.4), and the mass loss was recorded at different time points. After recording the initial mass of the dry hydrogel discs, samples were placed in centrifuge tubes with PBS equilibrated at 37˚C. At each time point, the discs were taken out from PBS and freeze dried. The PBS of the remaining samples was replaced with fresh solutions to maintain sink conditions.

4.2.5 Catalase Release

Catalase was radiolabeled with $Na^{125}I$ (Perkin Elmer, Boston, MA) using the Iodogen (Pierce Biotech., Rockford, IL) method, and unbound iodine was removed from the protein using gel permeation chromatography (Bio-spin 6 Columns, Bio-Rad Labs, Hercules, CA). Conditions were set based upon manufacturer's recommendations. ^{125}I-catalase-loaded PBAE hydrogel discs were degraded at 37˚C in 2 mL of PBS. Loaded hydrogels were degraded, and at each time point, the supernatant was removed. The ^{125}I concentration of the supernatants and hydrogel discs were counted using a Perkin-Elmer 2470 Wizard^2 Automatic Gamma Counter.

4.2.6 Vancomycin Release

Hydrogels loaded with 0.1 wt% catalase and/or 1.5 wt% vancomycin were degraded over a period of 7 days. At each time point, the supernatant was collected and replaced with fresh 10 mM PBS, pH 7.4. Vancomycin concentration was determined by reverse-phase high performance liquid chromatography (HPLC, Shimadzu Prominence) in 14%

acetonitrile/86% of 1% TFA water using a 150 X 4.6 mm Luna column (Phenomenex, Torrance, CA), calibrated using vancomycin standards. Vancomycin was detected using a Shimadzu UV-Vis detector at a wavelength of 280 nm.

4.2.7 Catalase Activity

Catalase activity of formed hydrogels was monitored directly by measuring hydrogen peroxide concentration as a function time. Briefly, 1 mg catalase-loaded hydrogel samples (n=3) were put in 1 mL of 10 mM H_2O_2 and allowed to react under constant mixing. Aliquots of 100 µL were collected at various time points, diluted 10x, and then three 100 µL aliquots of this dilution were added to a 96-well plate. Both 100 µL of a 0.4 mg/mL OPD working solution and 20 µL of 138 µg/mL HRP were added to each well. The concentration of OPD product was determined by measuring absorbance at 490 nm using a UV-visible spectrophotometer (Varian Cary 50 MPR). The concentration was compared to a calibration curve prepared with different concentrations of H_2O_2. The slope to report activity was calculated by (10 mM – conc. @ 20 min) / 20 min.

4.2.8 Antimicrobial Activity Studies

The Kirby-Bauer (KB) disc diffusion test was used to determine the antimicrobial activity of vancomycin released by hydrogels [375]. *Staphylococcus aureus* (ATCC 25923) was used as the test organism in this study. For seeding blood agar plates, 80 µL of an initial 0.5 OD_{600} culture was added to 5 mL of DI H_2O, and a 100 µL volume of diluted culture was spread on each plate for an approximate total count of 10^5 bacteria. Hydrogels with 1.5 mm thickness were cut to 7 mm discs, and discs were overlaid onto *S. aureus* seeded

blood agar plates. As a control, sterile Whatman #1 filter paper discs (Sigma, St. Louis, MO) of the same size loaded with varying amounts of vancomycin were used as a calibration. *S. aureus* was allowed to grow on blood agar plates for 24 h at 37ºC in 5% CO_2, after which zones of inhibition were measured. Disc diffusion tests were repeated every 24 hours using the same hydrogels as described above and zones of inhibition measured.

4.3 Results

4.3.1 Macromer and Hydrogel Synthesis

Macromers were synthesized using a Michael addition type reaction (Figure 4.1) with the acrylate groups in slight excess. This retention of double bonds permitted the subsequent free radical polymerization reaction that was used to crosslink the macromers. Free radical polymerization was used so as not to disrupt the enzymatic payload via other polymerization methods which could quickly denature proteins [377].

4.3.2 Hydrogel Degradation

To assess the ability to control the degradation rates of our hydrogels, *in vitro* degradation was carried out in PBS at 37˚C. As a preliminary study for testing the tunability of the hydrogel systems, a degradation rate pertinent to the range of wound-healing drug delivery devices was targeted. Hydrogels with a 75:25 (wt:wt) ratio of H6:A6 degraded in a period of 7 days, and showed two degradation phases (Figure 4.2 A). The 60:40 and 50:50 H6:A6 hydrogels degraded at a slower rate, with the 50:50 system degrading the slowest of the H6:A6 hydrogels. Compared to the co-macromer hydrogels (H6:A6), the monomacromer

hydrogels (AH6) produced a more uniform degradation profile, without the burst degradation found with the H6:A6 hydrogels (Figure 4.2 A).

4.3.3 Catalase Release

Catalase release was measured under sink conditions through ^{125}I-catalase tracing in both the hydrogels and supernatant. Hydrogels formed with AH6 or 60:40 H6:A6 macromers were co-loaded with catalase and vancomycin. Figure 4.2 B illustrates catalase release obtained from the supernatant and was confirmed by the radioactive counts remaining in the gel. There was an increased initial rate of catalase release of slightly over 20% in the first day for AH6, followed by a more sustained release pattern, which may in part be due to unbound ^{125}I being released from the gels (unbound ^{125}I content was calculated at 23%, as expected for catalase labeling). After 19 days, both the AH6 and H6:A6 hydrogels completely lost structural integrity and gained surface area for increased hydrogel degradation and subsequent release.

4.3.4 Vancomycin Release

Vancomycin release was highly dependent upon the macromer system employed. The 60:40 H6:A6 hydrogels released vancomycin more rapidly than did the AH6 hydrogels over a seven day period (Figure 4.2 C). As mesh size increased due to degradation of the hydrogel, catalase was retained much longer than vancomycin. Catalase is a much larger molecule (250 kDa) and thus was more tightly bound in the hydrogel network, while vancomycin (1.5 kDa) can more freely diffuse. Utilizing a vancomycin calibration curve (Figure 4.2 C inset), it can be seen that the total amount of vancomycin released did not

match the total loading of vancomycin in each hydrogel (Figure 4.2 D). This is possibly due to the nature of the hydrogel synthesis in which some vancomycin was deactivated through the redox reaction.

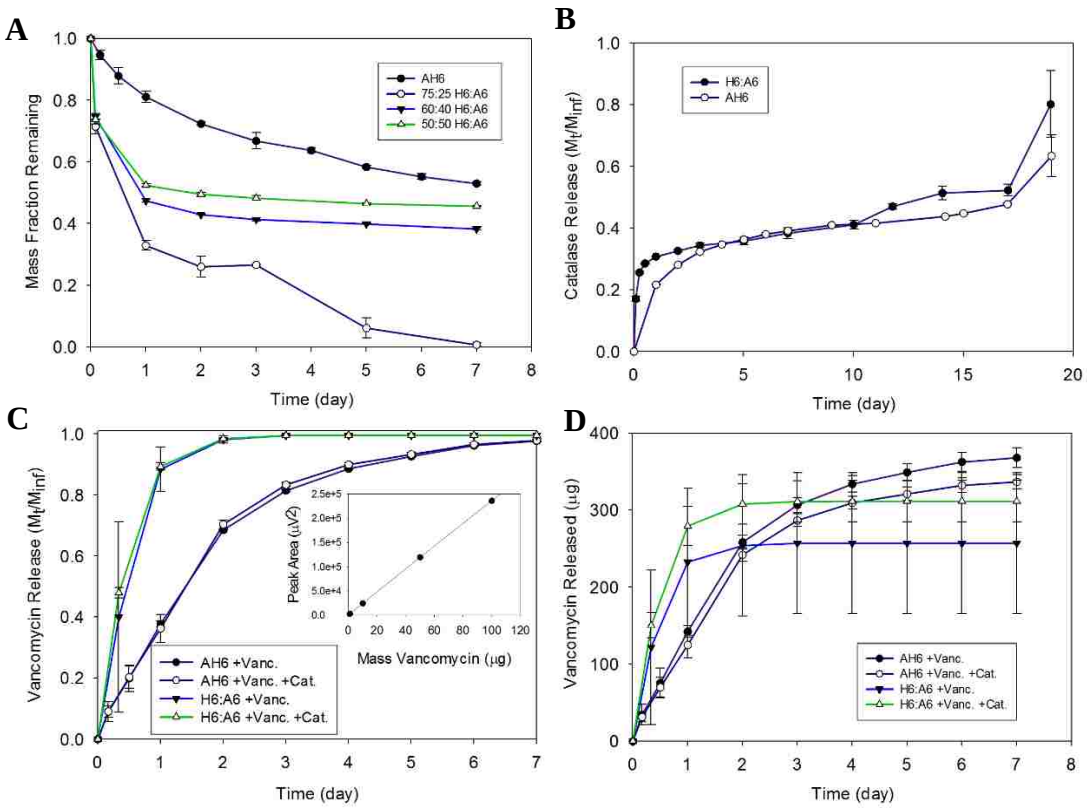

Figure 4.2. Drug release kinetics. A) Mass loss degradation profile comparison of hydrogels (n=3, standard deviation). B) Radiolabeled 125-I catalase release profiles in a PBS sink of 60:40 H6:A6 and AH6 (n=3, standard deviation) hydrogels. C) Vancomycin release profiles in PBS Sink with 60:40 H6:A6 and AH6 hydrogels. Inset in C) vancomycin HPLC calibration curve using standard samples in PBS. D) Vancomycin mass drug release from 7 mm x 1.5 mm hydrogel discs found via HPLC. n=3, standard deviation.

4.3.5 Catalase Activity

Catalase activity in hydrogels was directly measured by monitoring H_2O_2 degradation. Catalase loaded, vancomycin-loaded, catalase and vancomycin co-loaded, and control hydrogels were synthesized for activity studies. Enzymatic activity was determined assuming first order H_2O_2 degradation kinetics and is reported as units of catalase (1 U = 1 μmol H_2O_2 consumed per minute). Catalase loaded hydrogels displayed an ability to degrade H_2O_2 (Figure 4.3 A).

4.3.6 Vancomycin Activity

As antioxidants may elicit undesired bacterial protective effects by countering naturally occurring antibiotic oxidation [368], it was not clear if loaded catalase would inhibit the activity of vancomycin. Kirby-Bauer assays were carried out to evaluate the effectiveness of the vancomycin loaded hydrogels. Loaded and unloaded hydrogels (60:40 H6:A6 and AH6) were exposed to *S. aureus* inoculum, and the bacteria were incubated for 24 hours. Hydrogels that were not loaded with vancomycin did not show any inhibitory effects on the culture, exhibiting diameters equivalent to the hydrogel disc (Figure 4.3 B). Hydrogels loaded with vancomycin showed a large zone of inhibition, and importantly, catalase displayed no inhibitory effect on vancomycin activity in either system. Since the 60:40 H6:A6 hydrogels have a greater burst release than the AH6 hydrogels, the initial zone of inhibition was larger.

4.3.7 Vancomycin Activity Time Course

After the retention of vancomycin activity was confirmed, it was necessary to determine

whether the loaded hydrogels could present prolonged antimicrobial effects. Consequently, the zone of inhibition was measured as a function of time. Since unloaded control and catalase-only loaded hydrogels did not provide any antimicrobial function (Figure 4.3 B), evaluation was possible via the antimicrobial effect based on vancomycin activity. After four days and nine days of serial addition of the hydrogels to newly seeded *S. aureus* blood agar plates for the 60:40 H6:A6 and AH6 hydrogels, respectively, the zone of inhibition was reduced to the diameter of the disc itself (Figure 4.3 C). Both vancomycin loaded and vancomycin-catalase co-loaded hydrogels displayed similar vancomycin release activity.

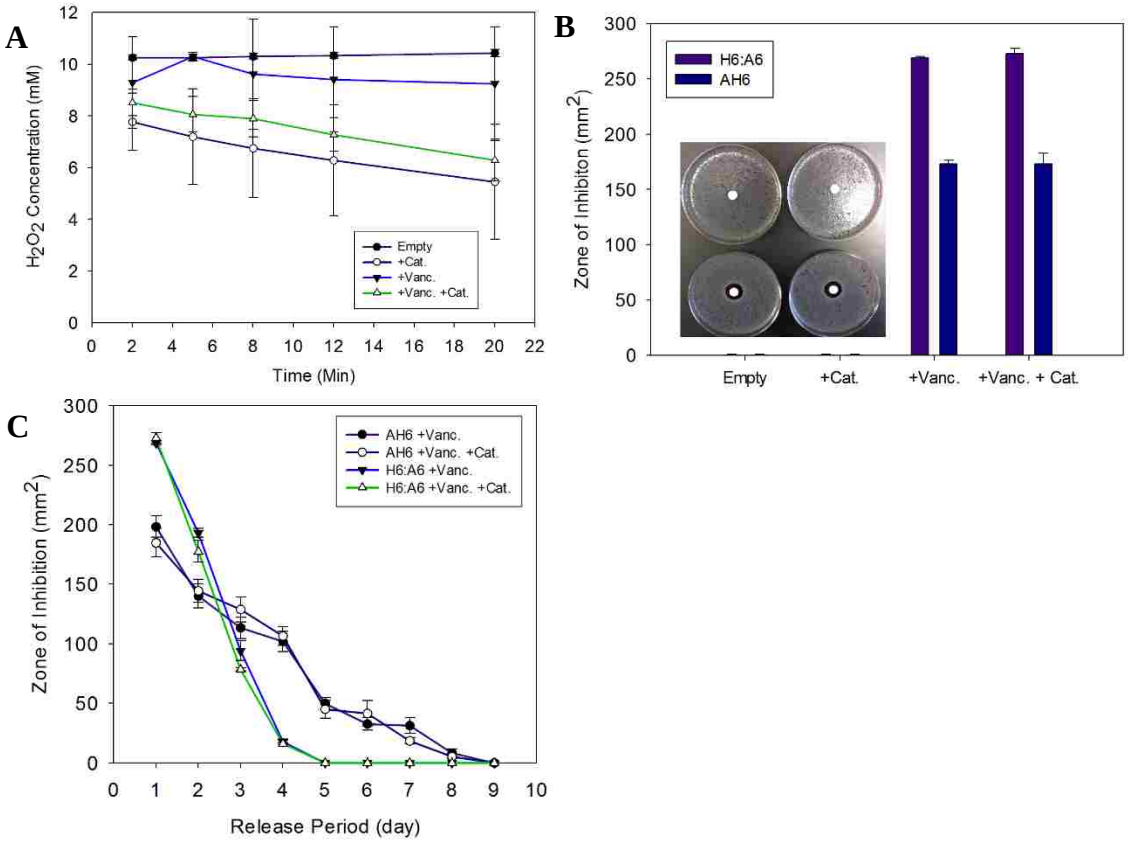

Figure 4.3. Activity of drug release. A) H_2O_2 concentration as a function of time with 60:40 H6:A6 hydrogels (n=4, standard deviation). B) Zone of inhibition areas at the initial time point. Inset of B) visual representation of Kirby-Bauer zones of inhibition on S. aureus agar plate. Upper left, empty; upper right, +Cat; lower left, +Vanc.; lower right, +Vanc. +Cat. The concentration of catalase and vancomycin used for both B) and inset of B) in AH6 (n=6, standard deviation) and 60:40 H6:A6 (n=3, standard deviation) hydrogels was 0.1 wt% and 1.5 wt% respectively. C) Zone of inhibition over time using 0.1 wt% catalase and 1.5 wt% vancomycin in both AH6 (n=6) and 60:40 H6:A6 (n=3, standard deviation) hydrogels.

4.4 Discussion

The macromers used in this study were selected for their tunable rate of degradation, allowing for a variety of degradation and release profile customizability [374]. Due to H6 (PEGDA and IBA) being more hydrophilic than A6 (DEGDA and IBA) due to its greater ethylene glycol content, this explains the observed increase in the degradation rate with increasing H6 content [374]. Of hydrogels formed, the initial degradation phase was proportional to the H6 content of the hydrogel, suggesting that the initial degradation phase could be a result of the loss of the H6 macromer content of the hydrogel network. The more hydrophilic portion enhanced aqueous interaction allowing increased swelling and degradation of the A6 networks. The more hydrophobic properties of these systems with increased A6 content shields ester bonds from hydrolysis, thereby resulting in slower degradation, as has been previously observed [378].

In order to alleviate this biphasic degradation profile, a monomacromer approach (AH6) was used to synthesize the hydrogels. This combined macromer possessed a more uniform distribution of PEG chains, resulting in a more uniform degradation rate (Figure 4.2 A) due to reacting the PEGDA and DEGDA together into a single macromer. Similar to the degradation profile changes, the slowed vancomycin release with AH6 compared to the co-macromer system is likely due to the homogeneity of the PEG chains in the AH6 system versus the heterogeneous H6:A6 hydrogels [376]. To this effect, vancomycin release was significantly extended and burst release reduced.

Catalase release, on the other hand, was sustained for a much longer period for both systems (19 days), likely due to the large molecular weight protein becoming entrapped in

the polymer network. This is demonstrated at the 7 day point with the 60:40 H6:A6 hydrogel degradation profile and catalase release, where degradation has produced a ~60% mass loss, whereas the catalase released ~40% in a similar trend as the bulk degradation profile. Similarly, the AH6 hydrogels produced ~50% mass loss and also showed ~40% catalase release over 7 days, without the initial burst in either catalase release nor hydrogel mass loss that the H6:A6 hydrogels produced. Interestingly, catalase-loaded gels possessed approximately 0.2 U/mg polymer, which is close to the same order of catalase activity achieved with other catalase/polymer formulations that possessed therapeutically relevant *in vivo* effects [97, 379]. While the application and form are different, this work supports the notion that levels of activity and loading already achieved are likely to be functionally significant.

The vancomycin activity time course on *S. aureus* on agar plates showed extended activity rates compared to PBS release. This extension of release was likely due to less aqueous interaction on the agar plates compared to PBS sink conditions. Nonetheless, The AH6 system showed superior release and degradation properties, allowing for a time period of vancomycin activity that is biologically relevant. The AH6 delivery system shows promise as a method of tandem delivery of both small and large molecules, and is without significant degradation or denaturation of the cargo tested due to any side effects of chemical free radical polymerization for *in situ* capable delivery.

4.5 Conclusions

Catalase and vancomycin were successfully loaded into poly(β-amino ester) hydrogels. These hydrogels exhibited tuneable degradation according to macromer ratio due to

hydrophilicity and hydrophobicity of the H6 and A6 macromers, respectively, as well as through macromer synthesis route. H6:A6 hydrogels degraded in two phases, with the H6 fraction degrading in the first phase, and AH6 hydrogels degraded in a single phasic manner perhaps due to a single macromer being used instead of co-macromers. Catalase retained activity in loaded hydrogels, and the activity was not inhibited by the presence of vancomycin.

Hydrogels loaded with vancomycin demonstrated the ability to inhibit *S. aureus* growth, showing viable vancomycin activity unaffected by the presence of catalase. Vancomycin encapsulation in poly(β-amino ester) hydrogels allowed for extended inhibition of bacteria due to controlled release. These results indicate that this hydrogel system may potentially be effective *in vivo*. The higher initial burst release of vancomycin in each hydrogel system can inhibit bacteria in a larger area initially and then locally sustain release for an extended period in the target region. These drug delivery systems will help to provide a means for tuning the co-release of large molecules with small, and potentially reduce risk of antibiotic resistance emergence in biomedical applications of infection and oxidative control.

Chapter 5. Synthesis and Characterization of an Antibacterial Hydrogel Containing Covalently-Bound Vancomycin

Based on the research article:

> Andrew L. Lakes, Rebecca Peyyala, Jeffrey L. Ebersole, David. A. Puleo, J. Zach Hilt, Thomas D. Dziubla. *Synthesis and characterization of an antibacterial hydrogel containing covalently bound vancomycin.* Biomacromolecules, 2014. **15**(8): p. 3009-18

5.1 Introduction

Traditionally, suppression of infection in severe wounds (e.g., combat trauma and motor vehicle accidents) is obtained through a prolonged course of intravenous and oral antibiotics requiring from multiple weeks to months of delivery to combat infection in the patients [318]. Despite these efforts, severe infections can emerge as a result of limited blood perfusion, as is the case with osteomyelitis, thus forming hard-to-eliminate biofilm infections that require potentially toxic concentrations of antibiotics [319]. To avoid this toxicity while still treating the wound, systemic antibiotic delivery is supplemented with local delivery [320, 321]. While local antibiotic delivery improves antibiotic access to the infected tissues, it is at the patient risk for invasive surgery required for implantation. Additionally, if a non-biodegradable implant, such as poly(methyl methacrylate) (PMMA) is used (as is current medical practice [17-19]), an additional follow-up extraction surgery is needed to remove the implant. Furthermore, non-biodegradable implants may create a solid anchorage point for bacterial adherence that interferes with the host's immune defenses, allowing for accretion and further distributed infection [20-22]. From these implants, drug release shows a large initial burst, followed by a very slow release, often below the minimum inhibitory concentration (MIC) for the infection agent [23-25]. As

such, research involving biodegradable drug delivery systems for the sustained release of antibiotics is increasing. In practice, however, biodegradable hydrogel and non-hydrogel drug delivery systems have shown little clinical success in preventing severe wound infections due to various issues, such as burst release of drug, host response with local inflammation and fibrous capsule formation, etc. [380, 381].

Research involving the controlled antibiotic release from degradable materials, including the use of bone cements [382-384] or synthetic polymers such as polyesters, have shown some improvement for antibiotic delivery [18, 319]. Yet, despite clever and effective approaches at slowing drug release (e.g. drug/polymer affinity based systems [385], or multilayered hybrid composite materials [386, 387]), there remains a significant burst release that makes matching degradation and release challenging. Through more closely coupling these two parameters, it may be possible for the scaffold to be completely degraded when the drug release falls below the bacterial MIC.

One way to couple drug release to degradation is through covalently linking an antibiotic into the degradable polymeric backbone. In this work, we sought to develop a drug delivery system in which we could engineer around those problems using poly(β-amino ester) (PBAE) hydrogels. These hydrogels can contain significant water content from swelling, and their highly cross-linked structure provides tissue-like properties, which make them useful for soft-tissue applications. These variable properties enable the physical capture of large molecules and allow for modification of hydrogels in numerous ways for application specific drug delivery [48]. The PBAEs used in this work hydrolyze into degradation products in biological systems over time, have tunable chemistry to allow modification of degradation rate through manipulation of hydrophobic:hydrophilic monomer and

macromer ratios affecting drug release rates for future potential with personalized medicine, and are formable *in situ* to treat irregular wounds. A previous publication of a similar PBAE hydrogel indicated cytocompatibility of small molecular weight degradation products [378]. With the intention of coupling the drug release rate and bulk degradation rate, vancomycin was covalently incorporated into the backbone hydrogel structure. This was performed by utilizing free primary amine sites on vancomycin in conjunction with PEG and DEG diacrylates. By adding vancomycin directly into the backbone of the macromer, the degradation rate of the ester bonds adjacent to vancomycin will be the limiting factor determining the release rate.

5.2 Materials and Methods

5.2.1 Reagents

Poly(ethylene glycol MW=400) diacrylate (PEGDA) and diethylene glycol diacrylate (DEGDA) were purchased from Polysciences Inc. (Warrington, PA), where vancomycin hydrochloride was purchased from PhytoTechnology Laboratories (Shawnee Mission, KS). Sodium ^{125}I was purchased through Perkin-Elmer (Waltham, MA). EGM-2 cell media and HUVEC were purchased through Lonza (Hopkinton, MA). Calcein AM was obtained from Life Technologies (Grand Island, NY). Ammonium persulfate (APS), tetramethylethylenediamine (TEMED), and isobutylamine (IBA) and other reagents were purchased from Sigma-Aldrich (St. St. Louis, MO). All reagents were used as received, unless otherwise stated.

5.2.2 PBAE Macromer Synthesis

All hydrogels were formed with a two-step synthesis: first a linear chain macromer was formed with acrylate end caps, and then polymerized into a hydrogel via free radical polymerization. PBAE macromers were synthesized based upon previously published methods [71, 378]. Briefly, macromers were first synthesized by Michael-Addition of diacrylates with isobutylamine and/or vancomycin, at 75ºC for 16 to 48 hours depending on synthesis starting materials. A deep orange color change was noted during the reaction. For all macromer syntheses, the ratio of diacrylate:amine was held constant at 1.2:1 to allow macromer end groups to be capped with acrylates. Figure 5.1 illustrates the synthesis scheme for the vancomycin PBAE hydrogel.

5.2.3 PBAE Macromer Characterization

Gel permeation chromatography (GPC) was used to determine number average molecular weight (M_n) and polydispersity index (PDI). High performance liquid chromatography (Shimadzu Prominence) with a Waters 2410 refractive index detector was used with two Resipore GPC columns (Agilent Technologies, Santa Clara, CA) running 100% tetrahydrofuran, using Agilent EasiVial as molecular weight standards. Fourier transform infrared spectroscopy (FTIR) was used to quantify carbonyl (C=O) and carbon double bonds (C=C) within samples of either starting materials, macromers, or hydrogels. Conversion was calculated via the division of the C=C / C=O ratio of either macromer or hydrogel, by the C=C / C=O ratio of the starting materials.

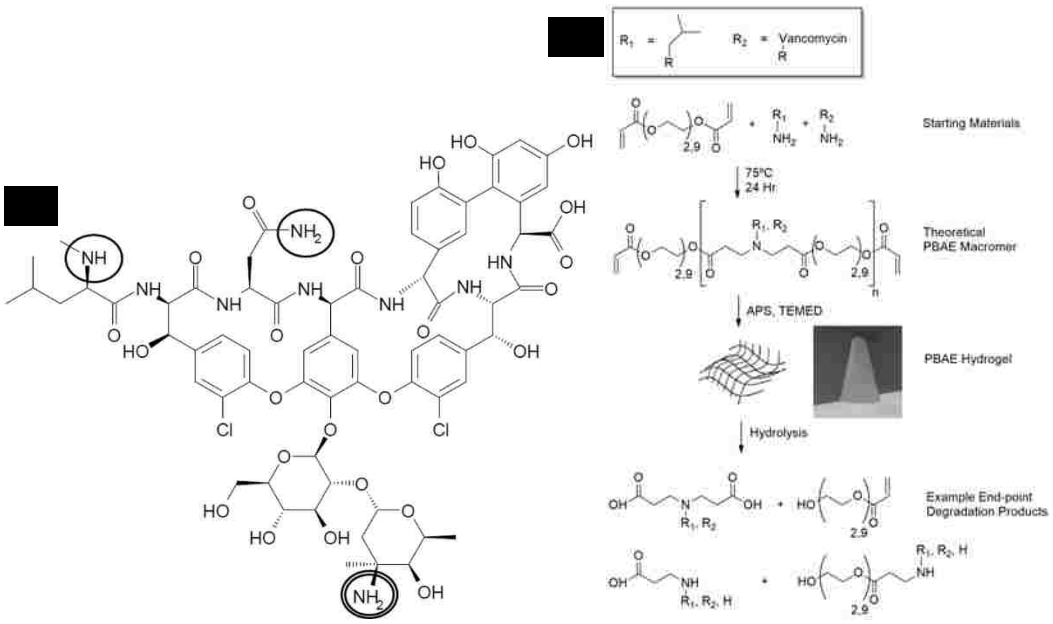

Figure 5.1. Incorporation of vancomycin into PBAE networks. A) Primary, secondary amine, and primary amide sites on vancomycin. The double-circled primary amine signifies the amine thought to participate in the Michael-Addition, whereas the primary amide group would not be as reactive due to resonance with the carbonyl. B) Overview of hydrogel formation reaction. While the degradation products shown are the theoretical terminal products, higher order degradation products potentially exist prior to complete degradation.

5.2.4 Hydrogel Synthesis

Hydrogels were synthesized through the free radical polymerization of PBAE macromers using red/ox initiators. All weight percentages (wt%) described herein are with respect to the total monomer added within each system. APS initiator (1.5 wt%) was dissolved in water (1.5 wt%) and used in conjunction with TEMED (0.5 wt% wrt total monomer), a reagent that catalyzes OH radical formation [388]. Hydrogels were formed over 24 hours at room temperature and used as is. A parallel plate mold, consisting of glass slides and Teflon spacers (1.5 mm thick), was used to form a slab from which 7 mm diameter discs are hole punched for sample analysis.

Two types of drug loaded hydrogels were formed: freely loaded vancomycin, and covalently loaded vancomycin (Table 5.1). For synthesis of free vancomycin loaded hydrogels, vancomycin was added (1.5 wt%) into the macromer prior to addition of the APS and TEMED, but after the macromer formation step. In contrast, covalently loaded vancomycin hydrogels were synthesized by addition of vancomycin (1.5 wt%) dissolved in DMSO (36 wt%) into the macromer solution during macromer synthesis, and then no further vancomycin is added prior to APS and TEMED addition. DMSO was removed from hydrogels via freeze-drying.

Table 5.1. Hydrogel synthesis schematic. A) Stepwise overview of freely loaded and covalently loaded hydrogel synthesis. The freely loaded hydrogel system was not freeze dried due to the lack of DMSO in the formation procedure. B) Macromer molecular weights found with GPC.

[redacted]

		Form Macromer	Form Hydrogel	Post
Freely Loaded Hydrogel	**Reactants**	DEGDA/PEGDA, isobutylamine	Free vancomycin, APS/water, TEMED	-
	Conditions	Heat 75ºC, stirred, 24hr	Parallel plate, room temperature	-
Covalently Loaded Hydrogel	**Reactants**	DEGDA/PEGDA, isobutylamine, vancomycin/DMSO	APS/water, TEMED	-
	Conditions	Heat 75ºC, stirred, 24hr	Parallel plate, room temperature	Freeze dry

[redacted]

DEGDA:PEGDA	M_n (Da)	PDI
2:1 VAH6	3970	1.96
3:1 VAH6	3890	1.87
4:1 VAH6	4130	2.00
5:1 VAH6	3560	1.92
3:1 AH6	3070	1.52

5.2.5 Hydrogel Degradation

Hydrogel discs (roughly 50 mg) were placed into 1 mL of 10 mM phosphate buffer saline (PBS), pH 7.4, maintained at 37 ºC in a shaker bath at 70 RPM, and release media were collected at specific times. At each sample point the entire releasate contents were replaced with fresh PBS. Aliquots of released media were stored at -80ºC prior to HPLC analysis.

5.2.6 Determination of Vancomycin Released

Vancomycin concentration was determined through use of a custom method reverse-phase high performance liquid chromatography (HPLC, Shimadzu Prominence) using a gradient of acetonitrile and 0.1% trifluoroacetic acid containing de-ionized-water using a 250 X 4.6 mm Luna C-18 column (Phenomenex, Torrance, CA). Samples started with 85% acetonitrile and 15% water with an increasing aqueous content over time. Vancomycin was detected using an in-line Shimadzu UV-Vis detector at a wavelength of 280 nm. Fractions of samples were collected manually through determination of retention time, detection time, and exit time from the system. For fractionation studies, effluent from the HPLC was collected in four fractions. These fractions were selected to match the following domains: 1) before the appearance of peaks, 2) containing free vancomycin and non-vancomycin degradation products, 3) containing covalent-vancomycin and non-vancomycin degradation products, and 4) containing later-stage degradation products. Initial HPLC fractions collected for mass spectroscopy utilized 24 hour release into PBS, whereby 20µL HPLC injections were used.

5.2.7 Mass Spectroscopy

HPLC fractions were collected of hydrogel releasate from 1.5 wt% vancomycin 3:1 DEGDA:PEGDA hydrogels. Mass spectroscopy (Bruker Ultraflextreme MALDI-TOFMS) was performed on these fractions and peaks were identified for correlation of an increase in molecular weight of vancomycin due to the addition of propionic acids. The positive-ion matrix-assisted laser desorption/ionization (MALDI) method was used as it is a soft ionization technique to reduce chance of vancomycin fragmentation.

5.2.8 Quantification of ^{125}I-Vancomycin Loaded Hydrogels

^{125}I-radiolabeling was utilized for detection of vancomycin concentration within HPLC fractions collected. Briefly, the Iodogen method was used for iodine coupling, where excess Iodogen reagent was dissolved in chloroform at 1 mg/mL, and evaporated into a film with dry nitrogen on a glass tube. Vancomycin was added at 1 mg/mL and Na-^{125}I was added at 150 µCi/mg vancomycin. After 5 minutes, 1000 MWCO dialysis tubing was used for purification. ^{125}I was mixed with free vancomycin and dialyzed with a 500-1000 MWCO Spectrum Laboratories Micro Float-A-Lyzer™ cassette to separate unbound ^{125}I. Two macromers were then formed (2:1 DEGDA:PEGDA + 1.5 wt% covalent vancomycin), but with only one containing the addition of 0.03 wt% radiolabeled vancomycin. After formation of hydrogels containing radiolabeled vancomycin, a controlled mass of hydrogel sample was degraded for 24 hours in PBS at 37ºC. Radiotracing was performed using a Perkin Elmer 2470 auto gamma counter. Since mass determination requires significantly higher sample concentration, 100 µL HPLC injections

were used from three days of hydrogel release compared to the initial samples run in HPLC for mass spectroscopy.

5.2.9 Bacterial MIC Assay

To compare planktonic antimicrobial activity, *Staphylococcus aureus* (ATCC 25923) was used as a target microbe. 2:1 DEGDA:PEGDA modified-vancomycin hydrogels (formed in tandem with the radiolabeled hydrogels) were degraded at 37ºC for 24 hours, and then fractions were collected as described earlier. Each fraction collected from the drug loaded hydrogels as well as unloaded hydrogels was serial diluted in two-fold, along with a series of free-vancomycin for a calibration curve. MIC_{90} value was determined as the highest concentration in which *S. aureus* showed 90% drop in absorbance from the positive growth control at OD_{600}. A 50/50 mixture of sample/BHI media was used, and the microtiter plate was mixed for 24 hours at 37ºC to discourage bacterial accumulation.

5.2.10 Modified Kirby-Bauer Assay

7 mm x 1.5 mm hydrogel discs (blank control, 3:1 DEGDA:PEGDA + 1.5 wt% free vancomycin, and 5:1 DEGDA:PEGDA covalently-linked vancomycin) were placed upon 10^5 CFU of *S. aureus* seeded agar plates and incubated overnight. After the incubation period, zones of inhibition were measured using image analysis software. Zone of inhibitions were calculated via the inhibition area minus the hydrogel disc area.

5.2.11 Cell Viability with Hydrogel Degradation Products

VAH6 5:1 and AH6 3:1 hydrogels were degraded to solubility in DI water. Human umbilical vein endothelial cells (HUVEC) of passage 5 were seeded at a density of 60,000

cells/cm^2 and cultured 48 hours in a 96 well plate with EGM-2 cell media supplemented with penicillin and streptomycin. Next, media was removed from wells, and dilutions in ¼-fold were made with the hydrogel degradation products in fresh cell media. After 24 hours, supernatant was removed, cells washed twice with fresh media. Live (untreated) and dead controls (0.1 M NaOH for 20 minutes) were used as comparison groups. Calcein AM was used as a live stain, and was incubated for 60 minutes, followed by two wash steps with fresh media. Fluorescence was measured using a BioTek Synergy Mx plate reader (Gen5 2.0, Winooski, VT).

5.3 Results

Based upon the mechanism of PBAE degradation via ester hydrolysis [7, 378], the released vancomycin product was expected to be modified by addition of propionic acid groups (Figure 5.1B). It is thought that both primary and secondary amines may play part in Michael-Addition, but that the primary amine double-circled is more likely to react compared to the secondary sites as a result of steric effects [389, 390]. As the vancomycin release product was expected to be modified, we performed HPLC, mass spectroscopy, and radiolabeling to identify this defining feature, as well as characterize the system overall for release kinetics and activity.

5.3.1 Characterization of PBAE Macromer

Macromer molecular weight (M_n) remained consistent, between roughly 3000 to 4000 Da (Table 1), indicating polymerization of the starting materials to 10-15 mers by mass. The PDI increased with the addition of vancomycin, the VAH6 samples in comparison to the AH6. FTIR data indicated a high yield of greater than 92-98% conversion of carbon double

bonds in the macromers, and 97-99% final conversion in the hydrogels (Figure 5.2A). After reaction, 0.6 to 1.7 acrylates per chain in the macromer were found. These were calculated through comparison of FTIR conversion and M_n found with GPC (Figure 5.2B).

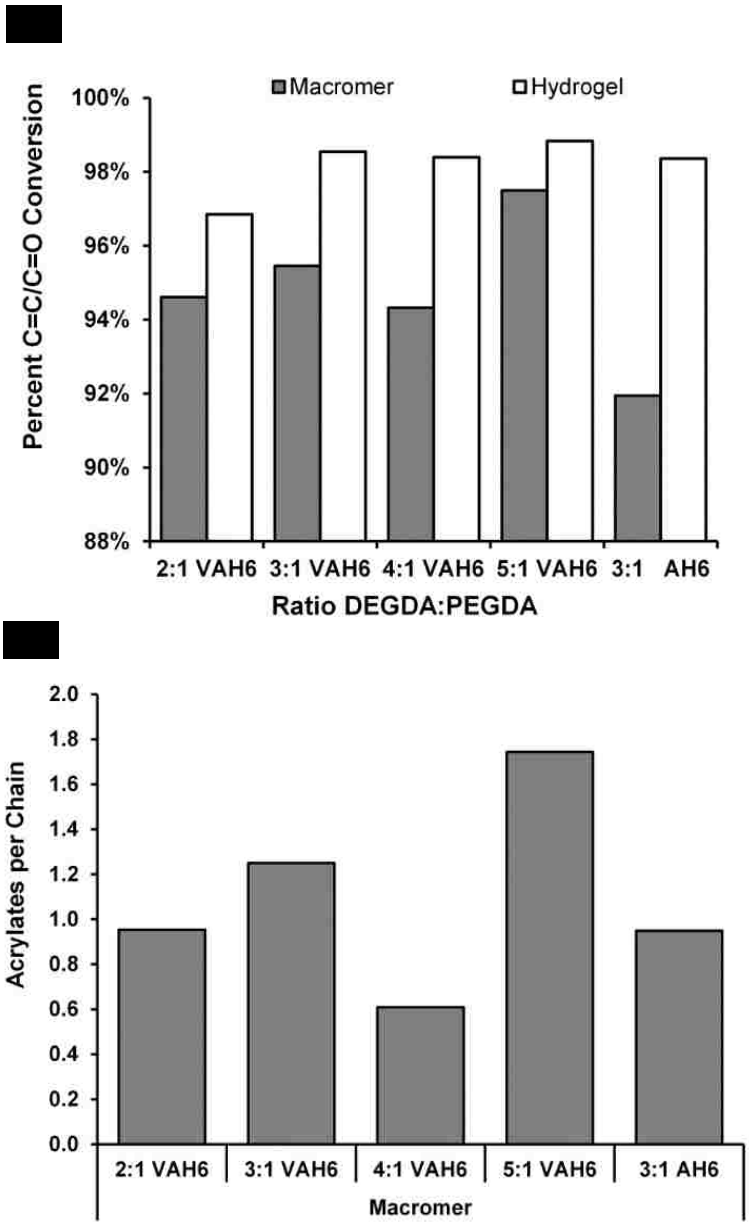

Figure 5.2. Macromer characteristics. A) Percent double bond conversion found after macromer and hydrogel polymerizations. B) Number of acrylates per polymer chain in the different macromers formed, based upon FTIR and GPC analysis. N=1 each.

5.3.2 HPLC Peak Comparison of degradation products

After formation of three different 2:1 DEGDA:PEGDA hydrogels (covalent-vancomycin, free-vancomycin, and unloaded), their releasate in PBS was collected after 24 hours. From the HPLC chromatograms, unique peaks between 4-8 minutes were detected at 280 nm in the covalently-loaded vancomycin samples that are not seen in the freely-loaded and unloaded degradation samples (Figure 5.3 A). These peaks also showed similar characteristics to that of vancomycin, with a peak at 280 and trough at 260 nm. It is hypothesized that these peaks contain vancomycin, and due to their difference in retention time, slower eluting species may be higher order intermediate degradation products.

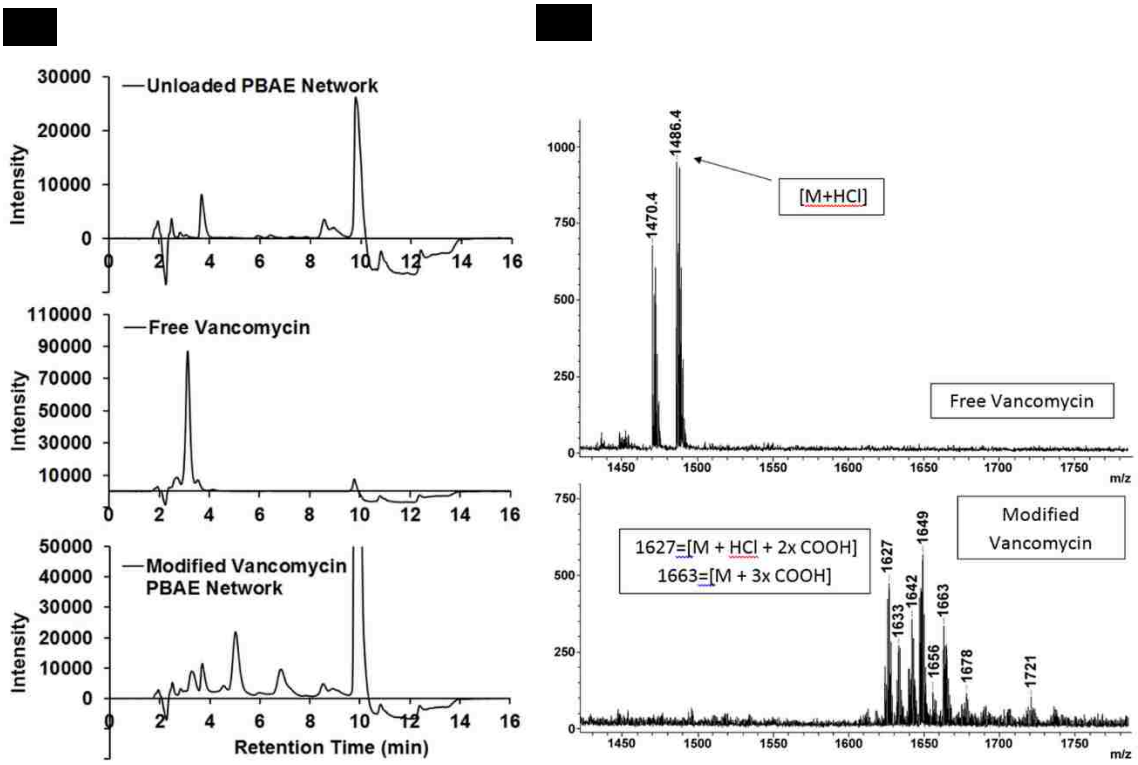

Figure 5.3. Analysis of covalently incorporated vancomycin hydrogel release into PBS over 24 hours. A) HPLC comparison of unloaded PBAE network, free vancomycin, and covalent vancomycin PBAE network releasate showing lack of a free vancomycin peak. B) MALDI mass spectroscopy comparison of free vancomycin (upper) and the releasate from covalently incorporated vancomycin (lower) HPLC peak fractions.

5.3.3 Mass Spectroscopy

To identify the new HPLC peaks which appeared, the 4-8 minute region was fraction collected, and mass spectroscopy was performed. It is theorized that the resulting vancomycin released from the polymer will increase the molecular weight from 1486 m/z [vancomycin HCl] in 72 m/z increments, as a result of the added propionic acid groups. The resulting analysis, indeed, indicated potential dual or triple propionic acid addition of vancomycin, correlating to m/z values in the range of 1627 = [M+HCl+2x COOH] to 1663 = [M+3x COOH], as possible outcomes (Figure 5.3 B).

5.3.4 Vancomycin Radiolabeling and HPLC Fractionation

In order to calculate mass release of the vancomycin products, ^{125}I was used to radiolabel vancomycin through use of the Iodogen reagent protocol, which covalently modifies double bonds that are ortho to the hydroxyl group on phenyl rings. HPLC fractions were collected in the retention periods as shown in Figure 5.4A, using the radiolabeled covalently-linked vancomycin hydrogel releasate (Figure 5.4 B panel 3). A different HPLC protocol was used than with Figure 5.3, so as to elute the hypothetical covalently linked vancomycin peaks into one region, while maintaining separation from free vancomycin. Specifically, Figure 5.4 B displays no free vancomycin peak at a retention time of 4.6 minutes, but does include unique peaks between 8 and 10 minutes that are not found in the unloaded hydrogel and free vancomycin controls. As these peaks were thought to be the release products of covalently modified vancomycin into the hydrogel backbone, fractions were collected to retain the areas of interest according to the retention times in Figure 5.4

A. Figure 5.4 C demonstrates successful collection of peaks via input of the collected fraction samples into HPLC for verification.

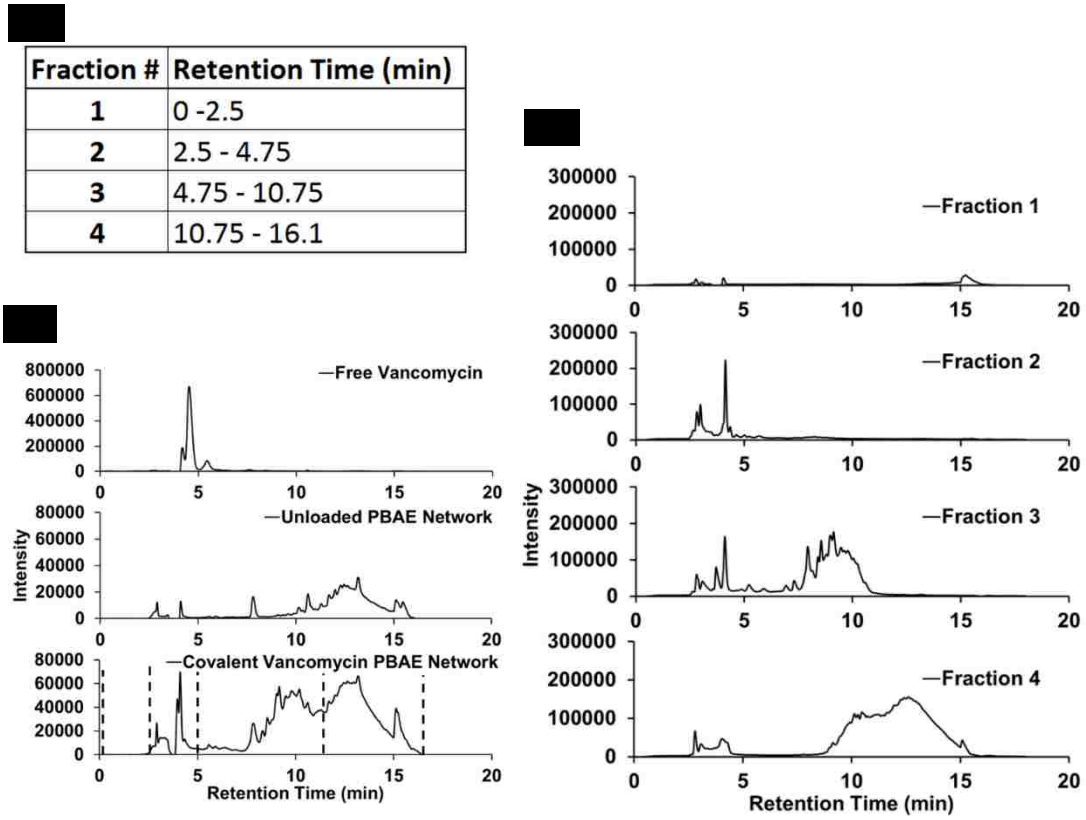

Figure 5.4. HPLC Fractionation of hydrogel degradation products. A) HPLC fraction collection periods of covalent vancomycin 2:1 DEGDA:PEGDA after 72 hours of release into PBS. Fraction numbers correlate to panel B. B) HPLC chromatogram comparison of full releasate samples (to be fraction collected). Vertical lines indicate fraction collection start and stop points. C) For verification of fractions collected, we re-analyzed samples of fractions collected from the covalent vancomycin hydrogel releasate shown in the third section of panel B.

Once the fractions were collected, each was run through a gamma counter. High counts per minute (CPM) were seen in fractions 3 and 4, but not in 1 and 2 using the same control volume (Figure 5.5). Using the calculated CPM/µg vancomycin from the radiolabeling process (7783 CPM/µg), both fraction 3 and 4 resulted in similar calculated concentrations of 1240 and 1214 µg/mL of vancomycin, respectively (Figure 5.5). Interestingly, fractions 1 and 2 were found to be at background CPM levels, indicating conversion of vancomycin into a polymerized product. The total injected CPM was 2835, and 1704 CPM was detected in total after HPLC analysis for a 60% recovery. The loss of sample activity was perhaps due to volatilization during lyophilization of the collected samples.

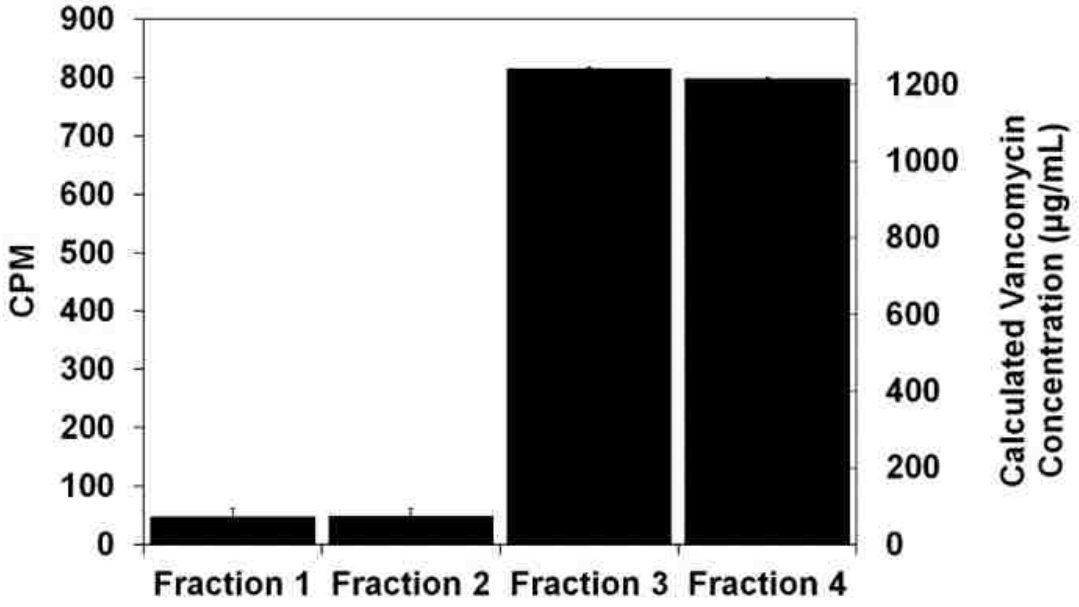

Figure 5.5. 125I tracing of HPLC fractions of covalent vancomycin 2:1 DEGDA:PEGDA fractions collected via HPLC after 24 hours of release into PBS. Secondary axis indicates the correlating vancomycin concentration based upon CPM/µg vancomycin radiolabeled with respect to the total loading of vancomycin.

5.3.5 Hydrogel Degradation and Drug Release

Degradation of hydrogels with covalently bound and free-loaded vancomycin is shown in Figure 5.6 A, which demonstrated various degradation rates depending upon the ratio of DEGDA and PEGDA, from 7 days for 2:1 to 22 days for 5:1. The 5:1 DEGDA:PEGDA covalent vancomycin hydrogel degraded at a similar rate to that of the 3:1 DEGDA:PEGDA free-loaded vancomycin hydrogel. This demonstrates that the addition of vancomycin into the polymer backbone increased the degradation rate, which is another indication of covalent-incorporation.

Figure 5.6 B shows the release of covalently-linked vancomycin from PBAE hydrogels of different DEGDA:PEGDA compositions, and a comparable hydrogel with freely loaded vancomycin. Mass release at time "t" divided the total mass released in the gel at completion is indicated as M_t/M_∞. It can be seen in that even though the 3:1 DEGDA:PEGDA free-loaded vancomycin hydrogel degraded at a similar rate to that of the 5:1 DEGDA:PEGDA covalently-loaded vancomycin (Figure 5.6 A), the 3:1 finished vancomycin release after 11 days, but the 5:1 released until the hydrogel finished degrading at 21 days (Figure 5.6 B). This result of a significant shift of the drug release rate/degradation rate plot (Figure 5.6 C) identifies the potential of a covalently-linked vancomycin drug delivery system.

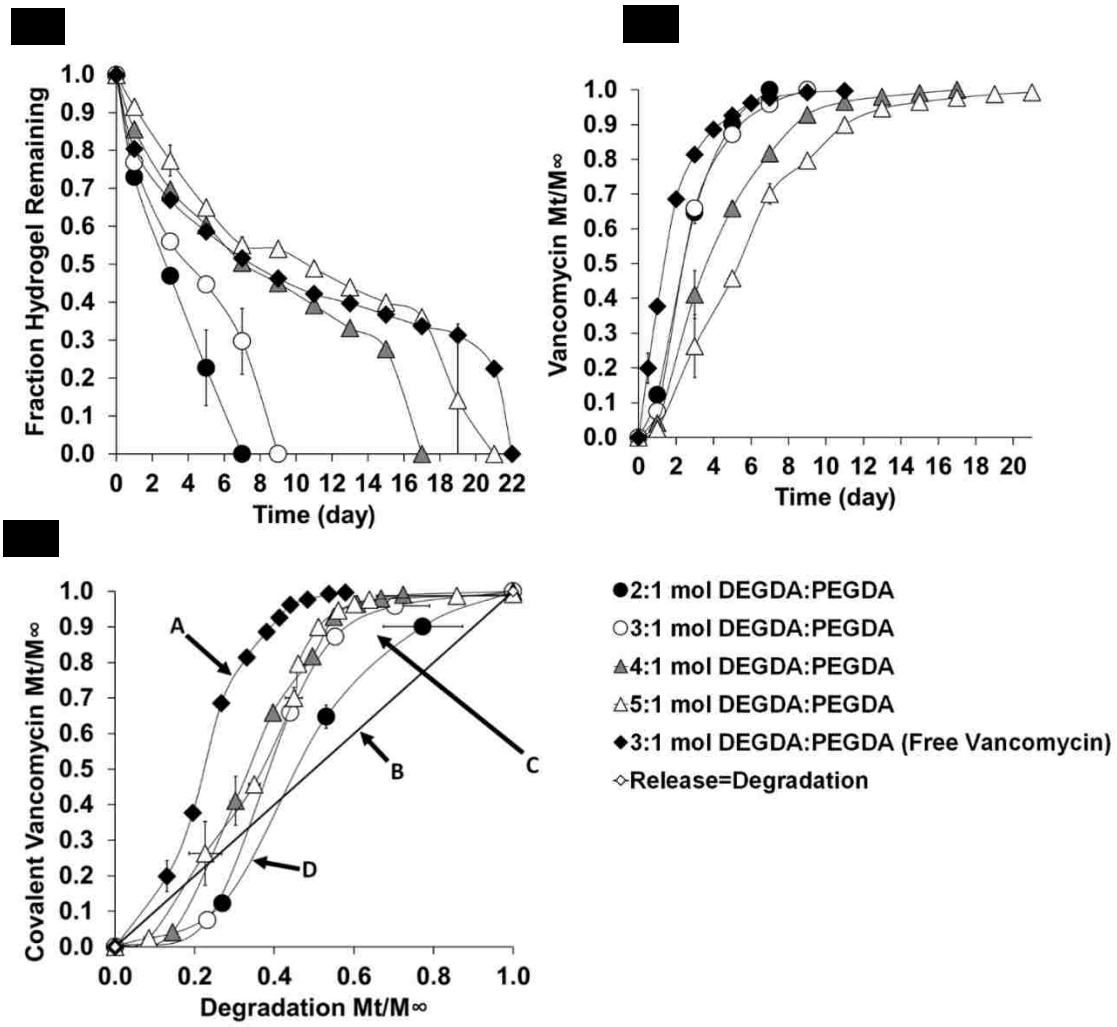
Fraction Hydrogel Remaining
Time (day)
Vancomycin Mt/M∞
Time (day)
Covalent Vancomycin Mt/M∞
Degradation Mt/M∞
A
B
C
D
2:1 mol DEGDA:PEGDA
3:1 mol DEGDA:PEGDA
4:1 mol DEGDA:PEGDA
5:1 mol DEGDA:PEGDA
3:1 mol DEGDA:PEGDA (Free Vancomycin)
Release=Degradation

Figure 5.6. Hydrogel degradation and vancomycin release. Panel A) Hydrogel degradation, comparing covalent vancomycin hydrogels to a free-vancomycin degradation profile. Panel B) Release of covalently vancomycin from hydrogels, with 1.5 wt% vancomycin, and freely loaded vancomycin for comparison. Measured using HPLC of degradation samples. Panel C) Comparison of covalent and freely-loaded vancomycin hydrogel drug release vs. hydrogel degradation. Arrows: A) Vancomycin's small molecular size (1.5 kDa) allows diffusion from the crosslinked network at a rate faster than the hydrogel degrades. B) This 45º line represents drug release at the same rate as the hydrogel degrades. C) Later, covalent vancomycin releases more quickly than the most hydrophobic regions of the covalent vancomycin hydrogels. D) Initially, covalent vancomycin releases more slowly than the most hydrophilic regions of the covalent vancomycin hydrogels.

5.3.6 Release Product MIC and Activity

In order to determine which fraction of hydrogel release contains antimicrobially active compounds of modified vancomycin, a planktonic bacterial growth inhibition assay was used (Figure 5.7). Comparison of the HPLC fractions (from Figure 5.4 A) after overnight incubation in media showed that fraction 3 had a higher activity (8x dilution before growth) than the 4th fraction (2x dilution before growth) and a significantly higher activity than fractions 1 and 2, which produced no growth inhibition. From analysis of Figure 5.4B, the third fraction was expected to show the most activity as it was thought to contain the covalently-linked vancomycin peaks. Additionally, using the collected radiolabeled concentrations from Figure 5.5, we were able to calculate the resulting activity of the modified vancomycin on *S. aureus* to be 155 and 607 µg/mL for the third and fourth fractions, respectively, compared to 2 µg/mL for free-vancomycin (Figure 5.8). Bacterial zones of inhibition measured after overnight incubation demonstrated that both free and covalent systems produce zones of active drug, at 237 mm^2 and 65 mm^2 respectively. However, comparing effects of freely loaded vancomycin and covalently loaded vancomycin hydrogels, we found that the free vancomycin hydrogel produced a larger zone than that of the covalent vancomycin gel (Figure 5.9).

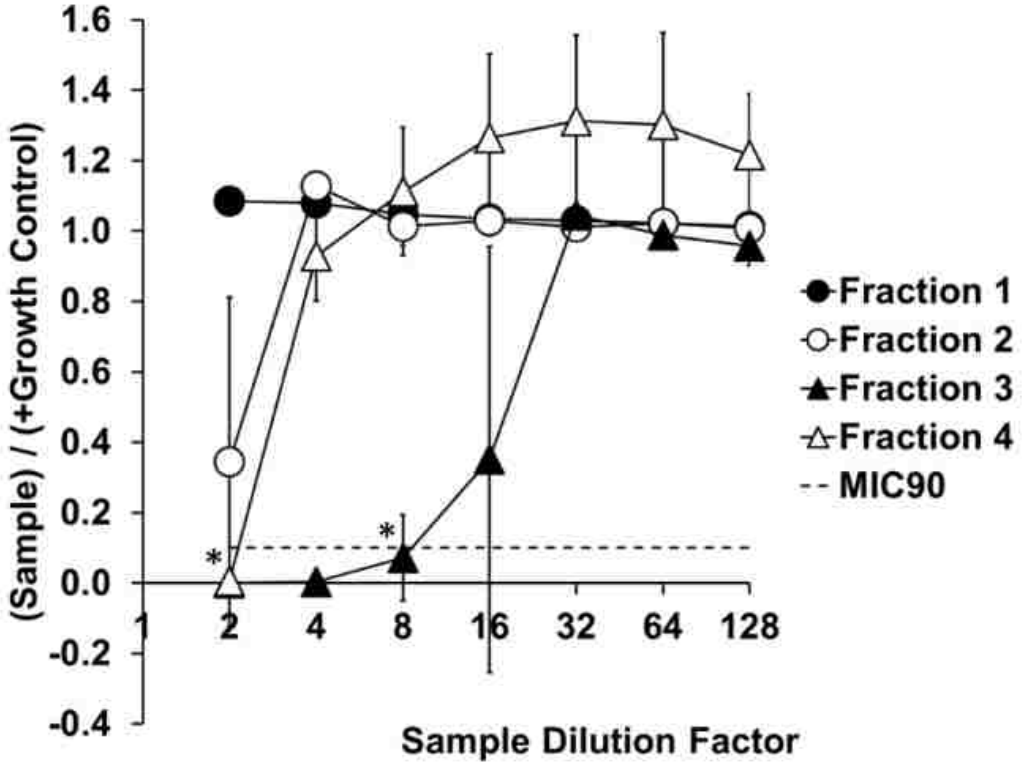

Figure 5.7. Growth inhibition test of overnight planktonic *S. aureus* using covalent vancomycin 2:1 DEGDA:PEGDA fractions collected via HPLC after 24 hours of release into PBS. Measurements taken at OD_{600} in a well plate. Negative control correlates to a fraction of 0, where positive growth (+Growth Control) is 1. * p-value < 0.01 from respective positive control.

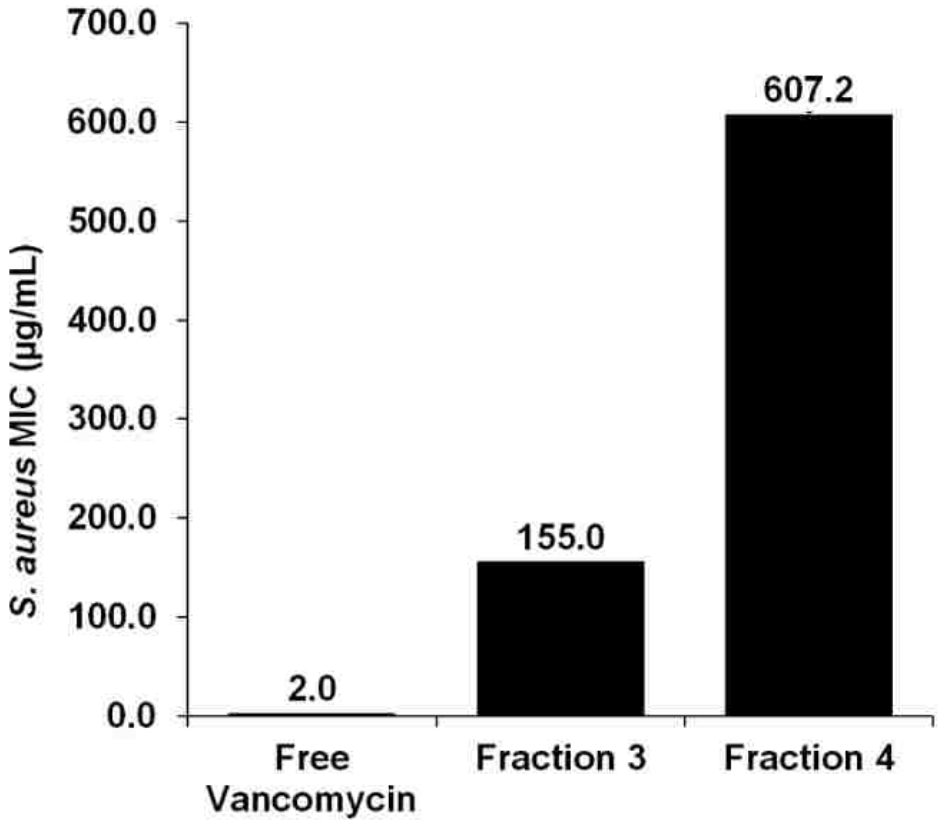

Figure 5.8. Specific activity of each fraction collected from covalent vancomycin 2:1 DEGDA:PEGDA fractions collected via HPLC after 24 hours of release into PBS. Fractions 1 and 2 did not achieve a MIC in the assay. The free vancomycin MIC is a literature value which has been verified in our lab using the same protocol.

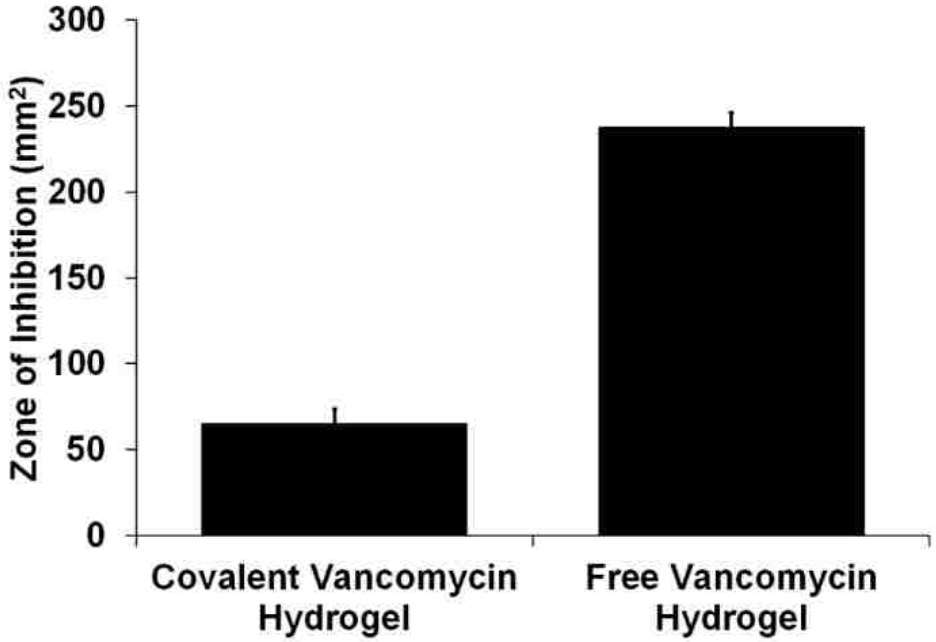

Figure 5.9. Zone of inhibition comparison. Degradation rate-matched (~21 days) covalent vancomycin (1.5 wt%) and free-vancomycin (1.5 wt%) hydrogels on a 24 hour modified Kirby-Bauer assay via placement of 7 mm x 1.5 mm hydrogel discs on *S. aureus* seeded agar petri dishes.

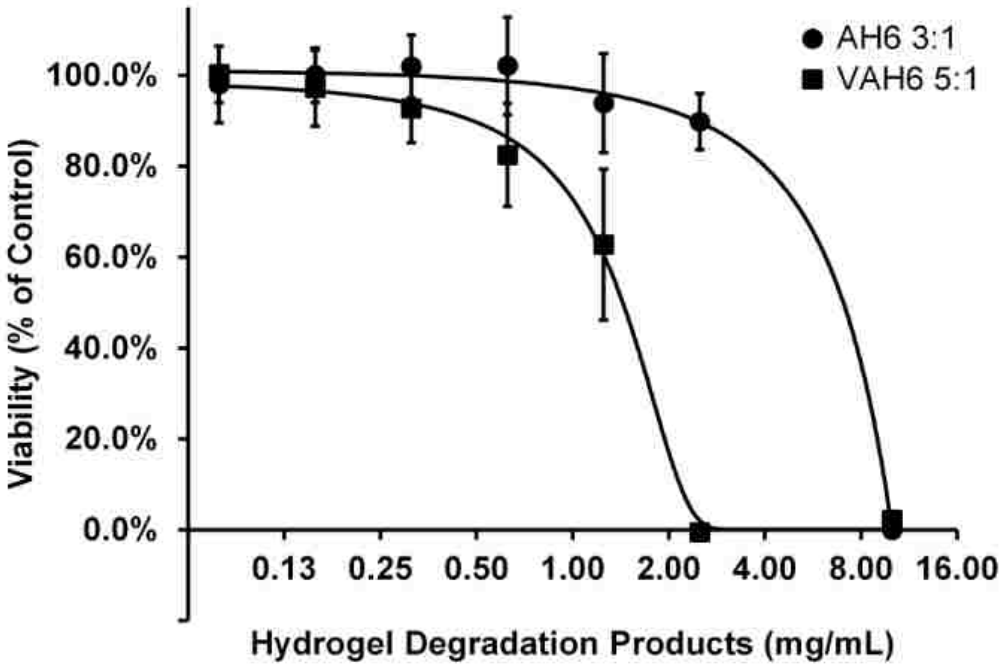

Figure 5.10. HUVEC viability after 24 hours incubation with VAH6 5:1 and AH6 3:1 hydrogel degradation products.

5.3.7 Cell Viability with Hydrogel Degradation Products

To determine cell toxicity of these hydrogel systems, hydrogels were degraded until complete solubility, and ran in a dose comparison on HUVEC (Figure 5.10). After 24 hours incubation, it was found that the TC_{50} were 1.5 mg/mL for the VAH6 5:1, and 7.0 mg/mL for the AH6 3:1, indicating an increased toxicity for the VAH6 5:1 system.

5.4 Discussion

S. aureus can colonize biomaterials at concentrations of 10^5 lower than what is required to overcome the body's immune system without the presence of a biomaterial [21, 22]. This large discrepancy in colonization underlines the importance of avoiding antimicrobial implants that release their contents prior to the complete degradation of the implant. Success in literature has been found concerning the covalent incorporation of drug into polymer design [7]. Through the use of therapeutic degradation products, drug release is bound to the degradation rate. This highly effective polymer design was integrated into our vancomycin containing hydrogels, to form a covalently linked antimicrobial biomaterial. Currently used PMMA beads, or modifications of such chemistries [391, 392] would require removal of inactive biomaterial remaining at the implant site beyond the drug release period, however, our hydrogel which releases covalently-bound vancomycin due to ester-based degradation, may avoid that problem. This PBAE material, synthesized, via acrylate-amine reaction between PEG and DEG diacrylates with vancomycin, allowed formation of an acrylate containing macromer that was redox polymerized into an antibiotic backbone with tunable degradation/release. While only hypothetical, side reactions during polymerization could potentially include other reactive sites of

vancomycin, such as double bond oxidation, leading to a reduction of antimicrobial activity. Through comparison of GPC results, analysis showed an increase in PDI for vancomycin containing macromers, perhaps due to the branching effects that vancomycin may add to the system. The addition of longer retention time peaks in HPLC indicated change of the vancomycin within the system away from the free form, as vancomycin addition was the only variation between the unloaded and loaded systems. Mass spectroscopy of the covalent vancomycin releasate samples produced several higher molecular weight peaks that support the hypothesis of vancomycin reaction with the diacrylates. As two Michael-Addition sites were hypothesized due to the glycosidic primary amine (see Figure 5.1B), a terminal molecular weight near 1630 was predicted, with variation potentially owing to the different PBS salts in solution and isotopes. Further validation of vancomycin incorporation was provided by radiotracing. After ^{125}I-radiolabeling of vancomycin, we found that the unique HPLC peaks in the covalent-vancomycin samples showed significantly higher CPM, compared to the fractions collected during, as well as prior to, the free vancomycin peaks which showed background CPM.

Comparison of the drug release:degradation ratio over time concluded that vancomycin release was patterned with degradation kinetics, as opposed to free loaded vancomycin where diffusion dominated drug release. To accomplish drug release tuned with matrix degradation, via a mechanism other than covalent drug addition, may not always be possible, however. It is often not attained using simple diffusion based drug release, where biodegradation outlasts drug burst release [25, 393, 394], as the kinetics for the bulk

degradation rate must either equal the drug diffusion rate or drive it through quick degradation.

In the case of hydrophilic drugs, like vancomycin, the high rate of drug diffusion would require a quickly degrading hydrogel matrix to match drug release/degradation, thereby denying the option of extended-release. Affinity-based drug-polymer interactions [385, 395] could encounter similar problems as well due to dependency on drug affinity for the polymer over other molecules in a complex system, compared to the more direct route of covalent addition. In comparison to our free vancomycin loaded system, the covalently loaded PBAE networks allowed for an elimination of the non-drug releasing period after the biomaterial was not yet fully degraded. This important factor is often absent in literature of vancomycin drug release from hydrogels [25, 393, 396-398]. Interestingly, even through covalent addition of vancomycin, exact synchronization of drug release to overall polymer degradation rate was not possible.

As shown in Figure 5.6 panel C, if the drug release;degradation ratio was 1 through the entire lifespan of the biomaterial, the data would have directly followed the 45º line. However, with variation of DEGDA:PEG400DA monomer ratios from 2:1 to 5:1, each hydrogel system degraded, swelled, and released drug differently. A potential source of this variation is likely heterogeneity within the network, resulting in domains with variable degradation rates. In previously published work, using a co-macromer hydrogel system [399], hydrogel heterogeneity was apparent via biphasic degradation trends, where this currently used system utilizes the co-monomer, single macromer method to form a hydrogel with single phase degradation trends. For example, the 2:1 DEGDA:PEG400DA hydrogel showed initial lag of drug release:degradation of less than 1 up to a degradation

M_t/M_∞ of just over 0.4, and then increased greater than 1 until completion. The PEG400DA rich regions may indeed degrade more quickly than the vancomycin regions, showing initial lag, whereas when DEGDA rich regions remain, the bulk degradation slows, and then vancomycin is released more rapidly. In contrast, the 5:1 DEGDA:PEG400DA hydrogel, being more hydrophobic to start with, the vancomycin ester bonds seemed to have degraded much faster than the much more prevalent DEGDA regions in comparison to the 2:1 hydrogels, showing the potential variation of kinetics possible with this system. Even with vancomycin only consisting of 1.5 wt% of the total hydrogel with respect to the polymeric monomer, the addition of vancomycin amine-acrylate esters to the backbone altered the total degradation period compared to the freely loaded system by 13 days for the 3:1 composition hydrogels, indicating a vast modification towards bulk hydrophilicity. A potential workaround for this stumbling block in degradation synchronization may be to selectively bond vancomycin to comparatively hydrophobic blocks (e.g. DEGDA), in order to offset the hydrophilicity of vancomycin and slow the release. However, without vancomycin comprising the amine content in entirety, disconnect will inevitably remain in release/degradation kinetics.

The antibacterial activity of vancomycin is due to the ability of the glycopeptide to traverse the cell wall of gram-positive bacteria, and bind to the D-alanyl-D-alanine moiety of N-acetylmuramic acid and N-acetylglucosamine. However, if the structure of vancomycin were to change, it is logical that the antimicrobial MIC may be affected as well, due to interference with hydrogen bonding regions within the peptide backbone to D-alanyl-D-alanine. Further, if vancomycin was still in its oligomeric form with backbone polymer, the ability of vancomycin to traverse the cell wall would likely be affected as well. And

thus, this may be a description for the resulting *S. aureus* MIC found for fraction 3 being 77.5 times greater than the MIC of neat vancomycin in Figure 5.7. Modified Kirby-Bauer results indicated a zone of inhibition similar to that of freely loaded vancomycin, albeit smaller. The resulting smaller inhibitory zone is thought to be due to a combination of the reduced activity of release products compared to free vancomycin, the reduced vancomycin release rate from degradation-based drug release found in PBS, and, hypothetically, the reduced diffusivity of larger oligomeric chains. In comparison to other groups utilizing covalent chemistries with vancomycin, one group has formed an antimicrobial surface with single-site vancomycin addition upon various chains, and found similar reductions in activity (up to a 60 fold decrease in activity) in some cases [389, 390]. Importantly, they reported that vancomycin still bound covalently to a modified surface film retained antimicrobial activity. Interestingly, this may also apply to our system as vancomycin is delivered from the hydrogel while remaining in oligomeric forms, and both of these moethods are required to exhibit properties of cell wall penetration to reach binding sites. In order to recover the antimicrobial activity back to the state of neat vancomycin, it is apparent that unmodified vancomycin may be necessary to be produced after cleavage from a polymer backbone. Our antimicrobial hydrogel system appears to show similar results, with a lowered activity in higher order degradation residues. Research looking into other covalent addition mechanisms may be warranted to produce this result.

Interestingly, while the VAH6 5:1 had a lower TC50, it was comparable to other published work using a similar PBAE hydrogel, where they used mouse pluripotent mesenchymal cells and found a TC50 value of between 0.4 to 1.8 mg/mL degradation products [400]. VAH6 products were also more toxic than vancomycin, which has been shown to become

toxic only above 5 mg/mL to HUVEC [401]. Yet, despite this decreased biocompatibility, the degradation products still possessed greater antimicrobial capacity as compared to mammalian cell toxicity. Future work will focus on a detailed evaluation of the modified Vancomycin and methods to improve the antimicrobial and toxicity thresholds.

5.5 Conclusions

Successful formation of an active antimicrobial hydrogel that releases drug throughout its degradative lifespan is important in the capacity to apply this strategy for infection treatment. With the ability to release vancomycin to the full extent of degradation, the covalent incorporation of vancomycin into the backbone of PBAE polymers indeed showed improved vancomycin kinetics over the freely-loaded system, where burst-release diffusion extinguished drug release well before degradation was complete. The resolution towards reduction of burst release may reduce the potential for bacterial colonization of this biomaterial as antibiotic was found to be released until the hydrogel loses structural integrity. Via Michael-Addition of vancomycin into the polymeric backbone hydrogel structure, vancomycin release was found to be much more closely correlated to the total degradation rate of the hydrogel compared to traditional free-loading. Tuning of the degradation profile between 7 and 21 days was possible through a 2.5-fold variation of the hydrophobic:hydrophilic content of the hydrogel from 2:1 to 5:1 DEGDA:PEGDA, an ability useful for wound healing applications requiring different release rates.

The specific activity on planktonic *S. aureus* of covalently-modified vancomycin was found to be reduced to that of un-modified vancomycin. This decrease in activity, however, is indeed an implication that vancomycin has been modified into the backbone of the material. This was corroborated by HPLC peak shifts and retention times of active

components. Since fraction 2 of Figure 5.3 is where the free-vancomycin peak would appear if present, it can be seen that there was high conversion of vancomycin into the modified form. As far as current literature is defined, this biodegradable hydrogel showing covalent release of vancomycin is an important step in degradative-based drug delivery for local antibiotic treatment.

Chapter 6. Reducible Disulfide Poly(beta-amino ester) Hydrogels for Antioxidant Delivery

Based on the research article:

> Andrew L. Lakes, Carolyn T. Jordan, Prachi T. Gupta, David A. Puleo, J. Zach Hilt, Thomas D. Dziubla. *Reducible Disulfide Poly(beta-amino ester) Hydrogels for Antioxidant Delivery.* Submitted to Advanced Materials.

6.1 Introduction

The natural redox state of human cells is a highly regulated system, where shifts in the balance of pro- and antioxidant levels may induce a state of cellular stress, [402] as is the case with an acute oxidative burden (e.g., radiation and reperfusion injury) or oxidative stress-based disease (e.g., pulmonary pneumonitis, atherosclerosis, and rheumatoid arthritis) [26-30]**.** Through carefully timed delivery of antioxidants, the redox buffering capacity may be temporarily increased, shifting the cytosol towards the reduced state, alleviating transient oxidative injury [31, 32]. To minimize potential oxidative stress caused by biomaterial-induced inflammation or toxicity, antioxidant delivery may aide the foreign body response, improving implant integration. On the other hand, biomaterials which lower antioxidant capacity may reduce biocompatibility in times of oxidative stress. Using a disulfide-containing poly(β-amino ester) (PBAE) hydrogel, similar to those used in literature for DNA delivery [403, 404], but which can be reduced to contain bound-thiols within the bulk matrix for antioxidant delivery, we found that a large differential existed between the cytotoxicity of the degradation products containing disulfides and those containing thiols (reduced disulfides). Further, oxidative stress was found to be significantly less with the thiol containing hydrogel degradation products, which indicated

the importance of biomaterial redox state and the potential for high biocompatibility compared to other antioxidant containing biomaterials.

Disulfide bonds are a common responsive crosslinking system used in polymeric biomaterials [405-408] and may be utilized as a means of biodegradation via disulfide cleavage for drug release to the cytosol [409, 410]**.** Human cells typically contain from 1 to 10 mM glutathione (GSH) and roughly 1/100 that content of glutathione disulfide (GSSG) [411, 412], which is enzymatically reduced back to glutathione mainly via glutathione reductase/$NADPH^+$ [31, 413, 414]**.** Unfortunately, cellular entry of disulfides may result in reduced antioxidant capacity through oxidation of glutathione in the cell via disulfide cleavage within the biomaterial or degradation products, and create mixed disulfides unable to participate in enzymatic regeneration of glutathione [415]**.** Delivery of reduced disulfide (thiol-containing) materials may be utilized to not only re-balance cellular response under oxidative stress conditions, but also enhance cell viability of biomaterials.

6.2 Materials and Methods

6.2.1 Materials

All reagents were used as received without further purification steps. Cystamine dihydrochloride, 4,7,10-trioxa-1,13-tridecanediamine (TTD), 5,5'-dithiobis(2-nitrobenzoic acid) (DTNB/Ellman's Reagent), diethyleneglycol diacrylate (DEGDA), and 2-mercaptoethanol (2-ME) was purchased from Polysciences Inc. (Warrington, PA). Immobilized tris(2-carboxyethyl)phosphine (TCEP) beads were purchased through Thermo Scientific (Waltham, MA). EGM-2 cell media and HUVEC were purchased

through Lonza (Hopkinton, MA). Hypoxanthine and xanthine oxidase were purchased through Sigma-Aldrich (St. Louis, MO). Calcein-AM was obtained from Life Technologies (Grand Island, NY). All solvents were purchased through either Fisher Scientific (Waltham, MA) or Pharmco-AAPER (Brookfield, CT).

6.2.2 Cystamine PBAE Hydrogel Synthesis

Throughout hydrogel synthesis, the total acrylate to total primary amine ratio was kept at a stoichiometric 1 to 1. First, cystamine was mixed with anhydrous dimethylsulfoxide (DMSO) at 133 mg/mL during sonication to aid in solubilization. Then, after mixing in TTD with the cystamine solution, it was added to the DEGDA. The mixture was then dispensed onto a casting ring upon a Teflon plate, and kept for 24 hours at 60ºC. After removal from the oven, thin film hydrogels were washed with DMSO to remove unreacted reagent, freeze dried for 48 hours, and stored with desiccant in argon at 2-5ºC.

6.2.3 Hydrogel Swelling and Mesh Size Calculations

Swelling studies proceeded via weighing the dry material before and after swelling in DMSO for at least 8 hours to achieve equilibrium. For reversible swelling steps, a new dry mass was calculated after freeze drying the material to account for any loss of mass washed away. The swelling ratios, $\boldsymbol{q}$, were found by dividing the swollen polymer $\boldsymbol{W_s}$ by the weight of the dry polymer $\boldsymbol{W_d}$ in equation 6.1. The polymer volume fractions, $\boldsymbol{v_2}$, were calculated by equation 6.2, where $\boldsymbol{\rho_p}$ and $\boldsymbol{\rho_s}$ are the densities of the dry polymer (1.3 g/cm^3) and DMSO solvent (1.1 g/cm^3) respectively [79].

$$\boldsymbol{q} = \frac{\boldsymbol{W_s}}{\boldsymbol{W_d}} \tag{6.1}$$

$$\boldsymbol{v_2} = \frac{\mathbf{1}}{\mathbf{1}+\frac{\boldsymbol{\rho_p}}{\boldsymbol{\rho_s}}(\boldsymbol{q}-\mathbf{1})} \tag{6.2}$$

Mesh size $\boldsymbol{\xi}$ calculations were performed using solvent interaction calculations using Flory-Rehner [81-83] equation 6.3 to find the number average crosslinking molecular weight $\boldsymbol{M_C}$ required for equation 6.4 [81, 86]. $\boldsymbol{M_N}$ is number average molecular weight of the polymer between crosslinks (from 217-194 Da for 0-66 mol% cystamine of the amines in the disulfide state, and 217-169 Da in the reduced), $\boldsymbol{\bar{v}_2}$ is the specific volume of the swollen amorphous hydrogel, $\boldsymbol{V_1}$ is molar volume of DMSO in the hydrogel (71.03 mL/mol), $\boldsymbol{l}$ is the repeat polymer bond length (1.54 Å for C-C), $\boldsymbol{C_n}$ is the Flory characteristic ratio (constant 4.0 used for ethylene glycol systems as an approximation [84, 85]), and $\boldsymbol{M_r}$ is the molecular weight of the repeating unit (44 Da for ethylene glycol assumed).

$$\frac{\mathbf{1}}{\boldsymbol{M_C}} = \frac{\mathbf{2}}{\boldsymbol{M_N}} - \frac{\boldsymbol{\bar{v}_2}}{\boldsymbol{V_1}} \frac{\left[\ln(\mathbf{1}-\boldsymbol{v_2}) + \boldsymbol{v_2} + \boldsymbol{\chi}\boldsymbol{v_2}^2\right]}{\boldsymbol{v_2}^{1/3} - \frac{\boldsymbol{v_2}}{\mathbf{2}}} \tag{6.3}$$

$$\boldsymbol{\xi} = \boldsymbol{l}\boldsymbol{v_2}^{-1/3}\left(\frac{\boldsymbol{2C_nM_C}}{\boldsymbol{M_r}}\right)^{1/2} \tag{6.4}$$

To determine the Flory-Huggins parameter, $\boldsymbol{\chi}$, equation 6.5 was used where $\boldsymbol{\chi_H}$ is the enthalpic contribution and $\boldsymbol{\chi_S}$ is the entropic contribution, typically used as 0.34 [416]. Equation 6.6 finds the enthalpic contribution, $\boldsymbol{R}$ is the universal gas constant, $\boldsymbol{T}$ is the absolute temperature, $\boldsymbol{\delta_2}$ and $\boldsymbol{\delta_1}$ are the Hildebrand solubility parameters of the polymer (equation 6.7) and solvent (12.0 cal/cm^3 [417]) respectively.

$$\boldsymbol{\chi} = \boldsymbol{\chi_H} + \boldsymbol{\chi_S} \tag{6.5}$$

$$\boldsymbol{\chi_H} = \frac{\boldsymbol{V_1}}{\boldsymbol{RT}}(\boldsymbol{\delta_2} - \boldsymbol{\delta_1})^2 \tag{6.6}$$

To calculate the Hildebrand solubility parameters, equation 6.7 was used, where $\boldsymbol{Ecoh_i}$ is the cohesive energy of each bond type in the crosslink, and $\boldsymbol{V_i}$ is the molar volume of the bond type in the crosslink.

$$\boldsymbol{\delta_2 = \left(\frac{\sum Ecoh_i}{\sum V_i}\right)^{0.5}} \quad \textbf{(6.7)}$$

Cohesive energies and molar volumes were used from Fedors values in Van Krevelen et al. [416]. The Flory-Huggins parameter for the initial oxidized state was used as an estimation in calculating the mesh size of the reduced, and then re-oxidized hydrogel.

6.2.4 Fourier Transform Infrared Spectroscopy

Using Fourier transform infrared spectroscopy (FTIR) (Varian 7000e) and a heated attenuated total reflectance (ATR) stage, the starting materials were added to the stage for real-time FTIR analysis. A spectrum was taken at each time point, and using Varian Resolutions Pro, peak areas were calculated for the carbonyl (C=O) and carbon double bonds (C=C) of acrylates.

6.2.5 X-ray Photoelectron Spectroscopy

A Thermo Scientific K-Alpha x-ray photoelectron spectrometer (XPS) was used with an EX06 ion source. Hydrogel samples were freeze dried overnight, then transferred to a high vacuum chamber for 24 hours. After this, the samples were scanned looking at the S2p binding energy range, and analyzed with Thermo Scientific Avantage Data System.

6.2.6 Hydrogel Degradation

For aqueous degradation, 10 mM phosphate buffered saline (PBS) was used for sink conditions. Samples were stored in a shaken 37ºC water bath for the indicated time periods, whereupon the total liquid supernatant was collected, and fresh PBS was added. For degradation performed in the presence of a reducing agent, TCEP or 2-ME was used with anhydrous DMSO.

6.2.7 Sample Reduction and Thiol Detection

To create reducing conditions, either TCEP or 2-ME was used. TCEP immobilized agarose beads were used to reduce any solvent soluble degradation products. Samples were kept at maximum equal to the molar reducing content of the beads for 30 minutes, well-mixed on a vortexer. To detect free/bound thiol, Ellman's reagent (DTNB) solution was first created at 0.0784 mg/ml using Ellman's buffer, and was kept out of light. After dilution of 17.8 µL of sample into 182.2 µL of Ellman's reagent solution, the mixture was incubated for 15 minutes before sample analysis using a UV-vis spectrophotometer at 412 nm. Thiol content was calculated based upon a calibration curve of reduced cystamine with TCEP beads and Ellman's assay.

6.2.8 Degradation of Reduced Hydrogel

A 25 mole ratio cystamine hydrogel was first reduced in 4x excess DMSO for 16 hours using 50 mM free TCEP. Due to the swelling ratio of the 50/50 mol% CA/TTD hydrogel being 4.2 wet/dry, and 11% of mass solubilized in reducing conditions, the gels were then washed 3 times with PBS to remove residual TCEP down to below 10 µM. Degradation samples were then taken at the time points compared to a control gel made of 50/50 mol%

CA/TTD, not exposed to reducing conditions, and a 0/100 mol% CA/TTD hydrogel exposed to reducing conditions to control for residual free TCEP not washed away.

6.2.9 Cytotoxicity Assay

Human umbilical vein endothelial cells (HUVECs) were seeded into 96 well plates (Costar) at 9,000 cells/well and grown to confluence. Cells were treated with neutralized (pH 7.4) degraded hydrogel materials in both oxidized and reduced states that were serially diluted in EGM-2 Endothelial Cell Growth Media (Lonza). Cells were incubated for 24 hours at 37ºC and 5% CO_2. Material was removed after 24 hours and cells were stained with Calcein-AM. HUVEC viability percentage was measured using a UV-vis spectrophotometer (Biotek SynergyMX) at excitation/emission wavelengths of 485/528 nm. Data was normalized to live controls.

6.2.10 Reduction of Oxidative Stress in HUVEC

HUVECs were seeded into 96 well plates at 9,000 cells/well and grown to confluence. Cells were incubated in neutralized hydrogel degradation products at concentrations between 2.5 and 10 mg/mL in EGM-2 endothelial cell growth media. After one hour, 18.75 mU/mL of xanthine oxidase (XO) was added followed by 200 µM hypoxanthine (HX) to cause injury via superoxide production. Cells were incubated with material and HX/XO for 24 hours at 37ºC and 5% CO_2. HUVEC viability was measured by Calcein-AM intensity using UV-vis spectrophotometry. Data was normalized to live controls.

6.2.11 Mitochondrial Respiratory Response in HUVEC

A Seahorse XF flux analyzer was used to monitor mitochondrial bioenergetics with the SS/SH hydrogel degradation products ± HX/XO by recording oxygen consumption rates (OCR) in pmol/min as well as extracellular acidification rates (ECAR) in terms of pH change. In this analysis, the assay parameters/treatments were set to determine changes in OCR to study the effect of HX/XO generated oxidative stress, and not changes in ECAR glycolytic flux. A 50/50 mol% CA/TTD hydrogel degradation product concentration was used which was below the Calcein-AM derived IC50 for both the SH and SS systems (both SS and SH used 0.156 mg/mL with SH at 0.363 ± 0.006 mM thiol, n=3, standard deviation). HX/XO (200 µM/18.75 mU/mL) was set at the same concentration as the Calcein-AM studies such that mitochondrial response may be deviated from non-treated controls. HUVECs were seeded at a density of 35000 cells/well in a 96-well tissue culture plate and were allowed to adhere overnight. A group of wells were media filled without cells to be used as a background during XF flux analysis. After overnight incubation, cells were treated with the hydrogel sample groups for 1 hour, whereupon HX/XO was added and incubated for 24 hours in total at 37ºC and 5% CO2. After 24 hours of treatment, the well plate was prepared for the mitochondrial stress assay using an XF flux analyzer.

The cell growth media was then washed with FX Assay Modified DMEM media (5.5 mM glucose, 1 mM pyruvate, 2 mM glutamine). After washing, wells were further incubated in the same FX media for 1 hour at 37ºC in a non-CO_2 chamber. The well plate was then subjected to the mitochondrial stress assay, which includes addition of electron transport inhibitors i.e. oligomycin (1 µM), FCCP (carbonyl cyanide p-trifluoromethoxyphenylhydrazone) (1 µM) and a mixture of rotenone (1 µM) and

antimycin A (1 µM) in a serial manner to study mitochondrial bioenergetics response. Each inhibitor serves the function of determining at least one bioenergetics component of the mitochondrion. Oligomycin acts as ATP synthase inhibitor and helps in determining the ATP production rate linked to that mitochondrion. FCCP is an uncoupling agent which gives an estimate of maximum respiration and mitochondrial spare respiratory capacity. Rotenone/antimycin A completely shuts down the mitochondrial function by inhibiting complex I and II function in electron transport chain and hence gives an estimate of any non-mitochondrial OCR which is further utilized in calculating basal respiration, and maximum respirations rates of mitochondrion. OCR and ECAR were measured every 3 minutes including addition of inhibitor drugs in series. Post XF analyzer measurement, cells in each well were fixed for BCA protein assay to estimate the protein content of the adhered cells. To proceed for the assay, FX media was removed and cells in each well were lysed by adding 25 µL of cell lysis buffer (0.32 mM sucrose, 2 mM EDTA, 2 mM EGTA, 20 mM HEPES at pH 7.4, containing protease inhibitors 4 µg/mL leupeptin, 4 µg/mL pepstatin, 5 µg/mL aprotinin, and 0.2 mM PMSF). The plate was incubated at -20oC overnight. The next day, the plate with lysed cells was analyzed for protein levels using BCA protein assay kit (Thermo Scientific, Rockford IL). The OCR (pmol/min) values were then normalized using the protein content values, and data was also obtained as pmol/min/µg of protein or %OCR from the third basal values of measurement for each group.

6.3 Results and Discussion

6.3.1 Hydrogel Formation

Disulfide cystamine-containing hydrogels were formed through aza-Michael addition of cystamine (CA) with diethylene glycol diacrylate (DEGDA) (Figure 6.1A). The relative content of thiol was controlled through the addition of another di-primary amine, 4,7,10-trioxa-1,13-tridecanediamine (TTD). To verify reaction between the acrylates and amines, real-time ATR-FTIR (attenuated total reflectance Fourier transform infra-red spectroscopy) analysis of the polymerization at 60ºC was completed, where the acrylate conversion was detected (Figure 6.1B). The carbon double bond of the acrylate groups present in DEGDA was found to decrease relative to the carbonyl group during reaction, indicating that Michael addition took place over the 24 hour reaction period. To verify cystamine incorporation into the networks, hydrogels were washed in dimethylsulfoxide (DMSO), which resulted in a mass loss of less than 7% (Figure 6.2A), indicating at least 93% of reactants added were incorporated into the hydrogel. Further, only 4 wt% of the total added cystamine was washed out for the 50/50 mol% CA/TTD hydrogel, demonstrating a high reactivity of cystamine (Figure 6.2B). Detection of the surface chemistry using X-ray photoelectron spectroscopy (XPS) revealed consistent proportionality of sulfur S2p orbitals (Figure 6.1C). Although disulfides and thiols contain overlapping binding energies, the presence of bound sulfur is nonetheless detected, with 163 eV hypothesized to be in disulfide configuration. Slight asymmetry may be due to 2p spin-orbit doublets of 1/2 and 3/2. Importantly, there are no oxidant shifts reflecting sulfones or sulfonates, which would appear at binding energies greater than 163 eV, around 168 eV.

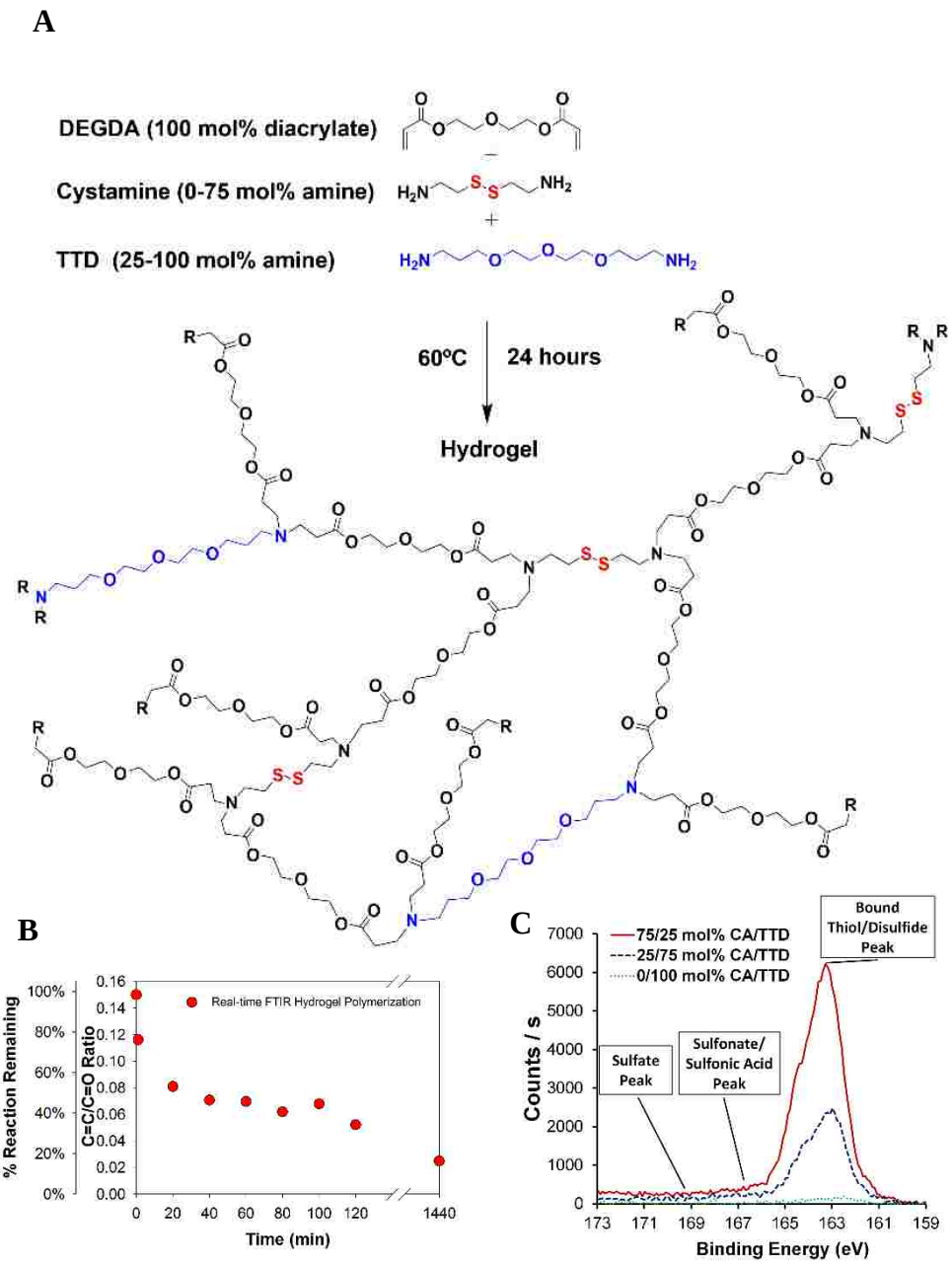

Figure 6.1. Disulfide PBAE and thiolated nanoparticle reaction scheme. A) PBAE disulfide hydrogel reaction scheme. B) Carbon double bond conversion using real-time FTIR polymerization on a heated ATR crystal, where the dashed abscissa line indicates the endpoint C=C/C=O ratio after 24 hours. C) XPS S2p spectra comparing sulfur (disulfide/bound thiol) binding energy at 163 eV. n=1 B,C.

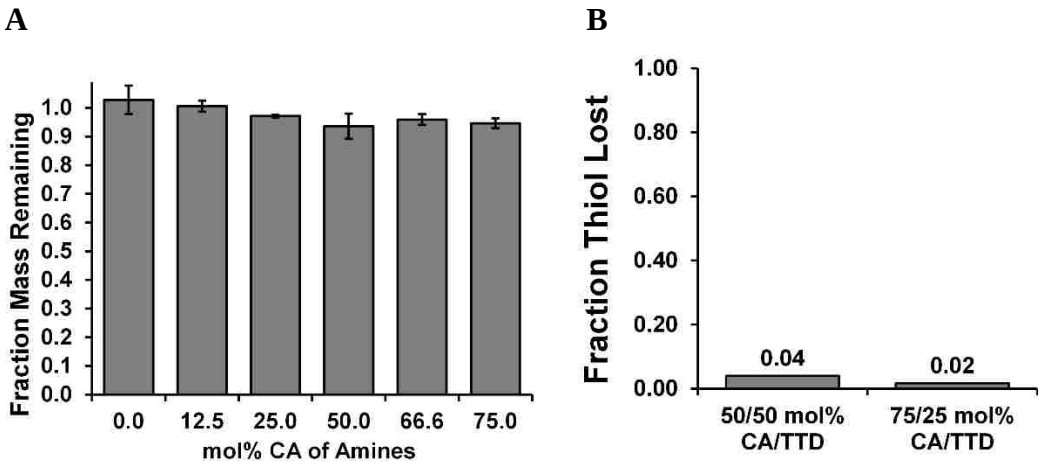

Figure 6.2. Washing results. A) Mass of hydrogels remaining after washing with DMSO and freeze drying (mass after wash / mass before wash), n=3, standard deviation. B) Thiol content of total lost in DMSO washing, n=1.

With intent to form a poly(beta-amino ester) hydrogel, hydrolytically cleavable ester bonds existed after reaction of DEGDA's acrylate groups to amines. The rate of degradation in 1x phosphate buffered saline (PBS) was expected to be dependent upon the relative hydrophilicity of the hydrogel. As cystamine is highly hydrophilic, it should increase the degradation rate with increasing content. By exposing CA/TTD hydrogels to PBS, degradation rate accelerated with increased cystamine content; the 75/25 mol% CA/TTD hydrogel degraded over 24 to 48 hours, compared to 48 to 72 hours for those with the lower cystamine content gels (50/50 mol% CA/TTD) (Figure 6.3A). Since these hydrogels degrade into ester-containing fragments of their backbone, these fragments should be released with intact disulfide bonds. Therefore, we gathered the supernatants and performed Ellman's free thiol assay to determine if the rate of disulfide release matched that of the degradation mass loss or if there was degradative preference to the disulfide regions due to their hydrophilicity. Release rates of disulfides were found over the same periods as the degradation products (Figure 6.4). By comparing the disulfide release rate to the degradation rate in M_t/M_∞, it can be seen whether cystamine release was diffusion controlled or degradation controlled. It was apparent, due to the closeness to the y=x line indicating coupled release between drug and degradation products, that release was degradation controlled throughout the lifespan of the material (Figure 6.3B).

6.3.2 Effect of a Reducing Environment

As hydrogels included disulfide bonds, it could be expected that if these were incorporated into the hydrogel backbone, a reducing environment would cleave these disulfides. Depending upon the extent of cystamine incorporation, a reducing environment could either decrease the crosslinking density or fully degrade the gel. Using the highest

cystamine content gel formed, a 75/25 mol% CA/TTD cystamine hydrogel, we added tris(2-carboxyethyl)phosphine (TCEP) reducing agent in excess and measured the mass remaining of the hydrogel over time. Indeed, it only took 2 hours to completely solubilize this hydrogel into DMSO (Figure 6.4B). We then varied the cystamine content from 0/100, 5/95, 25/75, 50/50, 66.6/33.3, and 75/25 mol% CA/TTD, and it was found that at 66.6/33.3 mol% CA/TTD and lower cystamine content, the hydrogels did not degrade completely into soluble degradation products after 12 hours with excess 2-mercaptoethanol reducing agent, but at concentrations above 66.6/33.3 mol% CA/TTD cystamine (e.g. 75/25), complete solubilization occurred (Figure 6.3C). This result indicates the ability for delivery of this material in a reduced state with antioxidant thiol groups that are likely exposed.

6.3.3 Drug Release of Pre-reduced Hydrogel

For reduced hydrogels below the 66.6/33.3 mol% CA/TTD cystamine content threshold at which bulk mass remains, these should contain antioxidant moieties as endcaps where disulfides previously existed. Upon introduction to an aqueous environment, the ester-cleaved fragments would thereby contain these thiol endcaps, and allow for antioxidant release proportional to the rate of degradation. To determine this, we first reduced a 50/50 mol% CA/TTD hydrogel in excess TCEP, and then after washing away free reducing agent, the thiol content was measured in degradation supernatants as a function of incubation time in PBS. As anticipated, the 50/50 mol% CA/TTD hydrogel previously reduced showed release of free thiol groups compared to controls (Figure 6.3D). The degradation time decreased substantially from a previous 48-72 hours in the oxidized state to 10-24 hours in the reduced form. This decrease was perhaps due to a combination of larger void volume, allowing for greater solvent interaction, and enhanced hydrophilicity with the extra thiol

endcap content. Roughly 10% of mass was lost due to initial reduction, with the remainder perhaps due to oxidation of thiols over time (compare with Figure 6.4C).

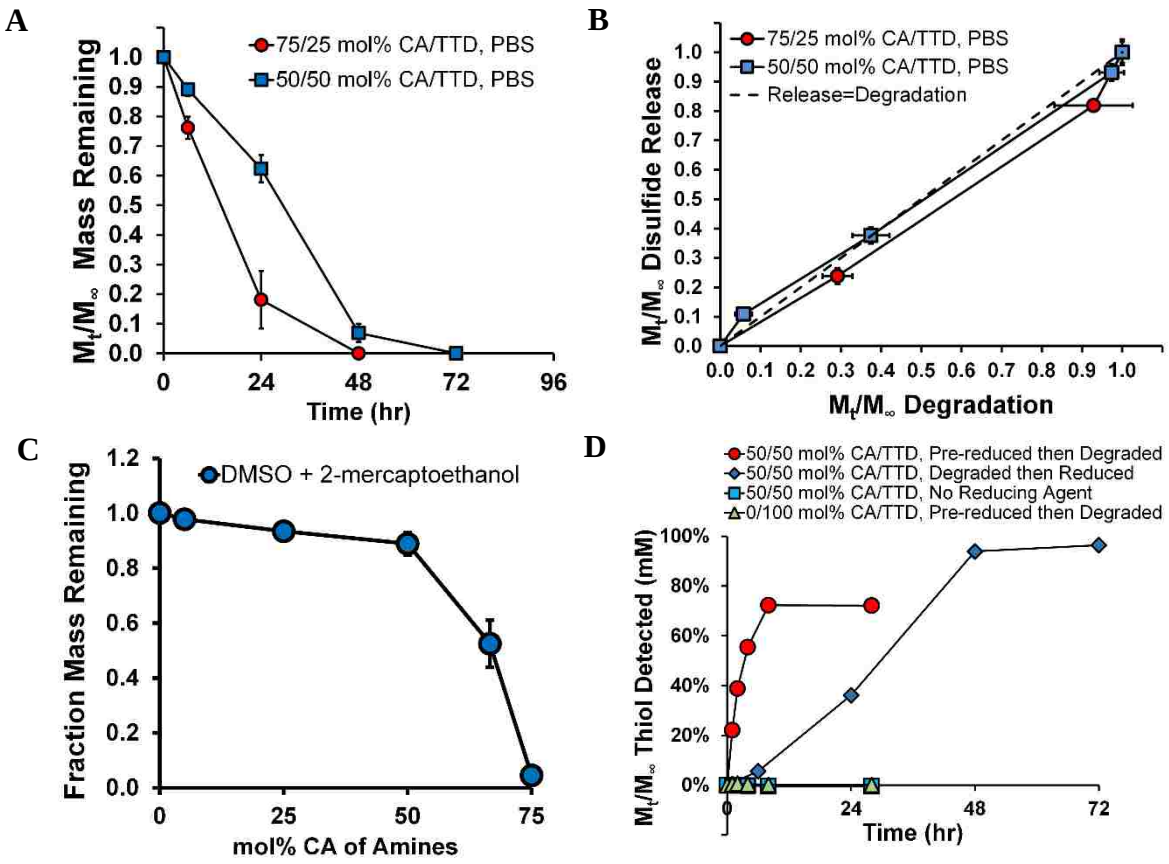

Figure 6.3. Disulfide hydrogel characteristics. A) Mass remaining of 50/50 and 75/25 mol% CA/TTD hydrogels via degradation in PBS at 37ºC in sink conditions. B) Comparison of disulfide release rate vs. bulk hydrogel degradation. C) Fraction of hydrogel mass remaining after washing with 2-mercaptoethanol in DMSO vs. cystamine molar content. D) Rate of thiol-containing species eluting from 50/50 mol% CA/TTD, or 0/100 mol% CA/TTD hydrogels in PBS which had been pre-reduced with TCEP in DMSO (16 hr) and washed, reduced post-degradation, or not reduced. n=3 each for A-D, standard deviation.

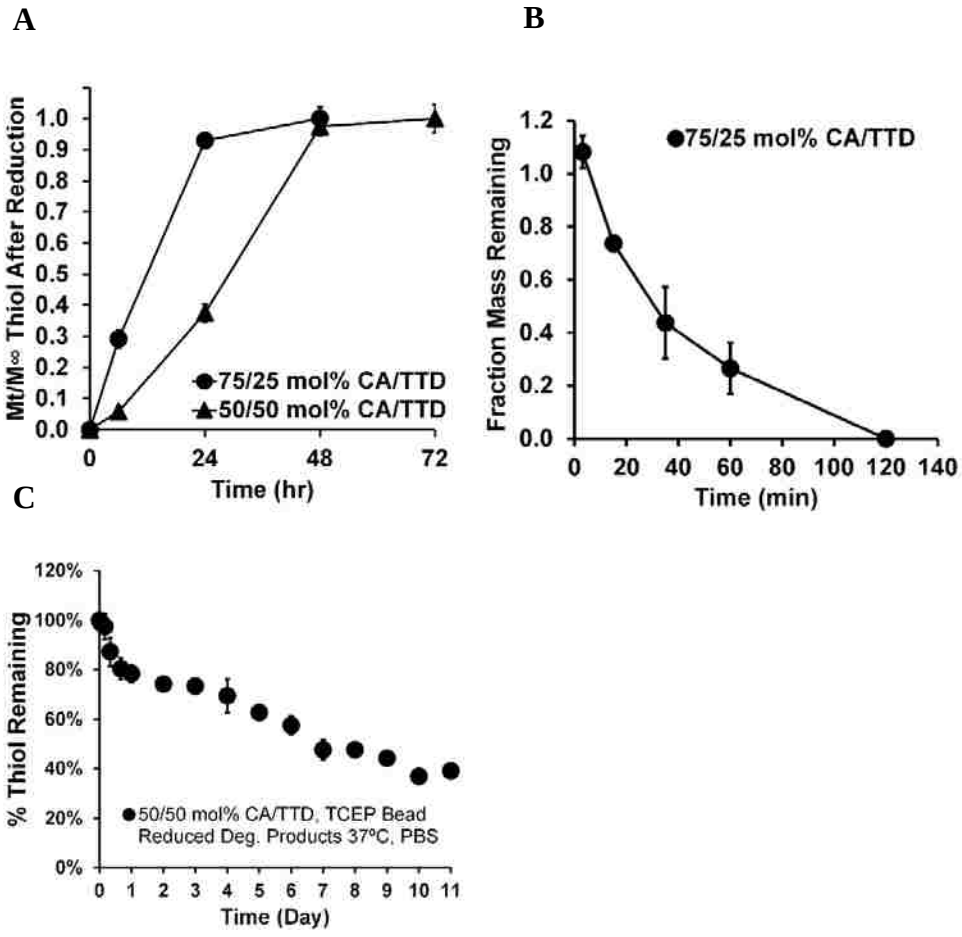

Figure 6.4. Reduced hydrogel characteristics. A) Release rate of disulfides post-reduced to thiols found in the soluble degradation products of Figure 6.3A hydrogels. B) Kinetics of reduction for a 75/25 mol% CA/TTD hydrogel in 2-mercaptoethanol and DMSO, detected via Ellman's assay. C) Percent of solubilized 50/50 mol% CA/TTD hydrogel degradation products remaining in the thiol state over time in PBS at 37ºC. n=3 for all, standard deviation.

6.3.4 Hydrogel Swelling and Mesh Size

Increasing the content of cystamine increased the degradation rate, which could be explained through swelling ratio observation. Further, if these hydrogels are exposed to reducing conditions, their swelling ratio should increase readily due to not only mass loss but from the increase in mesh size as a result of de-coupling disulfide bonds into thiol endcaps. We found this hypothesis to be validated after placing hydrogels of varying cystamine content in reducing conditions in anhydrous DMSO for 8 hours until equilibrium swelling occurred (Figure 6.5A). While the 75/25 mol% CA/TTD hydrogel solubilized completely, the lower content gels showed a dramatic spike in swelling ratio in DMSO, indicating backbone cleavage. To see if a margin of the crosslinking could be recovered, we re-oxidized these hydrogels in air after freeze drying and found that the swelling ratio was decreased slightly ($p=0.003$ for 50/50 mol% CA/TTD, $p=0.13$ for 66.6/33.3 mol% CA/TTD). Full recovery was not expected, however, as the solubilized products which diffused from the hydrogel into the DMSO solution were not recoverable and discarded, which precluded the hydrogel returning to its original state.

Flory-Huggins parameter calculation (Figure 6.5C) showed a decrease in value with increasing cystamine content, similarly for both the oxidized and reduced materials, indicating increased miscibility with DMSO. This correlated with the observed increase in swelling ratio. Since χ values were greater for the reduced (SH) backbone compared to oxidized (SS), the increase in swelling was not due to an increased polymer-solvent miscibility, and is further corroborated by disulfide cleavage. The mesh size calculation found sizes from 8.2 ± 0.2 Å to 9.0 ± 0.6 Å for the oxidized, and 8.0 ± 0.15 Å to 18.2 ± 2.8 Å for the reduced hydrogels, with increasing mesh size with increasing cystamine content.

After re-oxidation of the initially reduced hydrogel, the mesh size decreased, but was not significantly recovered at 16.7 ± 2.9 Å. n=3, standard deviation.

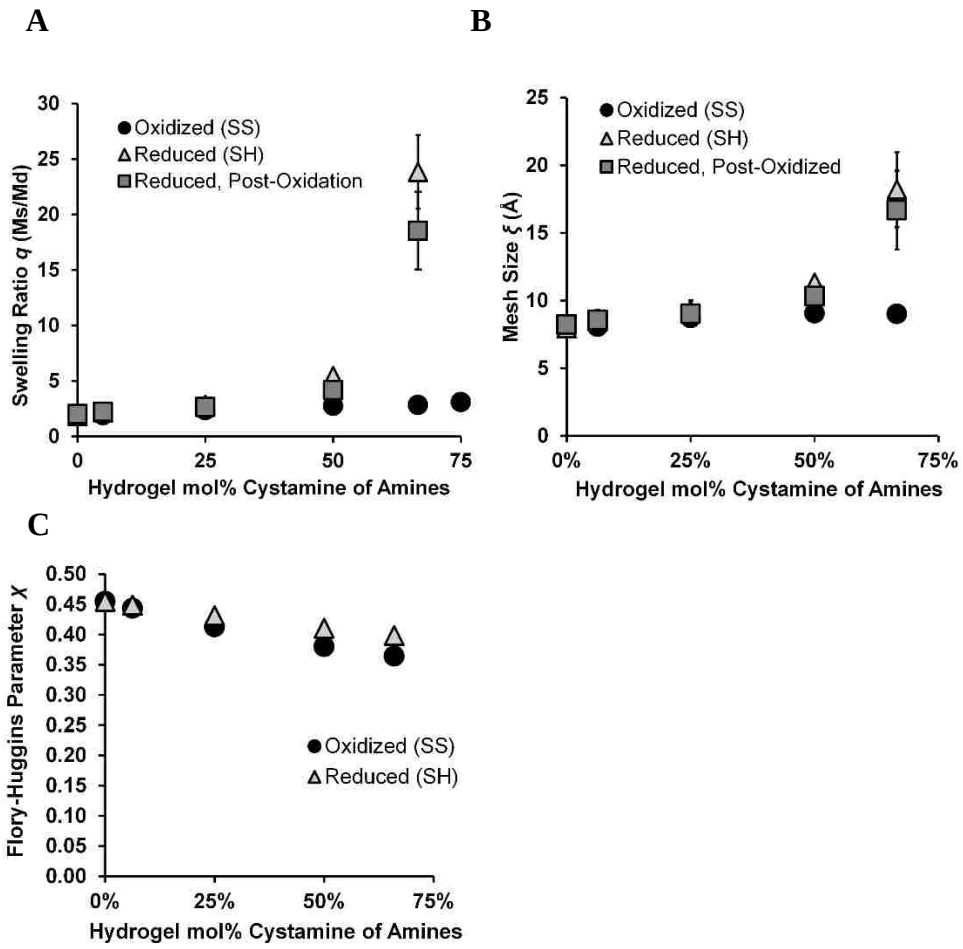

Figure 6.5. Equilibrium swelling of various cystamine content hydrogels in DMSO. A) Swelling ratio, B) calculated mesh size, and C) calculated Flory-Huggins parameter. n=3, standard deviation.

6.3.5 Cytotoxicity of Degradation Products on HUVEC

To evaluate cellular toxicity of the cystamine hydrogels, human umbilical vein endothelial cells (HUVEC) were exposed to serial dilutions of hydrogel degradation products for 24 hours, and viability was measured using Calcein-AM live stain. Degradation products were either reduced using TCEP beads or kept neat (disulfide state) and quantified for their thiol content in PBS. It was found that hydrogels containing cystamine showed large differential toxicity dependent upon their redox state, whereas treatment with TCEP reducing agent had only a small effect on cell response to the control hydrogel without cystamine (Figure 6.6A-C). This shift in half maximal toxic conentration (TC50) on the control with reducing agent was perhaps due to a low level of leached reducing agent from the TCEP beads at less than 1 mM (data not shown). Degradation products with reduced cystamine resulted in a cellular toxic concentration (TC50) between 13.5 and 15.5 times higher than their respective disulfide containing samples. TC50 values can be found in Table 1. It was originally hypothesized that the presence of disulfide would increase cytotoxicity, but this was not observed in this assay as TC50 values of the disulfide containing hydrogels were similar to those for the unloaded 0/100 mol% CA/TTD result, near 0.5 mg/mL. Yet, the reduced samples containing cystamine show much higher cytocompatibility than the 0/100 mol% CA/TTD control (near 7 mg/mL each), indicating antioxidant induced cytoprotection. Considering how there is higher thiol content at a lower bulk material concentration for the 75/25 mol% CA/TTD hydrogel, yet nearly equal for the 50/50 mol% CA/TTD, there may be a combination of effects occurring to determine cytotoxicity, with DEGDA and TTD being negative factors and thiol being a positive. Comparing these TC50 values to literature of other PBAE hydrogel supernatants, the unloaded 0/100 mol%

CA/TTD and oxidized samples show greater cytotoxicity, which was comparable to that for the PEGDA with TTD crosslinked hydrogels of Wattamwar et al. **[7]** In contrast, the thiol-containing samples show lower cytotoxicity, similar to Lakes et al. **[62]** using DEGDA/PEGDA/isobutylamine and vancomycin hydrogels but greater than the poly-antioxidant PBAE from Wattamwar et al. (1 mg/mL) **[75]**. It is apparent that the presence of thiol groups within the degradation products significantly lowered cellular viability compared to the hydrogel containing DEGDA and TTD only.

Table 6.1. Comparison of TC50 Values on HUVEC.

	TC50 (mg/mL)		TC50 (mM)	
Mol% CA/TTD	**-Reducing Agent**	**+Reducing Agent**	**-Reducing Agent (Disulfide)**	**+Reducing Agent (Thiol)**
0/100	0.56	1.0	0.00	1.0*
50/50	0.63	8.5	0.32	8.7
75/25	0.44	6.8	0.35	11
PLGA	16.6	—	0.00	—

*Contains residual TCEP, no thiol

6.3.6 Protection from Oxidative Stress on HUVEC

It was hypothesized that the reduced hydrogel form containing thiols would show protection against a reactive oxygen species insult, resulting in enhanced cellular viability compared to controls or the disulfide formulation. To demonstrate suppression of oxidative stress, HUVECs were exposed to a superoxide-producing hypoxanthine and xanthine oxidase (HX/XO) reaction in the presence of hydrogel degradation products in both forms. **[418]** A significant increase in cell viability was demonstrated with the reduced sample compared to a blank control containing only HX/XO and cells at two concentrations of 2.5 and 5 mg/mL (Figure 6.6D). In contrast, the oxidized samples showed no viability with or without superoxide insult at the same concentrations tested (Figure 6.6E). This result exemplifies the differential toxicity between the two material types in that the reduced form lowers oxidative injury, yet creates injury in the oxidized form.

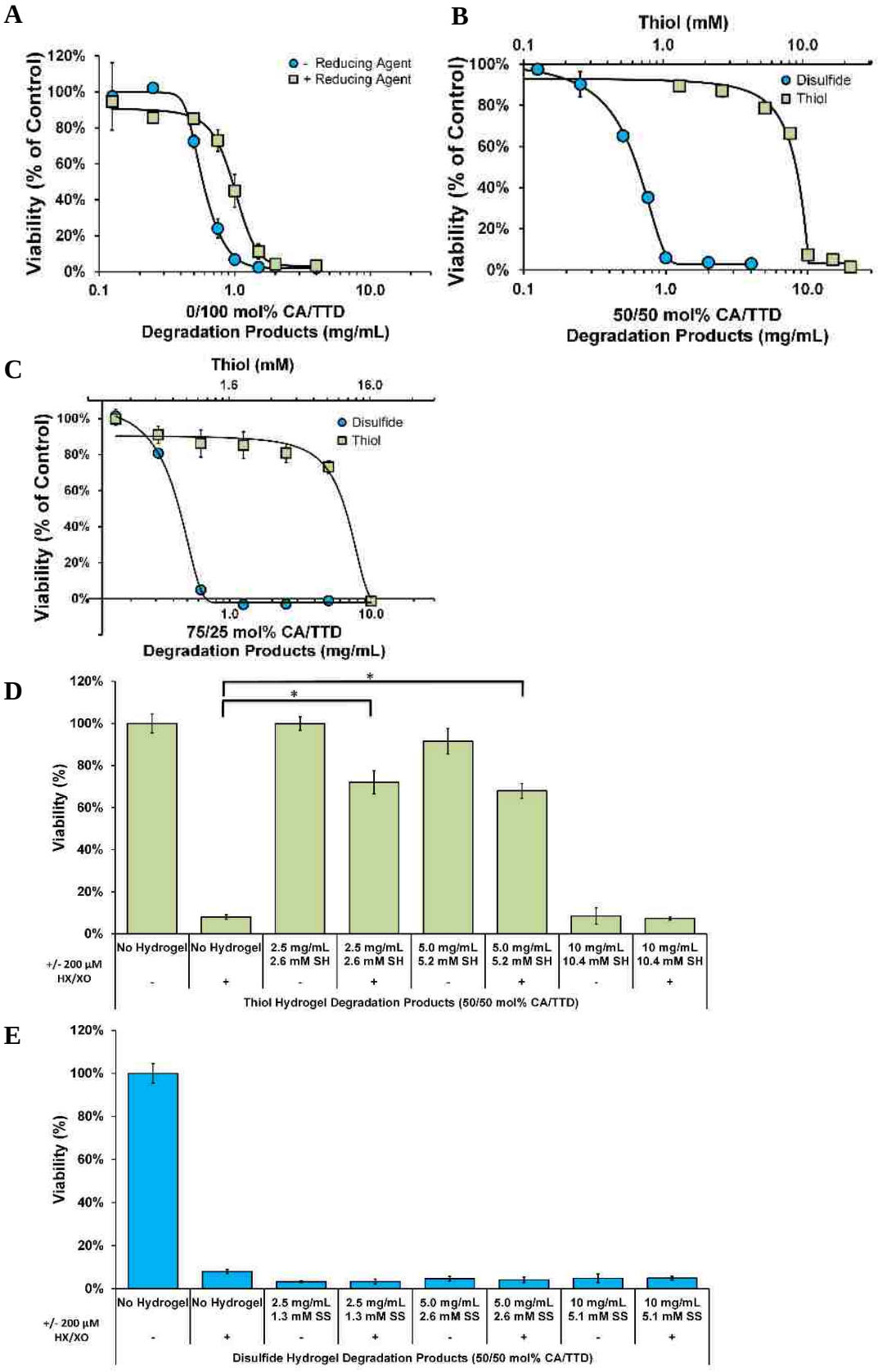
A
Viability (% of Control)
120%
100%
80%
60%
40%
20%
0%
0.1
1.0
10.0
- Reducing Agent
+ Reducing Agent
0/100 mol% CA/TTD
Degradation Products (mg/mL)
B
Thiol (mM)
0.1
1.0
10.0
Disulfide
Thiol
50/50 mol% CA/TTD
Degradation Products (mg/mL)
C
Thiol (mM)
1.6
16.0
75/25 mol% CA/TTD
Degradation Products (mg/mL)
D
Viability (%)
*
*
No Hydrogel
No Hydrogel
2.5 mg/mL 2.6 mM SH
5.0 mg/mL 5.2 mM SH
10 mg/mL 10.4 mM SH
+/- 200 µM HX/XO
Thiol Hydrogel Degradation Products (50/50 mol% CA/TTD)
E
Viability (%)
No Hydrogel
2.5 mg/mL 1.3 mM SS
5.0 mg/mL 2.6 mM SS
10 mg/mL 5.1 mM SS
+/- 200 µM HX/XO
Disulfide Hydrogel Degradation Products (50/50 mol% CA/TTD)

Figure 6.6. Cellular viability of degradation products. A-C) Cellular viability of hydrogel degradation products without (disulfide form) or with (reduced form) TCEP reducing agent beads with A) 0/100 mol% CA/TTD (unloaded), B) 50/50 mol% CA/TTD C) 75/25 mol% CA/TDD. D,E) HX/XO free radical generation assay comparing cell viability of 50/50 mol% CA/TTD hydrogels in the reduced state and oxidized state, with and without oxidative injury with dose response (200 uM HX, 18.75 mU XO). n=5 A-E, standard deviation. *$p<0.05$ with Bonferroni correction to the "No Hydrogel +HX".

6.3.7 Mitochondrial Response to Oxidative Stress on HUVEC

In order to further our mechanistic understanding behind the viability differences found between oxidized (SS) and reduced (SH) hydrogel degradation products, we performed a Seahorse Bioscience XF assay to determine changes in mitochondrial oxygen consumption rate, as under cellular distress, mitochondrial dysfunction may ultimately cause cell death. Using an equal hydrogel degradation product concentration (0.156 mg/mL) which was below the IC50 for both the SS and SH containing 50/50 mol% CA/TTD, we subjected the previous Calcein-AM HX/XO injury model to a Seahorse XF assay to analyze effects of mitochondrial oxygen consumption rate (OCR).

6.3.8 Total OCR Results

Without HX/XO treatment, the disulfide-containing material (SS) showed several significant differences in viability in total OCR values (Figure 6.7A-D) for ATP production, total respiration, and max respiration compared to live controls. The decreases in OCR in the SS groups is similar to the viability differences found in the Calcein-AM based HX/XO study of Figure 6.6E. Also similar to Figure 6.6E, with HX treatment, there were no statistical changes comparing the live control to the SS material, indicating no protection. Comparing the cellular protein content of Figure 6.8, there is an average decrease, but non-significant difference between the control and SS groups without HX treatment. This small decrease may be due to mitochondrial stress due to reduced ATP production, as can be seen by the significant decrease in SS total OCR without HX treatment compared to the control without HX treatment (Figure 6.7B).

Looking at the reduced thiol-containing material (SH) for total OCR without HX treatment,

results are again similar to the prior HX/XO viability assay (Figure 6.6D) in that there are no statistical changes in viability compared to the -HX live control for all four tests, and with HX treatment, SH viability remains statistically higher than the respective control for basal respiration and ATP production. These results indicate higher cellular viability after SH material addition compared to SS, and also a protective effect against HX/XO induced oxidative stress. Comparing the protein normalized % OCR may be more insightful to remove confounding protein differences that indicate cellular viability, and not necessarily mitochondrial function directly.

6.3.9 % OCR Results (Protein Normalized)

After normalizing for protein content (Figure 6.8), the statistical differences found in Figure 6.4A-D were not present in Figure 6.4E-H for both the SS and SH materials, with the only exception being for -HX SS spare respiration, and, while insignificant, lower averages were found for the SS material in ATP production and max respiration with HX treatment. Spare respiration determines how well mitochondria respond when there is increased cellular energy demand, defined as the difference between the basal and maximal OCR in the assay. The disulfide material responded poorly to spare respiration compared to the SH material, perhaps indicating that the SS material is causing mitochondria to shift ATP energy towards detoxification of the SS material, thus lowering the respiratory reserve energy. Total ATP production for the SH material with HX treatment remained very high, further identifying potential protection. The statistical power of these results could be improved through running multiple Seahorse XF plates to double our replication from 7 wells in the control and 5 in the samples. Further, multiple concentrations would identify if we are able to replicate the dose-response found in the HX/XO viability assay (Figure

6.6 D,E).

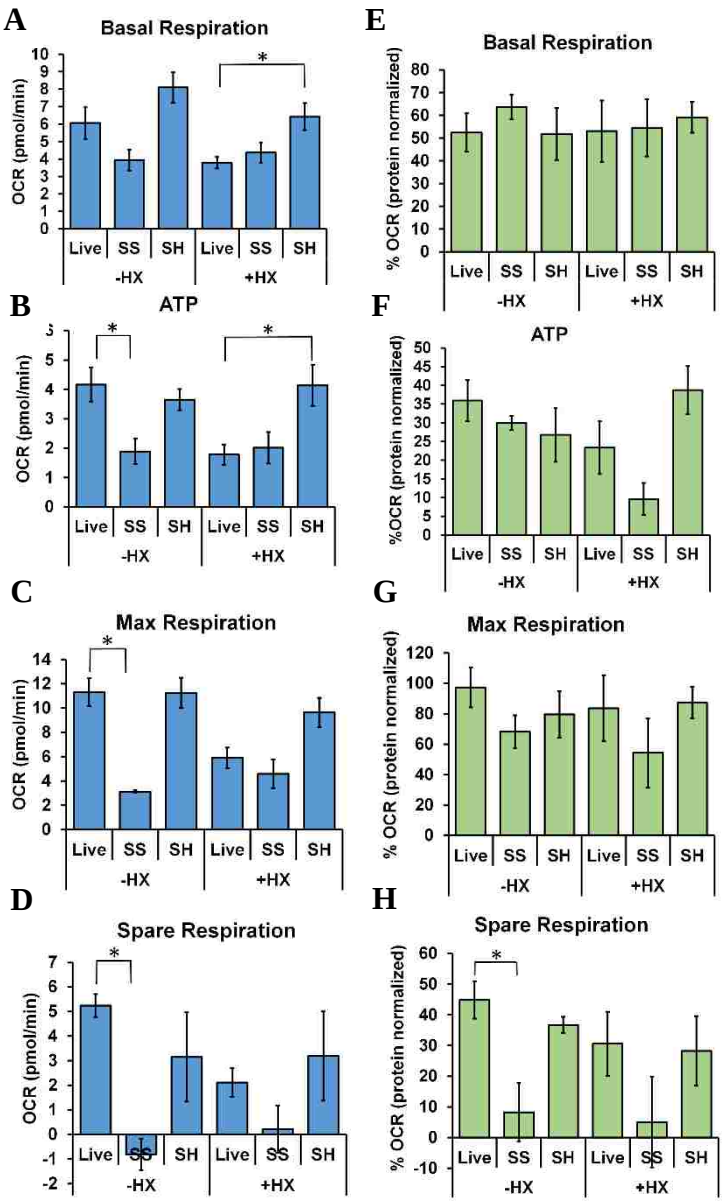

Figure 6.7. XF Seahorse assay on HUVEC. 50/50 mol% CA/TTD degradation products, ± HX/XO (200 µM/18.75 mU/mL). A-D) OCR result. E-H) %OCR result normalized for protein content. n=5 for treatments, n=7 for live control. Standard error. *p<0.05 with Bonferroni correction compared to respective controls.

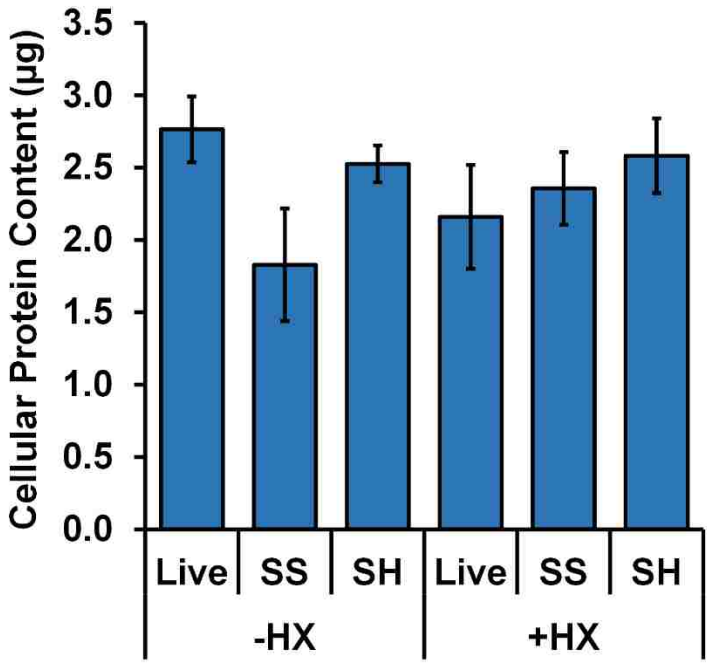

Figure 6.8. XF Seahorse assay cell protein data. Correlates to Figure 6.7. n=5 for treatments and n=7 for live control, standard error. ± HX/XO (200 µM/18.75 mU/mL). No statistical differences after Bonferroni correction to respective controls.

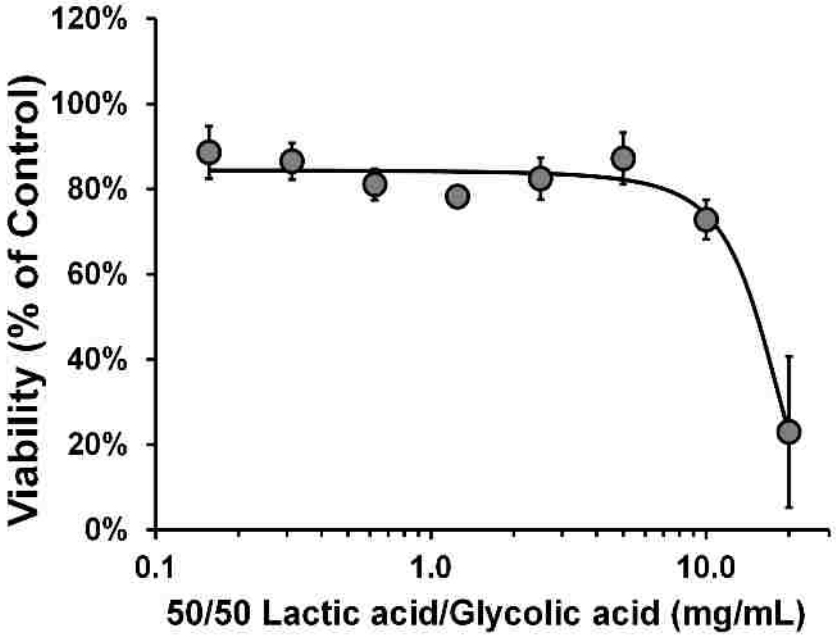

Figure 6.9. Calcein-AM viability on HUVEC. Treated with glycolic acid and lactic acid in PBS, pH shifted to 7.4 to mimic PLGA degradation products. IC_{50} = 16.6mg/mL. n=5, standard deviation.

6.4 Conclusions

Through variation of the cystamine content as a di-primary amine containing crosslinker, we were able to produce hydrogels that degrade in a reducing environment, as well as hydrolytically due to the presence of ester bonds. Interestingly, with a disulfide content lower than 75/25 mol% CA/TTD, hydrogels were shown to partially degrade in reducing conditions, leading to a thiol-containing bulk material. This thiol functionality provided utility to deliver these materials in either a disulfide-containing oxidized state or thiol-containing reduced state. With alteration of the redox state, cytotoxicity of a single base material spanned over an order of magnitude difference, with the reduced hydrogel byproducts being less toxic than other antioxidant-containing PBAEs described in the current literature and within an order of magnitude as PLGA (Figure 6.9). The reduced form also showed ability to greatly enhance cellular viability upon induction of HX/XO oxidative stress. In a similar light, stressed mitochondrial conditions (spare respiration) showcased large differences between spare respiratory capacity, as under increased oxidative duress, the disulfide material showed statistically lower total OCR and protein normalized %OCR perhaps due to material detoxification, contrary to the thiol material which was statistically no different from the live controls, and showed oxidative stress protection for total OCR values. It is hypothesized that this duality between antioxidant and oxidant state of the material is similar to the cellular redox state of GSH/GSSG, where with slight offset, oxidative toxicity or antioxidant protection is manifested, requiring mitochondrial metabolic shifts. This gives rise to potential applications of cellular antioxidant fortification for the reduced state and reduced viability the oxidized state, while using an identical concentration of materials.

Chapter 7: Thiolated Antioxidant PBAE Nanoparticles for Redox Applications

7.1 Introduction

Cellular oxidation is a key degenerative pathway in a variety of diseases, from atherosclerosis to radiation injury [419, 420]. However, cellular oxidation is also an essential, and unavoidable byproduct of cellular respiration through, among other pathways, the mitochondrial electron transport chain [421]. These oxidative processes are normally held in check by reducing agents/antioxidants produced intracellularly by essential amino acid building blocks, enzymatic antioxidants, or other materials ingested through diet such as vitamin E tocopherols and tocotrienols. A similar paradox exists with cellular reduction processes. Even antioxidants, which are an oxidative defense mechanism to keep the immune system and oxidative processes in check, can also be detrimental at high levels, such as in hypervitaminosis E or excessive immune suppression in sepsis therapy [258, 259]. It is therefore apparent that a fine balance must exist between redox molecules on the cellular level, as imbalance may lead to pathogenesis or inhibition of normal body processes [422]. This redox balance may be supplemented through selective, targeted drug delivery [423]. One approach to help re-establish redox homeostasis in times of oxidative stress is to supplement essential molecules already present in the cellular reactive oxygen species (ROS) defense system, including glutathione, N-acetyl cysteine (NAC), vitamins A and E, catalase, superoxide dismutase etc. or plant-derived polyphenols like curcumin or quercetin. Delivery of these agents has been widely studied, and yet have had mixed results depending on their delivery method and application. For instance, delivery of NAC, one of three ingredients for glutathione synthesis, has clinical application for treatment of acetaminophen overdose [290]. This is through competitive binding of the

acetaminophen metabolite N-acetyl-p-benzoquinone imine, blocking glutathione depletion. However, NAC delivery has also been shown to interrupt p53 pathways, a multifaceted protein which can initiate apoptosis and a key tumor suppressor implicated in DNA repair, hypoxia, and oncogene activation [306, 307]. In mice which inhaled *Cre* recombinase adenovirus for an increased lung cancer propensity, it was found that those given NAC (or vitamin E) supplements showed increased cancer progression rates. When *Trp53* knockout mice were used, there was no effect of antioxidant administration, identifying ROS-mediated p53 apoptosis inhibition as causing the increased cancer progression [308]. These findings implicate the risk of non-targeted antioxidant delivery to those already with cancer, especially to high risk individuals such as smokers, but do not directly identify changes in tumor initiation or prevention.

Intracellularly, glutathione (GSH) is the most abundant small biomolecule at a concentration of 1-10 mM depending on conditions within the cytosol [424, 425]. The thiol group on GSH participates in numerous redox reactions as a reducing agent, and is largely oxidized into glutathione disulfide (GSSG) whereupon glutathione reductase may regenerate the thiol groups at the expense of NADPH oxidizing to NADP+. Under normal conditions, the cytosol GSH:GSSG ratio is near 100:1, establishing the cytosolic reducing environment [426, 427]. However, under extreme cellular oxidative stress, the ratio may drop to 1-10:1, allowing for the oxidation mediated damage of important biomolecules to occur [428].

It is clear that specific local delivery to regions of the body and/or certain cell types is necessary for positive outcomes in complex oxidative stress diseases [429]. To target regions otherwise not bioavailable or accessible through direct local injection, active

targeting strategies of systemically administered drugs/complexes have been accomplished in the literature through use of monoclonal antibodies, ligands, aptamers, etc. [430]. Polymeric nanoparticles are a promising field of study to achieve local delivery of bioactive molecules to the site of interest whist minimizing non-specific interactions. However, not all nanoparticles allow for surface functionalization. If a nanoparticle is not amphiphilic enough for antibody coating, or a small molecule requires a specific orientation for reaction to occur, physadsorption may not be advantageous or even possible. Readily functionalizable nanoparticles are therefore a powerful asset for covalent addition of biomolecules, such as is the case with thiol/disulfide interchange reactions, which also has been shown in literature to be useful for redox-responsive drug release [404, 431-433].

With the intent of mimicking the glutathione redox found in the body, our group previously synthesized a highly biocompatible poly(β-amino ester) (PBAE) containing a disulfide crosslinker with di-primary amine functionality, cystamine [434]. These polymer networks were doped with the non-bioactive di-primary amine 4,7,10-trioxa-1,13-tridecanediamine (TTD), allowing for variation of cystamine content. These networks retained their bulk form while containing bound thiols within the matrix network under reducing conditions, allowing thiolated degradation products to be released upon degradation over a period of 2-3 days. Variation of cystamine content produced an effect of variable cellular viability of degradation products depending on being in the thiol (reduced) or disulfide (oxidized) form. Further, the thiol (reduced) degradation products were able to protect endothelial cells from oxidative damage. While we could form up to 75 mol% cystamine of the total amines (75/25 mol% cystamine/TTD), it was not possible to synthesize a hydrogel with cystamine accounting for 100 mol% of the amine used, due to cystamine solubility limits

in DMSO. In this work, we have overcome the reaction limitations of the 100 mol% cystamine system through using a non-nucleophilic base Michael addition catalyst, 1,8-diazabicycloundec-7-ene (DBU). With DBU to increase cystamine reaction, two network systems were made with 100 mol% cystamine, either using diethylene glycol diacrylate (DEGDA) or 1,6-hexanediol ethoxylate diacrylate (HEDA) making up the rest of the hydrogel at a 1:1 total acrylate to total amine ratio (stoichiometric based on reactive sites). Previously we found that when these hydrogels contained greater than 66 mol% of the amine of cystamine crosslinker, they would solubilize completely in reducing conditions with organic solvent due to disulfide cleavage. It was hypothesized that upon reduction of these 100 mol% cystamine of amines hydrogels, these thiolated oligomers would form nanoparticles upon single emulsion with an aqueous anti-solvent. It is the scope of this chapter to show the synthesis and characterization of these hydrogels formed and their transformation into thiolated PBAE nanoparticles, as well as discover the material properties and function as a thiol delivery vehicle for potential redox applications.

7.2 Materials and Methods

7.2.1 Materials

All reagents were used as received without further purification steps. Cystamine dihydrochloride, N-(1-pyrenyl)maleimide (NPM), 1,8-Diazabicycloundec-7-ene (DBU), 5,5'-dithiobis(2-nitrobenzoic acid) (DTNB/Ellman's Reagent), 1,6-hexanediol ethoxylate diacrylate (HEDA), and 2-mercaptoethanol (2-ME) were purchased from Sigma-Aldrich (St. Louis, MO). Diethylene glycol diacrylate (DEGDA) was purchased from Polysciences Inc. (Warrington, PA). Immobilized tris(2-carboxyethyl)phosphine (TCEP) beads were

purchased through Thermo Scientific (Waltham, MA). All solvents were purchased through either Fisher Scientific (Waltham, MA) or Pharmco-AAPER (Brookfield, CT).

7.2.2 Cystamine Hydrogel Synthesis and Washing

Cystamine was first dissolved at 185 mg/mL with a 25/75 vol% mixture of DBU catalyst/DMSO respectively during vortexing with sonication, and then added to the diacrylate (either HEDA or DEGDA) at a stoichiometric ratio between acrylate and amine reactive sites (33 mol% cystamine and 67 mol% diacrylate), and vortexed briefly. The mixture was then dispensed onto a casting ring upon a Teflon plate, and kept for 24 hours at 60ºC. Using 10x excess volume of DMSO, polymers were mixed for 3 time periods with the supernatant collected. The disulfide-containing supernatant was then reduced with immobilized TCEP beads for material loss analysis with Ellman's thiol detection assay. After DMSO washing, DMSO was removed from the gels using acetone extraction (10x volume) three times. Since cystamine is not soluble in acetone, we did not collect the acetone for cystamine detection. The washed hydrogels were then let to air dry for 1 hour, followed by freeze drying for 24 hours whereupon a change in mass was measured for based on the original mass of ingredients added. Washing of these hydrogels post-synthesis was necessary not only for quantification of unreacted cystamine and diacrylate, but also to attain FT-IR spectra. This was due to strong interference of DBU's protonated C=N form with the C=C peak from the diacrylate. Since DBU washed out after reaction, we were able to better assess the C=C conversion.

7.2.3 Extent of Hydrogel Conversion

Fourier Transform Infrared Spectroscopy (FT-IR) (Varian 7000e) was used to determine extent of reaction by tracking carbon double bond to carbonyl ratio on the acrylates before and after reaction (C=C/C=O ratio). Peak areas were measured using Varian Resolutions Pro software.

7.2.4 Bulk Hydrogel Degradation and Disulfide Release

Using excess 10 mM phosphate buffered saline at pH 7.4, sectioned hydrogels were degraded under sink conditions with PBS supernatant saved for analysis and replaced at each time point at 37 ºC. For each change in mass time point, a different hydrogel was removed from the PBS, freeze dried 24 hours, and weighed. Disulfide containing degradation product release was reduced with TCEP beads and measured for thiol content using Ellman's assay.

7.2.5 Nanoparticle Synthesis

Hydrogels were reduced with 2-ME and organic solvent (acetone or DMSO) at 20x molar excess and shaken vigorously under argon atmosphere to solubilize the thiolated linear chain PBAE oligomer. This oligomeric solution was either used as is or diluted with extra acetone or DMSO, and then added drop-wise to an aqueous solution under mild vortexing. With a final 8% organic concentration after initial single emulsion nanoparticle formation, nanoparticles were washed 3 times under appropriate centrifugation periods at 30000 G to remove organic solvent, reducing agent, and uncoupled oligomers.

7.2.6 Mass Spectroscopy

Mass spectroscopy data were obtained at the University of Kentucky Mass Spectrometry Facility using a Bruker Ultraflextreme time-of-flight mass spectrometer equipped with a smartbeam-II solid state laser (Nd:YAG, 355 nm), using dihydroxybenzoic acid as the matrix for matrix-assisted laser desorption/ionization (MALDI) sample preparation. Two sample types of reduced hydrogels were analyzed, 1) hydrogels reduced with 2-ME in acetone, and 2) hydrogels reduced with 2-ME in acetone, formed into nanoparticle in DI water which were washed, and then the solution freeze dried and reduced again using 2-ME and acetone.

7.2.7 Microscopy

Electron microscopy was performed at the University of Kentucky's Electron Microscopy Center. Scanning electron microscopy (SEM) was first performed with a Hitachi S4300 with a low concentration sample (0.01 mg/mL) of HEDA/CA nanoparticles formed in DI water which were washed, flash frozen, and freeze dried onto carbon tape. A high concentration nanoparticle sample (5 mg/mL) was formed with an HEDA/CA hydrogel, which was reduced with 2-ME and formed into DI water. This sample was then washed and air dried onto aluminum foil (instead of flash frozen and freeze dried). SEM and energy dispersive X-ray spectroscopy (EDS) were analyzed using an FEI Helios DualBeam FIB/SEM for imaging and elemental analysis.

For fluorescent conjugate nanoparticle imaging, the thiol-reactive fluorescent dye, N-(1-pyrenyl)maleimide (NPM), was reacted at 10x molar excess with HEDA/CA and DEGDA/CA thiolated nanoparticles for 1 hour in 50/50 vol% DMSO/DI water at room

temperature, and then washed out 3 times. Particle sizes were taken before and after conjugation. Fluorescent microspore images were taken at 1 ms for bright field and 60 s for UV filtered images.

7.2.8 Nanoparticle Size vs Feed Concentration

Using 2-ME reduced hydrogels in either acetone or DMSO at various concentrations, nanoparticle were added dropwise into a vortexed tube of 10 mM PBS containing 1 wt% of 78% hydrolyzed 6000 MW poly(vinyl alcohol) (PVA) and 1 mM EDTA. Size (z-average diameter) and polydispersity index (PDI) were determined with a Malvern Zetasizer Nano.

7.2.9 Nanoparticle Kinetic Size and Thiol Activity

Using three feed concentrations of 25, 50, and 75 mg/mL 2-ME reduced hydrogel in either DMSO (for HEDA/CA) or acetone (for DEGDA/CA), nanoparticles were formed from dropwise addition into the PBS/PVA/EDTA solution and washed 3 times. A 4^{th} wash was collected to determine the background reducing agent levels, and also to determine pellet mass after freeze drying for final nanoparticle concentrations formed (listed in plot legends of Figures 7.8 and 7.9). We chose DMSO for HEDA/CA and acetone for DEGDA/CA as they formed at the highest concentration of nanoparticles respectively, allowing for ease of pellet mass measurement. Nanoparticle-bound thiol content was measured using a modified version of Ellman's assay, where after 20 minutes of incubation of nanoparticles with 5,5'-dithiobis-(2-nitrobenzoic acid) (DTNB) solution, the mixture was centrifuged for 5 minutes at 30000 G to remove nanoparticle precipitates and the supernatant read at 412nm at each time point. Percent intensity of initial time point measurements were made

with derived total count rate measurements from the DLS. Theoretical max thiol was calculated from knowledge of the pellet mass and hydrogel cystamine mass fraction, assuming an equal distribution of cystamine-containing oligomers remained in the nanoparticle compared to what was washed out.

7.3 Results

7.3.1 Cystamine Hydrogel Material Characteristics

Through the use of the Michael addition catalyst, DBU [435], we were able to produce 100 mol% of the amine hydrogels (Figure 7.1 A). Two types of hydrogels were formed, the first with HEDA and cystamine (CA), and the second with DEGDA and CA. The ratio of acrylate to amine was kept constant at 1:1. The cystamine was added to the reactants at 20 wt% for HEDA and 26% for the DEGDA preparations. After polymerization, the samples were washed using DMSO to remove excess monomers and DBU catalyst, and analyzed for cystamine loss (Figure 7.2 A) and total mass loss (Figure 7.2 B). While the HEDA/CA hydrogel had a 1.0 ± 0.24% total mass loss with 0.2 ± 0.01% of that from the cystamine alone, the DEGDA/CA hydrogel saw 7.7 ± 6.7% total mass loss with 2.3 ± 0.23% loss being from cystamine. n=3, standard deviation.

After washing, freeze dried hydrogels were analyzed using FT-IR to determine the extent of reaction by comparing the remaining diacrylate ratio of the carbon double bond to carbonyl ratio (C=C/C=O) (Figure 7.2 C). The HEDA/CA hydrogel showed slightly fewer uncreacted diacrylates (greater conversion) with 0.036 ± 0.0063 (21 ± 3.7% of the C=C/C=O final/initial), where the DEGDA/CA hydrogel was found to have 0.045 ± 0.011 (28 ± 7.0% of the C=C/C=O final/initial) remaining. n=3, standard deviation.

These hydrogels, were theoretically predicted to show hydrolytic degradation of ester bonds in aqueous media. While the DEGDA/CA hydrogel degraded measurably over 7 days to roughly 26% ± 23% mass remaining (Figure 7.2 D) with 52% ± 2% disulfide-containing degradation products released (n=3, standard deviation) (Figure 7.2 E), the HEDA formulation remained within error of 100% mass remaining after 7 days, and less than 1% disulfide-containing degradation products released. Comparing the disulfide release to degradation rate (Figure 7.2 F), disulfide release appears to be degradation based (i.e. close to the 45º line), if not slightly slower than degradation, perhaps explained by over reporting of degradation by continual small undissolved hydrogel fragments being aspirated at later time points, and thus not detected in solution for Ellman's detection assay.

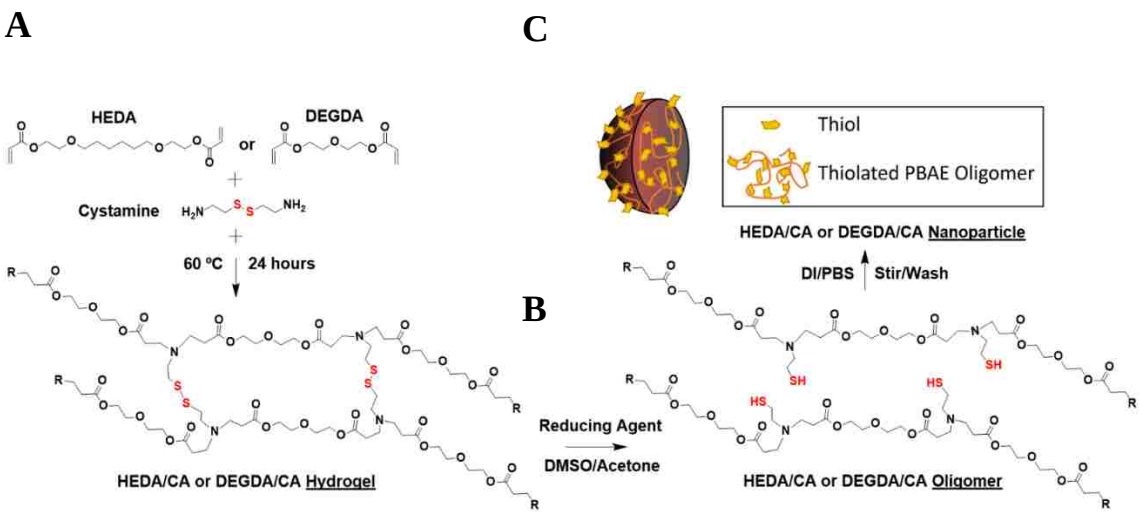

Figure 7.1. Synthesis schematic. A) disulfide PBAE hydrogel and conversion into B) thiolated oligomers via a reducing agent (2-mercaptoethanol), and C) single-emulsion into thiolated nanoparticles.

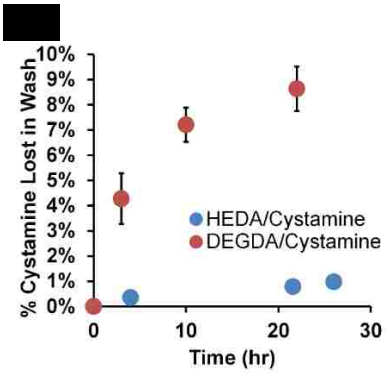
% Cystamine Lost in Wash
10%
9%
8%
7%
6%
5%
4%
3%
2%
1%
0%
0
10
20
30
Time (hr)
HEDA/Cystamine
DEGDA/Cystamine

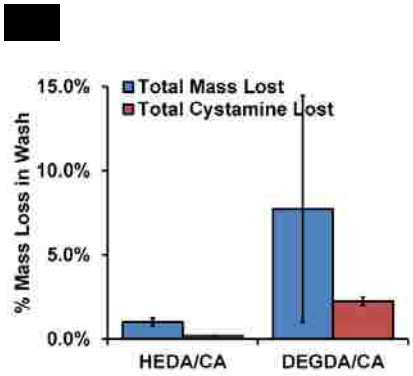
% Mass Loss in Wash
15.0%
10.0%
5.0%
0.0%
Total Mass Lost
Total Cystamine Lost
HEDA/CA
DEGDA/CA

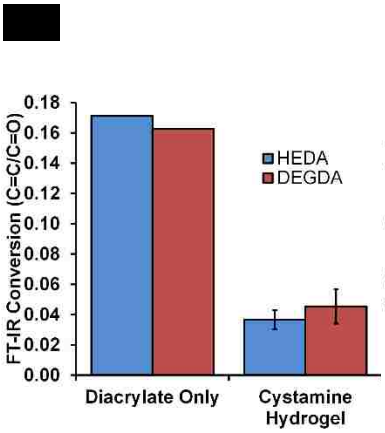
FT-IR Conversion (C=C/C=O)
0.18
0.16
0.14
0.12
0.10
0.08
0.06
0.04
0.02
0.00
HEDA
DEGDA
Diacrylate Only
Cystamine Hydrogel

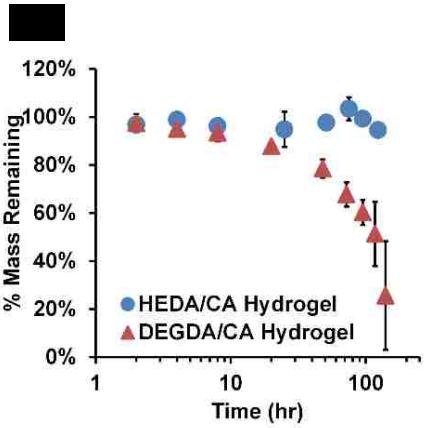
% Mass Remaining
120%
100%
80%
60%
40%
20%
0%
1
10
100
Time (hr)
HEDA/CA Hydrogel
DEGDA/CA Hydrogel

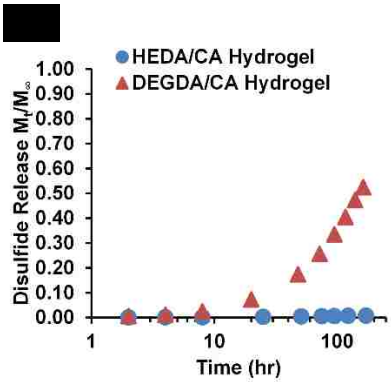
Disulfide Release Mt/M∞
1.00
0.90
0.80
0.70
0.60
0.50
0.40
0.30
0.20
0.10
0.00
1
10
100
Time (hr)
HEDA/CA Hydrogel
DEGDA/CA Hydrogel

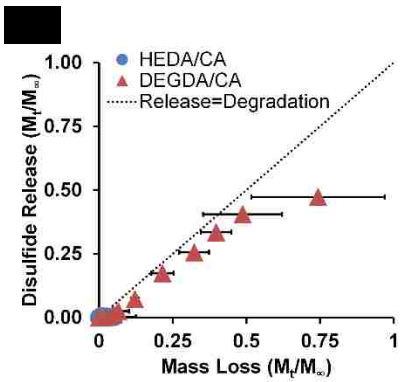
Disulfide Release (Mt/M∞)
1.00
0.75
0.50
0.25
0.00
0
0.25
0.5
0.75
1
Mass Loss (Mt/M∞)
HEDA/CA
DEGDA/CA
Release=Degradation

Figure 7.2. Disulfide hydrogel characteristics. A) kinetic cystamine mass loss after washing B) total mass and cystamine loss of theoretical total and C) conversion with FT-IR. D) % mass remaining during sink condition degradation at 37 ºC, E) disulfide release and F) comparison of disulfide release to mass loss over time. n=3, standard deviation, each time point other than C) “diacrylate only” where n=1.

7.3.2 Properties of Reduced Hydrogels

Due to the presence of disulfide crosslinks in the network backbone, reducing conditions will cleave those disulfide bonds to form a thiolated linear polymer. Reduction proceeded for 1 hour with a vigorously mixed solution under argon until the matrix was dissolved, using 50/50 vol% 20x stoichiometric reducing agent (2-ME) and acetone or DMSO. Following reduction, hydrogels were solubilized in either DMSO or acetone, whereupon they were analyzed for molecular weight with mass spectroscopy (#1). A second set, however, was also analyzed for molecular weight after the oligomer solution was used to form nanoparticles which were washed, freeze dried, and re-reduced with 2-ME in acetone (#2). The median molecular weight found for the reduced HEDA/CA hydrogel was 2000 m/z before nanoparticle formation (#1) and 2600 m/z after nanoparticle formation (#2) (Figure 7.3 A,B). Similarly for the reduced DEGDA/CA hydrogel, the molecular weight was 2400 m/z before (#1) and 2500 m/z after (#2) nanoparticle formation (Figure 7.3 C,D). More dramatic, however, was the increased higher molecular weight tail for the reduced materials after nanoparticle formation and washing. For a molecular weight of 2500 Da, approximately 10 mers are required for the thiolated oligomers formed from the reduced hydrogels. Due to the low ionization intensity of MALDI MS, it is typical to assume that z=1 for these polymers.

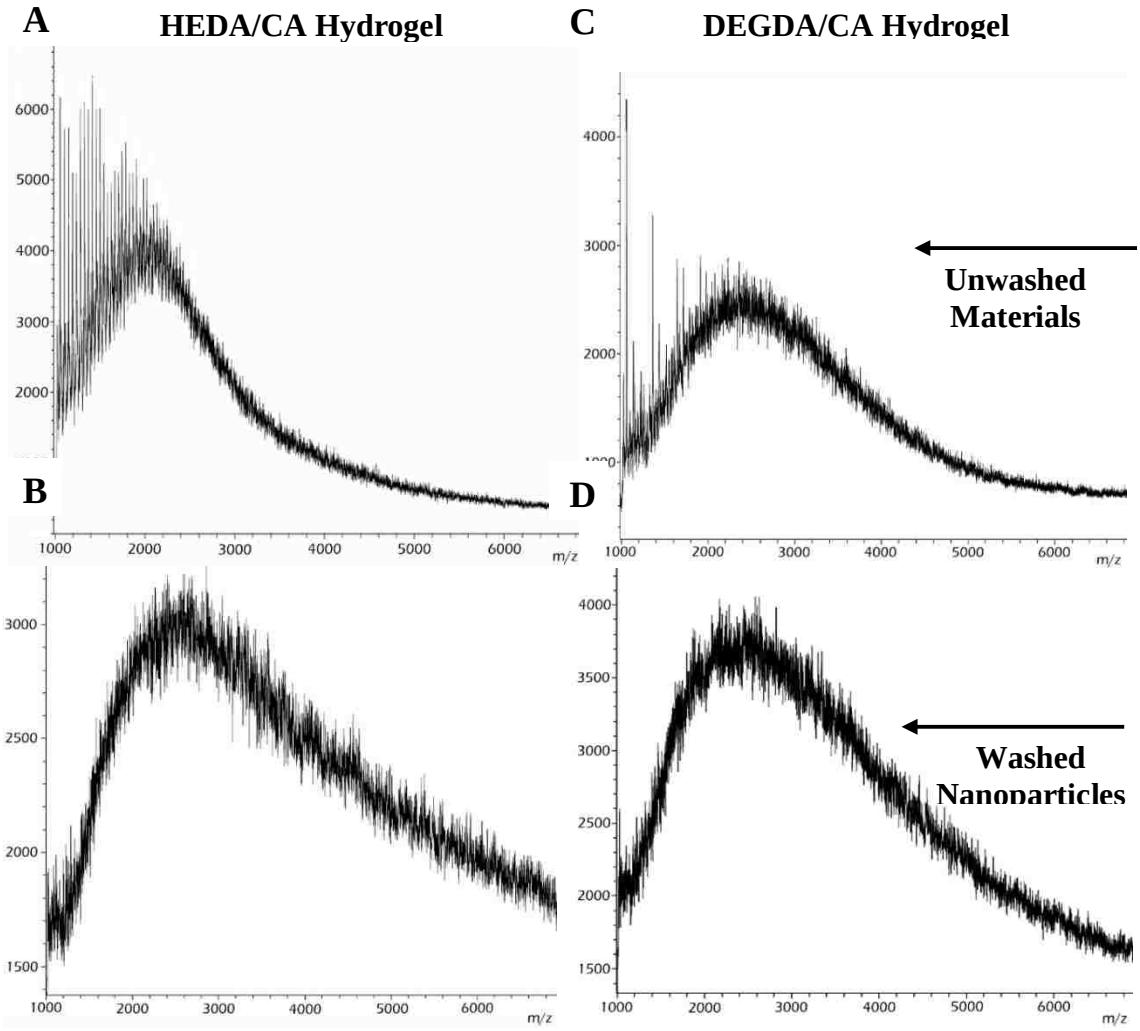

Figure 7.3. Mass spectroscopy of thiolated oligomers. A) and B) HEDA/CA reduced hydrogels before and after nanoparticle formation. B) and C) DEGDA/CA reduced hydrogels before and after nanoparticle formation. Y-axis is intensity (a.u.).

7.3.3 Thiolated Nanoparticles

Thiolated PBAE nanoparticles were formed through single emulsion of reduced oligomers (Figure 7.1 C). After adding hydrogels into organic solvent in the presence of a reducing agent, thiolated oligomers were formed (Figure 7.1 B) which were then added dropwise into an aqueous anti-solvent of PBS containing 1 wt% PVA for stabilization and 10 mM EDTA to inhibit thiol oxidation from divalent cations. Particle sizes were found to be dependent upon both feed concentration and organic solvent selection (DMSO or acetone). For both the HEDA/CA and DEGDA/CA systems, acetone resulted in larger z-average particle diameters, which increased with an increase in feed concentration. With the HEDA/CA formulation, the maximum particle feed concentration was 100 mg/mL for DMSO solvent, and 25 mg/mL for acetone for the particles to remain stable upon synthesis (Figure 7.4 A,B). For DEGDA/CA, particles were unstable at concentrations exceeding 75 mg/mL in acetone, and 25 mg/mL for DMSO (Figure 7.4 C,D).

For electron microscopy imaging, we used DI water instead of PBS to form HEDA/CA nanoparticles. Particles formed in DI water possessed a z-average diameter of 150 nm with a PDI of 0.150 from DLS readings (Figure 7.5 F). After washing, SEM images were obtained. Interestingly, we found that SEM samples prepared at a high concentration (4 mg/mL used) facilitated film formation upon the droplet drying onto the aluminum foil (Figure 7.5 A-C). EDS elemental analysis showed the film to contain 2.2% sulfur and 79.5% carbon (Figure 7.5 D). At low particle concentration (0.01 mg/mL), however, particles appeared to retain their solution morphology and were found to be in the correct size range as DLS measurements, albeit lightly agglomerated (Figure 7.5 E).

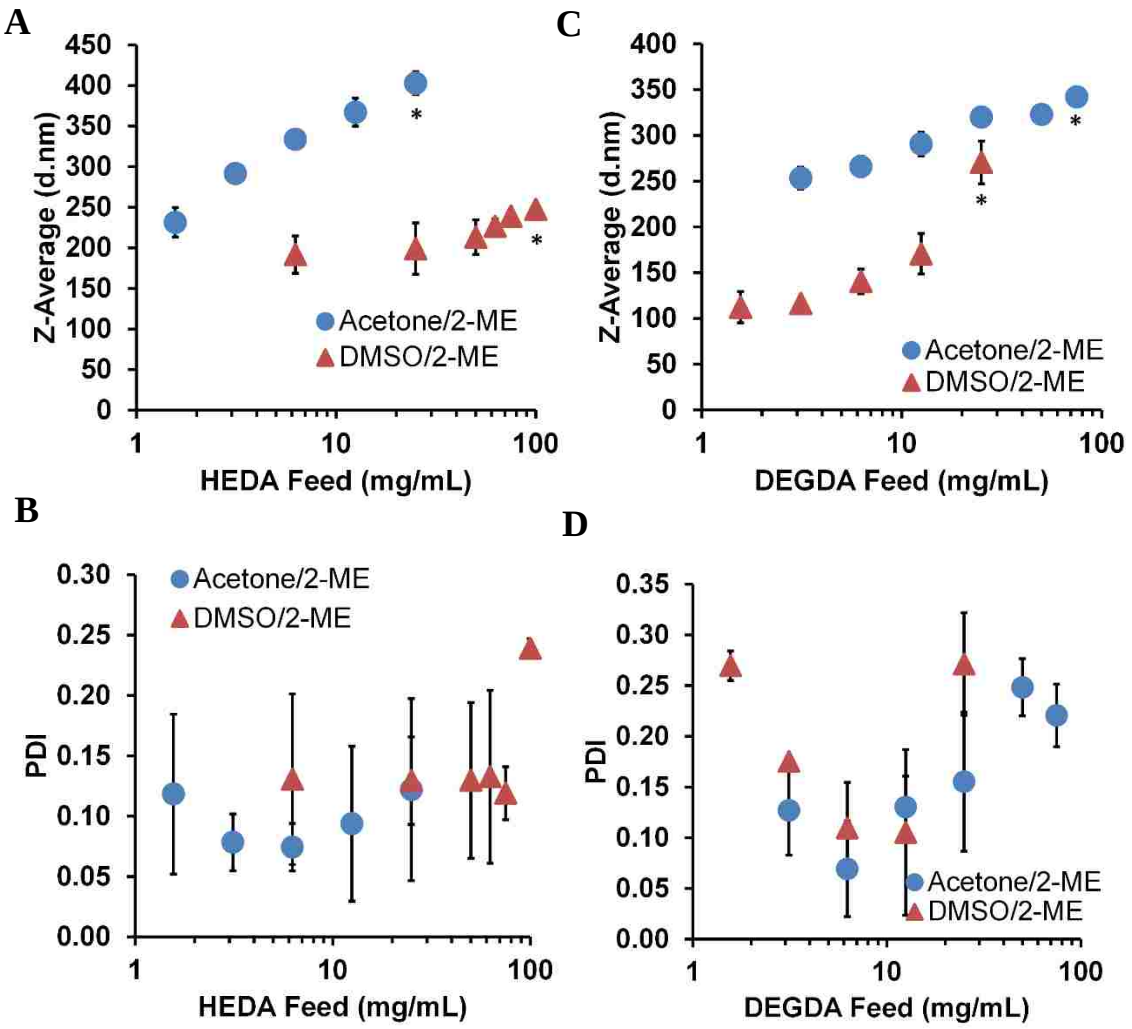

Figure 7.4. Comparison of feed concentration. A) and C) comparison of nanoparticle z-average diameter and B) and D) polydispersity index of HEDA/CA and DEGDA/CA thiolated nanoparticles respectively, in PBS/PVA/EDTA. n=3 each point, standard deviation. *Maximum concentration before particles became unstable.

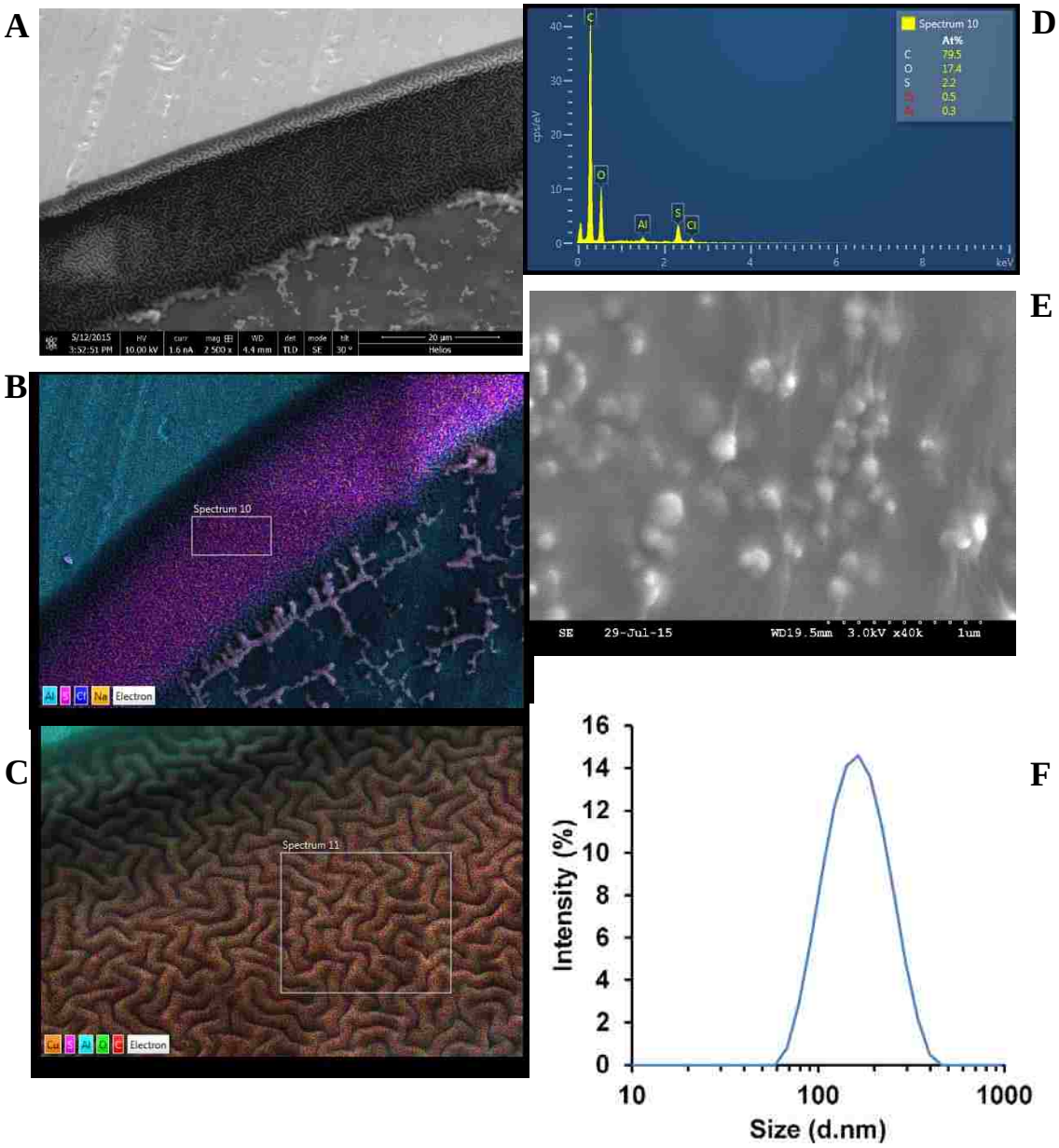
A
B
C
D
E
F
Spectrum 10
Spectrum 11
Electron
Spectrum 10
At%
C 79.5
O 17.4
S 2.2
Cl 0.5
Al 0.3
cps/eV
keV
SE 29-Jul-15 WD19.5mm 3.0kV x40k 1um
Intensity (%)
Size (d.nm)
10
100
1000

Figure 7.5. Scanning electron microscopy (SEM) of thiolated HEDA/CA nanoparticles at high concentration (4 mg/mL) forming a film at droplet boundary. A) Zoomed out micrograph, B) zoomed out micrograph overlaid with elemental analysis chromatogram – purple indicates sulfur from cystamine, blue indicates aluminum from the substrate. C) Zoomed in micrograph of film showing surface deformation upon solvent evaporation, and D) energy dispersive X-ray spectroscopy (EDS) spectrum of panel B. E) SEM of nanoparticles at low concentration (0.01 mg/mL) in DI water, and F) characteristic particle size in DI water of HEDA/CA nanoparticles.

7.3.4 Characterization of Thiol Functionality

In order to visualize the thiolated nanoparticles, we reacted HEDA/CA and DEGDA/CA nanoparticles with NPM in DMSO. SEM of particle sizes were found to be 375 nm with 50% DMSO vs 150 nm with 8% DMSO. With and without NPM addition did not affect particle sizes using 50% DMSO (Figure 7.5 F and Figure 7.7). Representative images of visible nanoparticle aggregates were taken with a fluorescent microscope using an ultraviolet filter or in bright field, before and after NPM addition, and with either HEDA/CA or DEGDA/CA nanoparticles (Figure 7.6). It was seen that both the HEDA/CA and DEGDA/CA nanoparticles/aggregates fluoresced with the addition of NPM, but not without, indicating thiol functionality.

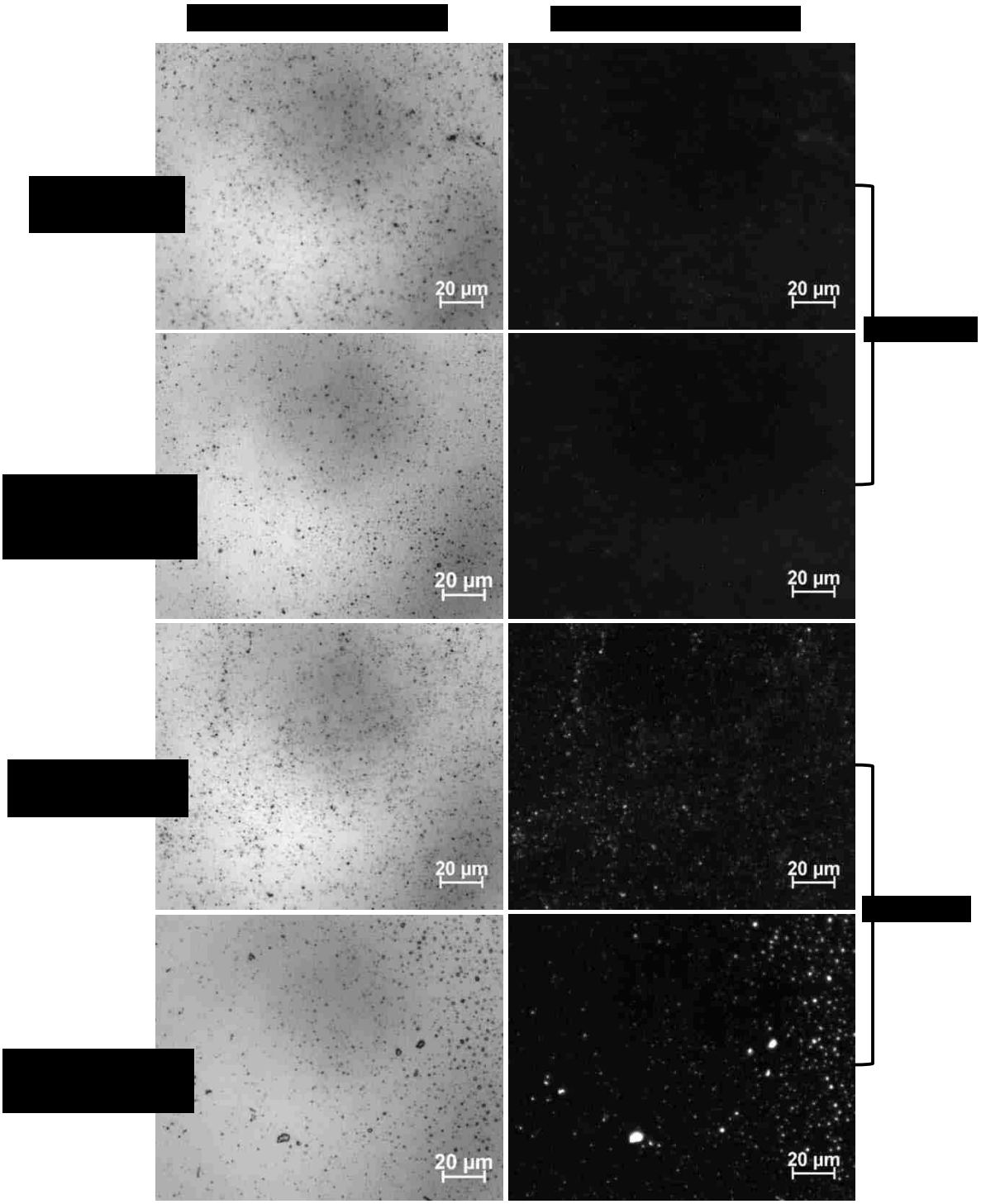

Figure 7.6. Comparison of HEDA/CA and DEGDA/CA nanoparticles formed in DI water and added to 50 vol% DMSO ± NPM fluorescent maleimide.

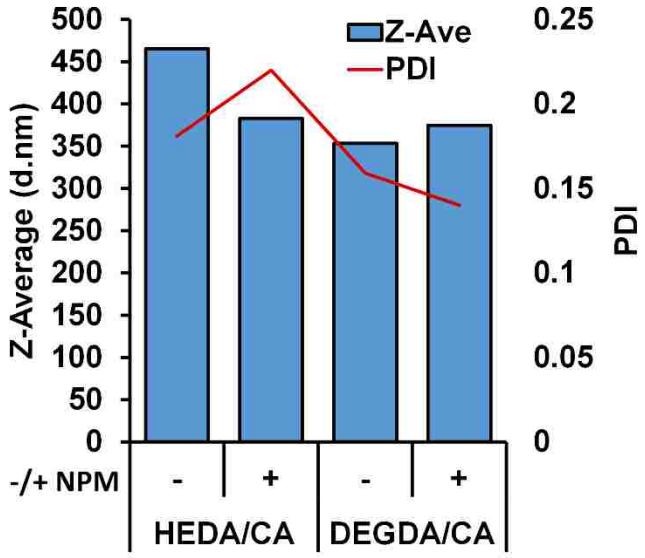

Figure 7.7. Addition of *N*-(1-pyrenyl)maleimide (NPM) (ex/em 338/375 nm) to already made nanoparticles in DI water. 1 hr incubation at room temperature with 50% DMSO, washed 3x. n=1 each.

7.3.5 Nanoparticle Kinetics

Activity, size, and degradation kinetics were measured with nanoparticles formed in PBS/PVA/EDTA, under 37ºC incubation. The HEDA/CA system formed with DMSO was compared with the DEGDA system formed with acetone. The HEDA/CA particles possessed sizes from 200–250 nm with PDI between 0.1–0.2 (Figure 7.8 A,B). Similar to the bulk hydrogel, there was no significant evidence of degradation occurring, as monitored by DLS scattering intensity over time (Figure 7.8 E).

Ellman's thiol assay was performed on the nanoparticle bulk solution at each time point without washing to include both nanoparticle bound thiols and any degradation products. Thiols were found to be present on the particles with Ellman's assay up to 7 days (Figure 7.8 C,D), with the maximum specific thiol release (mmol/g nanoparticles) at the highest particle concentration (4.0 mg/mL) depending on the formulation. These initial synthesis concentrations were taken as soon as possible after 3 wash steps were complete, which was after 3 hours from initial formation where 31, 47, and 59 % of the theoretical maximum thiols were detected (Figure 7.8 F). Comparing the DEGDA/CA nanoparticles to the HEDA/CA nanoparticles, the presence of thiols also lasted over 7 days, as beyond that minimal levels were being detected (Figure 7.9 C,D). However, the starting concentration was much closer to the theoretical maximum (Figure 7.9 F) at averages of 88 ± 1.5, 106 ± 8.2, and 103 ± 10.2 % of the theoretical maximum (n=3, standard deviation). The lower concentration nanoparticle system showed the lowest specific thiol content (mmol/g nanoparticles). In contrast to the HEDA/CA system where the bulk hydrogel and nanoparticles showed no degradation, the DEGDA/CA nanoparticle system showed signs of degradation to compliment the bulk hydrogel degradation. While the z-average particle

sizes did not change consistently across the concentrations starting between 300–350 nm with a PDI of 0.075–0.20 (Figure 7.9 A,B), the % intensity of the original were statistically different after 7 days of degradation, decreasing by 13–30 % from the original (Figure 7.9 E).

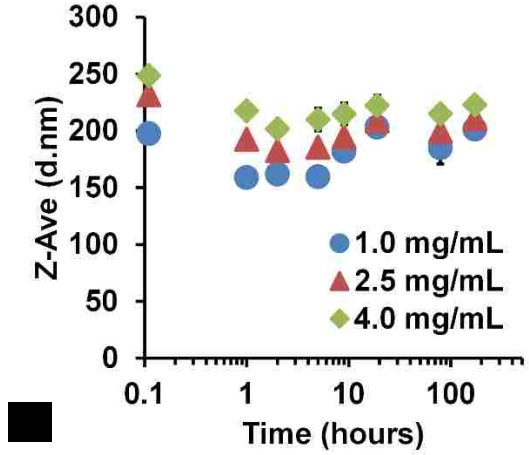
Z-Ave (d.nm)
300
250
200
150
100
50
0
0.1
1
10
100
Time (hours)
1.0 mg/mL
2.5 mg/mL
4.0 mg/mL

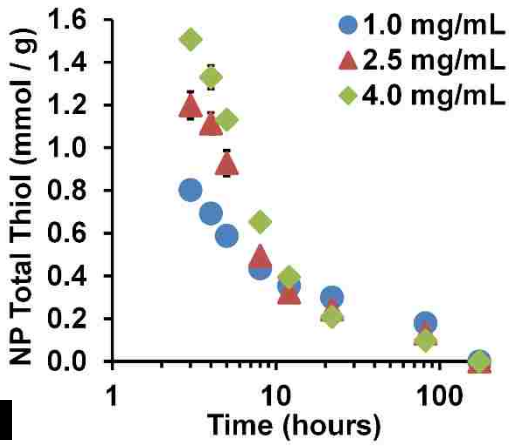
NP Total Thiol (mmol / g)
1.6
1.4
1.2
1.0
0.8
0.6
0.4
0.2
0.0
1
10
100
Time (hours)
1.0 mg/mL
2.5 mg/mL
4.0 mg/mL

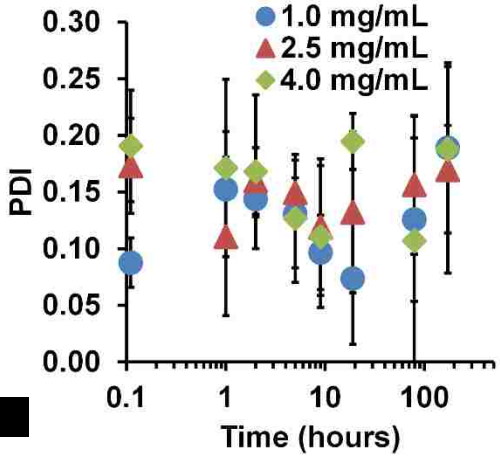
PDI
0.30
0.25
0.20
0.15
0.10
0.05
0.00
0.1
1
10
100
Time (hours)
1.0 mg/mL
2.5 mg/mL
4.0 mg/mL

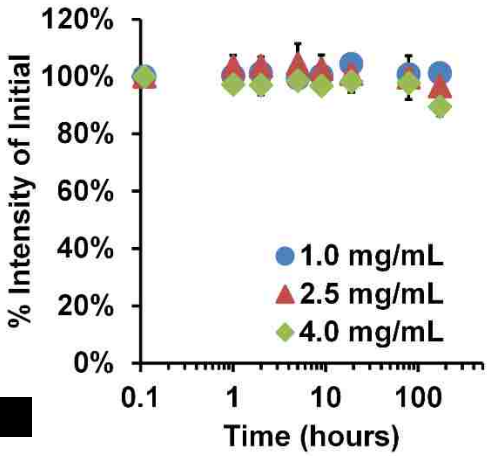
% Intensity of Initial
120%
100%
80%
60%
40%
20%
0%
0.1
1
10
100
Time (hours)
1.0 mg/mL
2.5 mg/mL
4.0 mg/mL

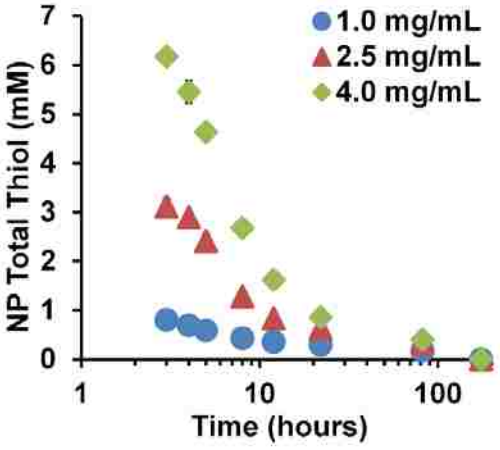
NP Total Thiol (mM)
7
6
5
4
3
2
1
0
1
10
100
Time (hours)
1.0 mg/mL
2.5 mg/mL
4.0 mg/mL

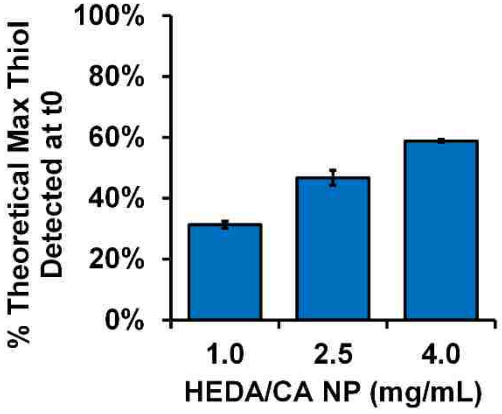
% Theoretical Max Thiol Detected at t0
100%
80%
60%
40%
20%
0%
1.0
2.5
4.0
HEDA/CA NP (mg/mL)

Figure 7.8. Kinetics plots of HEDA/CA nanoparticles in PBS/EDTA/EDTA. A) z-average diameter, B) polydispersity index (PDI), C) total thiol found, D) total thiol found per mass of nanoparticles, E) % intensity of dispersion over time, and F) % of the theoretical maximum thiol concentration found after washing.

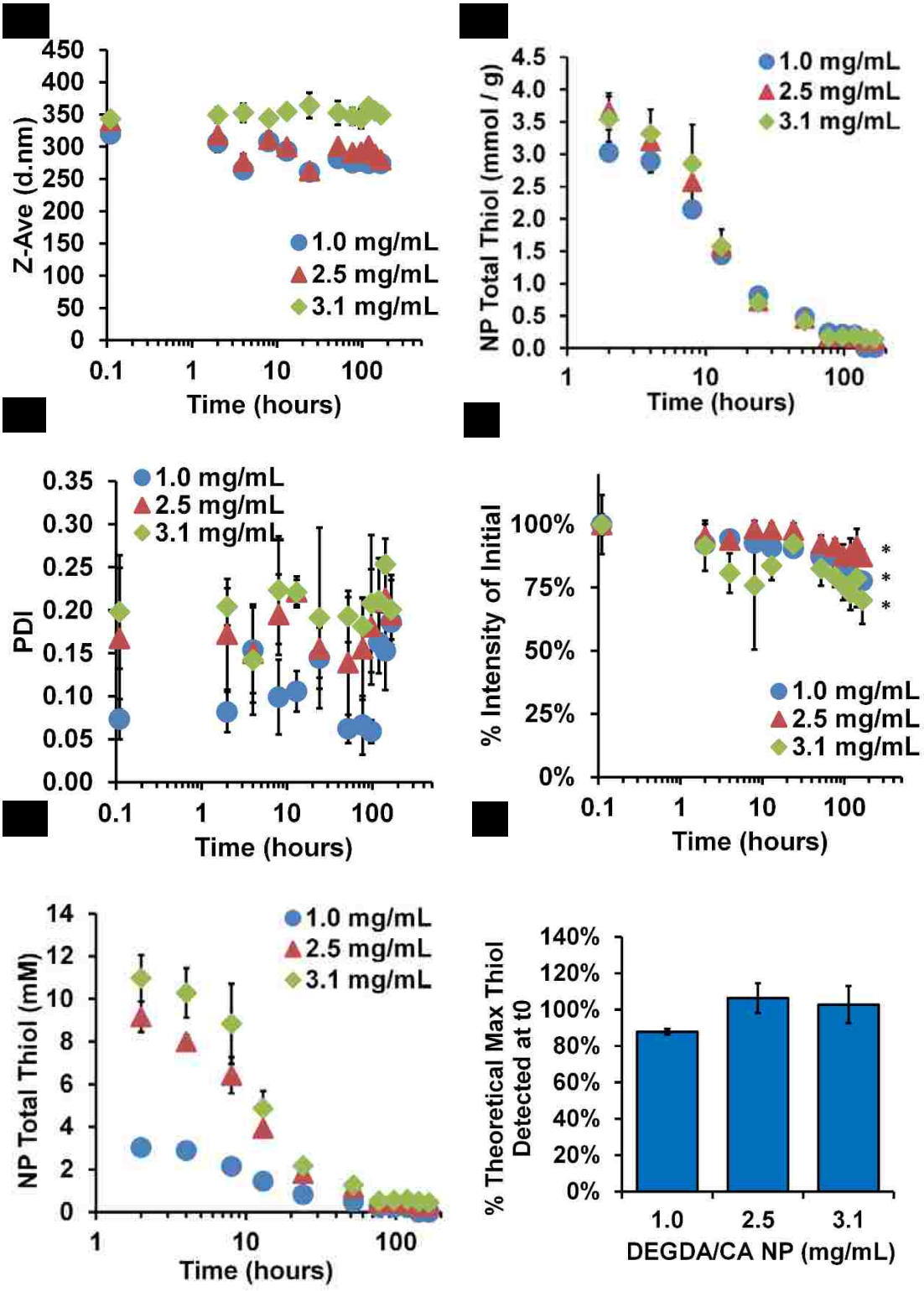
Z-Ave (d.nm)
Time (hours)
1.0 mg/mL
2.5 mg/mL
3.1 mg/mL
NP Total Thiol (mmol / g)
PDI
% Intensity of Initial
NP Total Thiol (mM)
% Theoretical Max Thiol Detected at t0
DEGDA/CA NP (mg/mL)

Figure 7.9. Size and activity kinetics of DEGDA/CA nanoparticles in PBS/PVA/EDTA. n=3 each nanoparticle set, standard deviation. *Indicates $p<0.05$ intensity change from original. A) z-average diameter, B) polydispersity index, C) total thiol found, D) total thiol found per mass of nanoparticles, E) % intensity of dispersion over time, and F) % of the theoretical maximum thiol concentration found after washing.

7.4 Discussion

Disulfide crosslinked hydrogels were formed with a content great enough to dissolve in the presence of a reducing agent in organic solvents. However, hydrogels precipitated in aqueous systems with the same reducing agent, leading to our formation of controlled nanoparticles via single emulsion. Even though it is thought that both the DEGDA/CA and HEDA/CA hydrogels were in PBAE configuration through Michael addition of the acrylates and amines to form ester linkages, only the DEGDA system showed a measurable degradation rate and disulfide release over 7 days (Figure 7.2 D,E). HEDA is more hydrophobic than DEGDA in that it contains an aliphatic 6 carbon chain compared to DEGDA with 2 carbons, and therefore may inhibit hydrolysis of the ester bonds. Swelling studies comparing the two hydrogel systems could aid in this hypothesis of decreased polymer-solvent interaction with HEDA/CA hydrogels.

The washing mass loss for the DEGDA/CA hydrogels was greater than the disulfide release found. This is explained by three different points: 1) increased hydrogel fragmentation occurred with the DMSO swollen hydrogels, where aspiration of small hydrogel particles may have occurred during the wash steps. This effect can be seen as well on the drug release vs mass loss (Figure 7.2 F) where after 50% of mass loss, the amount of drug release tapers off. 2) HEDA is more hydrophobic than DEGDA. 3) The extent of reaction with FTIR was greater for the HEDA/CA compared to DEGDA/CA, so it could also be partially explained by increased extent of reaction. However, these conversion numbers found are also similar to those recorded in our previous publication with the TTD-doped DEGDA/CA hydrogels, at 0.04 C=C/C=O, which showed fast hydrolysis in water [434].

With the HEDA/CA nanoparticles, mass spectroscopy showed that lower molecular weight fragments were washed out after nanoparticle formation, compared to before washing. As not all oligomers formed upon hydrogel reduction would be of equal chain length, it is unlikely that all oligomers were incorporated. After the centrifugation wash step, the nanoparticles could have been separated from unincorporated oligomers in solution. However, this result could also be explained by low molecular weight fragments diffusing from the nanoparticle during centrifugation, whereas large fragments would show diffusional limitations. Due to the stoichiometric excess of 2-mercaptoethanol used to reduce both the hydrogel and nanoparticles, this result cannot be explained by re-oxidation of oligomers.

Nanoparticles were prepared in a two-stage synthesis approach, first forming disulfide hydrogels, and then reducing them for formulation into thiolated nanoparticles. With this technique, the bulk material of disulfide hydrogels may be stored in a non-volatile state prior to nanoformulation. After reduction of the hydrogels into thiolated oligomers, the nanoparticles remained stable for over 8 days without aggregation in solution, even upon complete oxidation of thiols after 7 days. This stability was likely enhanced by the surfactant effects using PVA, and thiol activity was extended with the presence of EDTA to inhibit the effects of divalent cations (which are known to increase thiol oxidation rate [436]). Although not tested in this work, a biologically relevant serum-containing media would hinder thiol activity through thiol-disulfide exchange in proteins. It is also possible that in an intracellular environment which has high reducing potential, bound-thiols may persist longer and aid in glutathione/cysteine antioxidant capacity in times of oxidative

stress. Future experiments using a cellular environment may increase nanoparticle degradation rate due to the presence of esterases to cleave the PBAE ester bonds.

While thiolated nanoparticles did not aggregate at the solution concentrations of Figures 7.8 A and 7.9 A, they did when dried outside of solution. This was demonstrated with electron microscopy where nanoparticles formed a film, perhaps due to re-oxidation of the high concentration of thiols present. Where typical particle aggregation may show touching nanoparticles under SEM, the polymers were likely above the glass transition temperature (T_g), if not also the melting temperature (T_m) and showed formation of a film at high concentration, and individual soft spheres at low concentration. It is hypothesized that from the combination of capillary forces and droplet air drying, the higher concentration polymer on the droplet edge was from re-oxidation of polymer into a concentrated film. We attempted to run DSC on the reduced polymer as well as the disulfide hydrogel to verify this, but it was difficult to adequately remove reducing agents as well as solvent to get an adequate reading. Facilitating film formation, compared to similar applications in literature, our particles were highly thiolated up to 3.7 ± 0.28, and 1.5 ± 0.01 mmol SH/g nanoparticles for the DEGDA/CA formulation and HEDA/CA formulation respectively (n=3, standard deviation) [437, 438]. This high drug loading was intrinsic to the material via use of the inexpensive crosslinker, cystamine, without requirement of commonly used, and less economical crosslinkers such as SH-PEG-SH or SPDP (succinimidyl 3-(2-pyridyldithio)propionate)).

The increase in nanoparticle size based upon feed concentration was likely due to an intrinsic viscosity increase upon increased concentration. Similarly, the size dependence upon solvent variation was likely due to Flory-Huggins derived solvent miscibility

differences [81]. While fluorescent imaging of nanoparticles with the thiol-reactive dye, NPM, was not expected to show individual nanoparticles due to optical limitations, we did find fluorescence of the visible aggregates. Since NPM is only weakly fluorescent before maleimide reaction, this is further implication that thiols were present on the nanoparticles as is seen with the direct kinetic Ellman's assay.

Disulfide crosslinked nanoparticles are a popular design, whether for use as reducing agent-sensitive cross linkers that dissolve for drug release upon reduction [438-443], for extended circulation formulations [444], with thiol-ene type reactions as a reactive crosslinker [445, 446], or to expose thiols for antibody conjugation [447]. For the purpose of antioxidant delivery, however, nanoparticles delivered in the thiol state are not as widely reported compared to thiol-based small molecule systems, perhaps due to rapid oxidation rates in aqueous solution [437]. Where other antioxidant systems may show antioxidant drug release through fast [8] or slow [402] degradative processes, this nanoparticle system is different in that maximal antioxidant capacity is available at the initial treatment. For applications of antioxidant delivery, organ protection prior to radiotherapy, or post oxidation event, such as ischemia-reperfusion injury, a short thiol half-life formulation with high initial activity may be desirable.

7.5 Conclusions

Polymeric nanoparticles are part of a widely researched field showing promising results towards the advent of region-specific targeting and treatment through specialized functionality and drug delivery. Through reduction of disulfide containing hydrogels of high drug content, we formulated and characterized thiol-bound nanoparticles with tunable

degradability, size and activity. Nanoparticles formed were shown to be thiol containing via Ellman's assay, as well as reaction with NPM, demonstrating functionality of the thiol groups. As prior research has shown, these thiol groups are highly biologically relevant, and may aid in processes such as reduction of pathophysiological oxidative stress, and be useful as conjugate moieties found at high concentration using inexpensive starting materials.

Chapter 8. Conclusions and Future Directions

In the modern era, treatment options have advanced rapidly to the advent of personalized medicine. Since individual patients have different factors influencing their health, different medical histories, and different genetics, plug-and-play biomaterials of the past may not always be the best option. Through the formation of customizable materials, patients may receive treatments designed for their need. In our work, we have demonstrated PBAEs to be a highly customizable platform for drug delivery in a variety of applications using straightforward synthesis procedures. Through tailoring these PBAEs to exhibit not only tunable biomaterial properties, but also elicit bioactive responses, we demonstrate multiple applications in which PBAEs could be used to enhance the impact that modern biomaterials have on everyday medicine.

Initially, we formulated PBAE hydrogels with free loaded antibiotic (vancomycin) and antioxidant (catalase) as a potential method to improve upon local antibiotic delivery with reduced risk of antibiotic resistance emergence in a single delivery system. Through tuning of the comparatively hydrophilic and hydrophobic ethylene glycol-based monomers, these *in situ* formable, biodegradable hydrogels showed controllable degradation and drug release rates. While catalase release followed a degradative release profile over 19 days of release until hydrogels fragmented, vancomycin followed a diffusive release profile that was improved from 2 days up to 7 days of release, through modification of the single monomer, co-macromer system into a co-monomer, single macromer system. While this antibiotic hydrogel system is theoretically advantageous over non-degradable systems as second surgeries would not be required, antibiotic release concluded much earlier than the hydrogel degraded.

To overcome this mismatch of drug release and degradation periods, we utilized the free primary amine sites on vancomycin for covalent addition into the PBAE backbone and found the vancomycin drug release period matched to the degradation period at 21 days. However, vancomycin-containing degradation products minimum inhibitory concentration dropped from 2 μg/mL to 155 μg/mL against *Staphylococcus aureus*, likely due to remnant propionic acids found in mass spectroscopy after hydrogel ester hydrolysis. Nonetheless, covalent addition was found to be a useful method to extend vancomycin release and reduce chance of empty scaffold colonization through degradative drug release in local antibiotic therapies. These methods of covalent addition could be expanded to allow a library of other antibiotics to be covalently bound (see Table A.1). However, depending upon the bioactivity of the amine groups, different antibiotic activities may be produced.

Due to the large numbers of oxidative stress-related diseases experienced by the world's population, treatment and/or prevention of oxidative stress through sequestration of free radicals may be performed through delivery of antioxidant polymers. With our experience in synthesizing covalent-drug conjugated PBAE hydrogels, we synthesized a disulfide-containing (cystamine) PBAE for applications of supplementing the thiol/disulfide cellular redox system. Depending on the cystamine content, the hydrogel could be chemically reduced into either a thiol-bound hydrogel, or a soluble bound-thiol system. Conditional on the cystamine redox state, hydrogel degradation products showed large differential cellular toxicity concentrations, with the thiol-containing products being less cytotoxic. Further, the thiol-containing degradation products protected against cellular oxidative stress whereas the disulfide material did not. This was in part due to mitochondrial protection as shown by a Seahorse XF assay. The ability to powerfully inhibit oxidative

stress on endothelial cells with this material's degradation products indicates use as an antioxidant delivery system, perhaps useful in applications at high concentrations such as hydrogel radiation spacers where protection of normal tissue is paramount to delivering lethal doses to cancerous tissue alone. Further development of this material could include modification of bound thiol groups, where additional activity could be introduced as bound, or redox sensitive moieties. If disulfide cleavage were to dispense a greater antioxidant content than was required to reduce the disulfide bond, perhaps there would be a net antioxidant effect, something possible through using a double-disulfide linker with multiple covalently attached polyphenolic antioxidant in the center group, for instance, to increase the net equivalent antioxidant capacity.

Nanoparticle drug delivery research is an ever growing field due to the potential benefits of both the nanoscale properties and cellular interactions, allowing for effects like enhanced permeation and retention, but also for tissue specific, antigen-based drug targeting. Due to the antioxidant protective effects with the cystamine hydrogels, we created a nanoparticle formulation for applications with antioxidant delivery. Using a non-nucleophilic base catalyst to increase the Michael addition reaction, we formed high drug content hydrogels (20-26 wt%) previously unattainable. With these hydrogels in the reduced oligomeric form, we created biodegradable, thiolated nanoparticles which showed high thiol activity over 7 days while remaining stable. Similar to the bulk hydrogel version of this material, the nanoparticle formulation contained high antioxidant content initially on the nanoparticle-bound thiols, and thus may be desirable with applications in which a high initial antioxidant effect is required to block initial onset of acute oxidative stress, such as in initial radioprotection. Further, due to the decreased vapor pressure of bound-thiols versus free

thiols in solution, it could be a less odoriferous substitute of *N*-acetyl cysteine treatment of acetaminophen overdose, or even be formulated as an inhalable for cystic fibrosis mucus disintegration. These nanoparticles are also potentially useful for not only antioxidant delivery applications, but also as an inexpensive method to create high thiol content PBAE nanoparticles which could be used for specific targeting of thiol-reactive species, such as antibodies, maleimide conjugates, or gold substrates for theranostics. Future work with these nanoparticles may include more accurate identification of the glass transition and melting temperatures, and if as predicted it is below ambient conditions, then modifying the backbone materials to increase these. This would allow for enhanced ease of handling, electron microscopic imaging, and washing/storage methods, such as freeze drying.

APPENDIX

Table A.1. Primary Amine Containing Antibiotics Listed in the World Health Organization Essential Medicines. G+/- is Gram positive or negative activity.

					Useful Against	
Class	**Type**	**Name**	**Mechanism**	**Activity**	***S. aureus***	***P. aeruginosa***
Protein Synthesis Inhibitors	Aminoglycoside	Streptomycin	Ribosome 30S subunit	G+/-	No	No
	Aminoglycoside	Neomycin	Ribosome 30S subunit	G+/-	No	No
	Aminoglycoside	Kanamycin	Ribosome 30S subunit	G+/-	Yes	No
	Aminoglycoside	Gentamicin	Ribosome 30S subunit	G+/-	Yes	Yes
	Tetracycline	Doxycycline	Ribosome 30S subunit	G+/-	No	No
Cell Envelope Inhibitors	Glycopeptide	Vancomycin	D-alanyl-D-alanine	G+	Yes	No
	β-lactam	Amoxicillin	Penicillin binding protein	G+/-	No	No
	β-lactam	Ampicillin	Penicillin binding protein	G+/-	Yes	No
	Cephalosporin	Cefixime	Penicillin binding protein	G+/-	No	No
	Cephalosporin	Ceftriaxone	Penicillin binding protein	G+/-	No	Yes
	Cephalosporin	Ceftazidime	Penicillin binding protein	G+/-	No	Yes
Nucleic Acid Inhibitors	Antifolate	Trimethoprim	Dihydrofolate reductase inhibitor	G+/-	Yes	No
	Antifolate	Sulfadiazone	Dihydropteroate synthase inhibitor	G+/-	Yes	Yes

REFERENCES

1. Lynn, D.M. and R. Langer, *Degradable poly(beta-amino esters): Synthesis, characterization, and self-assembly with plasmid DNA.* J Am Chem Soc, 2000. **122**(44): p. 10761-10768.
2. Hawkins, A.M., et al., *Composite hydrogel scaffolds with controlled pore opening via biodegradable hydrogel porogen degradation.* J Biomed Mater Res A, 2014. **102**(2): p. 400-12.
3. Orellana, B.R., et al., *Bioerodible calcium sulfate/poly(beta-amino ester) hydrogel composites.* J Mech Behav Biomed Mater, 2013. **26**: p. 43-53.
4. Potineni, A., et al., *Poly(ethylene oxide)-modified poly(beta-amino ester) nanoparticles as a pH-sensitive biodegradable system for paclitaxel delivery.* J Control Release, 2003. **86**(2-3): p. 223-34.
5. Anderson, D.G., et al., *Structure/property studies of polymeric gene delivery using a library of poly(beta-amino esters).* Mol Ther, 2005. **11**(3): p. 426-434.
6. Liechty, W.B., et al., *Polymers for Drug Delivery Systems.* Annu Rev Chem Biomol, 2010. **1**: p. 149-173.
7. Wattamwar, P.P., et al., *Synthesis and characterization of poly(antioxidant beta-amino esters) for controlled release of polyphenolic antioxidants.* Acta Biomater, 2012. **8**(7): p. 2529-2537.
8. Gupta, P., et al., *Quercetin conjugated poly(beta-amino esters) nanogels for the treatment of cellular oxidative stress.* Acta Biomater, 2015.
9. Hawser, S.P., et al., *Rising incidence of Staphylococcus aureus with reduced susceptibility to vancomycin and susceptibility to antibiotics: a global analysis 2004-2009.* Int J Antimicrob Ag, 2011. **37**(3): p. 219-224.
10. Kohanski, M.A., M.A. DePristo, and J.J. Collins, *Sublethal Antibiotic Treatment Leads to Multidrug Resistance via Radical-Induced Mutagenesis.* Mol Cell, 2010. **37**(3): p. 311-320.
11. Kohanski, M.A., et al., *A common mechanism of cellular death induced by bactericidal antibiotics.* Cell, 2007. **130**(5): p. 797-810.
12. Organization, W.H., *Antimicrobial Resistance: Global Roport on Surveillance*. 2014, WHO Press.
13. Cap, M., L. Vachova, and Z. Palkova, *Reactive Oxygen Species in the Signaling and Adaptation of Multicellular Microbial Communities.* Oxid Med Cell Longev, 2012.
14. Hook, A.L., et al., *Combinatorial discovery of polymers resistant to bacterial attachment.* Nat Biotechnol, 2012. **30**(9): p. 868-75.
15. van Gysen, K., et al., *Feasibility of and rectal dosimetry improvement with the use of SpaceOAR (R) hydrogel for dose-escalated prostate cancer radiotherapy.* J Med Imag Radiat On, 2014. **58**(4): p. 511-516.
16. Masket, S., et al., *Hydrogel sealant versus sutures to prevent fluid egress after cataract surgery.* J Cataract Refr Surg, 2014. **40**(12): p. 2057-2066.
17. Kluin, O.S., et al., *Biodegradable vs non-biodegradable antibiotic delivery devices in the treatment of osteomyelitis.* Expert opinion on drug delivery, 2013. **10**(3): p. 341-51.

18. El-Husseiny, M., et al., *Biodegradable antibiotic delivery systems.* The Journal of bone and joint surgery. British volume, 2011. **93**(2): p. 151-7.
19. Lalidou, F., G. Kolios, and G.I. Drosos, *Bone Infections and Bone Graft Substitutes for Local Antibiotic Therapy.* Surgical technology international, 2014. **XXIV**.
20. Campoccia, D., et al., *Antibiotic-loaded biomaterials and the risks for the spread of antibiotic resistance following their prophylactic and therapeutic clinical use.* Biomaterials, 2010. **31**(25): p. 6363-77.
21. Bisno, A.L., *Molecular Aspects of Bacterial-Colonization.* Infect Cont Hosp Ep, 1995. **16**(11): p. 648-657.
22. Justinger, C., et al., *Antibiotic coating of abdominal closure sutures and wound infection (vol 145, pg 330, 2009).* Surgery, 2009. **146**(3): p. 468-468.
23. Kuechle, D.K., et al., *Elution of Vancomycin, Daptomycin, and Amikacin from Acrylic Bone-Cement.* Clin Orthop Relat R, 1991(264): p. 302-308.
24. Nelson, C.L., et al., *In vitro elution characteristics of commercially and noncommercially prepared antibiotic PMMA beads.* Clin Orthop Relat Res, 1992(284): p. 303-9.
25. Li, B., et al., *Sustained release of vancomycin from polyurethane scaffolds inhibits infection of bone wounds in a rat femoral segmental defect model.* Journal of Controlled Release, 2010. **145**(3): p. 221-230.
26. Ghafoori, P., et al., *Radiation-induced lung injury. Assessment, management, and prevention.* Oncology, 2008. **22**(1): p. 37-47; discussion 52-3.
27. Li, H., S. Horke, and U. Forstermann, *Vascular oxidative stress, nitric oxide and atherosclerosis.* Atherosclerosis, 2014. **237**(1): p. 208-219.
28. Taysi, S., et al., *Lipid peroxidation, some extracellular antioxidants, and antioxidant enzymes in serum of patients with rheumatoid arthritis.* Rheumatol Int, 2002. **21**(5): p. 200-204.
29. Gu, F., V. Chauhan, and A. Chauhan, *Glutathione redox imbalance in brain disorders.* Curr Opin Clin Nutr, 2015. **18**(1): p. 89-95.
30. Nishikawa, M., M. Hashida, and Y. Takakura, *Catalase delivery for inhibiting ROS-mediated tissue injury and tumor metastasis.* Advanced drug delivery reviews, 2009. **61**(4): p. 319-26.
31. Circu, M.L. and T.Y. Aw, *Glutathione and modulation of cell apoptosis.* Bba-Mol Cell Res, 2012. **1823**(10): p. 1767-1777.
32. Li, J.J., et al., *A chitosan-glutathione based injectable hydrogel for suppression of oxidative stress damage in cardiomyocytes.* Biomaterials, 2013. **34**(36): p. 9071-9081.
33. Costantino, L. and D. Boraschi, *Is there a clinical future for polymeric nanoparticles as brain-targeting drug delivery agents?* Drug Discovery Today, 2011.
34. Faraji, A.H. and P. Wipf, *Nanoparticles in cellular drug delivery.* Bioorgan Med Chem, 2009. **17**(8): p. 2950-2962.
35. Moghimi, S.M., A.C. Hunter, and J.C. Murray, *Long-circulating and target-specific nanoparticles: theory to practice.* Pharmacol Rev, 2001. **53**(2): p. 283-318.
36. Soppimath, K.S., et al., *Biodegradable polymeric nanoparticles as drug delivery devices.* Journal of Controlled Release, 2001. **70**(1-2): p. 1-20.

37. Keith R. Pine, B.H.S., Robert J. Jacobs, *Clinical Ocular Prosthetics. Ch 11: History of Ocular Prosthetics.* 2015.
38. Sellegren, K.R., *An Early History of Lower Limb Amputations and Prostheses.* Iowa Orthop J., 1982.
39. Langer, R. and D.A. Tirrell, *Designing materials for biology and medicine.* Nature, 2004. **428**(6982): p. 487-92.
40. Peppas, N.A., et al., *Physicochemical foundations and structural design of hydrogels in medicine and biology.* Annu Rev Biomed Eng, 2000. **2**: p. 9-29.
41. Williams, D.F., *On the mechanisms of biocompatibility.* Biomaterials, 2008. **29**(20): p. 2941-53.
42. Custer, P.L., et al., *Orbital implants in enucleation surgery: a report by the American Academy of Ophthalmology.* Ophthalmology, 2003. **110**(10): p. 2054-61.
43. Webster, T.J., *IJN's second year is now a part of nanomedicine history!* Int J Nanomed, 2007. **2**(1): p. 1-2.
44. Lu, C., et al., *Hydrogel containing silica shell cross-linked micelles for ocular drug delivery.* J Pharm Sci, 2013. **102**(2): p. 627-37.
45. Aslan, B., et al., *Nanotechnology in cancer therapy.* J Drug Target, 2013. **21**(10): p. 904-13.
46. Buddy D. Ratner, A.S.H., Frederick J. Schoen, Jack E. Lemons *Biomaterials Science: An Introduction to Materials in Medicine.* 1996.
47. Vasilakes, A.L., et al., *Controlled release of catalase and vancomycin from poly(β-amino ester) hydrogels.* Journal of Controlled Release: p. (submitted).
48. Brandl, F., et al., *Hydrogel-based drug delivery systems: comparison of drug diffusivity and release kinetics.* Journal of Controlled Release, 2010. **142**(2): p. 221-8.
49. Ruszczak, Z. and W. Friess, *Collagen as a carrier for on-site delivery of antibacterial drugs.* Advanced drug delivery reviews, 2003. **55**(12): p. 1679-1698.
50. Burdick, J.A., et al., *An investigation of the cytotoxicity and histocompatibility of in situ forming lactic acid based orthopedic biomaterials.* J Biomed Mater Res, 2002. **63**(5): p. 484-491.
51. Burkoth, A.K. and K.S. Anseth, *A review of photocrosslinked polyanhydrides: in situ forming degradable networks.* Biomaterials, 2000. **21**(23): p. 2395-2404.
52. Lee, C.H., A. Singla, and Y. Lee, *Biomedical applications of collagen.* Int J Pharm, 2001. **221**(1-2): p. 1-22.
53. Drury, J.L. and D.J. Mooney, *Hydrogels for tissue engineering: scaffold design variables and applications.* Biomaterials, 2003. **24**(24): p. 4337-51.
54. Peppas, N.A., et al., *Hydrogels in biology and medicine: From molecular principles to bionanotechnology.* Adv Mater, 2006. **18**(11): p. 1345-1360.
55. Marin, E., M.I. Briceno, and C. Caballero-George, *Critical evaluation of biodegradable polymers used in nanodrugs.* Int J Nanomed, 2013. **8**: p. 3071-3091.
56. Middleton, J.C. and A.J. Tipton, *Synthetic biodegradable polymers as orthopedic devices.* Biomaterials, 2000. **21**(23): p. 2335-2346.
57. Gilding, D.K. and A.M. Reed, *Biodegradable Polymers for Use in Surgery - Poly(Ethylene Oxide) Poly(Ethylene-Terephthalate) (Peo-Pet) Copolymers .1.* Polymer, 1979. **20**(12): p. 1454-1458.

58. Mathur, A.B., et al., *In vivo biocompatibility and biostability of modified polyurethanes.* J Biomed Mater Res, 1997. **36**(2): p. 246-257.
59. Putnam, D. and R. Langer, *Poly(4-hydroxy-L-proline ester): Low-temperature polycondensation and plasmid DNA complexation.* Macromolecules, 1999. **32**(11): p. 3658-3662.
60. Lim, Y.B., Y.H. Choi, and J.S. Park, *A self-destroying polycationic polymer: Biodegradable poly(4-hydroxy-L-proline ester).* J Am Chem Soc, 1999. **121**(24): p. 5633-5639.
61. Barrera, D.A., et al., *Synthesis and Rgd Peptide Modification of a New Biodegradable Copolymer - Poly(Lactic Acid-Co-Lysine).* J Am Chem Soc, 1993. **115**(23): p. 11010-11011.
62. Lakes, A.L., et al., *Synthesis and characterization of an antibacterial hydrogel containing covalently bound vancomycin.* Biomacromolecules, 2014. **15**(8): p. 3009-18.
63. Lakes, A.L., et al., *Reducible Disulfide Poly(beta-amino ester) Hydrogels for Antioxidant Delivery.* Adv Mater, Submitted.
64. Qiao, Z.Y., et al., *A pH-responsive natural cyclopeptide RA-V drug formulation for improved breast cancer therapy.* J Mater Chem B, 2015. **3**(22): p. 4514-4523.
65. Bui, Q.N., et al., *Redox- and pH-Sensitive Polymeric Micelles Based on Poly(beta-amino ester)-Grafted Disulfide Methylene Oxide Poly(ethylene glycol) for Anticancer Drug Delivery.* Macromolecules, 2015. **48**(12): p. 4046-4054.
66. Santra, S. and J.M. Perez, *Selective N-Alkylation of beta-Alanine Facilitates the Synthesis of a Poly(amino acid)-Based Theranostic Nanoagent.* Biomacromolecules, 2011. **12**(11): p. 3917-3927.
67. Clark, A., et al., *Mechanical properties and dual drug delivery application of poly(lactic-co-glycolic acid) scaffolds fabricated with a poly(beta-amino ester) porogen.* Acta Biomater, 2014. **10**(5): p. 2125-2132.
68. Meenach, S.A., et al., *Controlled synergistic delivery of paclitaxel and heat from poly(beta-amino ester)/iron oxide-based hydrogel nanocomposites.* Int J Pharmaceut, 2012. **427**(2): p. 177-184.
69. Lakes, A.L., et al., *Thiol Functionalized Poly(beta-amino ester) Nanoparticles for Redox Applications.* Acta Biomater, Submitted.
70. Lakes, A.L., et al., *Tandem Release of Vancomycin and Catalase for Local Control of Infection* AIMS Molecular Science, Submitted.
71. Hawkins, A.M., D.A. Puleo, and J.Z. Hilt, *Effect of Macromer Synthesis Time on the Properties of the Resulting Poly(beta-amino ester) Degradable Hydrogel.* J Appl Polym Sci, 2011. **122**(2): p. 1420-1426.
72. Nguyen, M.K. and D.S. Lee, *Injectable biodegradable hydrogels.* Macromol Biosci, 2010. **10**(6): p. 563-79.
73. Cui, Y., et al., *Preparation of hyaluronic acid micro-hydrogel by biotin-avidin-specific bonding for doxorubicin-targeted delivery.* Appl Biochem Biotechnol, 2013. **169**(1): p. 239-49.
74. Schulz, V., et al., *In-vitro investigations of a pH- and ionic-strength-responsive polyelectrolytic hydrogel using a piezoresistive microsensor.* Smart Struct Mater Nondestruct Eval Health Monit Diagn, 2009. **7287**.

75. Wattamwar, P.P., et al., *Synthesis and characterization of poly(antioxidant beta-amino esters) for controlled release of polyphenolic antioxidants.* Acta Biomater, 2012. **8**(7): p. 2529-37.
76. Carothers, W.H., *Polymers and polyfunctionality*. T Faraday Soc, 1936. **32**(1): p. 0039-0053.
77. Flory, P.J., *Principles of polymer chemistry*. The George Fisher Baker non-resident lectureship in chemistry at Cornell University. 1953, Ithaca,: Cornell University Press. 672 p.
78. Mequanint, A.P.a.K., *Biomedical Engineering - Frontiers and Challenges. Ch 14 Hydrogel Biomaterials*, ed. R. Fazel-Rezai. 2011.
79. Zustiak, S.P. and J.B. Leach, *Characterization of Protein Release From Hydrolytically Degradable Poly(Ethylene Glycol) Hydrogels.* Biotechnol Bioeng, 2011. **108**(1): p. 197-206.
80. Yui, N., R.J. Mrsny, and K. Park, *Reflexive polymers and hydrogels : understanding and designing fast responsive polymeric systems*. 2004, Boca Raton, FL: CRC Press. 452 p.
81. Peppas, N.A., et al., *Hydrogels in pharmaceutical formulations.* Eur J Pharm Biopharm, 2000. **50**(1): p. 27-46.
82. Nicholas A. Peppas, J.Z.H., J. Brock Thomas, *Nanotechnology in Therapeutics: Current Technology and Applications*. 2007.
83. Barbucci, R., *Hydrogels: Biological Properties and Applications*. 2009.
84. Mellott, M.B., K. Searcy, and M.V. Pishko, *Release of protein from highly cross-linked hydrogels of poly(ethylene glycol) diacrylate fabricated by UV polymerization.* Biomaterials, 2001. **22**(9): p. 929-41.
85. Merrill, E.W., K.A. Dennison, and C. Sung, *Partitioning and diffusion of solutes in hydrogels of poly(ethylene oxide).* Biomaterials, 1993. **14**(15): p. 1117-26.
86. Ebewele, R.O., *Polymer science and technology*. 2000, Boca Raton: CRC Press. 483 p.
87. Wichterle, O. and D. Lim, *Hydrophilic Gels for Biological Use.* Nature, 1960. **185**(4706): p. 117-118.
88. LaPorte, R.J., *Hydrophilic polymer coatings for medical devices : structure/properties, development, manufacture, and applications*. 1997, Lancaster, PA: Technomic Pub. xi, 186 p.
89. Ketelson, H.A., D.L. Meadows, and R.P. Stone, *Dynamic wettability properties of a soft contact lens hydrogel.* Colloids Surf B Biointerfaces, 2005. **40**(1): p. 1-9.
90. Ratner, B.D., *Biomaterials science : an introduction to materials in medicine*. 3rd ed. 2013, Amsterdam ; Boston: Elsevier/Academic Press. liii, 1519 p.
91. Mehdizadeh, M. and J. Yang, *Design strategies and applications of tissue bioadhesives.* Macromol Biosci, 2013. **13**(3): p. 271-88.
92. Park, J.H., et al., *Polymeric nanomedicine for cancer therapy.* Prog Polym Sci, 2008. **33**(1): p. 113-137.
93. Sahoo, S.K. and V. Labhasetwar, *Nanotech approaches to delivery and imaging drug.* Drug Discovery Today, 2003. **8**(24): p. 1112-1120.
94. Vinogradov, S.V., T.K. Bronich, and A.V. Kabanov, *Nanosized cationic hydrogels for drug delivery: preparation, properties and interactions with cells.* Advanced drug delivery reviews, 2002. **54**(1): p. 135-47.

95. Zhang, X.X., H.S. Eden, and X. Chen, *Peptides in cancer nanomedicine: Drug carriers, targeting ligands and protease substrates.* Journal of Controlled Release, 2011.
96. Kumari, A., S.K. Yadav, and S.C. Yadav, *Biodegradable polymeric nanoparticles based drug delivery systems.* Colloid Surface B, 2010. **75**(1): p. 1-18.
97. Dziubla, T.D., A. Karim, and V.R. Muzykantov, *Polymer nanocarriers protecting active enzyme cargo against proteolysis.* Journal of Controlled Release, 2005. **102**(2): p. 427-439.
98. Sutton, D., et al., *Functionalized micellar systems for cancer targeted drug delivery.* Pharmaceutical research, 2007. **24**(6): p. 1029-46.
99. Tang, R., et al., *Block copolymer micelles with acid-labile ortho ester side-chains: Synthesis, characterization, and enhanced drug delivery to human glioma cells.* Journal of Controlled Release, 2011. **151**(1): p. 18-27.
100. Felber, A.E., M.H. Dufresne, and J.C. Leroux, *pH-sensitive vesicles, polymeric micelles, and nanospheres prepared with polycarboxylates.* Advanced drug delivery reviews, 2012. **64**(11): p. 979-992.
101. Wadajkar, A.S., et al., *Cytotoxic evaluation of N-isopropylacrylamide monomers and temperature-sensitive poly(N-isopropylacrylamide) nanoparticles.* J Nanopart Res, 2009. **11**(6): p. 1375-1382.
102. Urbina, M.C., et al., *Investigation of magnetic nanoparticle-polymer composites for multiple-controlled drug delivery.* J Phys Chem C, 2008. **112**(30): p. 11102-11108.
103. Chen, W., et al., *Synthesis of PMMA and PMMA/PS nanoparticles by microemulsion polymerization with a new vapor monomer feeding system.* Colloid Surface A, 2010. **364**(1-3): p. 145-150.
104. Monasterolo, C., et al., *Sulfonates-PMMA nanoparticles conjugates: A versatile system for multimodal application.* Bioorg Med Chem, 2012. **20**(22): p. 6640-7.
105. Mohomed, K., et al., *Persistent interactions between hydroxylated nanoballs and atactic poly(2-hydroxyethyl methacrylate) (PHEMA).* Chem Commun, 2005(26): p. 3277-3279.
106. Oh, J.K., et al., *Preparation of nanoparticles of double-hydrophilic PEO-PHEMA block copolymers by AGET ATRP in inverse miniemulsion.* J Polym Sci Pol Chem, 2007. **45**(21): p. 4764-4772.
107. Calvo, P., et al., *Long-circulating PEGylated polycyanoacrylate nanoparticles as new drug carrier for brain delivery.* Pharmaceutical research, 2001. **18**(8): p. 1157-1166.
108. Reddy, L.H. and R.R. Murthy, *Influence of polymerization technique and experimental variables on the particle properties and release kinetics of methotrexate from poly(butylcyanoacrylate) nanoparticles.* Acta Pharm, 2004. **54**(2): p. 103-18.
109. Huang, C.Y., C.M. Chen, and Y.D. Lee, *Synthesis of high loading and encapsulation efficient paclitaxel-loaded poly(n-butyl cyanoacrylate) nanoparticles via miniemulsion.* Int J Pharmaceut, 2007. **338**(1-2): p. 267-75.
110. O'Hagan, D.T., K.J. Palin, and S.S. Davis, *Poly(butyl-2-cyanoacrylate) particles as adjuvants for oral immunization.* Vaccine, 1989. **7**(3): p. 213-6.

111. de Verdiere, A.C., et al., *Reversion of multidrug resistance with polyalkylcyanoacrylate nanoparticles: towards a mechanism of action.* British journal of cancer, 1997. **76**(2): p. 198-205.
112. Vauthier, C., et al., *Drug delivery to resistant tumors: the potential of poly(alkyl cyanoacrylate) nanoparticles.* Journal of Controlled Release, 2003. **93**(2): p. 151-60.
113. Sadekar, S. and H. Ghandehari, *Transepithelial transport and toxicity of PAMAM dendrimers: implications for oral drug delivery.* Advanced drug delivery reviews, 2012. **64**(6): p. 571-88.
114. Mukherjee, S.P., M. Davoren, and H.J. Byrne, *In vitro mammalian cytotoxicological study of PAMAM dendrimers - towards quantitative structure activity relationships.* Toxicology in vitro : an international journal published in association with BIBRA, 2010. **24**(1): p. 169-77.
115. Liu, Y., et al., *PAMAM dendrimers undergo pH responsive conformational changes without swelling.* J Am Chem Soc, 2009. **131**(8): p. 2798-9.
116. Liu, M. and J.M. Frechet, *Designing dendrimers for drug delivery.* Pharmaceutical science & technology today, 1999. **2**(10): p. 393-401.
117. Srinivas Uppuluri, et al., *The Properties of Dendritic Polymers II: Generation Dependence of the Physical Properties of Poly(amidoamine) Dendrimers.* ARL-TR-1774 ed. ARMY RESEARCH LABORATORY. 1999.
118. Feldstein, M.M., et al., *Relation of glass transition temperature to the hydrogen bonding degree and energy in poly(N-vinyl pyrrolidone) blends with hydroxyl-containing plasticizers: 3. Analysis of two glass transition temperatures featured for PVP solutions in liquid poly(ethylene glycol).* Polymer, 2003. **44**(6): p. 1819-1834.
119. Bharali, D.J., et al., *Cross-linked polyvinylpyrrolidone nanoparticles: a potential carrier for hydrophilic drugs.* J Colloid Interf Sci, 2003. **258**(2): p. 415-423.
120. Lee, W.C. and I.M. Chu, *Preparation and degradation behavior of polyanhydrides nanoparticles.* J Biomed Mater Res B, 2008. **84B**(1): p. 138-146.
121. Pfeifer, B.A., J.A. Burdick, and R. Langer, *Formulation and surface modification of poly(ester-anhydride) micro- and nanospheres.* Biomaterials, 2005. **26**(2): p. 117-124.
122. Ko, J., et al., *Tumoral acidic extracellular pH targeting of pH-responsive MPEG-poly (beta-amino ester) block copolymer micelles for cancer therapy.* Journal of Controlled Release, 2007. **123**(2): p. 109-115.
123. Gao, G.H., et al., *pH-responsive polymeric micelle based on PEG-poly(beta-amino ester)/(amido amine) as intelligent vehicle for magnetic resonance imaging in detection of cerebral ischemic area.* Journal of Controlled Release, 2011. **155**(1): p. 11-17.
124. Shen, Y., et al., *Degradable poly(beta-amino ester) nanoparticles for cancer cytoplasmic drug delivery.* Nanomedicine : nanotechnology, biology, and medicine, 2009. **5**(2): p. 192-201.
125. Min, K.H., et al., *Tumoral acidic pH-responsive MPEG-poly(beta-amino ester) polymeric micelles for cancer targeting therapy.* Journal of Controlled Release, 2010. **144**(2): p. 259-266.

126. Beck-Broichsitter, M., et al., *Development of a biodegradable nanoparticle platform for sildenafil: Formulation optimization by factorial design analysis combined with application of charge-modified branched polyesters.* Journal of Controlled Release, 2012. **157**(3): p. 469-477.
127. Zheng, X., et al., *Preparation of MPEG-PLA nanoparticle for honokiol delivery in vitro.* Int J Pharmaceut, 2010. **386**(1-2): p. 262-7.
128. Gaucher, G., R.H. Marchessault, and J.C. Leroux, *Polyester-based micelles and nanoparticles for the parenteral delivery of taxanes.* Journal of Controlled Release, 2010. **143**(1): p. 2-12.
129. Coffin, M.D. and J.W. Mcginity, *Biodegradable Pseudolatexes - the Chemical-Stability of Poly(D,L-Lactide) and Poly (Epsilon-Caprolactone) Nanoparticles in Aqueous-Media.* Pharmaceutical research, 1992. **9**(2): p. 200-205.
130. Lemoine, D., et al., *Stability study of nanoparticles of poly(epsilon-caprolactone), poly(D,L-lactide) and poly(D,L-lactide-co-glycolide).* Biomaterials, 1996. **17**(22): p. 2191-2197.
131. Musumeci, T., et al., *PLA/PLGA nanoparticles for sustained release of docetaxel.* Int J Pharmaceut, 2006. **325**(1-2): p. 172-179.
132. Mittal, G., et al., *Estradiol loaded PLGA nanoparticles for oral administration: effect of polymer molecular weight and copolymer composition on release behavior in vitro and in vivo.* Journal of Controlled Release, 2007. **119**(1): p. 77-85.
133. Mittal, A., et al., *Cytomodulin-functionalized porous PLGA particulate scaffolds respond better to cell migration, actin production and wound healing in rodent model.* Journal of tissue engineering and regenerative medicine, 2012.
134. Fonseca, C., S. Simoes, and R. Gaspar, *Paclitaxel-loaded PLGA nanoparticles: preparation, physicochemical characterization and in vitro anti-tumoral activity.* Journal of Controlled Release, 2002. **83**(2): p. 273-286.
135. Teixeira, M., et al., *Development and characterization of PLGA nanospheres and nanocapsules containing xanthone and 3-methoxyxanthone.* European journal of pharmaceutics and biopharmaceutics : official journal of Arbeitsgemeinschaft fur Pharmazeutische Verfahrenstechnik e.V, 2005. **59**(3): p. 491-500.
136. Hans, M.L. and A.M. Lowman, *Biodegradable nanoparticles for drug delivery and targeting.* Curr Opin Solid St M, 2002. **6**(4): p. 319-327.
137. Saez, A., et al., *Freeze-drying of polycaprolactone and poly(D,L-lactic-glycolic) nanoparticles induce minor particle size changes affecting the oral pharmacokinetics of loaded drugs.* European journal of pharmaceutics and biopharmaceutics : official journal of Arbeitsgemeinschaft fur Pharmazeutische Verfahrenstechnik e.V, 2000. **50**(3): p. 379-387.
138. Barakat, N.A.M., et al., *Biologically Active Polycaprolactone/Titanium Hybrid Electrospun Nanofibers for Hard Tissue Engineering.* Sci Adv Mater, 2011. **3**(5): p. 730-734.
139. Otsuka, H., Y. Nagasaki, and K. Kataoka, *PEGylated nanoparticles for biological and pharmaceutical applications.* Advanced drug delivery reviews, 2003. **55**(3): p. 403-419.
140. Cheng, J., et al., *Formulation of functionalized PLGA-PEG nanoparticles for in vivo targeted drug delivery.* Biomaterials, 2007. **28**(5): p. 869-876.

141. Li, Y.P., et al., *PEGylated PLGA nanoparticles as protein carriers: synthesis, preparation and biodistribution in rats.* Journal of Controlled Release, 2001. **71**(2): p. 203-211.
142. Ahmed, F. and D.E. Discher, *Self-porating polymersomes of PEG-PLA and PEG-PCL: hydrolysis-triggered controlled release vesicles.* Journal of Controlled Release, 2004. **96**(1): p. 37-53.
143. Vinogradov, S., E. Batrakova, and A. Kabanov, *Poly(ethylene glycol)-polyethyleneimine NanoGel (TM) particles: novel drug delivery systems for antisense oligonucleotides.* Colloid Surface B, 1999. **16**(1-4): p. 291-304.
144. Bivas-Benita, M., et al., *PLGA-PEI nanoparticles for gene delivery to pulmonary epithelium.* European journal of pharmaceutics and biopharmaceutics : official journal of Arbeitsgemeinschaft fur Pharmazeutische Verfahrenstechnik e.V, 2004. **58**(1): p. 1-6.
145. Lunov, O., et al., *Differential Uptake of Functionalized Polystyrene Nanoparticles by Human Macrophages and a Monocytic Cell Line.* Acs Nano, 2011. **5**(3): p. 1657-1669.
146. Pradip Paik and K.K. Kar, *Glass Transition Temperature of High Molecular Weight Polystyrene: Effect of Particle Size, Bulk to Micron to Nano.* Advanced Nano Engineering Materials Laboratory, 2006. **1**.
147. Acharya, S. and S.K. Sahoo, *PLGA nanoparticles containing various anticancer agents and tumour delivery by EPR effect.* Advanced drug delivery reviews, 2011. **63**(3): p. 170-183.
148. Kean, T. and M. Thanou, *Biodegradation, biodistribution and toxicity of chitosan.* Advanced drug delivery reviews, 2010. **62**(1): p. 3-11.
149. Agnihotri, S.A., N.N. Mallikarjuna, and T.M. Aminabhavi, *Recent advances on chitosan-based micro- and nanoparticles in drug delivery.* Journal of Controlled Release, 2004. **100**(1): p. 5-28.
150. Mundargi, R.C., et al., *Nano/micro technologies for delivering macromolecular therapeutics using poly(D,L-lactide-co-glycolide) and its derivatives.* Journal of Controlled Release, 2008. **125**(3): p. 193-209.
151. Panyam, J. and V. Labhasetwar, *Biodegradable nanoparticles for drug and gene delivery to cells and tissue.* Advanced drug delivery reviews, 2003. **55**(3): p. 329-347.
152. Lu, D.N., et al., *Dextran-grafted-PNIPAAm as an artificial chaperone for protein refolding.* Biochem Eng J, 2006. **27**(3): p. 336-343.
153. Jiang, W.W., et al., *Phagocyte responses to degradable polymers.* Journal of Biomedical Materials Research Part A, 2007. **82A**(2): p. 492-497.
154. Fu, K., et al., *Visual evidence of acidic environment within degrading poly(lactic-co-glycolic acid) (PLGA) microspheres.* Pharmaceutical research, 2000. **17**(1): p. 100-106.
155. Bat, E., et al., *In vivo behavior of trimethylene carbonate and epsilon-caprolactone-based (co)polymer networks: Degradation and tissue response.* Journal of Biomedical Materials Research Part A, 2010. **95A**(3): p. 940-949.
156. Albanese, A., P.S. Tang, and W.C. Chan, *The effect of nanoparticle size, shape, and surface chemistry on biological systems.* Annu Rev Biomed Eng, 2012. **14**: p. 1-16.

157. Storm, G., et al., *Surface Modification of Nanoparticles to Oppose Uptake by the Mononuclear Phagocyte System.* Advanced drug delivery reviews, 1995. **17**(1): p. 31-48.
158. Guo, J.W., et al., *Aptamer-functionalized PEG-PLGA nanoparticles for enhanced anti-glioma drug delivery.* Biomaterials, 2011. **32**(31): p. 8010-8020.
159. Veronese, F.M. and G. Pasut, *PEGylation, successful approach to drug delivery.* Drug Discovery Today, 2005. **10**(21): p. 1451-8.
160. Parveen, S. and S.K. Sahoo, *Long circulating chitosan/PEG blended PLGA nanoparticle for tumor drug delivery.* Eur J Pharmacol, 2011. **670**(2-3): p. 372-383.
161. Gref, R., et al., *'Stealth' corona-core nanoparticles surface modified by polyethylene glycol (PEG): influences of the corona (PEG chain length and surface density) and of the core composition on phagocytic uptake and plasma protein adsorption.* Colloid Surface B, 2000. **18**(3-4): p. 301-313.
162. Bader, R.A., A.L. Silvers, and N. Zhang, *Polysialic acid-based micelles for encapsulation of hydrophobic drugs.* Biomacromolecules, 2011. **12**(2): p. 314-20.
163. Simone, E.A., T.D. Dziubla, and V.R. Muzykantov, *Polymeric carriers: role of geometry in drug delivery.* Expert opinion on drug delivery, 2008. **5**(12): p. 1283-300.
164. Sharma, G., et al., *Polymer particle shape independently influences binding and internalization by macrophages.* J Control Release, 2010. **147**(3): p. 408-12.
165. Geng, Y., et al., *Shape effects of filaments versus spherical particles in flow and drug delivery.* Nature nanotechnology, 2007. **2**(4): p. 249-55.
166. Beningo, K.A. and Y.L. Wang, *Fc-receptor-mediated phagocytosis is regulated by mechanical properties of the target.* J Cell Sci, 2002. **115**(4): p. 849-856.
167. Authimoolam, S.P., et al., *Synthetic oral mucin mimic from polymer micelle networks.* Biomacromolecules, 2014. **15**(8): p. 3099-111.
168. Kim, T.Y., et al., *Phase I and pharmacokinetic study of Genexol-PM, a cremophor-free, polymeric micelle-formulated paclitaxel, in patients with advanced malignancies.* Clin Cancer Res, 2004. **10**(11): p. 3708-3716.
169. Kim, S.C., et al., *In vivo evaluation of polymeric micellar paclitaxel formulation: toxicity and efficacy.* Journal of Controlled Release, 2001. **72**(1-3): p. 191-202.
170. Poon, Z., et al., *Highly stable, ligand-clustered "patchy" micelle nanocarriers for systemic tumor targeting.* Nanomed-Nanotechnol, 2011. **7**(2): p. 201-209.
171. Nakanishi, T., et al., *Development of the polymer micelle carrier system for doxorubicin.* Journal of Controlled Release, 2001. **74**(1-3): p. 295-302.
172. Matsumura, Y., et al., *Phase I clinical trial and pharmacokinetic evaluation of NK911, a micelle-encapsulated doxorubicin.* British journal of cancer, 2004. **91**(10): p. 1775-1781.
173. Photos, P.J., et al., *Polymer vesicles in vivo: correlations with PEG molecular weight.* Journal of Controlled Release, 2003. **90**(3): p. 323-334.
174. Nassar, T., et al., *High Plasma Levels and Effective Lymphatic Uptake of Docetaxel in an Orally Available Nanotransporter Formulation.* Cancer Res, 2011. **71**(8): p. 3018-3028.
175. Nassar, T., et al., *Novel double coated nanocapsules for intestinal delivery and enhanced oral bioavailability of tacrolimus, a P-gp substrate drug.* Journal of Controlled Release, 2009. **133**(1): p. 77-84.

176. Sheng, Y., et al., *Long-circulating polymeric nanoparticles bearing a combinatorial coating of PEG and water-soluble chitosan.* Biomaterials, 2009. **30**(12): p. 2340-2348.
177. Shimoda, A., et al., *Dual crosslinked hydrogel nanoparticles by nanogel bottom-up method for sustained-release delivery.* Colloids Surf B Biointerfaces, 2011.
178. Hasegawa, U., et al., *Raspberry-like assembly of cross-linked nanogels for protein delivery.* Journal of Controlled Release, 2009. **140**(3): p. 312-317.
179. De Jesus, O.L.P., et al., *Polyester dendritic systems for drug delivery applications: In vitro and in vivo evaluation.* Bioconjugate Chem, 2002. **13**(3): p. 453-461.
180. Ihre, H.R., et al., *Polyester dendritic systems for drug delivery applications: Design, synthesis, and characterization.* Bioconjugate Chem, 2002. **13**(3): p. 443-452.
181. Gratton, S.E.A., et al., *Nanofabricated particles for engineered drug therapies: A preliminary Biodistribution study of PRINT (TM) nanoparticles.* Journal of Controlled Release, 2007. **121**(1-2): p. 10-18.
182. Parveen, S., R. Misra, and S.K. Sahoo, *Nanoparticles: a boon to drug delivery, therapeutics, diagnostics and imaging.* Nanomedicine : nanotechnology, biology, and medicine, 2011.
183. Lee, J.Y., et al., *Intracellular delivery of paclitaxel using oil-free, shell cross-linked HSA - Multi-armed PEG nanocapsules.* Biomaterials, 2011. **32**(33): p. 8635-8644.
184. Rawat, M., et al., *Nanocarriers: Promising vehicle for bioactive drugs.* Biol Pharm Bull, 2006. **29**(9): p. 1790-1798.
185. Lai, S.K., Y.Y. Wang, and J. Hanes, *Mucus-penetrating nanoparticles for drug and gene delivery to mucosal tissues.* Advanced drug delivery reviews, 2009. **61**(2): p. 158-171.
186. Beck-Broichsitter, M., O.M. Merkel, and T. Kissel, *Controlled pulmonary drug and gene delivery using polymeric nano-carriers.* Journal of Controlled Release, 2011.
187. Discher, B.M., et al., *Polymersomes: Tough vesicles made from diblock copolymers.* Science, 1999. **284**(5417): p. 1143-1146.
188. Discher, D.E. and A. Eisenberg, *Polymer vesicles.* Science, 2002. **297**(5583): p. 967-973.
189. Christian, D.A., et al., *Polymersome carriers: From self-assembly to siRNA and protein therapeutics.* European journal of pharmaceutics and biopharmaceutics : official journal of Arbeitsgemeinschaft fur Pharmazeutische Verfahrenstechnik e.V, 2009. **71**(3): p. 463-474.
190. Ahmed, F., et al., *Biodegradable polymersomes loaded with both paclitaxel and doxorubicin permeate and shrink tumors, inducing apoptosis in proportion to accumulated drug.* Journal of Controlled Release, 2006. **116**(2): p. 150-158.
191. Li, S.L., et al., *Self-assembled poly(butadiene)-b-poly(ethylene oxide) polymersomes as paclitaxel carriers.* Biotechnology Progress, 2007. **23**(1): p. 278-285.
192. Levine, D.H., et al., *Polymersomes: a new multi-functional tool for cancer diagnosis and therapy.* Methods, 2008. **46**(1): p. 25-32.
193. Bajpai, A.K., et al., *Responsive polymers in controlled drug delivery.* Prog Polym Sci, 2008. **33**(11): p. 1088-1118.

194. Morimoto, N., et al., *Hybrid nanogels with physical and chemical cross-linking structures as nanocarriers.* Macromolecular Bioscience, 2005. **5**(8): p. 710-716.
195. Shah, P.P., et al., *Skin permeating nanogel for the cutaneous co-delivery of two anti-inflammatory drugs.* Biomaterials, 2012. **33**(5): p. 1607-17.
196. Nagahama, K., T. Ouchi, and Y. Ohya, *Biodegradable Nanogels Prepared by Self-Assembly of Poly(L-lactide)-Grafted Dextran: Entrapment and Release of Proteins.* Macromolecular Bioscience, 2008. **8**(11): p. 1044-1052.
197. Shidhaye, S., et al., *Nanogel Engineered Polymeric Micelles for Drug Delivery.* Current Drug Therapy, 2008. **3**: p. 209-217.
198. Lee, E.S., et al., *A virus-mimetic nanogel vehicle.* Angew Chem Int Edit, 2008. **47**(13): p. 2418-2421.
199. Kopecek, J., *Polymer chemistry - Swell gels.* Nature, 2002. **417**(6887): p. 388-+.
200. Kettel, M.J., et al., *Aqueous nanogels modified with cyclodextrin.* Polymer, 2011. **52**(9): p. 1917-1924.
201. Shen, W., et al., *Thermosensitive, biocompatible and antifouling nanogels prepared via aqueous raft dispersion polymerization for targeted drug delivery.* Journal of Controlled Release, 2011. **152 Suppl 1**: p. e75-6.
202. Leo, E., et al., *In vitro evaluation of PLA nanoparticles containing a lipophilic rug in water-soluble or insoluble form.* Int J Pharmaceut, 2004. **278**(1): p. 133-141.
203. Nowak, A.P., et al., *Rapidly recovering hydrogel scaffolds from self-assembling diblock copolypeptide amphiphiles.* Nature, 2002. **417**(6887): p. 424-428.
204. Haley, B. and E. Frenkel, *Nanoparticles for drug delivery in cancer treatment.* Urol Oncol-Semin Ori, 2008. **26**(1): p. 57-64.
205. Davis, M.E., Z. Chen, and D.M. Shin, *Nanoparticle therapeutics: an emerging treatment modality for cancer.* Nat Rev Drug Discov, 2008. **7**(9): p. 771-782.
206. Lammers, T., W.E. Hennink, and G. Storm, *Tumour-targeted nanomedicines: principles and practice.* British journal of cancer, 2008. **99**(3): p. 392-397.
207. Lince, F., et al., *Preparation of polymer nanoparticles loaded with doxorubicin for controlled drug delivery.* Chem Eng Res Des, 2011. **89**(11A): p. 2410-2419.
208. Alexis, F., et al., *Factors affecting the clearance and biodistribution of polymeric nanoparticles.* Mol Pharmaceut, 2008. **5**(4): p. 505-515.
209. Makhof, A., Y. Tozuka, and H. Takeuchi, *pH-Sensitive nanospheres for colon-specific drug delivery in experimentally induced colitis rat model.* European journal of pharmaceutics and biopharmaceutics : official journal of Arbeitsgemeinschaft fur Pharmazeutische Verfahrenstechnik e.V, 2009. **72**(1): p. 1-8.
210. Zhang, W., et al., *The potential of Pluronic polymeric micelles encapsulated with paclitaxel for the treatment of melanoma using subcutaneous and pulmonary metastatic mice models.* Biomaterials, 2011. **32**(25): p. 5934-5944.
211. Yoo, H.S., E.A. Lee, and T.G. Park, *Doxorubicin-conjugated biodegradable polymeric micelles having acid-cleavable linkages.* Journal of Controlled Release, 2002. **82**(1): p. 17-27.
212. Ganta, S., et al., *A review of stimuli-responsive nanocarriers for drug and gene delivery.* Journal of Controlled Release, 2008. **126**(3): p. 187-204.
213. Gillies, E.R. and J.M.J. Frechet, *A new approach towards acid sensitive copolymer micelles for drug delivery.* Chem Commun, 2003(14): p. 1640-1641.

214. Sharon, J., M.A. Liebman, and B.R. Williams, *Recombinant polyclonal antibodies for cancer therapy.* J Cell Biochem, 2005. **96**(2): p. 305-313.
215. Qiu, X.Q., et al., *Small antibody mimetics comprising two complementarity-determining regions and a framework region for tumor targeting.* Nat Biotechnol, 2007. **25**(8): p. 921-9.
216. Ruoslahti, E., S.N. Bhatia, and M.J. Sailor, *Targeting of drugs and nanoparticles to tumors.* J Cell Biol, 2010. **188**(6): p. 759-768.
217. Garcia-Bennett, A., M. Nees, and B. Fadeel, *In search of the Holy Grail: Folate-targeted nanoparticles for cancer therapy.* Biochem Pharmacol, 2011. **81**(8): p. 976-984.
218. Sudimack, J. and R.J. Lee, *Targeted drug delivery via the folate receptor.* Advanced drug delivery reviews, 2000. **41**(2): p. 147-162.
219. Liu, G., et al., *Functional nanoparticles for molecular imaging guided gene delivery.* Nano Today, 2010. **5**(6): p. 524-539.
220. Xiao, L., et al., *Role of cellular uptake in the reversal of multidrug resistance by PEG-b-PLA polymeric micelles.* Biomaterials, 2011. **32**(22): p. 5148-57.
221. Muzykantov, V.R., et al., *Endotoxin reduces specific pulmonary uptake of radiolabeled monoclonal antibody to angiotensin-converting enzyme.* J Nucl Med, 1991. **32**(3): p. 453-60.
222. Trubetskoy, V.S., et al., *Use of N-terminal modified poly(L-lysine)-antibody conjugate as a carrier for targeted gene delivery in mouse lung endothelial cells.* Bioconjug Chem, 1992. **3**(4): p. 323-7.
223. Iijima, M. and H. Kamiya, *Surface Modification for Improving the Stability of Nanoparticles in Liquid Media.* Kona Powder Part J, 2009(27): p. 119-129.
224. Galperin, A., et al., *Radiopaque iodinated polymeric nanoparticles for X-ray imaging applications.* Biomaterials, 2007. **28**(30): p. 4461-4468.
225. Loudos, G., G.C. Kagadis, and D. Psimadas, *Current status and future perspectives of in vivo small animal imaging using radiolabeled nanoparticles.* Eur J Radiol, 2011. **78**(2): p. 287-295.
226. Rutman, A.M. and M.D. Kuo, *Radiogenomics: Creating a link between molecular diagnostics and diagnostic imaging.* Eur J Radiol, 2009. **70**(2): p. 232-241.
227. Rai, P., et al., *Development and applications of photo-triggered theranostic agents.* Advanced drug delivery reviews, 2010. **62**(11): p. 1094-1124.
228. Xie, J., S. Lee, and X.Y. Chen, *Nanoparticle-based theranostic agents.* Advanced drug delivery reviews, 2010. **62**(11): p. 1064-1079.
229. Sakamoto, J.H., et al., *Enabling individualized therapy through nanotechnology.* Pharmacol Res, 2010. **62**(2): p. 57-89.
230. Ringe, K., C.M. Walz, and B.A. Sabel, *Nanoparticle Drug Delivery to the Brain,* in *Encyclopedia of Nanoscience and Nanotechnology*. 2004. p. 91-104.
231. Kim, S., et al., *Cytotoxicity of, and innate immune response to, size-controlled polypyrrole nanoparticles in mammalian cells.* Biomaterials, 2011. **32**(9): p. 2342-2350.
232. Wang, P.W., S.M. Henning, and D. Heber, *Limitations of MTT and MTS-Based Assays for Measurement of Antiproliferative Activity of Green Tea Polyphenols.* Plos One, 2010. **5**(4).

233. Rejinold, N.S., et al., *Curcumin-loaded biocompatible thermoresponsive polymeric nanoparticles for cancer drug delivery.* J Colloid Interf Sci, 2011. **360**(1): p. 39-51.
234. Wattamwar, P.P., et al., *Tuning of the pro-oxidant and antioxidant activity of trolox through the controlled release from biodegradable poly(trolox ester) polymers.* Journal of Biomedical Materials Research Part A, 2011. **99A**(2): p. 184-191.
235. Dobrovolskaia, M.A., et al., *Ambiguities in applying traditional Limulus Amebocyte Lysate tests to quantify endotoxin in nanoparticle formulations.* Nanomedicine : nanotechnology, biology, and medicine, 2010. **5**(4): p. 555-562.
236. Siepmann, J. and N.A. Peppas, *Modeling of drug release from delivery systems based on hydroxypropyl methylcellulose (HPMC).* Advanced drug delivery reviews, 2001. **48**(2-3): p. 139-157.
237. Peppas, N.A. and J.J. Sahlin, *A Simple Equation for the Description of Solute Release .3. Coupling of Diffusion and Relaxation.* Int J Pharmaceut, 1989. **57**(2): p. 169-172.
238. Zeng, Q.H., A.B. Yu, and G.Q. Lu, *Multiscale modeling and simulation of polymer nanocomposites.* Prog Polym Sci, 2008. **33**(2): p. 191-269.
239. Perez-Herrero, E. and A. Fernandez-Medarde, *Advanced targeted therapies in cancer: Drug nanocarriers, the future of chemotherapy.* Eur J Pharm Biopharm, 2015. **93**: p. 52-79.
240. Hamaguchi, T., et al., *A phase I and pharmacokinetic study of NK105, a paclitaxel-incorporating micellar nanoparticle formulation.* British journal of cancer, 2007. **97**(2): p. 170-176.
241. Hawkins, M.J., P. Soon-Shiong, and N. Desai, *Protein nanoparticles as drug carriers in clinical medicine.* Advanced drug delivery reviews, 2008. **60**(8): p. 876-885.
242. WHO. *Fact sheet N°310*. 2014; Available from: http://www.who.int/mediacentre/factsheets/fs310/en/.
243. Van Boeckel, T.P., et al., *Global trends in antimicrobial use in food animals.* P Natl Acad Sci USA, 2015. **112**(18): p. 5649-5654.
244. Casali, N., et al., *Microevolution of extensively drug-resistant tuberculosis in Russia.* Genome Res, 2012. **22**(4): p. 735-745.
245. Boyman, L., G.S. Williams, and W.J. Lederer, *The growing importance of mitochondrial calcium in health and disease.* Proc Natl Acad Sci U S A, 2015. **112**(36): p. 11150-1.
246. Jackson, S., et al., *Mitochondrial abnormalities in the myofibrillar myopathies.* Eur J Neurol, 2015.
247. Orrenius, S., V. Gogvadze, and B. Zhivotovsky, *Mitochondrial oxidative stress: implications for cell death.* Annu Rev Pharmacol Toxicol, 2007. **47**: p. 143-83.
248. Manoilov, S.E. and K.P. Khanson, *[the Effect of Exogenous Cytochrome C on Oxidative Phosphorylation in Mitochondria Isolated from Tissues of Irradiated Animals].* Vopr Med Khim, 1964. **10**: p. 410-3.
249. Kerr, J.F., A.H. Wyllie, and A.R. Currie, *Apoptosis: a basic biological phenomenon with wide-ranging implications in tissue kinetics.* British journal of cancer, 1972. **26**(4): p. 239-57.
250. Go, Y.M. and D.P. Jones, *Redox compartmentalization in eukaryotic cells.* Biochim Biophys Acta, 2008. **1780**(11): p. 1273-90.

251. Ye, Z.W., et al., *Oxidative stress, redox regulation and diseases of cellular differentiation.* Biochim Biophys Acta, 2015. **1850**(8): p. 1607-21.
252. Lu, S.C., *Glutathione synthesis.* Biochim Biophys Acta, 2013. **1830**(5): p. 3143-53.
253. Eaton, D.L. and T.K. Bammler, *Concise review of the glutathione S-transferases and their significance to toxicology.* Toxicol Sci, 1999. **49**(2): p. 156-64.
254. Saito, G., J.A. Swanson, and K.D. Lee, *Drug delivery strategy utilizing conjugation via reversible disulfide linkages: role and site of cellular reducing activities.* Advanced drug delivery reviews, 2003. **55**(2): p. 199-215.
255. Hu, J., L. Dong, and C.E. Outten, *The redox environment in the mitochondrial intermembrane space is maintained separately from the cytosol and matrix.* J Biol Chem, 2008. **283**(43): p. 29126-34.
256. Hwang, C., A.J. Sinskey, and H.F. Lodish, *Oxidized redox state of glutathione in the endoplasmic reticulum.* Science, 1992. **257**(5076): p. 1496-502.
257. Banerjee, R., *Redox outside the box: linking extracellular redox remodeling with intracellular redox metabolism.* J Biol Chem, 2012. **287**(7): p. 4397-402.
258. Galley, H.F., *Bench-to-bedside review: Targeting antioxidants to mitochondria in sepsis.* Crit Care, 2010. **14**(4).
259. Rocha, M., et al., *Mitochondrial dysfunction and antioxidant therapy in sepsis.* Infect Disord Drug Targets, 2012. **12**(2): p. 161-78.
260. Hotchkiss, R.S. and I.E. Karl, *The pathophysiology and treatment of sepsis.* N Engl J Med, 2003. **348**(2): p. 138-50.
261. Amieva, M. and R.M. Peek, Jr., *Pathobiology of Helicobacter pylori-induced Gastric Cancer.* Gastroenterology, 2015.
262. Akira, S., S. Uematsu, and O. Takeuchi, *Pathogen recognition and innate immunity.* Cell, 2006. **124**(4): p. 783-801.
263. Banchereau, J. and R.M. Steinman, *Dendritic cells and the control of immunity.* Nature, 1998. **392**(6673): p. 245-52.
264. Zha, S., et al., *Cyclooxygenases in cancer: progress and perspective.* Cancer Lett, 2004. **215**(1): p. 1-20.
265. Singer, A.J. and R.A. Clark, *Cutaneous wound healing.* N Engl J Med, 1999. **341**(10): p. 738-46.
266. Martin, P., *Wound healing--aiming for perfect skin regeneration.* Science, 1997. **276**(5309): p. 75-81.
267. Dunon, D., L. Piali, and B.A. Imhof, *To stick or not to stick: the new leukocyte homing paradigm.* Curr Opin Cell Biol, 1996. **8**(5): p. 714-23.
268. Folkman, J. and Y. Shing, *Angiogenesis.* J Biol Chem, 1992. **267**(16): p. 10931-4.
269. Kleinman, H.K., R.J. Klebe, and G.R. Martin, *Role of collagenous matrices in the adhesion and growth of cells.* J Cell Biol, 1981. **88**(3): p. 473-85.
270. Zorov, D.B., M. Juhaszova, and S.J. Sollott, *Mitochondrial ROS-induced ROS release: an update and review.* Biochim Biophys Acta, 2006. **1757**(5-6): p. 509-17.
271. Lawrence, T., *The Nuclear Factor NF-kappa B Pathway in Inflammation.* Csh Perspect Biol, 2009. **1**(6).
272. Nuss, K.M. and B. von Rechenberg, *Biocompatibility issues with modern implants in bone - a review for clinical orthopedics.* Open Orthop J, 2008. **2**: p. 66-78.
273. Wiggins, M.J., et al., *Biodegradation of polyether polyurethane inner insulation in bipolar pacemaker leads.* J Biomed Mater Res, 2001. **58**(3): p. 302-307.

274. Conner, E.M. and M.B. Grisham, *Inflammation, free radicals, and antioxidants.* Nutrition, 1996. **12**(4): p. 274-277.
275. Ungersbock, A., O.E.M. Pohler, and S.M. Perren, *Evaluation of soft tissue reactions at the interface of titanium limited contact dynamic compression plate implants with different surface treatments: An experimental sheep study.* Biomaterials, 1996. **17**(8): p. 797-806.
276. El-Warrak, A.O., et al., *An animal model for interface tissue formation in cemented hip replacements.* Vet Surg, 2004. **33**(5): p. 495-504.
277. Illum, L., et al., *The Organ Distribution and Circulation Time of Intravenously Injected Colloidal Carriers Sterically Stabilized with a Blockcopolymer - Poloxamine 908.* Life Sci, 1987. **40**(4): p. 367-374.
278. Owens, D.E. and N.A. Peppas, *Opsonization, biodistribution, and pharmacokinetics of polymeric nanoparticles.* Int J Pharmaceut, 2006. **307**(1): p. 93-102.
279. Wang, R.L., et al., *The Acute Extracellular Flux (XF) Assay to Assess Compound Effects on Mitochondrial Function.* J Biomol Screen, 2015. **20**(3): p. 422-429.
280. Ricciotti, E. and G.A. FitzGerald, *Prostaglandins and inflammation.* Arterioscler Thromb Vasc Biol, 2011. **31**(5): p. 986-1000.
281. Laine, L., *Approaches to nonsteroidal anti-inflammatory drug use in the high-risk patient.* Gastroenterology, 2001. **120**(3): p. 594-606.
282. Dani, M., et al., *The local antinociceptive effects of paracetamol in neuropathic pain are mediated by cannabinoid receptors.* Eur J Pharmacol, 2007. **573**(1-3): p. 214-5.
283. Din, F.V., et al., *Effect of aspirin and NSAIDs on risk and survival from colorectal cancer.* Gut, 2010. **59**(12): p. 1670-9.
284. Cuzick, J., et al., *Aspirin and non-steroidal anti-inflammatory drugs for cancer prevention: an international consensus statement.* Lancet Oncol, 2009. **10**(5): p. 501-7.
285. Lopez-Olivo, M.A., et al., *Methotrexate for treating rheumatoid arthritis.* Cochrane Database Syst Rev, 2014. **6**: p. CD000957.
286. Malhotra, S., et al., *In vitro and in vivo antioxidant, cytotoxic, and anti-chronic inflammatory arthritic effect of selenium nanoparticles.* J Biomed Mater Res B Appl Biomater, 2015.
287. Duarte, J.H., *Experimental arthritis: Fullerene nanoparticles ameliorate disease in arthritis mouse model.* Nat Rev Rheumatol, 2015. **11**(6): p. 319.
288. Griffith, O.W. and A. Meister, *Origin and Turnover of Mitochondrial Glutathione.* P Natl Acad Sci USA, 1985. **82**(14): p. 4668-4672.
289. Anderson, M.E. and J.L. Luo, *Glutathione therapy: from prodrugs to genes.* Semin Liver Dis, 1998. **18**(4): p. 415-24.
290. Green, J.L., et al., *Oral and Intravenous Acetylcysteine for Treatment of Acetaminophen Toxicity: A Systematic Review and Meta-analysis.* The western journal of emergency medicine, 2013. **14**(3): p. 218-26.
291. Mell, L.K., et al., *Effect of amifostine on response rates in locally advanced non-small-cell lung cancer patients treated on randomized controlled trials: A meta-analysis.* Int J Radiat Oncol, 2007. **68**(1): p. 111-118.

292. Uzal, C., et al., *The protective effect of amifostine on radiation-induced acute pulmonary toxicity: Detection by (TC)-T-99m-DTPA transalveolar clearances.* Int J Radiat Oncol, 2004. **60**(2): p. 564-569.
293. Tsoutsou, P.G. and M.I. Koukourakis, *Radiation pneumonitis and fibrosis: Mechanisms underlying its pathogenesis and implications for future research.* Int J Radiat Oncol, 2006. **66**(5): p. 1281-1293.
294. Ishii, Y. and S. Kitamura, *Soluble intercellular adhesion molecule-1 as an early detection marker for radiation pneumonitis.* Eur Respir J, 1999. **13**(4): p. 733-738.
295. Rube, C.E., et al., *Dose-dependent induction of transforming growth factor beta (TGF-beta) in the lung tissue of fibrosis-prone mice after thoracic irradiation.* Int J Radiat Oncol, 2000. **47**(4): p. 1033-1042.
296. Antonadou, D., et al., *Randomized phase III trial of radiation treatment +/- amifostine in patients with advanced-stage lung cancer (vol 51, pg 915, 2001).* Int J Radiat Oncol, 2002. **52**(5): p. 1458-1458.
297. Antonadou, D., et al., *Effect of amifostine on toxicities associated with radiochemotherapy in patients with locally advanced non-small-cell lung cancer.* Int J Radiat Oncol, 2003. **57**(2): p. 402-408.
298. Komaki, R., et al., *Effects of amifostine on acute toxicity from concurrent chemotherapy and radiotherapy for inoperable non-small-cell lung cancer: Report of a randomized comparative trial.* Int J Radiat Oncol, 2004. **58**(5): p. 1369-1377.
299. Andreassen, C.N., C. Gran, and J.C. Lindegaard, *Chemical radioprotection: A critical review of amifostine as a cytoprotector in radiotherapy.* Semin Radiat Oncol, 2003. **13**(1): p. 62-72.
300. Lawrence, Y.R., et al., *The addition of amifostine to carboplatin and paclitaxel based chemoradiation in locally advanced non-small cell lung cancer: Long-term follow-up of Radiation Therapy Oncology Group (RTOG) randomized trial 9801.* Lung Cancer, 2013. **80**(3): p. 298-305.
301. Rades, D., et al., *Serious adverse effects of amifostine during radiotherapy in head and neck cancer patients.* Radiother Oncol, 2004. **70**(3): p. 261-264.
302. Bourhis, J., et al., *Effect of Amifostine on Survival Among Patients Treated With Radiotherapy: A Meta-Analysis of Individual Patient Data.* J Clin Oncol, 2011. **29**(18): p. 2590-2597.
303. Sarna, L., et al., *Clinically Meaningful Differences in Patient-Reported Outcomes with Amifostine in Combination with Chemoradiation for Locally Advanced Non-Small-Cell Lung Cancer: An Analysis of Rtog 9801.* Int J Radiat Oncol, 2008. **72**(5): p. 1378-1384.
304. Sasse, A.D., et al., *Amifostine reduces side effects and improves complete response rate during radiotherapy: Results of a meta-analysis.* Int J Radiat Oncol, 2006. **64**(3): p. 784-791.
305. Bjelakovic, G., et al., *Antioxidant supplements for prevention of mortality in healthy participants and patients with various diseases.* Cochrane Db Syst Rev, 2012(3).
306. Faraonio, R., et al., *p53 suppresses the Nrf2-dependent transcription of antioxidant response genes.* J Biol Chem, 2006. **281**(52): p. 39776-84.
307. Vazquez, A., et al., *The genetics of the p53 pathway, apoptosis and cancer therapy.* Nat Rev Drug Discov, 2008. **7**(12): p. 979-87.

308. Sayin, V.I., et al., *Antioxidants accelerate lung cancer progression in mice.* Sci Transl Med, 2014. **6**(221): p. 221ra15.
309. Barnes, P.J. and M. Karin, *Nuclear factor-kappaB: a pivotal transcription factor in chronic inflammatory diseases.* N Engl J Med, 1997. **336**(15): p. 1066-71.
310. Fan, Z., et al., *Anti-inflammatory and antioxidant effects of curcumin on acute lung injury in a rodent model of intestinal ischemia reperfusion by inhibiting the pathway of NF-Kb.* Int J Clin Exp Pathol, 2015. **8**(4): p. 3451-9.
311. Mishra, A., et al., *Curcumin modulates cellular AP-1, NF-kB, and HPV16 E6 proteins in oral cancer.* Ecancermedicalscience, 2015. **9**: p. 525.
312. Ohtomo, Y., et al., *Evidence for biogenic graphite in early Archaean Isua metasedimentary rocks.* Nat Geosci, 2014. **7**(1): p. 25-28.
313. Schloss, P.D. and J. Handelsman, *Status of the microbial census.* Microbiol Mol Biol R, 2004. **68**(4): p. 686-+.
314. McFall-Ngai, M., et al., *Animals in a bacterial world, a new imperative for the life sciences.* P Natl Acad Sci USA, 2013. **110**(9): p. 3229-3236.
315. Guo, L.H., X.S. He, and W.S. Shi, *Intercellular communications in multispecies oral microbial communities.* Front Microbiol, 2014. **5**.
316. Zoetendal, E.G., E.E. Vaughan, and W.M. de Vos, *A microbial world within us.* Mol Microbiol, 2006. **59**(6): p. 1639-1650.
317. Wyklicky, H. and M. Skopec, *Ignaz Philipp Semmelweis, the prophet of bacteriology.* Infect Control, 1983. **4**(5): p. 367-70.
318. Nandi, S.K., et al., *Local antibiotic delivery systems for the treatment of osteomyelitis - A review.* Mat Sci Eng C-Mater, 2009. **29**(8): p. 2478-2485.
319. Gogia, J.S., et al., *Local antibiotic therapy in osteomyelitis.* Seminars in plastic surgery, 2009. **23**(2): p. 100-7.
320. Gitelis, S. and G.T. Brebach, *The treatment of chronic osteomyelitis with a biodegradable antibiotic-impregnated implant.* J Orthop Surg (Hong Kong), 2002. **10**(1): p. 53-60.
321. Mohanty, S.P., M.N. Kumar, and N.S. Murthy, *Use of antibiotic-loaded polymethyl methacrylate beads in the management of musculoskeletal sepsis--a retrospective study.* J Orthop Surg (Hong Kong), 2003. **11**(1): p. 73-9.
322. Kaplan, J.B., et al., *Low Levels of beta-Lactam Antibiotics Induce Extracellular DNA Release and Biofilm Formation in Staphylococcus aureus.* Mbio, 2012. **3**(4).
323. Norowski, P.A., Jr. and J.D. Bumgardner, *Biomaterial and antibiotic strategies for peri-implantitis: a review.* J Biomed Mater Res B Appl Biomater, 2009. **88**(2): p. 530-43.
324. Cirz, R.T. and F.E. Romesberg, *Controlling mutation: intervening in evolution as a therapeutic strategy.* Crit Rev Biochem Mol, 2007. **42**(5): p. 341-354.
325. Arce Miranda, J.E., et al., *Oxidative and nitrosative stress in Staphylococcus aureus biofilm.* FEMS microbiology letters, 2011. **315**(1): p. 23-9.
326. Voyich, J.A., et al., *Insights into mechanisms used by Staphylococcus aureus to avoid destruction by human neutrophils.* J Immunol, 2005. **175**(6): p. 3907-3919.
327. Keshavjee, S., et al., *Treatment of extensively drug-resistant tuberculosis in Tomsk, Russia: a retrospective cohort study.* Lancet, 2008. **372**(9647): p. 1403-9.
328. Alekshun, M.N. and S.B. Levy, *Molecular mechanisms of antibacterial multidrug resistance.* Cell, 2007. **128**(6): p. 1037-1050.

329. McCallum, N., B. Berger-Bachi, and M.M. Senn, *Regulation of antibiotic resistance in Staphylococcus aureus.* Int J Med Microbiol, 2010. **300**(2-3): p. 118-129.
330. WHO, *Antimicrobial resistance: global report on surveillance 2014*. 2014.
331. Hoiby, N., et al., *Antibiotic resistance of bacterial biofilms.* Int J Antimicrob Ag, 2010. **35**(4): p. 322-332.
332. Smith, A.W., *Biofilms and antibiotic therapy: Is there a role for combating bacterial resistance by the use of novel drug delivery systems?* Advanced drug delivery reviews, 2005. **57**(10): p. 1539-1550.
333. Stewart, P.S., *Mechanisms of antibiotic resistance in bacterial biofilms.* Int J Med Microbiol, 2002. **292**(2): p. 107-113.
334. Cabiscol, E., J. Tamarit, and J. Ros, *Oxidative stress in bacteria and protein damage by reactive oxygen species.* International microbiology : the official journal of the Spanish Society for Microbiology, 2000. **3**(1): p. 3-8.
335. D'Autreaux, B. and M.B. Toledano, *ROS as signalling molecules: mechanisms that generate specificity in ROS homeostasis.* Nat Rev Mol Cell Bio, 2007. **8**(10): p. 813-824.
336. Veal, E.A., A.M. Day, and B.A. Morgan, *Hydrogen peroxide sensing and signaling.* Mol Cell, 2007. **26**(1): p. 1-14.
337. Mookherjee, N. and R.E. Hancock, *Cationic host defence peptides: innate immune regulatory peptides as a novel approach for treating infections.* Cell Mol Life Sci, 2007. **64**(7-8): p. 922-33.
338. Ouhara, K., et al., *Increased resistance to cationic antimicrobial peptide LL-37 in methicillin-resistant strains of Staphylococcus aureus.* J Antimicrob Chemother, 2008. **61**(6): p. 1266-9.
339. El-Gamal, M.I., M.S. Abdel-Maksoud, and C.H. Oh, *Recent advances in the research and development of marine antimicrobial peptides.* Curr Top Med Chem, 2013. **13**(16): p. 2026-33.
340. Boles, B.R. and P.K. Singh, *Endogenous oxidative stress produces diversity and adaptability in biofilm communities.* P Natl Acad Sci USA, 2008. **105**(34): p. 12503-12508.
341. Hospenthal, D.R., et al., *Guidelines for the prevention of infection after combat-related injuries.* Journal of Trauma-Injury Infection and Critical Care, 2008. **64**(3): p. S211-S220.
342. Scott, P., et al., *An outbreak of multidrug-resistant Acinetobacter baumannii-calcoaceticus complex infection in the US military health care system associated with military operations in Iraq.* Clinical Infectious Diseases, 2007. **44**(12): p. 1577-1584.
343. Charbonneau, H., et al., *Mediastinitis due to Gram-negative bacteria is associated with increased mortality.* Clinical microbiology and infection : the official publication of the European Society of Clinical Microbiology and Infectious Diseases, 2014. **20**(3): p. O197-202.
344. Lepelletier, D., et al., *Risk factors for mortality in patients with mediastinitis after cardiac surgery.* Archives of cardiovascular diseases, 2009. **102**(2): p. 119-25.
345. Tang, G.H., et al., *Prevention and management of deep sternal wound infection.* Seminars in thoracic and cardiovascular surgery, 2004. **16**(1): p. 62-9.

346. Bratzler, D.W., et al., *Antimicrobial prophylaxis for surgery: an advisory statement from the National Surgical Infection Prevention Project.* Clinical infectious diseases : an official publication of the Infectious Diseases Society of America, 2004. **38**(12): p. 1706-15.
347. Daar, E.S., *Emerging resistance profiles of newly approved antiretroviral drugs.* Top HIV Med, 2008. **16**(4): p. 110-6.
348. D'Agata, E.M.C., et al., *The Impact of Different Antibiotic Regimens on the Emergence of Antimicrobial-Resistant Bacteria.* Plos One, 2008. **3**(12).
349. Michel, J.B., et al., *Drug interactions modulate the potential for evolution of resistance.* P Natl Acad Sci USA, 2008. **105**(39): p. 14918-14923.
350. Pepper, J.W., *DEFEATING PATHOGEN DRUG RESISTANCE: GUIDANCE FROM EVOLUTIONARY THEORY.* Evolution, 2008. **62**(12): p. 3185-3191.
351. Morero, N.R. and C.E. Argarana, *Pseudomonas aeruginosa deficient in 8-oxodeoxyguanine repair system shows a high frequency of resistance to ciprofloxacin.* FEMS microbiology letters, 2009. **290**(2): p. 217-226.
352. Park, S., X. You, and J.A. Imlay, *Substantial DNA damage from submicromolar intracellular hydrogen peroxide detected in Hpx- mutants of Escherichia coli.* Proc Natl Acad Sci U S A, 2005. **102**(26): p. 9317-22.
353. Dwyer, D.J., M.A. Kohanski, and J.J. Collins, *Role of reactive oxygen species in antibiotic action and resistance.* Current opinion in microbiology, 2009. **12**(5): p. 482-9.
354. Fajardo, A. and J.L. Martinez, *Antibiotics as signals that trigger specific bacterial responses.* Current opinion in microbiology, 2008. **11**(2): p. 161-167.
355. Farr, S.B., R. Dari, and D. Touati, *Oxygen-Dependent Mutagenesis in Escherichia-Coli Lacking Superoxide-Dismutase.* P Natl Acad Sci USA, 1986. **83**(21): p. 8268-8272.
356. Lu, T.K. and J.J. Collins, *Engineered bacteriophage targeting gene networks as adjuvants for antibiotic therapy.* P Natl Acad Sci USA, 2009. **106**(12): p. 4629-4634.
357. Miller, C., et al., *SOS response induction by beta-lactams and bacterial defense against antibiotic lethality.* Science, 2004. **305**(5690): p. 1629-31.
358. Driffield, K., et al., *Increased mutability of Pseudomonas aeruginosa in biofilms.* J Antimicrob Chemoth, 2008. **61**(5): p. 1053-1056.
359. Imlay, J.A., *Cellular defenses against superoxide and hydrogen peroxide.* Annu Rev Biochem, 2008. **77**: p. 755-776.
360. Chatti, A., et al., *Effects of hydrogen peroxide on the motility, catalase and superoxide dismutase of dam and/or seqA mutant of Salmonella typhimurium.* World J Microb Biot, 2012. **28**(1): p. 129-133.
361. Storz, G. and J.A. Imlay, *Oxidative stress.* Current opinion in microbiology, 1999. **2**(2): p. 188-194.
362. Storz, G., et al., *Bacterial Defenses against Oxidative Stress.* Trends Genet, 1990. **6**(11): p. 363-368.
363. Sakai, A., et al., *Impact of reactive oxygen species on spontaneous mutagenesis in Escherichia coli.* Genes Cells, 2006. **11**(7): p. 767-778.
364. Woodford, N. and M.J. Ellington, *The emergence of antibiotic resistance by mutation.* Clin Microbiol Infec, 2007. **13**(1): p. 5-18.

365. Campoccia, D., et al., *Antibiotic resistance in Staphylococcus aureus and Staphylococcus epidermidis clinical isolates from implant orthopedic infections.* Int J Artif Organs, 2005. **28**(11): p. 1186-1191.
366. Muro, S., et al., *Control of endothelial targeting and intracellular delivery of therapeutic enzymes by modulating the size and shape of ICAM-1-targeted carriers.* Mol Ther, 2008. **16**(8): p. 1450-1458.
367. Simone, E.A., et al., *Loading PEG-Catalase into Filamentous and Spherical Polymer Nanocarriers.* Pharmaceutical research, 2009. **26**(1): p. 250-260.
368. Wang, X.H. and X.L. Zhao, *Contribution of Oxidative Damage to Antimicrobial Lethality.* Antimicrob Agents Ch, 2009. **53**(4): p. 1395-1402.
369. Bergman, K., et al., *Injectable cell-free template for bone-tissue formation.* J Biomed Mater Res A, 2009. **91**(4): p. 1111-8.
370. Kretlow, J.D., L. Klouda, and A.G. Mikos, *Injectable matrices and scaffolds for drug delivery in tissue engineering.* Advanced drug delivery reviews, 2007. **59**(4-5): p. 263-273.
371. Nair, L.S. and C.T. Laurencin, *Polymers as biomaterials for tissue engineering and controlled drug delivery.* Adv Biochem Eng Biot, 2006. **102**: p. 47-90.
372. Hawkins, A.M., N.S. Satarkar, and J.Z. Hilt, *Nanocomposite degradable hydrogels: demonstration of remote controlled degradation and drug release.* Pharmaceutical research, 2009. **26**(3): p. 667-73.
373. Lin, C.C. and A.T. Metters, *Hydrogels in controlled release formulations: network design and mathematical modeling.* Advanced drug delivery reviews, 2006. **58**(12-13): p. 1379-408.
374. Anderson, D.G., et al., *A combinatorial library of photocrosslinkable and degradable materials.* Adv Mater, 2006. **18**(19): p. 2614-2618.
375. Andrews, J.M. and B.W.P.S. T, *BSAC standardized disc susceptibility testing method (version 6).* J Antimicrob Chemoth, 2007. **60**(1): p. 20-41.
376. Hawkins, A.M., et al., *Tuning Biodegradable Hydrogel Properties via Synthesis Procedure.* Submitted.
377. Andreopoulos, F.M., et al., *Photoimmobilization of organophosphorus hydrolase within a PEG-based hydrogel.* Biotechnol Bioeng, 1999. **65**(5): p. 579-88.
378. Hawkins, A.M., et al., *Synthesis and analysis of degradation, mechanical and toxicity properties of poly(beta-amino ester) degradable hydrogels.* Acta Biomater, 2011. **7**(5): p. 1956-1964.
379. Dziubla, T.D., et al., *Endothelial targeting of semi-permeable polymer nanocarriers for enzyme therapies.* Biomaterials, 2008. **29**(2): p. 215-27.
380. Gao, P., et al., *Recent advances in materials for extended-release antibiotic delivery system.* J Antibiot, 2011. **64**(9): p. 625-634.
381. Bhattarai, N., J. Gunn, and M.Q. Zhang, *Chitosan-based hydrogels for controlled, localized drug delivery.* Advanced drug delivery reviews, 2010. **62**(1): p. 83-99.
382. Huang, J.G., et al., *Dual-delivery of vancomycin and icariin from an injectable calcium phosphate cement-release system for controlling infection and improving bone healing.* Molecular medicine reports, 2013. **8**(4): p. 1221-7.
383. Schnieders, J., et al., *The effect of porosity on drug release kinetics from vancomycin microsphere/calcium phosphate cement composites.* J Biomed Mater Res B Appl Biomater, 2011. **99**(2): p. 391-8.

384. Cui, X., et al., *A novel injectable borate bioactive glass cement for local delivery of vancomycin to cure osteomyelitis and regenerate bone.* Journal of materials science. Materials in medicine, 2014.
385. Thatiparti, T.R., A.J. Shoffstall, and H.A. von Recum, *Cyclodextrin-based device coatings for affinity-based release of antibiotics.* Biomaterials, 2010. **31**(8): p. 2335-2347.
386. Brooks, B.D., et al., *Molded polymer-coated composite bone void filler improves tobramycin controlled release kinetics.* J Biomed Mater Res B Appl Biomater, 2013.
387. Bastari, K., et al., *A controlled release of antibiotics from calcium phosphate-coated poly(lactic-co-glycolic acid) particles and their in vitro efficacy against Staphylococcus aureus biofilm.* Journal of materials science. Materials in medicine, 2013.
388. Mohan, Y.M., P.S.K. Murthy, and K.M. Raju, *Preparation and swelling behavior of macroporous poly(acrylamide-co-sodium methacrylate) superabsorbent hydrogels.* J Appl Polym Sci, 2006. **101**(5): p. 3202-3214.
389. Lawson, M.C., et al., *Polymerizable Vancomycin Derivatives for Bactericidal Biomaterial Surface Modification: Structure-Function Evaluation.* Biomacromolecules, 2009. **10**(8): p. 2221-2234.
390. Lawson, M.C., C.N. Bowman, and K.S. Anseth, *Vancomycin derivative photopolymerized to titanium kills S. epidermidis.* Clin Orthop Relat R, 2007(461): p. 96-105.
391. Moojen, D.J.F., et al., *In Vitro Release of Antibiotics from Commercial PMMA Beads and Articulating Hip Spacers.* J Arthroplasty, 2008. **23**(8): p. 1152-1156.
392. Shinsako, K., et al., *Effects of bead size and polymerization in PMMA bone cement on vancomycin release.* Bio-Med Mater Eng, 2008. **18**(6): p. 377-385.
393. Overstreet, D.J., et al., *In situ forming, resorbable graft copolymer hydrogels providing controlled drug release.* Journal of Biomedical Materials Research Part A, 2013. **101A**(5): p. 1437-1446.
394. Chilukuri, D.M. and J.C. Shah, *Local delivery of vancomycin for the prophylaxis of prosthetic device-related infections.* Pharmaceutical research, 2005. **22**(4): p. 563-572.
395. Harth, K.C., et al., *Antibiotic-Releasing Mesh Coating to Reduce Prosthetic Sepsis: An In Vivo Study.* J Surg Res, 2010. **163**(2): p. 337-343.
396. Baral, A., et al., *Assembly of an injectable noncytotoxic peptide-based hydrogelator for sustained release of drugs.* Langmuir : the ACS journal of surfaces and colloids, 2014. **30**(3): p. 929-36.
397. Khodaverdi, E., et al., *Sustained delivery of amphotericin B and vancomycin hydrochloride by an injectable thermogelling tri-block copolymer.* PDA journal of pharmaceutical science and technology / PDA, 2013. **67**(2): p. 135-45.
398. Shukla, A., et al., *Release of vancomycin from multilayer coated absorbent gelatin sponges.* J Control Release, 2012. **157**(1): p. 64-71.
399. Hawkins, A.M., et al., *Tuning biodegradable hydrogel properties via synthesis procedure.* Polymer, 2013. **54**(17): p. 4422-4426.

400. Hawkins, A.M., et al., *Synthesis and analysis of degradation, mechanical and toxicity properties of poly(beta-amino ester) degradable hydrogels.* Acta biomaterialia, 2011. **7**(5): p. 1956-64.
401. Robibaro, B., et al., *Endothelial cell compatibility of glycopeptide antibiotics for intravenous use.* J Antimicrob Chemother, 1998. **41**(2): p. 297-300.
402. Wattamwar, P.P., et al., *Tuning of the pro-oxidant and antioxidant activity of trolox through the controlled release from biodegradable poly(trolox ester) polymers.* J Biomed Mater Res A, 2011. **99**(2): p. 184-91.
403. Green, J.J., R. Langer, and D.G. Anderson, *A combinatorial polymer library approach yields insight into nonviral gene delivery.* Accounts of chemical research, 2008. **41**(6): p. 749-59.
404. Zugates, G.T., et al., *Synthesis of poly(beta-amino ester)s with thiol-reactive side chains for DNA delivery.* J Am Chem Soc, 2006. **128**(39): p. 12726-34.
405. Peng, H.H., et al., *Synthesis of a disulfide cross-linked polygalacturonic acid hydrogel for biomedical applications.* J Mater Sci-Mater M, 2013. **24**(6): p. 1375-1382.
406. Zarembinski, T.I., et al., *Thiolated hyaluronan-based hydrogels crosslinked using oxidized glutathione: An injectable matrix designed for ophthalmic applications.* Acta Biomater, 2014. **10**(1): p. 94-103.
407. Gaulding, J.C., et al., *Reversible Inter- and Intra-Microgel Cross-Linking Using Disulfides.* Macromolecules, 2012. **45**(1): p. 39-45.
408. Yang, F., et al., *PEG-based bioresponsive hydrogels with redox-mediated formation and degradation.* J Mater Sci-Mater M, 2012. **23**(3): p. 697-710.
409. Lee, Y.S. and S.W. Kim, *Bioreducible polymers for therapeutic gene delivery.* Journal of Controlled Release, 2014. **190**: p. 424-439.
410. Sunshine, J.C., et al., *Effects of Base Polymer Hydrophobicity and End-Group Modification on Polymeric Gene Delivery.* Biomacromolecules, 2011. **12**(10): p. 3592-3600.
411. Bull, R., et al., *Ischemia enhances activation by Ca2+ and redox modification of ryanodine receptor channels from rat brain cortex.* J Neurosci, 2008. **28**(38): p. 9463-9472.
412. Zitka, O., et al., *Redox status expressed as GSH:GSSG ratio as a marker for oxidative stress in paediatric tumour patients.* Oncol Lett, 2012. **4**(6): p. 1247-1253.
413. Blahova, L., et al., *Simultaneous determination of reduced and oxidized glutathione in tissues by a novel liquid chromatography-mass spectrometry method: application in an inhalation study of Cd nanoparticles.* Analytical and bioanalytical chemistry, 2014. **406**(24): p. 5867-76.
414. Ballatori, N., et al., *Molecular mechanisms of reduced glutathione transport: role of the MRP/CFTR/ABCC and OATP/SLC21A families of membrane proteins.* Toxicology and applied pharmacology, 2005. **204**(3): p. 238-55.
415. Moreno, M.L., et al., *Disulfide stress: a novel type of oxidative stress in acute pancreatitis.* Free radical biology & medicine, 2014. **70**: p. 265-77.
416. Krevelen, D.W.v. and K.t. Nijenhuis, *Properties of polymers : their correlation with chemical structure : their numerical estimation and prediction from additive*

group contributions. 4th, completely rev. ed. 2009, Amsterdam: Elsevier. xxvi, 1004 p.
417. Dziubla, T.D., et al., *Compounds and methods for reducing oxidative stress*. 2014.
418. Shuvaev, V.V., et al., *Platelet-endothelial cell adhesion molecule-1-directed endothelial targeting of superoxide dismutase alleviates oxidative stress caused by either extracellular or intracellular superoxide.* The Journal of pharmacology and experimental therapeutics, 2007. **323**(2): p. 450-7.
419. Valko, M., et al., *Free radicals and antioxidants in normal physiological functions and human disease.* Int J Biochem Cell B, 2007. **39**(1): p. 44-84.
420. Ray, P.D., B.W. Huang, and Y. Tsuji, *Reactive oxygen species (ROS) homeostasis and redox regulation in cellular signaling.* Cell Signal, 2012. **24**(5): p. 981-990.
421. Murphy, M.P., *How mitochondria produce reactive oxygen species.* Biochem J, 2009. **417**: p. 1-13.
422. Jones, D.P. and Y.M. Go, *Redox compartmentalization and cellular stress.* Diabetes, obesity & metabolism, 2010. **12 Suppl 2**: p. 116-25.
423. Ratnam, D.V., et al., *Role of antioxidants in prophylaxis and therapy: A pharmaceutical perspective.* J Control Release, 2006. **113**(3): p. 189-207.
424. Ballatori, N., et al., *Molecular mechanisms of reduced glutathione transport: role of the MRP/CFTR/ABCC and OATP/SLC21A families of membrane proteins.* Toxicol Appl Pharm, 2005. **204**(3): p. 238-255.
425. Arrigo, A.P., *Gene expression and the thiol redox state.* Free Radical Bio Med, 1999. **27**(9-10): p. 936-944.
426. Bull, R., et al., *Ischemia enhances activation by Ca2+ and redox modification of ryanodine receptor channels from rat brain cortex.* The Journal of neuroscience : the official journal of the Society for Neuroscience, 2008. **28**(38): p. 9463-72.
427. Hwang, C., A.J. Sinskey, and H.F. Lodish, *Oxidized Redox State of Glutathione in the Endoplasmic-Reticulum.* Science, 1992. **257**(5076): p. 1496-1502.
428. Chai, Y.C., et al., *S-thiolation of individual human neutrophil proteins including actin by stimulation of the respiratory burst: evidence against a role for glutathione disulfide.* Archives of biochemistry and biophysics, 1994. **310**(1): p. 273-81.
429. Kamaly, N., et al., *Targeted polymeric therapeutic nanoparticles: design, development and clinical translation.* Chemical Society reviews, 2012. **41**(7): p. 2971-3010.
430. Vasilakes, A.L., T.D. Dziubla, and P.P. Wattamwar, *Polymeric Nanoparticles.* Engineering Polymer Systems for Improved Drug Delivery, 2014: p. 117-161.
431. Meng, F., W.E. Hennink, and Z. Zhong, *Reduction-sensitive polymers and bioconjugates for biomedical applications.* Biomaterials, 2009. **30**(12): p. 2180-98.
432. Yameen, B., et al., *Drug Delivery Nanocarriers from a Fully Degradable PEG-Conjugated Polyester with a Reduction-Responsive Backbone.* Chemistry, 2015. **21**(32): p. 11325-9.
433. Nguyen, C.T., et al., *Redox-sensitive nanoparticles from amphiphilic cholesterol-based block copolymers for enhanced tumor intracellular release of doxorubicin.* Nanomedicine : nanotechnology, biology, and medicine, 2015.
434. Lakes, A.L., et al., *Reducible Disulfide Poly(β-amino ester) Hydrogels for Antioxidant Delivery.* Submitted.

435. Yeom, C.-E., M.J. Kim, and B.M. Kim, *1,8-Diazabicyclo[5.4.0]undec-7-ene (DBU)-promoted efficient and versatile aza-Michael addition.* Tetrahedron, 2007. **63**(4): p. 904-909.
436. Stevens, R., L. Stevens, and N.C. Price, *The Stabilities of Various Thiol Compounds Used in Protein Purifications.* Biochem Educ, 1983. **11**(2): p. 70-70.
437. Verheul, R.J., S. van der Wal, and W.E. Hennink, *Tailorable thiolated trimethyl chitosans for covalently stabilized nanoparticles.* Biomacromolecules, 2010. **11**(8): p. 1965-71.
438. Novo, L., et al., *Decationized crosslinked polyplexes for redox-triggered gene delivery.* J Control Release, 2013. **169**(3): p. 246-56.
439. Deng, H., et al., *Balancing the stability and drug release of polymer micelles by the coordination of dual-sensitive cleavable bonds in cross-linked core.* Acta Biomater, 2015. **11**: p. 126-36.
440. Morales-Cruz, M., et al., *Activation of caspase-dependent apoptosis by intracellular delivery of Cytochrome c-based nanoparticles.* J Nanobiotechnology, 2014. **12**: p. 33.
441. Cui, Y., et al., *Mesoporous silica nanoparticles capped with disulfide-linked PEG gatekeepers for glutathione-mediated controlled release.* ACS Appl Mater Interfaces, 2012. **4**(6): p. 3177-83.
442. Abdullah Al, N., et al., *Development of disulfide core-crosslinked pluronic nanoparticles as an effective anticancer-drug-delivery system.* Macromol Biosci, 2011. **11**(9): p. 1264-71.
443. Wang, Y., et al., *Disulfide bond bridge insertion turns hydrophobic anticancer prodrugs into self-assembled nanomedicines.* Nano Lett, 2014. **14**(10): p. 5577-83.
444. Huang, C.H., et al., *Biodegradable polydisulfide dendrimer nanoclusters as MRI contrast agents.* Acs Nano, 2012. **6**(11): p. 9416-24.
445. Zou, J., et al., *Clicking well-defined biodegradable nanoparticles and nanocapsules by UV-induced thiol-ene cross-linking in transparent miniemulsions.* Adv Mater, 2011. **23**(37): p. 4274-7.
446. Williams, S.R., et al., *Synthesis and Characterization of Poly(ethylene glycol)-Glutathione Conjugate Self-Assembled Nanoparticles for Antioxidant Delivery.* Biomacromolecules, 2009. **10**(1): p. 155-161.
447. Nobs, L., et al., *Biodegradable nanoparticles for direct or two-step tumor immunotargeting.* Bioconjug Chem, 2006. **17**(1): p. 139-45.

VITA

Andrew Lakes received a Bachelor of Science in Chemical Engineering from the University of Minnesota Duluth in 2010, and is currently a PhD candidate under advisement of Dr. Thomas Dziubla in Chemical Engineering at the University of Kentucky, starting in 2010. Andrew is a former NSF-IGERT trainee, and former NCI-CNTC trainee where he worked on drug delivery with poly(beta-amino ester) antibiotic and antioxidant polymers for treatment of infectious and oxidative stress related disease applications. Andrew Lakes changed his name from Andrew Vasilakes in 2014.

RESEARCH ADVISORS

- **Dr. Thomas Dziubla** – Primary advisor. Associate Professor of Chemical and Materials Engineering, U of Kentucky.
- **Dr. J. Zach Hilt** – Co-advisor. Associate Professor of Chemical and Materials Engineering, U of Kentucky.
- **Dr. David Puleo** – Co-advisor. Director of Biomedical Engineering, U of Kentucky.
- **Dr. Ronald McGarry** – Clinical advisor. Clinical Associate Professor and Vice Chairman in Department of Radiation Medicine, U of Kentucky.

PUBLICATIONS

- **Andrew L. Lakes**, David. A. Puleo, J. Zach Hilt, Thomas D. Dziubla. *Thiol Functionalized Poly(beta-amino ester) Nanoparticles for Redox Applications.* (In prep.)
- **Andrew L. Lakes**, Justin P. Byarski, Dipti Biswal, Paritosh P. Wattamwar, Rebecca Peyyala, David. A. Puleo, J. Zach Hilt, Thomas D. Dziubla. *Tandem Release of Vancomycin and Catalase for Local Control of Infection*. (In prep.)
- **Andrew L. Lakes**, Carolyn T. Jordan, Prachi T. Gupta, David A. Puleo, J. Zach Hilt, Thomas D. Dziubla. *Reducible Disulfide Poly(beta-amino ester) Hydrogels for Antioxidant Delivery.* (Submitted, Advanced Materials)
- Prachi T. Gupta, **Andrew L. Lakes**, Thomas D. Dziubla. *A Free Radical Primer*, In Dziubla: Oxidative Stress and Biomaterials: the Science, Challenges and Opportunity. (In prep.)
- Sundar P. Authimoolam, **Andrew L. Lakes**, David A. Puleo, Thomas D. Dziubla. *Layer-by-layers of Polymeric Micelles as a Biomimetic Drug-Releasing Network.* Accepted, Macromolecular Bioscience 2015. **15**(8): p. 3099-111

- **Andrew L. Lakes**, Rebecca Peyyala, Jeffrey L. Ebersole, David. A. Puleo, J. Zach Hilt, Thomas D. Dziubla. *Synthesis and characterization of an antibacterial hydrogel containing covalently bound vancomycin.* Biomacromolecules, 2014. **15**(8): p. 3009-18
- Sundar P. Authimoolam, **Andrew L. Vasilakes**, Nihar M. Shah, David A. Puleo, Thomas D. Dziubla. *Synthetic Oral Mucin Mimic from Polymer Micelle Networks. Biomacromolecules, 2014.*
- **Andrew L. Vasilakes**, Thomas D. Dziubla, Paritosh P. Wattamwar. *Ch. 5: Polymeric Nanoparticles*, In Rebecca A. Bader, Engineering Polymer Systems for Improved Drug Delivery. Hoboken, NJ: Wiley & Sons, Inc. 2014

SELECTED PRESENTATIONS

- **Andrew L. Lakes**, Carolyn T. Schumer, David A. Puleo, J. Zach Hilt, Thomas D. Dziubla, *Reducible Disulfide Poly(β-amino ester) Hydrogels for Antioxidant Delivery.* UK CCTS. Lexington, KY Mar. 2015 – Poster.
- **Andrew L. Lakes**, Ron C. McGarry, David A. Puleo, J. Zach Hilt, Thomas D. Dziubla, *Synthesis and Characterization of Disulfide Poly(beta-amino ester) Nanoparticles for Lung Cancer Radioprotection*. AAPS. San Diego, CA Nov. 2014 – Poster.
- **Andrew L. Vasilakes**, Ron C. McGarry, David A. Puleo, J. Zach Hilt, Thomas D. Dziubla, *Disulfide Containing Poly(β-amino esters) for Biomedical-related Applications*, Spring Symposium, Lexington, KY, 2014 – Poster.
- **Andrew L. Vasilakes**, David A. Puleo, J. Zach Hilt, Thomas D. Dziubla, *Development of Disulfide Containing Poly(β-amino esters) for Cancer-Related Applications*, Markey Cancer Center Day, Lexington, KY, 2014 – Poster.
- **Andrew L. Vasilakes**, David A. Puleo, J. Zach Hilt, Thomas D. Dziubla, *Formation of a Covalently-Linked Vancomycin Containing Hydrogel for Local Antibiotic Delivery*, Biomaterials Day, Lexington, KY, 2013 – Oral.
- **Andrew L. Vasilakes**, David A. Puleo, J. Zach Hilt, Thomas D. Dziubla, *Covalent Release of Vancomycin from an Antibiotic Hydrogel Wound Dressing*, Annual AIChE Conference, San Francisco, CA, 2013 – Oral.
- **Andrew L. Vasilakes**, David A. Puleo, J. Zach Hilt, Thomas D. Dziubla, *Development of Vancomycin-Linked Poly(β-amino ester) Hydrogels*, Society for Biomaterials, Boston, MA, 2013 – Poster.
- **Andrew L. Vasilakes**, David A. Puleo, J. Zach Hilt, Thomas D. Dziubla, *Tandem Drug Delivery from Hydrogels for Inhibition of Antibiotic Resistance Emergence*, American Institute for Chemical Engineers Annual Conference, Pittsburgh, PA, 2012 – Oral.
- **Andrew L. Vasilakes**, Rebecca Peyyala, David A. Puleo, J. Zach Hilt, Thomas D. Dziubla, *Synthesis and Characterization of PBAE Hydrogel for the Controlled Release*

of Vancomycin and Catalase, Biomaterials Day, University of Kentucky, Lexington, KY, 2012 – Poster.

- **Andrew L. Vasilakes**, David A. Puleo, J. Zach Hilt, Thomas D. Dziubla, *Development of biodegradable hydrogels for controlled-release of antimicrobial and antioxidant agents*, Appalachian Health Summit, Lexington, KY, 2012 - Poster.
- **Andrew L. Vasilakes**, Justin P. Byarski, Dipti Biswal, Rebecca Peyyala, David A. Puleo, J. Zach Hilt, T.D. Dziubla, *Development of biodegradable hydrogels for controlled-release of antimicrobial/antioxidant agents*, Biomaterials Day, Purdue University, West Lafayette, IN, 2011 – Poster.
- **Andrew L. Vasilakes**, D. Biswal, R. Peyyala, D.A. Puleo, J.Z. Hilt, T.D. Dziubla, *Development of biodegradable hydrogels for the controlled release of antimicrobial and antioxidant agents*, American Institute for Chemical Engineers Annual Conference, Minneapolis, MN, 2011 – Oral.

UNDERGRADUATE MENTEES

- Elysha Calhoun, *Redox Behavior of Disulfide-crosslinked PBAE Hydrogels*, CME 395 and IGERT Research Experience for Undergraduates (REU) participant, University of Kentucky, 2014-2015
- Nic Quammen, *Extrusion of antioxidant polymers for use with 3D printing*, LaFayette High School, 2014-2015
- Alexandra May, *3D Printed Meshes for Antioxidant Delivery*, IGERT Research Experience for Undergraduates (REU) participant, Florida State University, 2013
- Stephanie Cleaver, *Multiphase Drug Release Through a Loaded Biodegradable Hydrogel*, IGERT Research Experience for Undergraduates (REU) participant, DePauw University, 2012
- Adam Lyvers, *Poly(β-amino ester) Coated Iron Oxide Nanoparticles as Biomimetic Sinks for Polychlorinated Biphenyl Detoxification*, IGERT Research Experience for Undergraduates (REU) participant. University of Kentucky, 2011

AWARDS

- President of the University of Kentucky local chapter for the Society for Biomaterials (UKY-SFB) (2013-2014).
- Coordinated Sixth Annual Biomaterials Day conference on September 27th, 2014.
- NCI-CNTC Fellowship (Cancer Nanotechnology Training Center) (2013-2015)
- Certificate in Bioactive Interfaces and Devices (2013)
- Third place overall oral presentation, Biomaterials Day, Case Western (2013)
- NSF-IGERT Fellowship **(**Integrative Graduate Education and Research Traineeship) (2010-2013)

COMMUNITY OUTREACH

- Engineers Day 2015 – CNTC Poster – Discovering the world of nanotechnology

- Science Fair Judge 2015 – 31th Annual KAW-FCPS (Chemistry Leader)
- Science Fair Judge 2014 – 30th Annual KAW-FCPS
- Science Fair Judge 2013 – Lexington Traditional Magnet School
- Engineers Day 2013 – pH responsiveness of enteric coated/uncoated omega-3 tablets.
- Vineyard Church 2012 – Identification of unknown powders via scientific method
- Vineyard Church 2012 – Formation of a cornstarch-based children's toy
- Engineers Day 2012 – Fluorescent quenching of riboflavin in egg whites
- Engineers Day 2011 – Chromatographic analysis of colored markers

FUNDING SOURCES

- CNTC-NCI (R25CA153954).
- IGERT-NSF (DGE-0653710).
- US Army Medical Research Acquisition Activity (W81XWH-09-1-0461).